

¹H PULSED SOLID-STATE NMR T₂ RELAXATION STUDIES OF MACROMOLECULAR STRUCTURES OF ARGONNE PREMIUM COALS

X. Yang, A. R. Garcia, J. W. Larsen, and B. G. Silbernagel
Exxon Research and Engineering Company, Annandale, NJ 08801

Keywords: Coal Structures, NMR Relaxation, Argonne Premium Coals

Abstract

NMR studies of free induction decay (FID) have been made for as received and dried samples of North Dakota, Illinois #6 and Pittsburgh #8 coals.

Modifications of the NMR measurement and data treatment lead to an unambiguous separation of the FID signal into three components: two gaussians and one lorentzian. The two gaussians can be related to the macromolecular structures of coal, and their relaxation behaviors are comparable with model polymer systems. The lorentzian is almost entirely due to absorbed water, and the water content determined for the coals as received agrees very well with those reported using other methods.

High vacuum dried coal samples are also studied, and the results are compared with those of as-received coals. The drying is very effective, evidenced by almost complete loss of the lorentzian component. Interestingly, neither T_2 nor $I_2(0)$ is changed after drying, indicating that the drying process does not have a damaging effect on coal structures.

Introduction

The determination of moisture in coals, the investigation of effective ways for coal drying, and the evaluation of the effect of the drying process on coal structures are both of fundamental importance in coal science and of commercial value in industry applications.

Several experimental methods have been developed in the analysis of moisture in coals, e.g., ASTM (1) and ¹⁸O isotope dilution (2). NMR relaxation measurement has been used for a long time in water quantification in coals (3). A recent work by Wroblewski et al. (4) using ³¹P NMR relaxation technique not only provided a new method for coal moisture quantification, but also presented an excellent review and comparison among different techniques and results in the literature on coal moisture determination.

Coal drying is often the first step in coal experiments and coal treatment both in laboratory and industry scale. However, contrary to the studies of wet coals, much less work has been done for dried coals. Although both wet and dried coals were

studied using solid-state NMR a long time ago (5), much of the attention lately have been given to the kinetics of the drying process (6). In other words, there is a need of a systematic evaluation of the effectiveness of various drying methods, and a investigation of the impact of the drying processes on coal structures.

Recently, we have conduct a series of experiments on as-received, dried (in different ways), and solvent swelled Argonne Premium coals using pulsed solid-state NMR techniques (7). Here, we present part of these results, i.e., ^1H NMR T_2 relaxation measurement of as-received and high vacuum dried Illinois #6, Pittsburgh #8 and North Dakota coals. The main purpose of this paper is to demonstrate:

- (1) a new method for coal moisture quantification,
- (2) a establishment of the relationship between NMR relaxation behaviors and coal structures, and
- (3) an evaluation of the effectiveness of drying, and its impact on coal structures.

Experimental

The as-received samples were prepared by directly transferring well-shaken 100 mesh Argonne premium coals from the original ampules to a 5 mm NMR tube under nitrogen atmosphere. The dried coal samples are prepared using high vacuum pumping at about 1×10^4 torr for 48 hours. The NMR tube was sealed under a vacuum of 1×10^2 torr while the sample was frozen with liquid nitrogen. The sealed tube is about same length as that of the NMR probe coil (2 cm), and about two-thirds of it is filled with the sample.

The relaxation measurements were carried out on a Bruker MSL-360 spectrometer operated at 360 MHz. A two-pulse (the output of the RF pulse is about 1kW) $90_x - \tau - 90_y$ solid-echo sequence was used in order to get the entire FID. The signal is recorded by a Bruker BC-131 transient digitizer with a sampling speed of $0.2 \mu\text{s}$. The data was stored in an Aspect 3000 computer and treated with the Lotus-123 data spreadsheet. The parameters used in the measurement, e.g., pulse width D1, pulse spacing τ , repetition time D0, and number of scans NS were systematically optimized, and the typical values used in the data collection are $1.0 \mu\text{s}$, $4.0 \mu\text{s}$, 6s and 512 for D1, τ , D0 and NS respectively.

Effort was made to shim the NMR magnet to reduce the inhomogeneity as much as possible. With liquid cyclohexane, the line width measured is less than 100 Hz.

A Kel-f probe base was made to reduce the background proton signal to about 0.3% relative to the intensity of dried coals (the original Bruker probe base gives a background proton signal of about 4% due to absorbed water).

Results and Discussion

The coal structure is complex. The protons measured by ^1H NMR can be of different structural origins. In terms of the free induction decay, these 'different' protons can relax to equilibrium by different mechanisms and at different rates. Thus, a proper deconvolution of the FID into different components is crucial, and also valuable, in understanding coal structures. Following, a brief discussion of the fitting routine used in the present experiment is given.

In this work, a step-by-step least-linear-square analysis of the natural logarithm of the FID intensity was used to deconvolute the FID signal. For both as-received and dried coals, the FID signal can be fitted best by minimum of two gaussian and one lorenzian functions:

$$I = I_{g1}(0) \text{EXP}[-(t/T_{2g1})^2/2] + I_{g2}(0) \text{EXP}[-(t/T_{2g2})^2/2] + I_l(0) \text{EXP}(-t/T_{2l}) \quad [1]$$

where T_2 is the transverse relaxation time and $I(0)$ is the intensity extrapolating to $t=0$ for any one of the components. The subscriptions g and l abbreviate gaussian and lorenzian respectively.

It was found previously (8) that, by using a nonlinear-least-square fitting method, the FID signal can be fitted by either two gaussians and one lorenzian or two lorenzians and one gaussian (those authors chose the later). However, we find that our fitting procedure provides an unambiguous deconvolution of the FID signal into two gaussians and one lorenzian, as demonstrated in Figure 1 for as-received Illinois #6.

In Figure 1(A), the long decaying component is clearly a lorenzian function. After subtracting the lorenzian component, the natural logarithm of the rest of the signal is plotted in Figure 1(B) as a function of t (lorenzian) and in Figure 1(C) as a function of t^2 (gaussian). The lorenzian fitting in Figure 1(B) for the second component would lead to an erroneous extrapolation to $t=0$, while the gaussian fitting in Figure 1(C) not only gives a reasonable value to $I_{g2}(0)$, but also leads to an almost-perfect gaussian fitting for the last component in Figure 1(D).

All the measured relaxation parameters defined in Equation 1 are listed in Table 1 for both as-received and dried coals. By inserting the values of Table 1 into Equation 1, it can be easily verified that the three components are indeed well separated in each of their time regions. Generally, the accuracy in determination of the relaxation time T_2 is greater than that of $I(0)$ since the former is derived from the slope of the plots as showed in Figure 1, while the later is obtained from the extrapolation to $t=0$ where fluctuation at the beginning of the decay could cause more uncertainty. For the dried coals, uncertainty in both T_{2l} and $I_l(0)$ can be even higher since water concentration in dried coals is so low. Nevertheless, the accuracy in present experiment is good enough for the following discussions.

From Table 1, it can be seen clearly that water has a profound effect on the relaxation dynamics of coals, mainly the lorenzian component. A slow lorenzian decay is usually due to protons with high isotropic rotational mobility. The fact that the lorenzian component for the coals as received is almost completely gone after drying leads to a speculation that this lorenzian component is entirely due to the contribution from physically absorbed water protons. This speculation is strengthened by the fact that the weight percentage of water in coals $W\%$, derived from $I_t(0)$ in the present experiment, compares very well with those obtained using other established methods for coal moisture determination. The comparison is made in Table 2, where the literature values of $W\%$ are listed and compared with ours derived from $I_t(0)$ using the following equation:

$$W\% = \frac{I_t(0) \times 18/2}{I_t(0) \times 18/2 + [100 - I_t(0)] / H_{\text{coal}}} \quad [2]$$

where H_{coal} is the weight percentage of proton in dried coal obtained from elemental analysis (1). Thus, the ^1H NMR relaxation measurement not only serves for understanding coal structures, but also provides a new method for quantitative determination of moisture in coals.

It is known that strongly coupled rigid-lattice structures usually give a FID signal of gaussian shape (9). The coal structure, which is represented by the two gaussian components, seems indeed a tight one. As shown in Table 1, neither wetting nor drying has a significant effect on the structure, which evidenced by the fact that almost same values of T_{2g} and $I_t(0)$ are obtained for both as-received and dried coals.

The shorter time gaussian component is dominant, accounting for more than 90% of the FID signal, and its T_2 values are nearly same for all of the three coals. It has been proposed that the coal structure consists mainly of a three-dimensional cross-linked polymer network (10). The present experimental observations are consistent with this picture. Further support for this model comes from the fact that similar NMR experiments on a cross-linked polystyrene in this laboratory (7) gives just one gaussian component with a T_2 of 9.7 μs which is very close to the T_{2g1} values for the first gaussian component of the coals.

The second gaussian component also presents part of the coal structure not only because the decay has a gaussian form, but also because the relative intensity of this component, $I_{22}(0)$, is independent of the water present in the coals. The clear correlation between T_{2g1} and T_{2g2} (a ratio about 1/2) indicates that certain kind of relationship exists between the two types of coal structures. It has been suggested (11) that the restricted rotation of methyl groups and hydrocarbon chains in the macromolecular framework of coals is likely responsible for this component of higher mobility. Further experiments on model polymers might lead to a more definite structural identification.

Conclusions

A step-by-step least-linear-square fitting in the present work leads to an unambiguous deconvolution of the FID signal into two gaussian and one lorentzian components. The lorentzian arises from the protons of physically absorbed water in coals, and the quantitative measurement of the lorentzian component provides a new way for the moisture determination in coals.

More than 90% of the coal structure behaves as a rigid-lattice. The relaxation time measured for coals is very similar to that of cross-linked model polymer. Less than 10% of the coal structures shows higher mobility, and a possible source for this intermediate component may be the hindered rotation of methyl groups or hydrocarbon chains of the coal macromolecular structure.

The drying by high vacuum pumping is almost complete, and no significant structural change in coal was observed during the drying process.

Acknowledgement

We thank Philip Mulieri of Lehigh University for preparing the high vacuum dried samples.

References

1. Vorres, K. S. "User's Handbook for the Argonne Premium Coal Sample Program", U.S. Department of Energy, October 1, 1989. See also: Vorres, K. S. *Energy and Fuel* 1990, 4, 420.
2. Finseth, D. *Prepr. Pap. - Am. Chem. Soc., Div. Fuel Chem.* 1987, 32, 260.
3. Lynch, L. J. and Webster, D. S. *Fuel* 1979, 58, 429.
4. Wroblewski, A. E.; Reinartz, K.; Verkade J. G. *Energy and Fuel* 1991, 5, 786.
5. Gerstein, B. C.; Chow, C.; Pembleton, R. G.; Wilson, R. C. J. *Phys. Chem.* 1977, 81, 565.
6. For example, Vorres, K. S. and Kolman, R. *Prepr. Pap. - Am. Chem. Soc., Div. Fuel Chem.* 1988, 33, 7.
7. Yang, X; Garcia, A; Larsen, J. W.; Silbernagel, B. G., unpublished results.
8. Gerstein, B. C., unpublished results.
9. For example, see Abragam, A. "The Principles of Nuclear Magnetism", Clarendon Press: Oxford, 1961.
10. Larsen, J. W.; in "New Trends in Coal Science", Yürüm, Y. Ed., Kluwer Academic Publisher: New York, 1988, 73-84.
11. Kamieński, B; Pruski, M; Gerstein, B. C.; Given, P. H. *Energy and Fuel* 1987, 1, 45.

Table 1: Summary of the ^1H NMR relaxation measurements

Coals		Gaussian 1		Gaussian 2		Lorenzian	
		$T_{2g1}^{\#}$	$I_{g1}(0)$	T_{2g2}	$I_{g2}(0)$	T_{2l}	$I_l(0)$
Pittsburgh #8	as*	10.1	90	19.6	5	23.3	5
	dried	10.1	95	20.6	5	25	1
Illinois #6	as	9.9	76	18.8	5	155	19
	dried	10.0	95	20.9	5	27	1
North Dakota	as	9.5	35	16.5	9	258	56
	dried	9.6	91	19.8	7	25	2

$\#$ The unit for T_2 is 10^{-6} sec.

* as = as received.

Table 2: Moisture in coals (W%) determined with various methods

Coals	H_{coal}	^{31}P NMR	Moisture W%		
	(Dry%) Ref(1)		ASTM Ref(1)	^{18}O dilt. Ref(2)	^1H NMR This work
Pittsburgh #8	4.83	2.85	1.65	2.5	2.2
Illinois #6	4.23	9.35	7.94	9.6	8.2
North Dakota	4.36	31.05	32.24	34.4	33

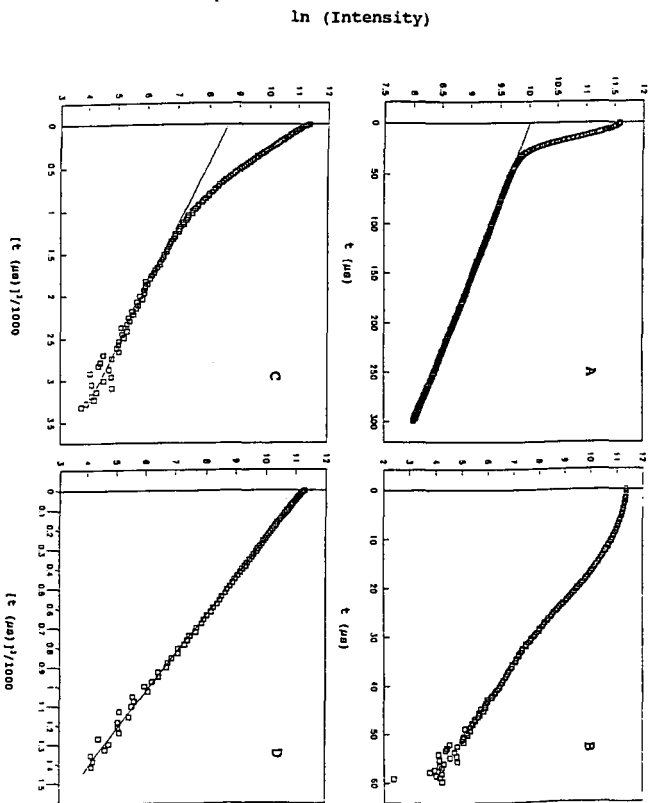


Figure 1: The natural logarithm of the FID intensity of as-received Illinois #6 as a function of relaxation time t and t^2 . D is the experimental data point and the solid line is the least-square fitting. (A) the original FID, (B) after subtracting the lorentzian component from (A), (C) same as (B) except plotted as function of t^2 , and (D) after subtracting the intermediate gaussian component from (C).

CARBON RADICAL RELAXATION PROPERTIES IN ARGONNE PREMIUM COALS

M. Bernardo, B.G. Silbernagel, and H. Thomann
Exxon Research and Engineering Co.
Annandale, NJ 08801

Key Words: Electron Paramagnetic Resonance, Relaxation, Coal

ABSTRACT

We have applied Electron Spin Echo (ESE) spectroscopy to the analysis of demineralized samples of Argonne Premium Coals. The goal of the present work has been to examine the detailed form of the magnetization recovery in spin lattice relaxation (T_{1e}) and phase memory decay measurements and to trace the temperature dependence of the T_{1e} processes to get a clearer understanding of the mechanisms responsible for carbon radical relaxation. The demineralized coal samples have been chosen for this study because the presence of paramagnetic transition metal ions tends to obscure the effects in the starting coal samples. We find a significant degree of non-exponentiality in the recovery of the carbon radical magnetization, to the best of our knowledge the first of such observations in coals. Such a result could have three sources: spectral spin diffusion among the radical species, a distribution of T_{1e} values due to inequivalent structures for the radicals, or non-uniform spatial distributions of the radicals. A comparison of the T_m and the temperature dependence of these properties suggests that this non-exponentiality is intrinsic to the radicals.

INTRODUCTION

There has been considerable recent interest in the application of transient Electron Paramagnetic Resonance (EPR) techniques to the studies of a variety of materials [1]. These techniques are widely varied, including Electron Spin Echo (ESE) determinations of the relaxation properties of the paramagnetic species as well as more elaborate Electron Nuclear Double Resonance (ENDOR) techniques. Recent studies in coal samples indicate a significant potential for important results in these areas [2, 3]. The present report will focus on the former of these advanced transient EPR techniques: a study of the functional dependence of the magnetization dynamics for carbon radicals in coal using ESE techniques.

The early work in this laboratory on the ESE properties of carbon radicals in coal was performed on a series of coal macerals (vitrinites, exinites, and inertinites) isolated from the starting coal by gravity density centrifugation techniques [4]. In this previous survey [5], the magnetization recovery of the samples was found to be closely approximated by an exponential. For the vitrinite members of this series, the phase memory decay rate, T_m^{-1} , the analog of the spin-spin relaxation time in nuclear magnetic resonance, was found to be proportional to the density of the carbon radicals in the sample, suggesting that the T_m relaxation arose from dipolar coupling. The spin-lattice relaxation rate for the radicals, T_{1e}^{-1} , was found to increase dramatically for higher rank coals, the increase initiating in the vicinity of ~ 82% carbon. It was suggested that this increase in T_{1e}^{-1} resulted from the onset of short range local order with increasing rank for the aromatic molecules which serve as the hosts for the radicals.

While these results were encouraging, there was some concern about whether they reflected the intrinsic properties in the native coal. These materials were prepared from samples of coal from the Penn State (PSOC) coal bank. The history and storage conditions of these samples were not carefully documented. Furthermore, these materials were exposed to air during the grinding and centrifugation processes. At the time, conventional EPR techniques were used

to trace variations in g -value, linewidth, and lineshape of the radicals at each stage of the process [6]. While no major changes were noted, there were still concerns about the chemical nature of the as-received PSOC samples and the chemical forms of the carbon radicals. Finally, the scale of the centrifugation process, as practiced at that time, produced very small amounts of material (~ 10 mg) which severely affected the signal to noise in the ESE experiments.

The availability of the Argonne Premium Coal samples [7] has provided the opportunity to address these concerns about the nature of the radical chemistry. Prior to receipt in this laboratory, the samples have been handled to avoid air exposure. However, a previous survey [3] indicated that the g -values, linewidths, radical densities, and relaxation properties for these samples—as received—were not consistent with the chemical variations expected during the maturation process. An EPR survey of the samples indicated high levels of transition metal ions, especially Fe^{3+} , in the as-received samples, with the effect being particularly pronounced in the highly functionalized lower rank coals. Subsequent removal of the transition metal impurities, by acid wash (e.g. with citric acid) or by HCl/HF demineralization, removed these transition metal ions and produced a much more consistent carbon radical behavior [8]. Now that these mineral effects are understood, we are returning to a detailed study of the organic matter in coal. There have been concomitant advances in the ESE systems in which the experiments are performed. In particular, the introduction of loop gap resonators provides higher microwave power levels and approximately a hundred fold increase in sensitivity for the ESE signals, greatly improving the precision of a study of the functional dependence of the magnetization dynamics.

EXPERIMENTAL

Samples of the demineralized Argonne Premium Coal samples have been examined at room temperature by the ESE techniques. For the radical spin-lattice relaxation measurements, a distinctly non-exponential magnetization recovery is observed. We will characterize this recovery in the following form:

$$(1) \quad (M_z(t) - M_0)/M_0 = \exp\{-(t/T_1')^\beta\},$$

where T_1' is a relaxation time (not a T_{1e}) and β is the exponent of the magnetization recovery. An example of this magnetization recovery is shown in Figure 1. In examinations of Beulah-zap, Illinois #6, and Pittsburgh #3 samples from the Argonne Premium Coal series, values of β ranging from ~ 0.5 to ~ 0.8 have been observed.

To test for possible instrumental effects, we have examined the effect of sample size and position in the resonator. The results suggest that we are not observing an instrumental effect.

DISCUSSION

In addition to these effects, there are several other sources for non-exponential magnetization recovery during spin-lattice relaxation measurements. Spectral spin diffusion among the radicals during the magnetization recovery process can lead to the effect. Alternatively, a distribution in T_{1e} values among the radicals in the sample could also lead to non-exponentiality, since in that case:

$$(M_z(t) - M_0)/M_0 = \int \rho(\alpha) \exp\{-\alpha t\} d\alpha \quad (2)$$

where α represents the T_{1e} value for a given class of radicals and $\rho(\alpha)$ represents the

probability distribution for radicals with that T_{1e} value in the coal sample. This distribution in radical types might not be so prominent in weathered coal samples like the isolated coal macerals observed previously. A third alternative might be that the *spatial distribution* of the radicals in the coal might be causing a distribution in recovery properties, which has been examined in some detail for other systems (e.g. γ -irradiated frozen solutions) [9]. The spatial inhomogeneity will influence both T_{1e} and T_m , and is currently under investigation.

ACKNOWLEDGEMENTS

We would like to thank Dr. R.A. Flowers of Lehigh University for the preparation of the demineralized samples and A.R. Garcia of this laboratory for the sample preparation.

REFERENCES

- 1 Keijzers, C.P., Reijerse, E.J., and Schmidt, J. Pulsed EPR: A New Field of Applications, North Holland, Amsterdam, 1989.
- 2 Thomann, H. and Bernardo, M. in Magnetic Resonance of Solid Carbonaceous Fuels (R.E. Botto, ed.), ACS Advances in Chemistry Series 229, (1992).
- 3 Silbernagel, B.G., Gebhard, L.A., Bernardo, M. and Thomann, H. in Magnetic Resonance in Solid Carbonaceous Fuels (R.E. Botto, ed.), ACS Advances in Chemistry Series 229, (1992).
- 4 Dyrkacz, G.R., and Horwitz, E. Energy and Fuels, 1982, 61, 3-12.
- 5 Thomann, H., Silbernagel, B.G., Jin, H., Gebhard, L.A., Tindall, P., and Dyrkacz, G.R. Energy and Fuels, 1988, 2, 333-339.
- 6 Silbernagel, B.G., Gebhard, L.A., Dyrkacz, G.R., and Bloomquist, C.A.A. Fuel, 1986, 65, 558-565.
- 7 Vorres, K.S. Energy and Fuels, 1990, 4, 420-426.
- 8 Silbernagel, B.G., Gebhard, L.A., Flowers, R.A., and Larsen, J.W. Energy and Fuels, 1991, 5, 561-568.
- 9 For a discussion of non-exponential magnetization recovery, see, e.g. Bowman, M.K., and Kevan, L. in Time Domain Electron Spin Resonance (L. Kevan and R.N. Schwartz, eds.), John Wiley and Sons, New York, 1979, 73-80.
- 10 For a discussion of the effects of the spatial distribution of paramagnetic species, see, e.g. Salikov, K.M. and Tsvetkov, Yu.D. in Time Domain Electron Spin Resonance (L. Kevan and R.N. Schwartz, eds.), John Wiley and Sons, New York, 1979, 258-271.

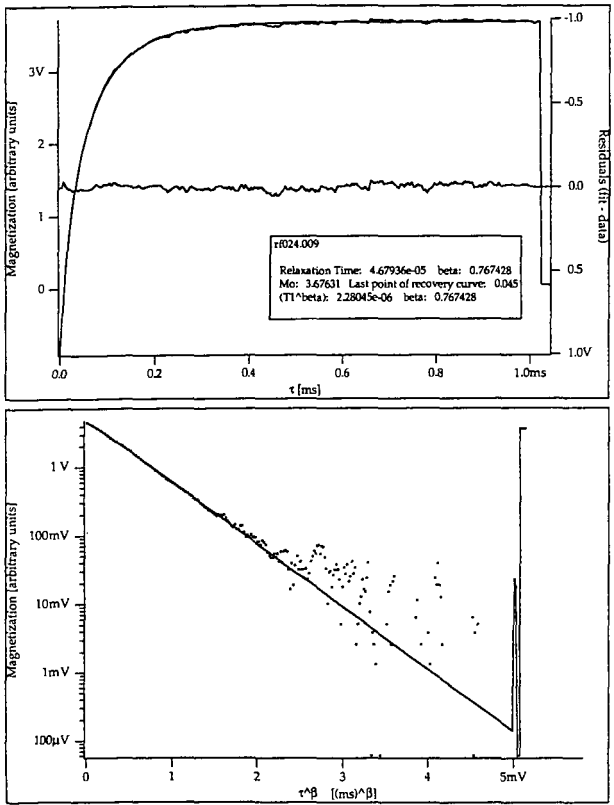


Fig 1 Non-exponential magnetization recovery for a sample of Pittsburgh #3 coal. An exponent of $\beta = 0.767$ is observed in this case. The residuals shown in the upper portion of the figure provide some measure for the goodness of fit for the data.

Solid-State CPMAS ^{13}C NMR and Pyrolysis-GC-MS Studies of Coal Structure and Liquefaction Reactions

Chunshan Song, Harold H. Schobert and Patrick G. Hatcher

Fuel Science Program, Department of Materials Science and Engineering, 209 Academic Projects Building, The Pennsylvania State University, University Park, PA 16802, USA

Keywords: Solid-state C-13 NMR, Pyrolysis-GC-MS, Coal Liquefaction

Abstract

The objective of this work is to delineate the chemical reactions during liquefaction of low rank coal by characterizing the resultant structural changes in coal macromolecular network, using cross-polarization magic angle spinning (CPMAS) solid-state ^{13}C NMR and flash pyrolysis-GC-MS (Py-GC-MS). We analyzed the THF-insoluble residues from liquefaction of a Montana subbituminous coal at different final temperatures ranging from 300 to 425°C in three different solvents under temperature-programmed (TPL) and non-programmed (N-PL) conditions. The combined use of CPMAS ^{13}C NMR and Py-GC-MS on the residues from TPL revealed a progressive loss of oxygen-containing species, and the gradual loss of aliphatic-rich species from the coal macromolecular network with increasing temperature from 300 to 425°C. The higher efficiency of TPL in the presence of H-donor, compared with conventional runs, is closely associated with H-transfer from tetralin to reactive species and removal of specific oxygen functional groups such as carboxyl and catechol groups from the coal during the programmed heat-up. Loss of these specific functional groups in early stage of TPL probably moderates or minimizes the occurrence of retrogressive reactions, thus increasing the conversion.

Introduction

Modern solid state nuclear magnetic resonance (NMR) spectroscopy originated in 1970s when cross-polarization (CP) and magic angle spinning (MAS) techniques were developed and combined (CPMAS) [1-3]. Since the first paper on NMR of coals was published by Vander Hart and Retcofsky in 1976 [4], solid-state NMR has been applied extensively in characterization of coals. The techniques of CPMAS and dipolar dephasing MAS (DDMAS) ^{13}C NMR can provide useful structural information on insoluble organic solids. In recent years, solid-state NMR has rapidly become one of the most important non-destructive techniques for studying the structure of solid coal, coal macerals, coal-derived products, geochemical samples, and other organic solids [5-12]. Flash pyrolysis-gas chromatography-mass spectrometry (Py-GC-MS) is also an important analytical technique for structural study of polymeric materials [13-16]. Py-GC-MS is relatively simple in theory, and can be viewed as a combination of the well known MS techniques with pyrolysis-GC [17,18]. While these techniques have been applied in many investigations, very few applications have been made in coal liquefaction studies.

The present work is a part of our research on temperature-programmed liquefaction of low rank coals, and involves the spectroscopic study of coal structure and liquefaction reactions using the combination of CPMAS ^{13}C NMR and Py-GC-MS [19-21]. The NMR technique has an advantage of providing the information related to the type and distribution of aromatic and aliphatic carbons in a non-destructive and quantitative fashion. Its disadvantage is that the information from NMR does not provide a direct picture of the molecular components and their environments. This is partly because the coal organic matrix is a complex mixture, whose individual components can not be resolved by NMR. Py-GC-MS is a very useful technique for studying the molecular components or structural units of polymeric organic solids. Py-GC-MS is also a fingerprinting technique [16]. However, the major drawback to Py-GC-MS is that the proportion of coal that can be volatilized and analyzed by GC-MS is relatively small. For many coals more than half of the organic material remains as a residue. Since each technique has advantages and disadvantages, we can make complementary use of these techniques by using them in tandem. The combined use of solid state NMR and Py-GC-MS has the potential to provide both average structural information and specific molecular components, and when applied to properly selected samples, can provide insights into the major and minor changes in coal structures and structural transformations involved in coal liquefaction processes [19,20].

Experimental

The coal used was a Montana subbituminous coal obtained from the Penn State Coal Sample Bank (DECS-9 or PSOC-1546). The characteristics of this coal are as follows: 33.5% volatile matter, 37.1% fixed carbon, 4.8% ash, 24.6% moisture, on a raw coal basis; 76.1% C, 5.1% H, 0.9% N, 0.3% organic S, and 17.5% O, on a dmmf basis. The coal was dried in a vacuum oven at 95°C for 2 h before use. The vehicle used was tetralin, a known H-donor. Liquefaction was carried out in 25 ml microautoclaves using 4 g coal (< 60 mesh) and 4 g tetralin under 6.9 MPa H₂. After the reaction, the liquid and solid products were separated by sequential extraction with hexane, toluene and THF.

The THF-insoluble residues were analyzed by solid state ¹³C NMR and Py-GC-MS. Our preliminary tests showed that a trace amount of THF remains in the residue even after vacuum drying at 100 °C for over 6 h, which significantly interferes with the spectroscopic characterization using CPMAS ¹³C NMR and Py-GC-MS. Therefore, prior to analyses, all the THF-insoluble residues were washed first by using acetone and then n-pentane, followed by vacuum drying at 100°C for 6 h. This procedure was found to be very effective for removing trace amount of THF.

The NMR spectra were acquired on a Chemagnetics M-100 NMR spectrometer by using the combined high power proton decoupling, cross-polarization and magic-angle-spinning (CPMAS) techniques. The measurements were carried out at a carbon frequency of 25.1 MHz. About 0.4-0.6 g of a sample was packed in a bullet-type Kel-F rotor (0.4 ml capacity); the spinning speed of the rotor was about 3.5 kHz. The experimental conditions for all the samples are as follows: a cross-polarization contact time of 1 ms and a pulse delay time of 1 s. An instrumental calibration test was performed with the rotor containing hexamethylbenzene, which was adjusted to the magic angle (54.7°) to give the correct chemical shifts. To assure good spectra with high signal-to-noise ratios, the number of pulses accumulated for obtaining a spectrum was at least 10,000, and most of the spectra were obtained with numbers of scans between 20,000 to 35,000.

Py-GC-MS analysis was performed on a Du Pont 490B GC-MS system fitted with a 30 m x 0.25 mm i.d. capillary column DB-17 coated with 50% phenylmethylsilicone stationary phase with a film thickness of 0.25 μm, and interfaced to a Chemical Data Systems Pyroprobe-1000 pyrolyzer. Helium was used as a carrier gas. The data acquisition and data processing were controlled through a computer-aided system. Prior to the start of data acquisition, the samples were flash-pyrolyzed at 610°C for 10 seconds, during which the pyrolysates (pyrolysis products) were retained in the close-to-inlet part of the capillary column by colling with liquid nitrogen. The column was held at 40°C for 5 minutes and subsequently programmed to 280°C at a rate of 4°C/min. The mass spectrometer was operated in the electron impact mode at 70 eV. In order to derive information related to the macromolecular network, the low molecular species in the coal and coal liquefaction products were removed by THF extraction prior to Py-GC-MS analysis. The other experimental details about the NMR and Py-GC-MS are similar to those described elsewhere [7].

Results and Discussion

Characterization of DECS-9 Subbituminous Coal

Because the liquefaction residues are THF-insoluble, it was necessary to obtain a corresponding baseline spectrum with the THF-insoluble residual part of the raw coal. Figure 1 shows the CPMAS ¹³C NMR spectra of the fresh DECS-9 coal and the unreacted but THF-extracted DECS-9 coal. It is interesting to note that the THF-extracted coal, which lost about 8 % THF-soluble materials, gave a spectrum similar to that of the raw coal in terms of the aromaticity and functionality (see below). Integration of the spectra gives only a slightly higher aromaticity (fa) value for the THF-extracted coal than for the raw coal. It should be noted that for some coals, the THF-extracted samples may display substantially different spectra. In addition, a general observation is that these NMR spectra are relatively poorly resolved, as compared to the spectra of pure materials, primarily because of the presence of a large number of different molecular species that have only slightly different chemical shifts.

Figure 2 shows the total ion chromatogram (TIC) obtained from Py-GC-MS of the THF-extracted raw coal. With the aid of computer-based data processing, it is now possible to perform a compound type analysis of coal pyrolysis products by using the selective ion monitoring technique in Py-GC-MS, as has been used for hydrocarbon type analysis of liquid fuels by GC-MS [22]. Low rank coals are known to have higher oxygen functionalities [23], and therefore we have examined the oxygen compounds in the pyrolysis products by using the characteristic ion masses for phenol (m/z 94), cresol (m/z 108), xylenol (m/z 122), and catechol (m/z 110). Figure 3 shows the total ion chromatogram (TIC) and selected ion chromatograms (SIC) in the extended retention time (RT) region of 2-22 min, which is a part of Figure 2. Within this range, the four most predominant peaks in the TIC are all phenolic compounds. Also found in this sample are catechol and methylcatechol. The two relatively large peaks around RT of 3 min are p- and o-xylene, in that order. It should be noted that there are a number of major hydrocarbon peaks which appeared between 0 to 2 min (Figure 2) and whose intensities are higher than the largest peak phenol in Figure 3. Those peaks are C₅-C₈ alkanes plus

alkenes, which are not well separated, and toluene, the second largest peak. There are many other small peaks appeared over the whole RT region, and selective ion monitoring at m/z 71 indicates that they are long-chain alkanes and alkenes. Overall, these results show that the DECS-9 coal contains significant amounts of oxygen-containing structural units such as phenol and alkylphenols as well as alkylbenzenes. It is also interesting to note that the long-chain aliphatics still exist after long time Soxhlet extraction with toluene and THF.

Characterization of Liquefaction Residues

CPMAS ^{13}C NMR

The temperature-programmed liquefaction (TPL) of DECS-9 Montana subbituminous coal was carried out at final temperature ranging from 300 to 425°C. Detailed discussion of the TPL may be found elsewhere [21]. For the sake of comparing the amount of organic materials in the THF-insoluble residues, Figure 4 shows the yields of THF- and toluene-soluble products plus gas from duplicate runs of Montana coal, as a function of final TPL temperature.

Figure 5 presents the NMR spectra. The spectrum of THF-extracted unreacted coal serves as a baseline. The THF-insoluble residue from TPL at final temperature of 300°C has a spectrum (Figure 5B) similar to that of the THF-extracted coal (Figure 5A). In this spectrum, an intense peak is present for aliphatic carbons (0-60 ppm) which may also include trace amounts of aliphatic ether (-C-O-X). This aliphatic peak becomes progressively smaller with increasing severity of liquefaction. The aromatic region has three peaks: an intense peak around 130 ppm (aromatic C), and two shoulders, one at about 142 ppm (possibly catechol-like C), and another at 152 ppm (phenolic or aromatic ether C). A peak at 181 ppm (carboxyl C), and a broad band around 212 ppm (ketone or aldehyde C) define the rest of the spectrum. The peaks at 142 and 212 ppm almost disappear after TPL at 350°C, and the peak at 181 also diminishes after TPL at 375°C. A decrease in intensity of the peak at 152 ppm is only observed after 375°C, and this is accompanied by further loss in aliphatic carbons. Concomitant with the decrease in total aliphatic carbons, the relative contribution from methyl carbons (0-25 ppm) increases. In general, the intensity of the aliphatic region (0-60 ppm) decreases, and the aromaticity increases with an increase in severity of TPL. Integration of the ^{13}C NMR spectra shown in Figure 5 indicates a progress increase in carbon aromaticity of the remaining organic materials in the residue. We are currently exploring the ways to quantitatively calculate the contents of different carbons both in the aromatic and aliphatic regions, and their changes with the TPL temperature by using the curve-fitting methods with the aid of computer-software.

Pyrolysis-GC-MS

Figure 5 shows the selected retention time region of 2-22 minutes of the Py-GC-MS chromatograms of the THF-extracted raw coal (A) and the residue from TPL at 300°C, the major peaks in which are identified in Table 1. Phenol, alkyl phenols, alkylbenzenes, catechols as well as alkanes and alkenes are formed from flash pyrolysis of the THF-extracted raw coal. Relative to this sample, there is apparent change in Py-GC-MS profile of the residue from TPL at 300°C. The appearance of a major peak for naphthalene and disappearance of catechol differentiate the latter from the former. This is especially interesting, since the NMR spectra of these two samples (Figure 4) and the corresponding yields of THF-solubles (7-9%) are similar to each other. From these results, it is clear that the reaction at 300°C did cause some structural change. The naphthalene peak in Figure 3 is due mainly to the use of tetralin solvent, because this peak was found to be very small with other solvent or without solvent. Since the residue has been extracted by THF for over 24 h, washed by acetone and pentane (to remove THF completely) and dried in vacuum at 90-100°C for 6 h, the naphthalene/tetralin remained in the residue must be either chemically bound to other species or physically entrapped in solvent-inaccessible micropores or closed pores which can not be removed by solvent extraction.

Also, it appeared that Py-GC-MS can detect some subtle differences in coal structure which are not easily detectable by CPMAS NMR. Combination of the NMR and Py-GC-MS data suggests that the original coal contains considerable quantities of catechol-like structures, which seem to disappear in the liquefaction residues above 300°C, and carboxyl groups, which almost disappear after 350°C, and also phenolic structures which diminish in concentration with increasing temperature. The analytical results point to the progressive loss of oxygen functional groups and aliphatic species from the macromolecular network of the subbituminous coal during its depolymerization in tetralin under TPL conditions. The higher conversions in TPL runs (relative to the conventional runs in tetralin) suggest that the removal of carboxylic and catechol groups from the coal during the programmed heat-up ($\leq 350^\circ\text{C}$) in tetralin may have contributed to minimizing the retrogressive crosslinking at higher temperatures.

Low-rank coals are characterized by low aromaticities and high oxygen functionalities. It seems possible from comparative examination of the coal conversion data and spectroscopic data that the TPL conditions may facilitate the reduction of crosslinking reactions of the thermally sensitive groups such as oxygen-functional groups at low temperatures in H-donor. Further work on the quantitative evaluation of coal structural change during liquefaction is

now in progress.

ACKNOWLEDGEMENTS.

C. Song gratefully acknowledges the financial support of this work (Fund No. 424-04-2404 LG-4-91) by the Cooperative Program for Coal Research at the Pennsylvania State University. We thank Mr. J. McConnie for assistance with some liquefaction experiments, and Mr. L. Hou for measuring some of the NMR spectra.

REFERENCES

1. Pines, A.; Gibby, M.G.; Waugh, J.S., *J. Chem. Phys.* 1972, 56, 1776; 1973, 59, 569.
2. Schaefer, J.; Stejskal, E.O., *J. Am. Chem. Soc.* 1976, 98, 1031
3. Yannoni, C.S., *Acc. Chem. Res.* 1982, 15, 201
4. Van Der Hart, D.L.; Retcofsky, H.L., *Fuel*, 1976, 55, 202
5. Alemany, L.B.; Grant, D.M.; Pugmire, R.J.; Alger, T.D.; Zilm, K.W. *J. Am. Chem. Soc.* 1983, 105, 2142.
6. Wilson, M.A.; Pugmire, R.J.; Karas, J.; Alemany, L.B.; Woolfenden, W.R.; Grant, D.M., *Anal. Chem.* 1984, 56, 933-943.
7. Hatcher, P.G., Wilson, M.A., Vassallo, A.M. and Lerch III, H.E. *Int. J. Coal Geol.* 1989, 13, 99.
8. Dennis, L.W.; Maciel, G.E.; Hatcher, P.G., *Geochimica et Cosmochimica Acta* 1982, 46, 901-907
9. Yoshida, T.; Maekawa, Y., *Fuel Processing Technol.* 1987, 15, 385-395.
10. Supaluknari, S.; Larkins, F.P.; Redlich, P.; Jackson, W.R., *Fuel Processing Technology* 1989, 23, 47-61.
11. Botto, R.E.; Wilson, R.; Winans, R.E., *Energy & Fuels* 1987, 1, 173.
12. Solum, M.S.; Pugmire, R.J.; Grant, D.M., *Energy & Fuels* 1989, 3, 187-193.
13. Nip, N.; de Leeuw, J.W.; Schenck, P.H.; Meuzelaar, H.L.; Stout, S.A.; Given, P.H.; Boon, J.J., *J. Anal. Appl. Pyrol.* 1985, 8, 221-240.
14. Philip, R.P.; Gilbert, T.D., *J. Anal. Appl. Pyrol.* 1987, 1, 93-108.
15. Hatcher, P.G.; Lerch, H.E.; Koura, R.K.; Verheyen, T.V., *Fuel* 1988, 67, 1069-1075.
16. Saiz-Jimenez, C.; De Leeuw, J.E., *J. Anal. Appl. Pyrol.* 1986, 9, 99-119.
17. Gallegos, E.J., "Pyrolysis Gas Chromatography", in "Chromatography in Petroleum Analysis", K.H. Altgelt and T.H. Gouw Eds., Marcel Dekker, New York, 1979, pp.163-184.
18. Meuzelaar, H.L.C.; Haverkamp, J.; Hileman, F.D., "Pyrolysis Mass Spectrometry of Recent and Fossil Biomaterials", Elsevier, Amsterdam, 1982, 287pp.
19. Song, C.; Schobert, H.H.; Hatcher, P.G., *Proc. 1991 Int. Conf. Coal Sci. U.K.*, 1991, p.664
20. Song, C.; Schobert, H.H.; Hatcher, P.G., *Energy & Fuels* 1992, in press.
21. Song, C.; Schobert, H.H., *Am. Chem. Soc. Div. Fuel Chem. Prepr.* 1992, 37, in press.
22. Song, C.; Hatcher, P.G., *Am. Chem. Soc. Div. Petrol. Chem. Prepr.* 1992, 37, in press.
23. Schobert, H.H., *Resources, Conservation and Recycling*, 1990, 3, 111-123.

Table 1 Major identified peaks in Figure 6

No.	MW	Identified Compound
1	106	p-Xylene
2	106	o-Xylene
3	120	C ₃ -benzene
4	120	C ₃ -benzene
5	94	Phenol
6	108	o-Cresol
7	108	m- + p-Cresol
8	122	Dimethylphenol
9	122	Ethylphenol
10	128	Naphthalene
11	136	C ₃ -phenol
12	110	Catechol
13	124	Methylcatechol
14	142	Methylnaphthalene
15	124	Methylcatechol

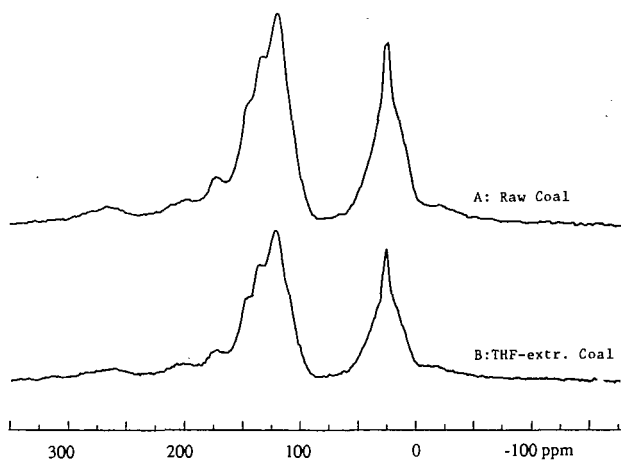


Figure 1 CPMAS ^{13}C NMR spectra of DECS-9 Montana subbituminous coal (A) and the THF-extracted coal (B).

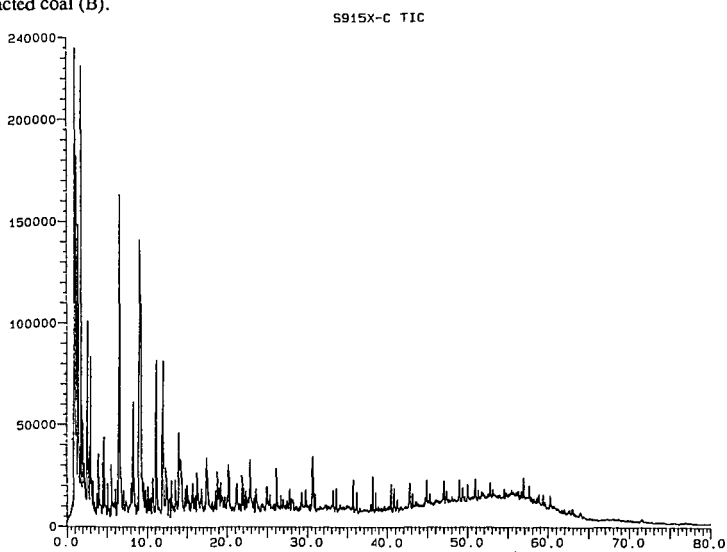


Figure 2 Total ion chromatogram for pyrolysis-GC-MS (610°C for 10 s) of THF-extracted DECS-9 Montana coal.

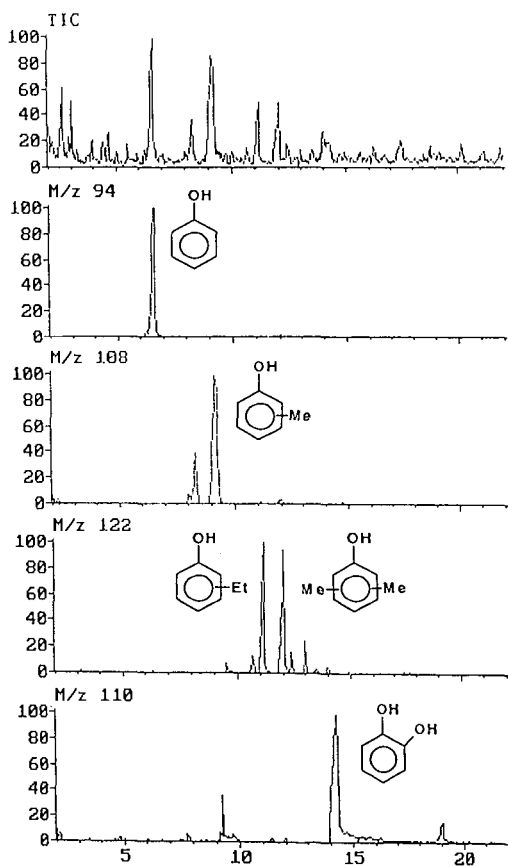


Figure 3 Specific ion chromatograms (SIC) and TIC from Py-GC-MS of THF-extracted, unreacted DECS-9 Montana subbituminous coal (pyrolysis at 610°C for 10 s)

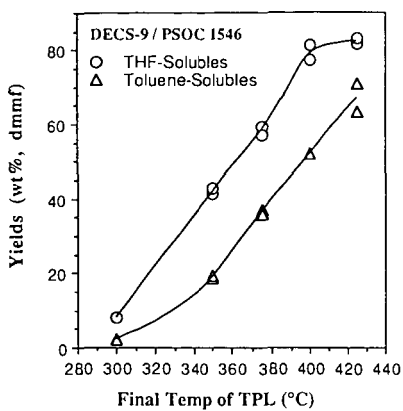


Figure 4 Conversion of DECS-9 Montana coal to THF- and toluene-solubles as a function of final temperature of temperature-programmed liquefaction (TPL) in tetralin.

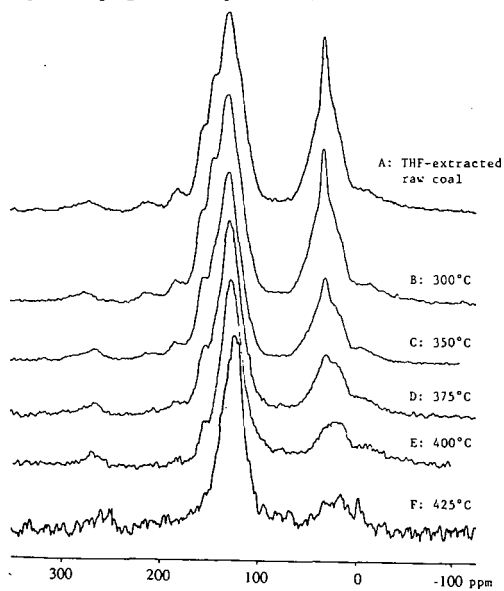


Figure 5 CPMAS ^{13}C NMR spectra of THF-insoluble residues from TPL of DECS-9 Montana coal in tetralin at different final temperature.

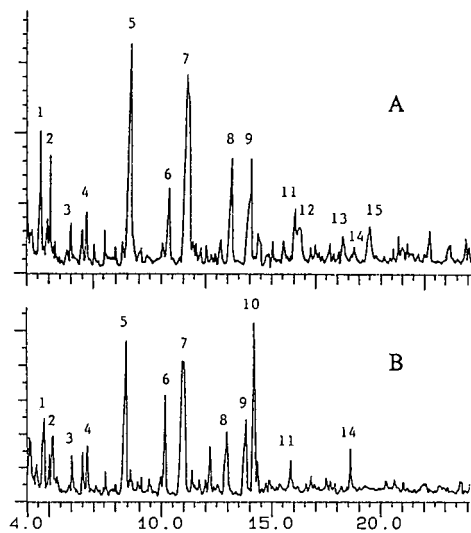


Figure 6 Py-GC-MS profiles of THF-extracted unreacted DECS-9 Montana subbituminous coal (A) and the residue (B) from TPL at final temperature of 300°C (pyrolysis at 610°C for 10 s).

Selective Saturation and Inversion of Multiple Resonances in High Resolution Solid State ^{13}C CP/MAS Experiments

Jian Zhi Hu,* Ronald J. Pugmire,+ Anita M. Orendt,* David M. Grant,* and C. Ye**

Department of Chemistry*, and Department of Fuels Engineering,+
University of Utah, Salt Lake City, Utah 84112, U.S.A.

**Wuhan Institute of Physics, Chinese Academy of Sciences, Wuhan
430071, The People's Republic of China

Abstract

Taking advantage of the long ^{13}C T_1 values generally encountered in solids, selective saturation and inversion of more than one resonance in ^{13}C CP/MAS experiments can be achieved by sequentially applying several DANTE pulse sequences centered at different transmitter frequency offsets. A new selective saturation pulse sequence is introduced composed of a series of 90° DANTE sequences separated by interrupted decoupling periods during which the selected resonance is destroyed. Applications of this method, including the simplification of the measurement of the principal values of the ^{13}C chemical shift tensor under slow MAS conditions are described. The determination of the aromaticity of coal using a relatively slow MAS spinning rate is also described.

Keywords: DANTE, multiple offset DANTE, coal structure, ^{13}C NMR

INTRODUCTION

It is well known that high resolution isotropic chemical shift spectra in solids can be obtained by applying high power heteronuclear decoupling in combination with MAS at a spinning rate larger than the width of the chemical shift anisotropy (CSA). Although isotropic chemical shifts are very useful in determining chemical structure, they come at a high price as the sample spinning averages the tensorial parameters which provide a great deal of information about the local electronic environment of the nuclei and molecular dynamics. However, when the sample spinning rate is less than the width of the chemical shift anisotropy (i.e., the slow MAS condition), the CSA powder pattern collapses to a group of spinning sidebands (SSB) spaced at the sample rotation rate with the center band located at the isotropic chemical shift position. As was demonstrated by Herzfeld and Berger (1), the tensorial principal values can be retrieved through digital simulation of the intensities of just a few spinning sidebands. However, when there are several chemically inequivalent nuclei in a molecule, the spinning sideband patterns are superimposed in the classical one dimensional CP/MAS experiment and it becomes very difficult to separate the individual sideband patterns and measure accurate intensities due to overlapping of lines. In order to simplify this measurement, a few two dimensional MAS experiments have been developed in which the isotropic chemical shift is obtained in one dimension while the spinning sideband patterns for each spin are separated in the second dimension (2,3). However, these methods suffer from either the need for specialized equipment and relaxation difficulties in the case of the switched speed method (2) or from intensity distortion problems in the case of the TOSS-Reversed TOSS method (3). It will be shown in this paper that undistorted spinning sideband patterns for only the aliphatic carbons can be readily obtained by saturating the entire aromatic, carbonyl and carboxyl sideband families using several DANTE sequences at different transmitter offset frequencies.

There are basically three categories of selective pulses; 1) the soft pulse (4-6) which is a single long, weak rectangular pulse; 2) the shaped pulse (7,8); and 3) the DANTE pulse sequence which consists of a series of short intense rf pulses (9-11). It has been known for a decade that selective excitation experiments in liquid state high resolution spectroscopy are quite informative (12). In solid state experiments, attention has initially been focused on selective excitation of multiple quantum coherence in quadrupolar systems (13-17) and on the application of selective excitation to either a static or high speed MAS sample. In both cases no spinning sidebands need be considered (18). In 1983, Caravatty et al. (19) demonstrated the usefulness of selective irradiation under slow MAS conditions and concluded that uniform excitation of one spinning sideband family can be achieved by synchronizing the pulse train of the DANTE sequence with sample rotation. It is possible to saturate the longitudinal magnetization of an entire sideband family by selective irradiation of one of its sidebands, while it is not possible to excite the whole sideband family via selective sideband irradiation. An example of this important feature is provided by Tekely et al. (20), where an incomplete elimination of the broad aromatic band and its spinning sidebands in a ^{13}C CP/MAS spectrum of coal at high magnetic field was achieved by applying a long DANTE sequence. Recently, Tekely et al (21) have reported a new selective pulse sequence named SELDOM; this sequence employs the normal 90° hard pulse and takes advantage of the short T_2 values generally encountered with solids. This pulse sequence preserves the magnetization of the preferred spin along the z axis while destroying all components of magnetization corresponding to the other spins presented in the spectrum. Selective pulses have also been successfully applied to simplify ^{13}C CSA measurement in 1D MAS-OFFMAS switched-angle experiments (22-23).

However, selective experiments to date have mainly focused on the selective excitation or saturation of one particular resonance or chemical shift range in the spectrum. If more than one resonance or chemical shift range could be inverted or saturated before the detection period, these experiments would have a broad range of applications. Some efforts have been made in the past to selectively excite more than one resonance. In the Double-DANTE sequence (11), selective excitation at two arbitrary frequencies can be achieved by the modulation of the phase of the DANTE sequence. Another demonstration provided by Ashida et al (23) in their 1D switched angle experiment showed that the inversion of two signals can be realized by sequentially applying two long soft pulses at different frequencies.

It will be demonstrated in this paper that selective saturation or inversion of multiple resonances can be achieved in spin systems with long spin lattice relaxation times by sequentially applying multiple DANTE sequences at different transmitter frequency offsets. In addition, a variation of the basic DANTE sequence which efficiently saturates the selected resonance is introduced. Several applications will be presented of this multiple resonance selective method which we will denote as "multiple offset DANTE". Experiments presented include spectra of complex organic compounds containing only one or two sideband families by saturation of the remaining resonances. This allows for more accurate determination of the sideband intensities and resultant principal components of the chemical shift tensor through removal of overlapping lines. The carbon aromaticity of coals can also be determined by the saturation of the entire aromatic region. Finally, with the addition of standard dipolar dephasing techniques to the multiple offset DANTE method, a spectrum containing only the spinning sideband family of a single aromatic carbon type (i.e., protonated, substituted, condensed, or phenolic) of a low rank coal can be obtained.

EXPERIMENTAL

All of the ^{13}C CP/MAS and selective irradiation experiments were performed on a Varian VXR-200 NMR spectrometer with a ^{13}C frequency of 50.318 MHz, using a CP/MAS probe from Doty Scientific Inc. A 50 KHz rf field strength was applied during the cross polarization period for both the ^{13}C and ^1H spin systems. When either higher decoupling rf field or higher selectivity for the DANTE sequence was necessary, the transmitter power levels of both channels were switched to the required level separately.

The basic pulse sequence used to perform the multiple offset DANTE is shown in Figure 1a. It starts with a classical cross polarization procedure to enhance the sensitivity of the observed rare nuclei (^{13}C), followed by a nonselective 90° pulse used to rotate the prepared magnetization back along the z axis. This is then followed by a series of DANTE sequences in which the transmitter frequency offset is changed. For the *i*th DANTE sequence, the parameters are as follows: transmitter frequency offset ω_i , pulse width T_{pi} , pulses interval T_{di} , and number of pulses N_i . Each DANTE sequence is, as shown in Figure 1b, a series of small tip angle pulses. If the cumulative total of the small tip angles is 180° , the net effect is inversion of the selected resonance whereas the selected resonance is saturated or destroyed by a long pulse train. An interrupted decoupling period DD_i is inserted between the DANTE sequences to allow the residual transverse magnetization to be fully destroyed before the next DANTE sequence starts; this delay time also serves for the switching time of the transmitter frequency offset. At the end of the DANTE group, a nonselective 90° pulse is used to return the magnetization to the x-y plane. Data acquisition then starts under the condition of high power proton decoupling.

In order to understand how these sequences work, several important features of the DANTE sequence must be reviewed. The selectivity of irradiation, v_i , is approximately determined by the average rf strength $v_i = \gamma H_1 [T_{pi} / (T_{pi} + T_{di})]$, where γH_1 is the pulse field strength in Hz. The magnetization corresponding to those non-selected spins is nearly unperturbed at the end of each individual DANTE sequence, i.e., after the first DANTE sequence they remain at their original longitudinal position. The second DANTE sequence acts in an identical manner, preparing the magnetization situated at ω_2 from its longitudinal position to its predesignated state, while the other resonances outside the selectively irradiated range, including the resonance at ω_1 , remain unperturbed. The first irradiated resonance still remains in its prepared state as long as its T_1 is relatively long compared to the length of the DANTE sequence. In the same manner, additional resonances can be prepared by the application of more DANTE sequences at different transmitter offsets.

A variation of the DANTE sequence which has been found to be very powerful in performing saturation in solids is shown in Figure 1c. In this variation the classical long DANTE sequence, shown in Figure 1b, is replaced by a group of sub-DANTE sequences with the cumulative flip angle for each sub-DANTE sequence set to 90° . A dipolar dephasing period inserted between each of the sub-DANTE sequences destroys the transverse magnetization selectively produced by each sub-DANTE sequence. The dephasing time needed depends on the strength of the C-H dipolar coupling; however, a longer time can be used since the magnetization of the spins of interest remains along the z axis during these dephasing periods. This variation of the normal DANTE sequence is called the "dephased DANTE" sequence in the following discussion. It functions in a manner opposite to the SELDOM pulse sequence (21), by destroying only the longitudinal magnetization corresponding to the resonance line selected while leaving the remaining resonances unperturbed.

Hexamethylbenzene (HMB) and 1,2,3-trimethoxybenzene (TMB) were obtained from Aldrich and used as received. The Lewiston Stockton coal sample is from the Argonne Premium Coal Sample Bank. Simulation of the intensity pattern of a spinning sideband family was performed using a program similar to that described in the literature by Fenzke et al (24).

RESULTS AND DISCUSSIONS

The efficiency of the dephased DANTE sequence, demonstrated on HMB, is shown in Figure 2. In this test case the resonance for the methyl carbons in HMB is saturated by using both the classical long DANTE pulse train (Figure 2b) and the dephased DANTE sequence (Figure 2c). It is obvious that the longitudinal magnetization of the methyl carbons is still appreciable after the application of 400 pulses using the classical DANTE sequence, whereas 60 pulses are sufficient to destroy the magnetization with the use of the dephased DANTE sequence. The dephased DANTE sequence can be used to replace the individual DANTE sequence in Figure 1a to perform signal saturation. It should be noted that the efficiency of the dephased DANTE sequence decreases as the number of spinning sideband of the saturated resonance increases unless synchronized sample rotation is used.

A typical example of the multiple offset DANTE method is given in Figure 3. Figure 3a is the ^{13}C CP/MAS spectrum of TMB under fast spinning conditions. There are four peaks in the aromatic region with isotropic chemical shifts of 105, 124, 138 and 154 ppm. Figure 3b shows the resultant spectrum obtained by inverting the two outer peaks using the classical 180° -DANTE at $t_{01}=105$ and $t_{02}=154$ ppm and saturating the two inner peaks using the dephased DANTE sequence at $t_{03}=124$ and $t_{04}=138$ ppm. It is clear that the multiple offset DANTE pulse sequence works.

The application of this pulse sequence in cases of slow MAS spinning in order to retrieve the shielding tensor components is shown in Figure 4. Figure 4a is the classical ^{13}C CP/MAS SSB spectrum of TMB obtained at a spinning rate of 1106 Hz. This spectrum is very crowded and the sidebands from the aromatic carbons and aliphatic carbons overlap as expected. By using three DANTE sequences at different transmitter frequency offsets, one is left with the spinning sideband spectrum containing only the three methyl carbons and the C2 aromatic carbon (138 ppm), as shown in Figure 4b. The frequency offset is chosen such that the selectively irradiated frequency is on one of the spinning sidebands with relatively high intensity in the selected sideband family. In addition, this irradiated sideband should not be superimposed with the sidebands from any of the carbons whose magnetization is to be preserved. Figure 4c contains only the sideband patterns from the methyl carbons and was obtained by saturation of all of the aromatic carbon resonances using four DANTE sequences. In order to avoid perturbation of the methyl groups, the transmitter frequency offsets were set to the downfield first sideband positions instead of the central isotropic peaks for the two protonated carbons (105 and 124 ppm). The chemical shift tensor principal values for the three methyl carbons, obtained by simulation of the intensity distribution patterns, along with the values obtained from a single crystal study (25) are listed in Table 1. The two sets of data are consistent within experimental error. It should also be noted that the SSB pattern for the unsaturated C2 aromatic carbon in Figure 4b looks very similar to that in the classical CP/MAS spectrum (Figure 4a), demonstrating the selectivity of the pulse sequence. The intensity of the lines in Figure 4b for the non-saturated C2 are not perturbed even though there are sidebands of this carbon within 300 Hz of the saturating frequency. The principal values for C2 obtained for both experiments are within the experimental error for this technique, and these values are also close to the single crystal results (see Table 1). Similar

experiments were performed to isolate the sideband pattern of the other aromatic carbons, with the resulting tensor components also reported in Table 1. Thus, this multiple offset DANTE method can be used to perform tailored excitation to obtain the tensor components of carbons in complex solids where either a single crystal or 2D experiments were previously required.

The application of the multiple offset DANTE sequence to an even more complex sample is demonstrated in Figure 5 for a Lewiston-Stockton coal sample. This coal has been well characterized by NMR measurements in our laboratory (26) as well as by other researchers (27). In this case, the experiments are performed under conditions of moderate (2-4 KHz) spinning rates in order not to attenuate the cross polarization magnetization transfer mechanism for carbons with weak dipolar interactions (28). However, at this spinning rate the sidebands produced by the aromatic carbons will be superimposed on the aliphatic signal as is shown in Figure 5a. A second spectrum, Figure 5b is obtained by total elimination of the aromatic spinning sideband family using four DANTE sequences with transmitter frequency offsets of 110, 126, 138, 150 ppm (26). It is clear from this figure that the elimination of the aromatic signal is complete. Figure 5c is the difference between Figures 5a and 5b, and shows only the signal from the aromatic carbons. From the integrated signal intensities of these spectra a carbon aromaticity of 0.77 is calculated, in good agreement with the value of 0.75 obtained from a Bloch decay measurement performed at 100 MHz with a spinning rate of 4 KHz (29). This agreement again lends confidence in the high degree of selectivity of this method.

This type of tailored excitation is even more efficient for extracting the ^{13}C CSA information from a complex compound such as a low rank coal under slow MAS condition when combined with the dipolar dephasing technique. In this case, a rotational synchronized dipolar dephasing sequence (30) is incorporated into the pulse sequence in Figure 1a to suppress the signal from protonated carbons. The data in Figures 6a and 6b were obtained in the same fashion as in Figures 5a and 5b on the Lewiston Stockton coal but with the addition of a 50 μs dephasing period to suppress the signal from the protonated carbons. Only the sideband families from the nonprotonated aromatic carbons as well as the mobile methyl resonances remain in Figure 6a and only the mobile methyl carbons remain in Figure 6b. Figure 6c is obtained by inserting a 50 μs dipolar dephasing time followed by three DANTE sequences centered at 155, 145, and 138 ppm in order to achieve complete saturation of the rather large chemical shift range of the phenolic and substituted carbons. The resulting spectrum contains signals due to the condensed aromatic carbons (i.e., bridgehead), and the mobile methyl carbons. A 50 μs dephasing time is again inserted and followed by four DANTE sequences with transmitter frequencies at 150, 125, 120 and 110 ppm, respectively, in order to saturate the phenolic and inner aromatic carbons, leaving essentially only the signal from the substituted aromatic carbons along with that from the mobile methyl carbons (Figure 6d). By a linear combination of the spectra in Figures 5 and 6, it is possible to obtain the sideband patterns for the protonated, the condensed, as well as the substituted aromatic carbons. For example, the condensed aromatic sideband family is obtained by subtracting 6b from 6c, and the substituted aromatic sideband family can be isolated by subtracting 6b from 6d. The ^{13}C CSA tensor principal values obtained by digital simulation of these sideband patterns for each type of carbon are listed in Table 2. These values are similar to those reported in coals by using static powder pattern simulation and variable angle spinning experiments (31).

Now, let us consider the limitations of the multiple offset DANTE discussed above. First, the prepared magnetization before the last DANTE sequence will relax to its equilibrium state according to its individual spn-lattice relaxation time, T_1 . It generally takes 5 to 20 ms to prepare each resonance, thus limiting the number of resonances that can

be prepared. Fortunately, ^{13}C T_1 values in solids are generally very long, ranging from seconds to tens of seconds. If different values of T_1 exist, the resonance with the longest T_1 should be selectively irradiated first while the resonance with the shortest T_1 should be selected last. A second limitation arises from using normal rectangular pulses in the DANTE sequence which cause excitation not only at the center frequency, but also at other frequencies determined by the pulse length and spacing applied (10). This leads to a slight intensity loss at these other frequencies, or to a distortion in the baseline. Although this loss is small, it can become significant as the number of DANTE sequences increases. This loss could be reduced or eliminated with the use of a more selective pulse, such as shaped pulses (7-8).

CONCLUSIONS

Multiple resonance saturation and inversion in a solid state spin system with relatively long T_1 values can be easily achieved by using multiple DANTE pulse sequences at different transmitter frequency offsets. A powerful saturation pulse sequence (i.e., the dephased DANTE sequence) is proposed. This type of multiple resonance saturation method can be successfully applied to perform the spinning sideband separation in slow MAS experiments, including tailored excitation of a spinning sideband family of a single aromatic carbon type in a low rank coal. This method can also be applied to additional problems in solids, such as monitoring the spin diffusion process among carbons. In addition, the selective pulse sequence is not limited to the DANTE sequence; other sequences such as a soft pulse or a shaped pulse could be used in place of the DANTE sequence. This type of multiple resonance method based on changing the transmitter frequency offsets should also be useful in high resolution liquid state NMR, as long as the spin system under investigation has relatively long spin-lattice relaxation times.

ACKNOWLEDGMENT

This work is supported by the Pittsburgh Energy Technology Center through the Consortium for Fossil Fuel Liquefaction Science (Contract No. DE-FC22-89PC89852). Mr. Fu Ruqiang is acknowledged for providing the spinning sideband simulation program.

REFERENCES

1. Herzfeld, J. and Berger, A.E. *J. Chem. Phys.* 1980, 73 (12), 6021.
2. Kolbert, A.C.; DeGroot, H.J.M. and Griffin, R.G. *J. Magn. Reson.* 1989, 85, 60.
3. Kolbert, A.C. and Griffin, R.G. *Chem. Phys. Letts.* 1990, 166 (1), 87.
4. Alexander, S. *Rev. Sci. Instrum.* 1961, 32, 1066.
5. Freeman, R. and Wittekoek, S. *J. Magn. Reson.* 1969, 1, 238.
6. Freeman, R.; Wittekoek, S. and Ernst, R.R. *J. Chem. Phys.*, 1970, 52, 1529.
7. Silver, M.S.; Joseph, R.I. and Hoult, D.I. *J. Magn. Reson.* 1984, 59, 347.
8. McCoy, M.A. and Warren, W.S. *J. Magn. Reson.* 1985, 65, 178.
9. Morris, G.A. and Freeman, R. *J. Magn. Reson.* 1978, 29, 433.
10. Xi-Li Wu; Ping Xu; Friedrich, J. and Freeman, R. *J. Magn. Reson.* 1989, 81, 206.
11. Geen, H.; Xi-Li Wu; Ping Xu; Friedrich, J. and Freeman, R. *J. Magn. Reson.* 1989, 81, 646.
12. Freeman, R. *Chem. Rev.* 1991, 91, 1397.
13. Vega, S. and Pines, A. *J. Chem. Phys.* 1977, 66, 5624.
14. Polak, M. and Vaughan, R.W. *Phys. Rev. Lett.* 1977, 39, 1677.

15. Vega, S. and Naor, Y. *J. Chem. Phys.* 1981, 75, 75.
16. Brunner, P.; Reinhold, M. and Ernst, R.R. *J. Chem. Phys.* 1980, 73, 1086.
17. Reinhold, M.; Brunner, P. and Ernst, R.R. *J. Chem. Phys.* 1981, 74, 184.
18. Vanderhart, D.L. *J. Magn. Reson.* 1989, 72, 13.
19. Caravatti, P.; Bodenhausen, G. and Ernst, R.R. *J. Magn. Reson.* 1983, 55, 88.
20. Tekely, P.; Brondeau, J.; Marchal, J.-P.; and Delpuech, J.-J. *Fuel*, 1986, 65, 997.
21. Tekely, P.; Brondeau, J.; Elbayed, K.; Retourmard, A. and Canet, D. *J. Magn. Reson.* 1988, 80, 509.
22. Iwamiya, J.H.; Davis, M.F. and Maciel, G.E. *J. Magn. Reson.* 1990, 88, 199.
23. Ashida, J.; Nakal, T. and Terao, T. *Chem. Phys. Letts.* 1990, 168, 523.
24. Fenzke, D.; Maeb, B. and Pfeifer, H. *J. Magn. Reson.* 1990, 88, 172.
25. Carter, C.M.; Facelli, J.C.; Alderman, D.W. and Grant, D.M. *J. Chem. Soc., Faraday Trans. 1*, 1988, 84 (11), 3673.
26. Solum, M.S.; Pugmire, R.J. and Grant, D.M. *Energy & Fuels*, 1989, 3 (2), 187-193.
27. Wind, R.A.; Jurkiewicz, A. and Maciel, G.E. *Fuel*, 1989, 68, 1189.
28. Snape, C.E.; Axelson, D.E.; Botto, R.E.; Delpuech, J.J.; Tekely, P.; Gerstein, B.C.; Pruski, M.; Maciel, G.E.; Wilson, M.A. *Fuel*, 1989, 68, 547.
29. Solum, M.S.; Yi Jiang, Jian; Pugmire, R.J.; Grant, D.M. Manuscript in preparation.
30. Munowitz, M.G.; Griffin, R.G.; Bodenhausen, G. and Huang, T.H. *J. Am. Chem. Soc.* 1981, 103, 2529.
31. Orendt, A.M.; Solum, M.S.; Sethi, N.K.; Hughes, C.D.; Pugmire, R.J.; and Grant, D.M. "Measurement of ^{13}C Chemical Shielding Anisotropy in Coal", in "Techniques in Magnetic Resonance: Advances in Chemistry Series No. 229". Botto, R.E. and Sanada, Y. Editors (1992) ACS Publications.

Table 1. Principal values of ^{13}C chemical-shift tensors obtained through digital simulation of sideband intensity patterns^a

Assignment	σ_{11}	σ_{22}	σ_{33}	σ_{avg}
1,2,3-trimethoxybenzene				
M ₁	82(83)	72(71)	9(9)	54
M ₂	87(88)	84(83)	10(10)	60
M ₃	81(82)	71(70)	13(13)	55
C _{1,3}	221(218)	168(172)	72(73)	154
C ₂ ^b	174(179)	169(164)	71(71)	138
C ₂ ^c	172	171	71	138
C _{4,6}	190(187)	119(123)	10(7)	106
C ₅	229(227)	133(136)	11(10)	124

^aData in parentheses are single crystal results (25).

^bObtained using sideband intensities from Figure 4a.

^cObtained using the sideband intensities in Figure 4b.

Table 2. Principal values of ^{13}C chemical shift tensors obtained through digital simulation of sideband intensity patterns for the Lewiston Stockton Coal

Assignment	σ_{11}	σ_{22}	σ_{33}	σ_{avg}
Protonated	230	126	14	123
condensed	192	184	2	126
substituted	238	158	18	138

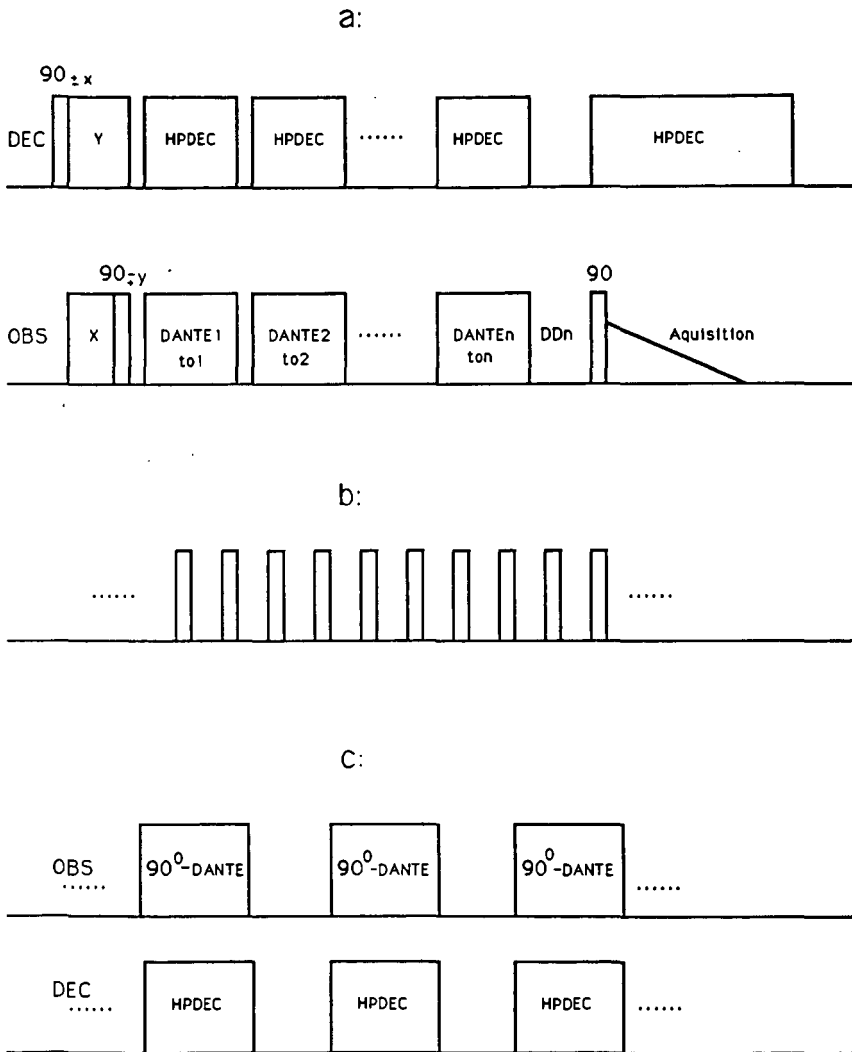


Figure 1. Pulse sequences: a) the general pulse sequence used to perform multiple resonance saturation and inversion, with the parameters for the i th DANTE sequence: transmitter frequency offset ω_i , pulse width T_{pi} , pulse interval T_{di} , and the number of pulses N_i ; b) the classical DANTE sequence; c) the dephased DANTE sequence.

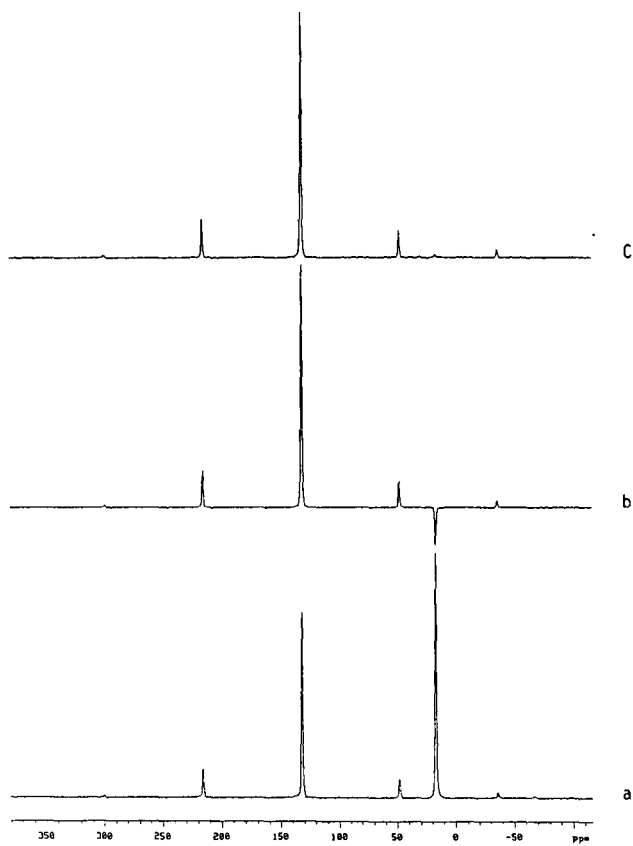


Figure 2. ^{13}C CP/MAS spectra of HMB obtained with sample spinning rate of 4.2 KHz, contact time of 3 ms, and 64 scans: a) the normal ^{13}C CP/MAS spectrum; b) saturation of the methyl carbon using the classical DANTE sequence with 400 hard pulses, pulse width $0.25\ \mu\text{s}$ and the interval between pulses $50\ \mu\text{s}$; c) saturation of the methyl carbon using the dephased DANTE sequence with three sub-DANTE sequences, each containing 20 hard pulses with the same parameters as in b, and a dephasing time of 16 ms.

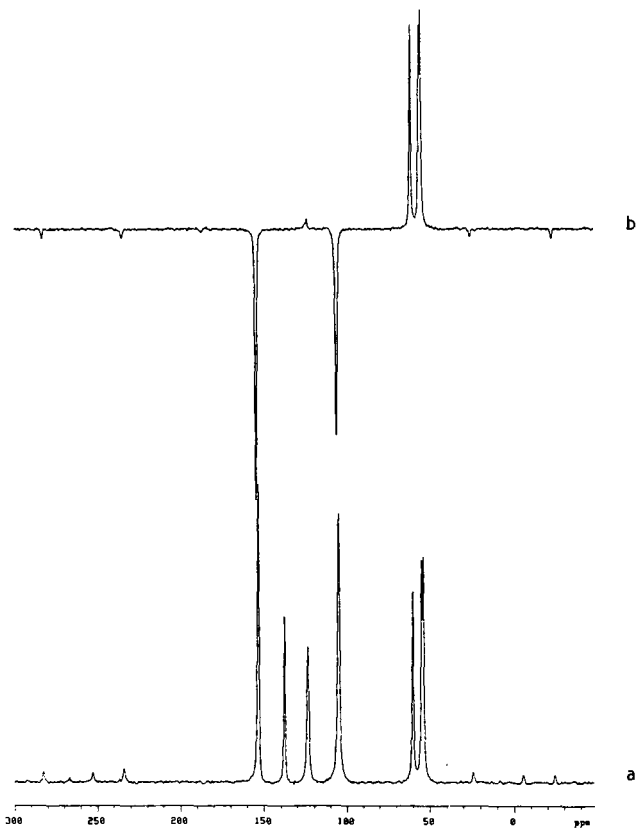


Figure 3. ^{13}C CP/MAS spectra of 1,2,3-Trimethoxybenzene (TMB) obtained with sample spinning rate of 6.0 KHz, contact time of 4 ms: a) the normal ^{13}C CP/MAS spectrum; b) spectrum obtained using the sequence in Figure 1a. The inner two aromatic resonances were saturated using the dephased DANTE sequence with offset frequencies centered at $\tau_1=124$ ppm and $\tau_2=138$ ppm and the outer two aromatic resonances were inverted using two 180° DANTE sequences with offset at $\tau_3=154$ ppm and $\tau_4=104$ ppm. Each dephased DANTE contains three 90° -DANTE of 20 pulses with pulse width 0.25 μs and a dephasing time between the sub-DANTE sequences of 16 ms.

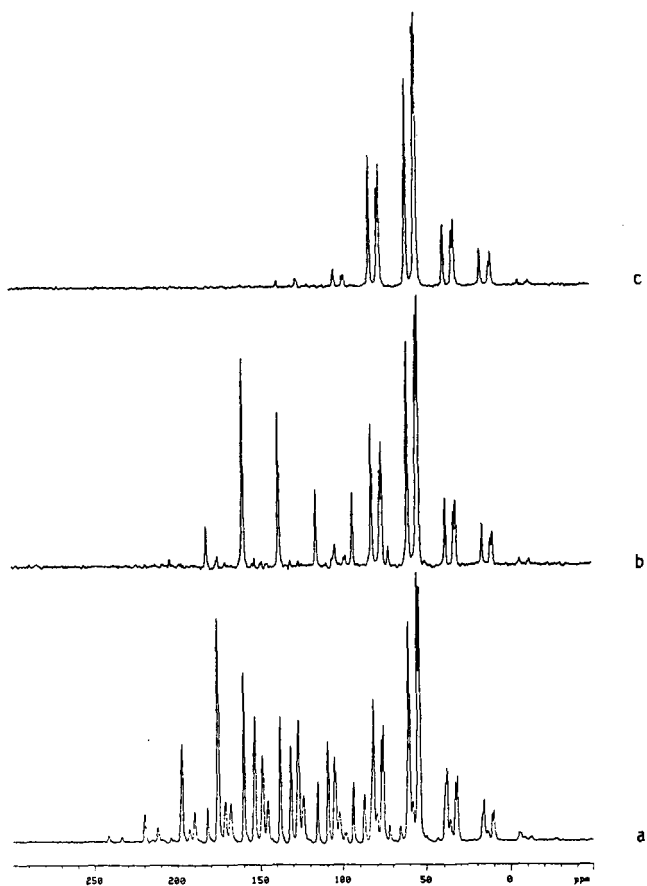


Figure 4. Spectra of TMB obtained with sample spinning rate 1106 ± 5 Hz and contact time of 4 ms: a) normal ^{13}C CP/MAS spectrum; b) spectrum obtained using three long DANTE sequences at transmitter frequency offsets of 126, 146 and 154 ppm in order to saturate these three spinning sideband families; c) spectrum obtained using four long DANTE sequences at 126, 146, 138, and 154 ppm to saturate the entire aromatic sideband family. The parameters for each long DANTE sequence are $T_{pi}=0.25 \mu\text{s}$, $T_{di}=100 \mu\text{s}$, $N_i=150$ and $DD_i=8$ ms.

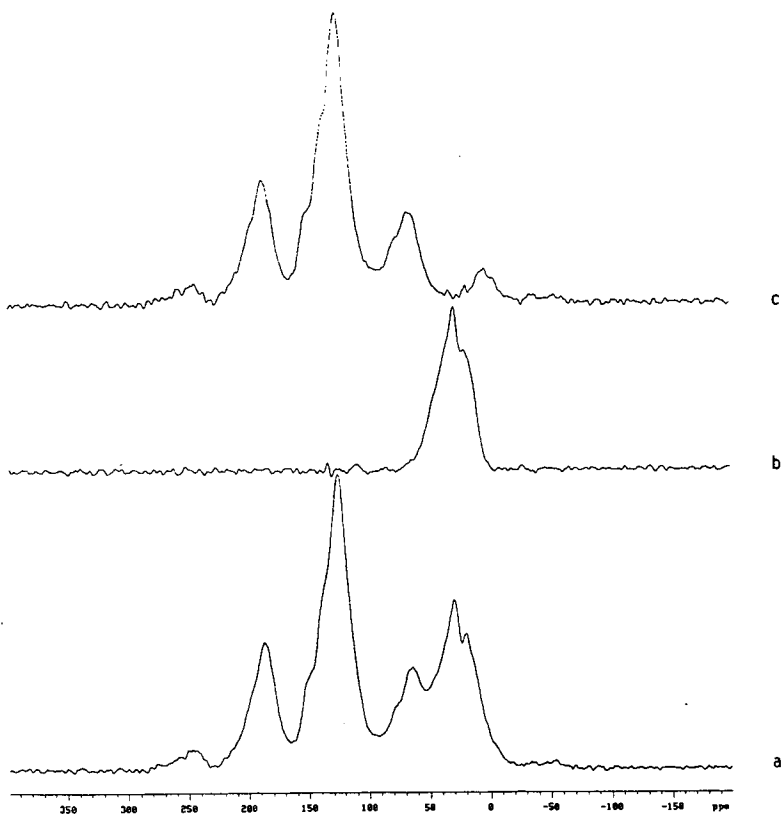


Figure 5. ^{13}C CP/MAS spectrum of Lewiston Stockton coal obtained with a sample spinning rate 3000 ± 30 Hz, and 1 ms contact time: a) the classical ^{13}C CP/MAS spectrum; b) application of four long DANTE sequences at 110, 126, 138 and 150 ppm to saturate the entire aromatic carbon spinning sideband family; c) subtraction of a from b. The parameters for each DANTE sequence are: $T_{pi}=0.5 \mu\text{s}$, $T_{di}=30 \mu\text{s}$, $N_i=150$, $DD_i=2$ ms;

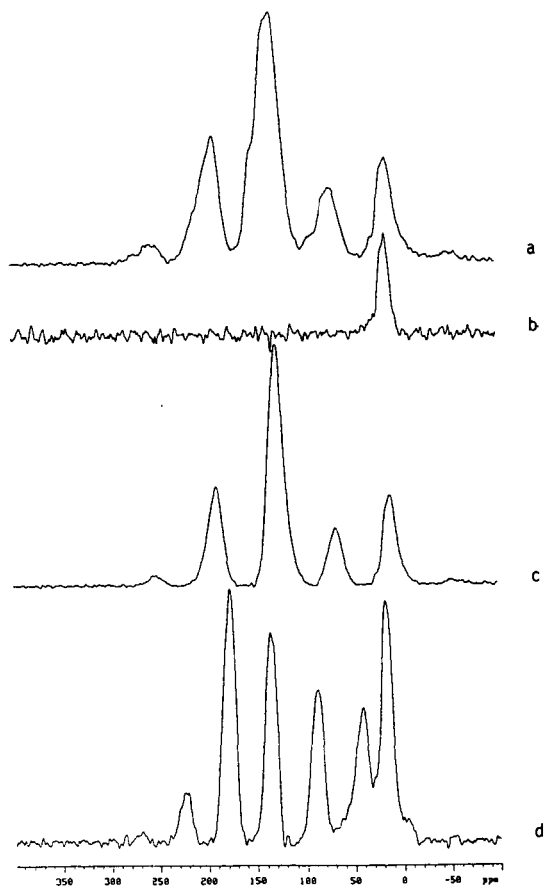


Figure 6. Tailored excitation of the spinning sideband family for various types of carbons in Lewiston Stockton coal by combining the multiple offset DANTE method with the dipolar dephasing technique with a contact time of 1 ms, recycle delay time of 4s and sample spinning rate 3000 ± 30 Hz (6d with sample spinning rate 2100 ± 50 Hz), and $T_{pi}=0.5 \mu\text{s}$, $T_{di}=30 \mu\text{s}$, $N_i=150$, $DD_i=2$ ms; a) dipolar dephasing spectrum with dephasing time of $50 \mu\text{s}$; b) spectrum obtained in a similar manner to Figure 5b except with a dephasing time of $50 \mu\text{s}$ inserted between the contact time and the first 90° pulse in the pulse sequence shown in Figure 1a; c) spectrum obtained in a similar manner to (b) except with three DANTE sequences at 138, 145 and 155 ppm used to saturate the phenolic and substituted aromatic sideband families; d) spectrum was again obtained in a similar manner to (b) but with four DANTE sequences used at 110, 120, 125 and 150 ppm to saturate the sideband families of the condensed and phenolic aromatic carbons. The remaining signals are due to methyl and substituted aromatic carbons.

QUANTITATIVE DECONVOLUTION OF ^{13}C NMR SPECTRA OF ILLINOIS #6 COAL

M.A. Jacintha,^a C.R. Dybowski,^a W.H. Calkins,^b W.D. Provine,^b M.T. Klein^b

Center for Catalytic Science and Technology

^aDepartment of Chemistry and Biochemistry

and

^bDepartment of Chemical Engineering

University of Delaware

Newark, DE 19716

Keywords: coal, deconvolution, ^{13}C NMR

INTRODUCTION

The quantification of chemical functionality is necessary to construct a picture of the structure of coal. The aromaticity of coal has been determined in a relatively quantitative manner using solid-state ^{13}C NMR spectroscopy,¹ although there has been a great deal of discussion about how this process can be carried out.² In this study, we discuss how one might further deconvolute the carbon spectrum of coal, into various aromatic and aliphatic components.

EXPERIMENTAL

Illinois #6 coal was obtained from the Argonne Premium Coal Sample Bank. The solid coal was analyzed by variable-contact-time solid-state ^{13}C CPMAS NMR spectroscopy, with a Chemagnetics m100S spectrometer operating at 25.1 MHz for carbon. Samples were kept in Kel-F[®] spinners to avoid spurious resonances from spinner material. Typical spinning speeds were 3 kHz. The acquisition time was 50 ms with a ^1H 90° pulse width of 6.5 μs and a pulse delay of 1 s. Quantification of both the original and the deconvoluted spectra were performed by fitting the integral intensities to the magnetization-recovery equation.³ The CPMAS spectra obtained at the various contact times were digitized using a TANDY Digitizer Pad, corrected for baseline roll and analyzed with the Peakfit[®] computer fitting program.

RESULTS

Various combinations of functions were tried. Of the many sets tried, only the combination of Lorentzian and Voigt functions given in Tables 1 and 2 fit the CPMAS spectra

obtained at various contact times over the full range of contact times. The aromatic region was resolved into three Lorentzians and one Voigt function. Similarly, the aliphatic region was resolved into two Lorentzians and two Voigts. The chemical-shift range, type of line-shape function, $T_{1\rho H}$, T_{CP} and ρ for each of the aromatic and aliphatic components are listed in Tables 1 and 2, respectively.

From the data in Tables 1 and 2, one sees that the parameters determining the cross-polarization behavior of the various components vary by up to a factor of 4 for $T_{1\rho H}$, and by a factor of 15 for T_{CP} . With such a wide variation of the values of the parameters for various components of the coal, it is readily understandable why integration of a CP-MAS spectrum taken at a single contact time cannot properly represent the distribution of carbon as accurately as possible. These results are related to the usual time constants determined for the aromatic and aliphatic regions, in that weighted averages of the $1/T_{1\rho H}$ and $1/T_{CP}$ of the components in a region are equal to those determined by variation of the integrals with contact time.⁴

In Figure 1, a simulated spectrum of this coal (based only on CPMAS-derived parameters) is compared with a fully relaxed Bloch-decay (BD) spectrum of the same coal. While the BD spectrum is relatively noisy, the simulated spectrum closely approximates its features. The BD spectrum was obtained with a pulse delay of 120 s. We have found that, to obtain fully relaxed spectra one must wait much longer than the suggested pulse delay of 20 s.⁵

One may be tempted to assign the components generated by this process, through comparison of the mean chemical shifts to those of pure model compounds. However, this is an oversimplification of the speciation. The range of shifts for each component as indicated by the half-width in the Tables is rather wide. In these ranges fall many different carbon functionalities. Thus, an analysis of this type will only coarsely describe the results. For example, the two downfield aromatic components may be associated with carbon-oxygen linkages. One possible solution to assigning the NMR components is correlation of these results with other measures of the coal structure (obtained by wet-chemical analysis or other spectroscopic investigation) using the techniques of factor analysis.⁶ To do this requires the analysis of many different coal samples such as the Argonne Premium Coal Samples. We are exploring this possibility.

References

1. Maciel, G.E.; Sindorf, D.W. *J. Am. Chem. Soc.* **1980**, *102*, 7607.
2. Snape, C.E.; Axelson, D.E.; Botto, R.E.; Delpuech, J.J.; Tekely, P.; Gerstein, B.C.; Pruski, M.; Maciel, G.E.; Wilson, M.A. *Fuel* **1989**, *68*, 547.
3. Botto, R.E.; Winans, R.E. *Energy and Fuels* **1987**, *1*, 173.
4. Solum, M.; Pugmire, R. J.; Grant, D. M. *Energy and Fuel* **1989**, *3*, 187.
5. Snape, C.E.; Love, G.D. *Prepr. of the Fuel Chem. Div.* **1991**, *36*, 877.
6. Malinowski, E.F.; Howery, D.F. *Factor Analysis in Chemistry*; Wiley: New York, 1980.

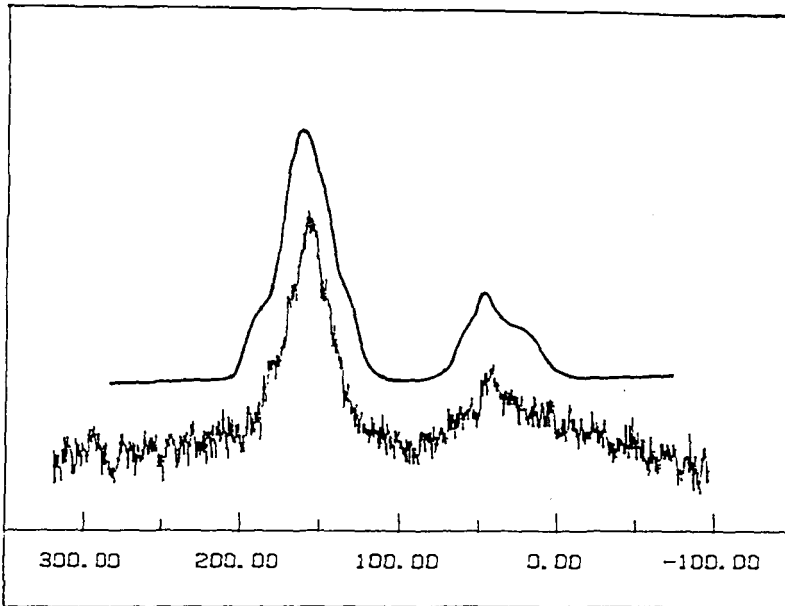
Table 1. Aromatic Components of Argonne Illinois #6 Coal

$\langle \delta \rangle$ (ppm)	Function	$T_{1\rho H}$ (ms)	T_{CP} (ms)	f
170 ± 5	Lorentzian	1.7 ± 0.05	0.39 ± 0.004	0.14 ± 0.02
160 ± 7.5	Lorentzian	3.0 ± 0.05	0.43 ± 0.004	0.16 ± 0.02
150 ± 12	Voigt	6.0 ± 0.05	0.30 ± 0.004	0.27 ± 0.02
125 ± 5	Lorentzian	3.5 ± 0.05	0.13 ± 0.004	0.12 ± 0.02

Table 2. Aliphatic Components of Argonne Illinois #6 Coal

$\langle \delta \rangle$ (ppm)	Function	$T_{1\rho H}$ (ms)	T_{CP} (ms)	f
75 ± 5	Lorentzian	4.0 ± 0.05	0.05 ± 0.004	0.07 ± 0.02
65 ± 7.5	Voigt	3.8 ± 0.05	0.18 ± 0.004	0.12 ± 0.02
50 ± 7.5	Lorentzian	7.0 ± 0.05	0.14 ± 0.004	0.09 ± 0.02
25 ± 2	Voigt	1.0 ± 0.05	0.75 ± 0.004	0.04 ± 0.02

Figure 1. Comparison between a simulated fully-relaxed spectrum and a Bloch-decay spectrum



¹³C NMR ANALYSIS OF MODEL SULFONIUM SALTS

T. K. Green, W. G. Lloyd, L. Gan, P. Whitley, K. Wu

Department of Chemistry, Western Kentucky University
Bowling Green, KY 42101

INTRODUCTION

The speciation and quantification of organic sulfur forms in fossil fuels is an area of research which has received much attention in recent years (1). Most of the techniques employed either chemically change the sulfur structures or fail to fully detect sulfur structures due to their nonvolatility. Exceptions are X-ray absorption spectroscopy (XAS) and X-ray absorption near edge spectroscopy (XANES) used recently by Gorbaty et al. to quantify sulfur forms in coals and heavy petroleum (2,3). This paper describes a new, nondestructive NMR method which offers potential for identifying and quantifying sulfur forms in fossil fuels. The method is based on the methylation of sulfur compounds to form sulfonium salts. We demonstrate that the ¹³C chemical shift of the added methyl carbon is very sensitive to the nature of the sulfur atom to which it is bonded. Thus, in principle, dialkylsulfides, alkylarylsulfides, diarylsulfides, benzothiophenes and dibenzothiophenes can be distinguished by this technique. A preliminary study using crude petroleum is presented to illustrate the potential of this technique for identifying sulfur compounds in fossil fuels.

EXPERIMENTAL

Methylation of Model Compounds

The procedure for methylation is similar to that given by Acheson and Harrison (4). Approximately 1 mmol of the sulfur compound and 1.2 mmol of AgBF₄ were dissolved and stirred in 3.0 mL of dichloroethane under argon. Methyl iodide (2.0 mmol) was added via syringe to the stirred solution. A yellow precipitate (AgI) immediately formed in all cases. The reaction was allowed to stir overnight after which the solution was filtered to remove AgI. The AgI precipitate was washed with acetonitrile. The filtrate was then rotovaporized at 40-50 °C to remove excess solvent. The residue was triturated with ether to give a precipitate. In some cases an oil formed which could not be precipitated, in which case the oil was dissolved in d₃-acetonitrile or d₆-acetone and analyzed directly by NMR. If a precipitate formed, it was filtered and washed with ten drops of water to remove excess AgBF₄. The solid was then dissolved in acetonitrile. Ether was then added until the solution became slightly turbid. The solution was then cooled in dry ice/acetone to effect crystallization. The yields ranged from 40 to 80%.

Methylation of Crude Petroleum

The same basic procedure was used to effect methylation of an Arabian crude petroleum sample. The sample was obtained from Ashland Oil and contains 2.8% sulfur. The amounts of the reagents were the same except that 1 g of petroleum was used in place of the sulfur compound. The solution was stirred overnight and then the AgI was filtered off. The solvents were removed by rotovaporization at 40-50°C and the residue was then placed in a vacuum oven overnight at room temperature. A small amount of residue (100 mg) was then dissolved in about 1 mL of d₃-acetonitrile. Not all of the residue dissolved so the solution was filtered and then placed in an NMR tube for analysis.

FT-NMR Analysis

¹³C spectra were obtained at 270 MHz using a JEOL CPF 270 FT-NMR. A pulse width of 2.8 us and a pulse delay of 3.0 sec were used. The number of transients ranged from 1500-5000 for the petroleum samples, depending on the concentration.

RESULTS AND DISCUSSION

Model Compounds

Sulfur is an excellent nucleophile. As such, sulfides and thiophenes react with alkyl iodide to yield sulfonium ions as shown below (5,6).



The reaction is favored by polar solvents such as acetonitrile and acetone. Since iodide is also a good nucleophile, the reaction is reversible. However, if the reaction is carried out in the presence of silver tetrafluoroborate (AgBF_4), silver iodide is precipitated, leaving the poor nucleophile tetrafluoroborate as the solute anion. Alkyl and aryl sulfides and thiophenes have all been successfully alkylated by this method.

Only limited ^{13}C chemical shift information exists on methyl sulfonium salts (7,8). Therefore, we prepared models for examination by NMR spectroscopy. The results are shown in Table I, where the chemical shifts of the added methyl carbon (relative to TMS) are listed.

The S-CH₃ chemical shifts cover a 15 ppm range for the model compounds examined. Among the sulfides, the chemical shift increases with the number of aryl groups bonded to the sulfur atom. This same trend is observed for the thiophenes, with the chemical shift increasing with increased aryl substitution about the central thiophenium ring. Comparing the chemical shifts of the S-methylbenzo[b]naphtho[2,1d]thiophenium (7) and S-methyldibenzothiophenium cations (6) reveals the effect of an additional fused ring - a slight upfield shift. Although more model compound work is required, these initial results indicate the potential for speciation of sulfur forms by the NMR technique.

Methylation of Crude Petroleum

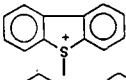
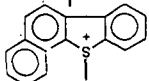
To demonstrate the usefulness of this approach, we have methylated an Arabian crude petroleum sample. The aliphatic region of the ^{13}C NMR spectrum of the crude dissolved in CDCl_3 is shown in Figure 1 (spectrum A). The major peak in the spectrum is at approximately 30 ppm (relative to TMS). This peak is attributed to aliphatic methylene groups by distortionless enhanced polarization transfer techniques (DEPT). The spectrum of the product from S-methylation using ordinary methyl iodide as methylating reagent is shown above this spectrum (spectrum B). The solvent is this case was d_3 -acetonitrile. This spectrum is very similar to that of the original crude, with the same set of major peaks. The small differences in chemical shifts might be attributed to a solvent effect. There is no apparent evidence of added methyl groups in the spectra of the methylated crude.

The spectrum of the product using 99% ^{13}C -enriched methyl iodide is also shown in Figure 1 (spectrum C). This spectrum is strikingly different than the other two spectra. The difference is most logically attributed to added methyl groups whose signals are enhanced due to the isotopic enrichment of the methyl iodide. This spectrum is expanded in Figure 2 to illustrate more detail. Although complex, this spectrum was highly reproducible in a duplicate run. Some of the peaks can be attributed to the original petroleum and are indicated with an asterisk (*).

Obviously, the spectrum in Figure 2 contains a considerable amount of information most of which is presently not interpretable. However, some preliminary assignments can be made. The region from 32.0 to 36.0 ppm is expanded and shown in Figure 3. There are six major peaks in this region with only one peak at 32.7 attributed to the original petroleum. In order to make possible assignments for these peaks, we have spiked the sample with known samples of S-methyldibenzothiophenium and S-methylbenzo[b]naphtho[1,2d]thiophenium tetrafluoroborate salts (compounds 6 and 7, Table I, respectively). The spectrum of the spiked sample is shown above the unspiked sample. The peaks at 34.9 and 34.2 ppm are seen to grow, indicating that these peaks correspond to compounds 6 and 7, respectively. Thus a tentative assignment can be made to these two peaks in the spectrum.

TABLE I

NMR Data on Model Sulfonium Salts

Cation ^a	δ , ppm (CH ₃) ^b
(1) $\text{CH}_3\text{CH}_2-\overset{+}{\text{S}}(\text{CH}_3)-\text{CH}_2\text{CH}_3$	21.0, 19.8 ^c
(2) $\text{C}_6\text{H}_5-\overset{+}{\text{S}}(\text{CH}_3)-\text{C}_6\text{H}_5$	25.0
(3) $\text{C}_6\text{H}_5-\overset{+}{\text{S}}(\text{CH}_3)-\text{C}_6\text{H}_5$	28.4
(4) 	28.3
(5) 	31.7
(6) 	34.9
(7) 	34.2

^a Tetrafluoroborate salts^b Relative to TMS^c Reference 7

CONCLUSIONS

We have determined the S-CH₃ ¹³C chemical shifts for a variety of model sulfonium salts. The data reveal that the chemical shift is very sensitive to the nature of the sulfur atom bonded to the methyl group. Thus a variety of model sulfur compounds can be readily distinguished by S-methylation with subsequent NMR analysis. The ¹³C NMR spectrum of methylated crude petroleum using isotopically-enriched methyl iodide reveals a number of peaks, most of which are unidentified at this time. More model compound work is obviously needed in order to more fully interpret the spectrum. However, it is clear that the technique offers potential for speciation of sulfur forms in fossil fuels. The technique might be particularly useful for analyzing sulfur forms in coals, since many of the sulfur-containing compounds are nonvolatile and are not readily analyzed by other techniques.

ACKNOWLEDGEMENTS

TKG acknowledges the Faculty Research Committee at WKU for a grant to initiate this study. We thank Howard Moore of Ashland Oil for the petroleum sample.

REFERENCES

1. Stock, L. M.; Wolney, R.; Basdrichna, B. Energy Fuels 1989, **3**, 651-61.
2. George, G. N.; Gorbaty, M. L., J. Am. Chem. Soc. 1989, **111**, 3182
3. George, G. N.; Gorbaty, M. L.; Keleman, S. R.; Sansone, M. Energy Fuels 1991, **5**, 93-97.
4. Acheson, R. M.; Harrison, D. R. J. Chem. Soc. C 1970, 1764.
5. Lowe, P. A. in "The Chemistry of the Sulphonium Group," Stirling, C. J. M.; Patai, S.; Eds.; John Wiley, New York, 1981, Chapter 11.
6. Trost, B. M.; Melvin, L. S., "Sulfur Ylids," Academic Press, New York, 1975.
7. Barabrella, C.; Dembach, P.; Garbassi, A. Tetrahedron Lett. 1980, **21(21)**, 2109-12.
8. Heldeweg, R. F., Hogeveen, H. Tetrahedron Lett. 1974, (1), 75-78.

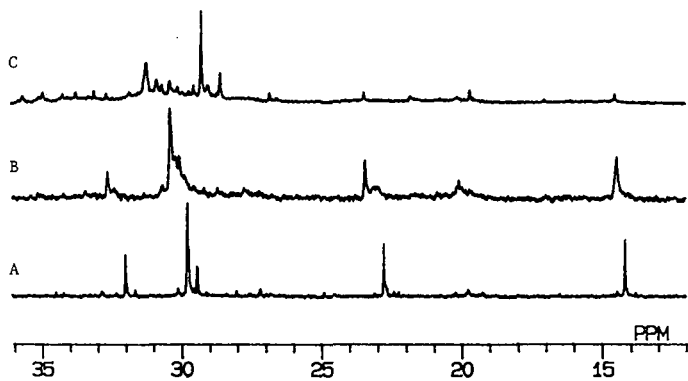


Figure 1. ^{13}C NMR Spectra of Arabian Crude. A - original crude in CDCl_3 . B - methylated crude in d_3 -acetonitrile. C - methylated crude in d_3 -acetonitrile using 99% ^{13}C -enriched methyl iodide.

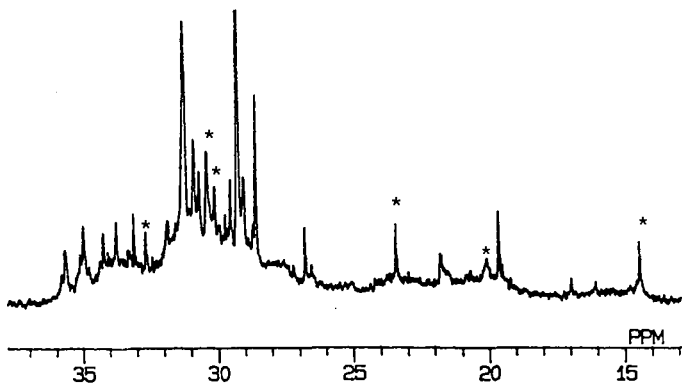


Figure 2. ^{13}C NMR Spectrum of Methylated Arabian Crude using 99% ^{13}C -enriched methyl iodide. Asterick indicates peak attributed to original crude.

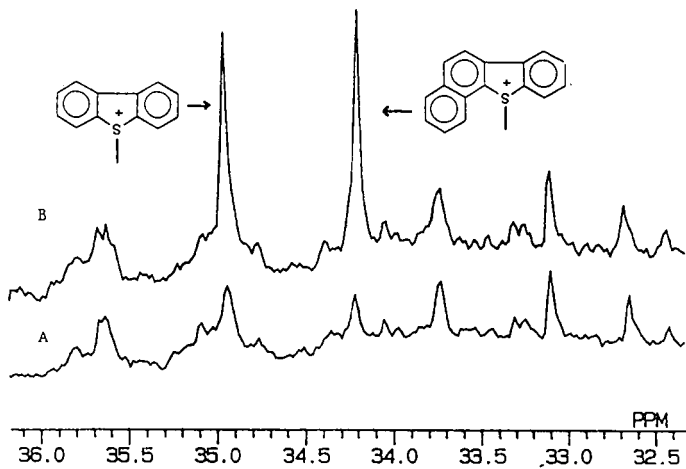


Figure 3. ^{13}C NMR Spectrum of Methylated Arabian Crude using 99% ^{13}C -enriched methyl iodide. A - unspiked sample. B - sample spiked with Compounds 6 and 7.

¹³C NMR SPECTROSCOPIC STUDIES OF ILLINOIS #6 COAL AND THE PRODUCTS OF ITS LIQUEFACTION

W.D. Provine,^a M. A. Jacintha,^b M.T. Klein,^a W. H. Calkins,^a and Cecil Dybowski^b

Center for Catalytic Science and Technology

^aDepartment of Chemical Engineering
and

^bDepartment of Chemistry and Biochemistry
University of Delaware
Newark, DE 19716

Keywords: coal, liquefaction, short contact time, ¹³C NMR

INTRODUCTION

The direct liquefaction of coal involves the cleavage of a variety of bonds, both covalent and otherwise, having a wide range of activation energies.^{1,2} The weaker bonds of lower activation energy are expected to break first, forming somewhat different products than are formed later in the process. As the coal becomes liquefied, the liquid products are also subject to further reaction. A practical application of these concepts is the observation that higher yields of liquids are obtained when the liquefaction process is carried out in two or more stages under somewhat different conditions.³ While the specific bonds that are first broken is still not known, examination of the process at very low conversions even before the coal has become a liquid should be of great interest. To do this, one requires a sampling system capable of providing samples at very short, well-defined reaction times (low conversions) of less than one minute to perhaps 5 to 15 minutes with mass and heat transfer not limiting and temperature and residence times accurately known. It is to report the preliminary results of such a study using solid-state NMR spectroscopy that this paper is presented.

EXPERIMENTAL

Reactor and sampling system. The system selected for study is a 1 liter CSTR (continuous stirred tank reactor) [Fig. 1] with a constant flow of tetralin (7 liters/hour) as a hydrogen-donor solvent in a 900psig nitrogen atmosphere (450 sccm nitrogen) at a selected temperature (390°C). 50-gram charges of coal in a tetralin slurry (1:2 coal to solvent) are injected through a rupture disk almost instantaneously by diverting the pressurized solvent into the charging bomb. Isothermal and isobaric conditions are achieved within 20s after injection. Product samples taken in an automated sampling manifold at 2, 23, 55, 87, 119, and 155s after injection are quenched to

150°C with a countercurrent water heat exchanger. The system was tested with samples of dibenzylether (with the inert biphenyl run as a blank) to check the behavior of a compound with well-known kinetics in the system and to determine the distribution of residence times. More details about the reactor system can be found in another paper.⁴

Sample work-up. The solids were filtered and washed with methylene chloride and dried in a vacuum oven. The liquefaction products were placed in a rotary evaporator to remove tetralin and lower-boiling products. The light fraction was analyzed by GC/MS and the heavy fraction by NMR spectroscopy.

Ash measurements. Conversion of the coal was determined by measuring the low-temperature ash content of the solid residue and comparing it to that of the unreacted coal. A low-temperature asher [LFE Corporation, LTA-302] was operated around 75-100 watts. The oxygen flow rate was kept at 100 cc/min.

NMR spectroscopic experiments. Residual solids were analyzed by variable-contact-time solid-state ¹³C CPMAS NMR spectroscopy,⁵ with a Chemagnetics m100S spectrometer operating at 25.1 MHz for carbon. Samples were kept in Kel-F[®] spinners to avoid spurious resonances from spinner material. Typical spinning speeds were about 3 kHz. The acquisition time was 50 ms with a ¹H 90° pulse width of 6.5 μs and a pulse delay of 1 s. Carbon aromaticities were derived by fitting integrated signal intensities for the aliphatic and aromatic carbon bands to the magnetization-recovery equation.⁶ We checked this procedure on known model compounds (hexamethylbenzene, adamantane and high-molecular-weight polystyrene), and in each case found that we could determine the relative fraction of intensity in one NMR peak to within ±0.01 of the known stoichiometric value. The Bloch-decay experiments were done with pulse delays of 5 s, 20 s and 120 s.

ESR experiments. ESR spectra were recorded on a Varian E-109 spectrometer at 9.1 GHz with 100 kHz modulation. All spectra were recorded at ambient temperature (295 ± 2 K) and DPPH was used as an external spin standard.

RESULTS

All of the experiments reported here were carried out on an Illinois #6 coal obtained from AMOCO Corporation.

One point of concern in measurements with NMR spectroscopy of solids is that the presence of paramagnetic centers may render some of the carbon NMR-invisible.⁶ If that process affected one carbon type more than another, aromaticities determined with NMR techniques could be skewed so that they do not reflect actual changes in the carbon, but rather the increase in paramagnetic centers. To address this point, we determined the paramagnetic concentrations in a set of residual solids as a function of residence time, as well as the aromaticity. These data are plotted against each other in Figure 2. As can be seen, the concentration of paramagnetic centers did change by more than a factor of four with processing. [The spin density is reported as the ratio of that in the residue to that of the unprocessed Illinois #6 coal.] The comparison of the ¹³C-derived aromatic fractions with the spin densities shows that there is very little, if any, correlation between these two variables. We assume,

therefore, that for this system the changes in aromaticity with residence time are not attributable to changes in paramagnetic concentrations.

Another issue regarding quantitation is the contention that Bloch-decay experiments give reliably quantitative information on the aromaticity of coal as compared to the variable-contact-time CPMAS experiments. When a Bloch-decay experiment was performed with a pulse delay of 20 s, the aromaticity value obtained was 0.77, whereas with a pulse delay of 120 s, the aromaticity value obtained was 0.66. The larger relative aromaticity value obtained in the experiment with a shorter pulse delay may be due to insufficient aromatic carbon nuclear relaxation toward equilibrium magnetization. The value of 0.66 is within experimental error, the same value found by fitting the entire build-up and decay curve in a CPMAS experiment.

The f_a values for Illinois #6 and the residual solids obtained upon liquefaction are given in Fig. 3 (as determined by fitted carbon magnetization curves) as a function of residence time. Conversions are reported as a function of residence time in Table 1.⁷ The graph in Fig. 3 is roughly divided into three regions: (a) a very early, almost instantaneous, decrease in aromatic fraction, (b) an intermediate regime in which the aromatic fraction increases and (c) a regime in which the aromatic fraction again decreases with time. The initial sharp decrease in aromaticity (after a residence time of only 2s) may be attributed to the removal of small aromatic moieties not covalently bound to the coal structure. An increase in the number of condensed aromatic protons in the liquid phase, as determined by NMR, (Fig. 4) is consistent with these results. The light fraction of the liquid products was found by GC/MS to contain only tetralin and its degradation products, to any measureable degree. An explanation for the intermediate regime, in which the aromatic fraction of the solid increases, is not clear. Aliphatic side chains may be removed⁸ or internal transfers of protons to liquefying fragments⁹ may produce an increase in aromaticity of the solid material. At residence times greater than about 2 minutes, the aromaticity of the residual solids is again seen to decrease. This decrease in aromaticity is probably due to hydrogen transfer from tetralin to the aromatic structures as the dominant process.¹⁰

CONCLUSIONS

Preliminary coal liquefaction experiments in a specially designed CSTR using NMR spectroscopy of the residual solid and the liquid products show that the kinetics of this process are very complex. There are at least three regimes that can be distinguished, with several different processes contributing to the overall process. These are readily distinguished by their effects on the aromaticity as determined by NMR techniques. Such processes as the flash desorption of small aromatics not covalently bonded to the framework, disruption of the coal with release of aliphatic material, proton transfer within the coal and from tetralin to the coal all presumably contribute to the observed changes.

REFERENCES

1. Szladow, A. J.; Given, P. H. *Ind. Eng. Chem. Proc. Res. Dev.* **1981**, *20*, 27-33.
2. Shabtai, J.; Skulthai, T.; Saito, I. *ACS Fuel Div. Preprints* **1986**, *31 (4)*, 15.
3. *Coal Liquefaction, A Research Needs Assessment: Technical Background*, DOE/ER-O400; volume II, pp. 4-89 to 4-115.
4. Provine, W. D.; Porro, N. D.; LaMarca, C.; Foley, H. C.; Bischoff, K. B.; Scouten, C. G.; Cronauer, D. C.; Tait, A. M.; Klein, M. T., "Development of a Pulse-Injection CSTR coal Liquefaction Flow Reactor," presented at the AIChE National Meeting, Chicago, IL, November, 1990.
5. Maciel, G. E.; Sindorf, D. W. *J. Am. Chem. Soc.* **1980**, *102*, 7607-7608.
6. Botto, R. E.; Wilson, R.; Winans, R. E. *J. Energy and Fuels* **1987**, *1*, 173.
7. Shou, J.K.; Pitts, W.S. *Fuel* **1977**, *56*, 343.
8. Calkins, W.H.; Tyler, R. J. *Fuel* **1984**, *63*, 1119.
9. Finsath, D. H.; Bockrath, B. C.; Illig, E. G.; Thames, B. M. *ACS Fuel Div. Preprints* **1986**, *31(4)*, 124.
10. Bockrath, B. C.; Illig, E. G.; Hough, M. *ACS Fuel Div. Preprints* **1990**, *35(1)*, 232.

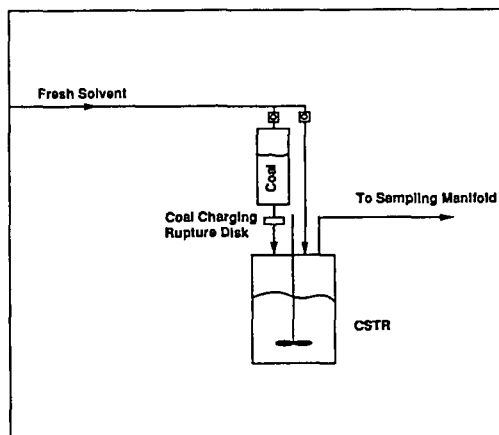


Figure 1 Schematic diagram of the CSTR.

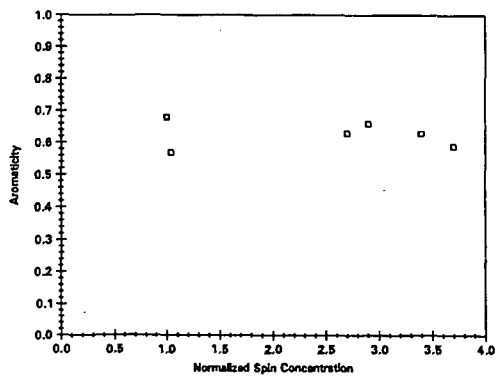


Figure 2 Aromaticity versus spin concentration for several solid residues.

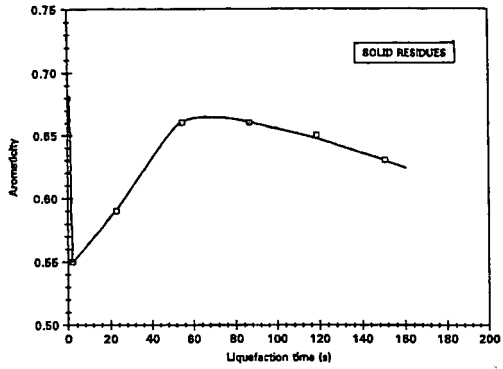


Figure 3 Aromaticity of solid residues as a function of liquefaction time.

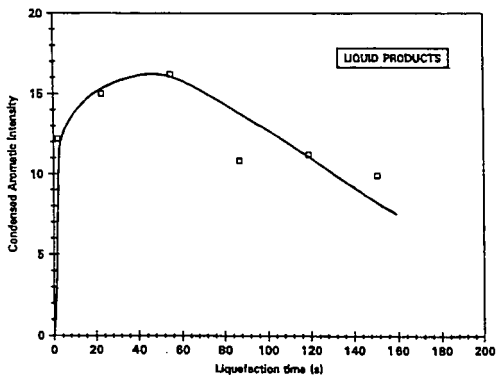


Figure 4 Aromaticity of liquid products as a function of liquefaction time.

Table 1. Weight % Conversion as a Function of Residence Time

Residence time (s)	Weight % Conversion
2	5.0
23	9.5
55	16.4
87	19.5
119	17.6
151	20.1

$$\text{Weight \% Conversion} = \frac{(A_t - A_0)}{A_0(1 - A_0)} \times 100$$

A_0 = Ash fraction of coal at time, $t = 0$

A_t = Ash fraction of coal at time, t

Chemical Structure of Char in the Transition from Devolatilization to Combustion

Thomas H. Fletcher*
Chemical Engineering Department
Brigham Young University, Provo, UT, 84602

Mark S. Solum, David M. Grant, and Ronald J. Pugmire
Departments of Chemistry and Fuels Engineering
The University of Utah, Salt Lake City, UT, 84112

Introduction

Recent coal devolatilization efforts have focused on relating coal devolatilization behavior to the chemical structure of the parent coal.¹⁻⁶ Gas and tar yields, as well as tar molecular weights, can be predicted based on correlations related to elemental compositions or from measured chemical characteristics of the parent coal. However, char is an important product produced during coal devolatilization, and must be characterized as a function of temperature and heating rate in a manner similar to volatile devolatilization products. Quantitative measurements of chemical structure are performed on the coals and chars using ¹³C nuclear magnetic resonance (NMR) techniques described by Solum and coworkers.⁷

The chemical structures of char and tar during devolatilization for an Illinois #6 coal and a lignite were published previously, and discussed relative to devolatilization behavior.^{8,9} These data showed that during the tar release period, the percentage of aromatic carbon for the bituminous coal char changed by less than 5%, while the carbon aromaticity in the lignite char changed in the early stage of pyrolysis. The carbon aromaticities for both sets of chars ultimately reached comparable values, but the parent lignite had a lower carbon aromaticity value ($f_a' = 0.57$) than the parent bituminous coal ($f_a' = 0.67$). The number of aromatic carbons per cluster indicated restructuring of the aromatic species earlier in the lignite than in the Illinois No. 6 coal.

In this work, the chemical structure of chars from five coals of different rank are examined, and implications on char reactivity are discussed. Chars were obtained as a function of residence time in two flow reactors generally used for devolatilization and char combustion experiments, respectively. The examination of five coals and their respective chars from two reactors allows better distinction of trends than was possible with the limited data previously published.

Experimental Approach

Char samples were collected as a function of residence time in an entrained flow, laminar reactor in the Sandia Coal Devolatilization Laboratory (CDL) in 100% nitrogen to isolate the pyrolysis reactions, with typical particle heating rates of 2×10^4 K/s, gas temperatures of 1250 K, and particle temperatures as high as 1200 K.^{2,3} Additional char samples were collected in an entrained flow, laminar flow reactor in the Sandia Char Combustion Laboratory (CCL), with a laminar CH₄/H₂/O₂/N₂ flat flame providing a high temperature environment (maximum gas temperature = 1600 K).¹⁰ Stoichiometric conditions were used in the flame, yielding less than 50 ppm O₂ in the post-flame gases. Char samples in the CCL were collected subsequent to the visible region of coal devolatilization, with particle heating rates of about 5×10^4 K/s and particle temperatures of

* Experiments performed at the Combustion Research Facility, Sandia National Laboratories, Livermore, CA.

approximately 1300 to 1500 K, depending on residence time and oxygen concentration.¹⁰ Common coal samples were used in the coal devolatilization and char oxidation experiments discussed here.

Helium-quench probes were used to collect char samples,^{2,10} and chars were analyzed for organic and inorganic elemental composition. The experiments in the CCL with no post-flame oxygen required modifications to the sampling system to aerodynamically separate tars, soot and aerosols from char particles. The extent of mass release from the char particles was determined from the trace mineral species (Si, Al, Ti, and total ash). Samples were obtained in the CDL at different residence times in the 1250 K gas condition, with residence times ranging from 20 to 250 ms. Samples were taken just subsequent to the pyrolysis zone (47 ms, 6.4 cm above the burner) in the CCL.

Results

The elemental compositions of the five coals used in these experiments are shown in Table 1, along with their total volatiles yields in the two reactors. The coals range in rank from a lignite to a low-volatile bituminous coal. The volatiles yields in the CCL are slightly higher than those in the CDL, and are much higher than the ASTM analyses.¹¹ Results of the ¹³C NMR chemical structure analyses of CDL chars are presented first, followed by data for the CCL chars.

Table 1
Elemental Analyses of Coals Used

PSOC-	Coal	Size Fraction (μm)	C (% daf)	H (% daf)	O (% daf)	N (% daf)	S (% daf)	Ash (% dry)	CDL Volatiles Yield (% daf)	CCL Volatiles Yield (% daf)
1507D	Beulah Zap (lignite)	75-106	66.56	4.26	25.16	1.12	2.89	18.7	53.7	58.6
1445D	New Mexico Blue (subbituminous)	106-125	75.6	5.26	17.33	1.32	0.49	3.48	53.4	56.2
1493D	Illinois No. 6 (hvb bituminous)	106-125	74.12	4.96	13.18	1.45	6.29	11.30	53.5	58.3
1451D	Pittsburgh No. 8 (hva bituminous)	63-75	84.23	5.54	7.56	1.65	1.01	3.73	53.1	52.2
1508D	WV Pocahontas (lv bituminous)	106-125	88.83	4.37	5.14	1.06	0.6	16.72	15.9	17.4

A. Chemical Structure of Coal Chars from the CDL

Attachments per Cluster. Attachments to aromatic clusters consist of alkyl groups and oxygen functional groups (e.g., phenols and/or alkyl and aryl ethers). These attachments are either bridges and loops between aromatic clusters or side chains. The bond strengths of the aromatic rings are much greater than the bond strengths of the labile bridges and loops. During devolatilization the labile bridges break, generating finite-size fragments containing one or more aromatic clusters. The light fragments are released as tar, while the heavier fragments stay in the char as metaplast and eventually reattach to the infinite char matrix. Broken bridge fragments (i.e., side chains)¹ are eventually released as light gas. In this analysis, it is assumed that the broken bridge fragments may be distinguished from intact bridges by the presence of methyl groups. Hence, the number of side chains per cluster can be estimated together with the number of intact bridges and loops per cluster. It is important to note that aliphatic carbons still remain at the end of the pyrolysis process and represent the presence of stable aliphatic bridge material and/or side chains that have not been expelled at the pyrolysis temperatures employed.

The total number of attachments per cluster (referred to as the coordination number, $\sigma+1$) is shown in Fig. 1 for char samples from all five coals. The coordination number either remains relatively constant or decreases slightly during devolatilization for all five coals. This means that no new attachment sites are generated during pyrolysis; any reattachment of metaplast occurs at existing side chain sites. Decreases in the coordination number can be explained by the release of side chains with no subsequent crosslinking at that site.

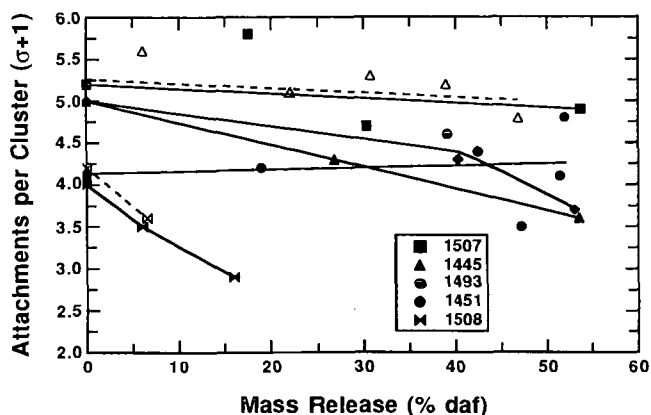


Figure 1. The total number of attachments per cluster vs. the extent of mass release due to devolatilization for chars collected at different residence times in the 1050 K (dashed lines and open symbols) and 1250 K (solid lines and filled symbols) gas temperature conditions.

The number of bridges and loops (i.e., bridges between aromatic rings and aliphatic loops on aromatic rings, such as tetralin) per cluster does not change significantly in the Illinois #6 coal char until the end of the mass release period, as shown in Fig. 2. The increase in the number of bridges and loops per cluster is an indication of the extent of crosslinking that occurs between neighboring aromatic clusters. The total number of attachments per aromatic cluster ($\sigma+1$), however, does not change significantly, indicating that bridge material is released at a rate proportional to the formation of crosslinking bridges. These stable char bridges likely are formed at the site of the original bridge. These data at rapid heating conditions clearly indicate that the average molecular structure of the Illinois No. 6 coal does not undergo major changes in functional group distribution until after most of the tar is released, at which time reactions occur in the char/metaplast that are associated with gas release.

The crosslinking behaviors of the chars from other coals, as indicated by the NMR data, are different from that observed in Illinois No. 6. The changes in the number of bridges and loops per cluster in the late stages of mass release for the other bituminous coal (PSOC-1451) are more scattered, and do not exhibit the clear indication of crosslinking observed in the Illinois #6 coal (PSOC-1493). In the lignite, the initial number of bridges and loops is slightly higher than in the bituminous coals, and increases in a monotonic progression with the extent of mass release, as reported earlier.⁹ The lignite data reflect the early crosslinking that is observed in solvent swelling measurements of lignites as compared to the high volatile bituminous coals.^{12,13} This early crosslinking is only indicated in Fig. 2 for the lignite; none of the other coals show significant increases in the number of bridges and loops

per cluster until the late stages of mass release (including the subbituminous coal). The highest rank coal (PSOC-1508 Pocahontas lv bituminous) shows a slight decrease in the number of bridges and loops per cluster as mass release proceeds.

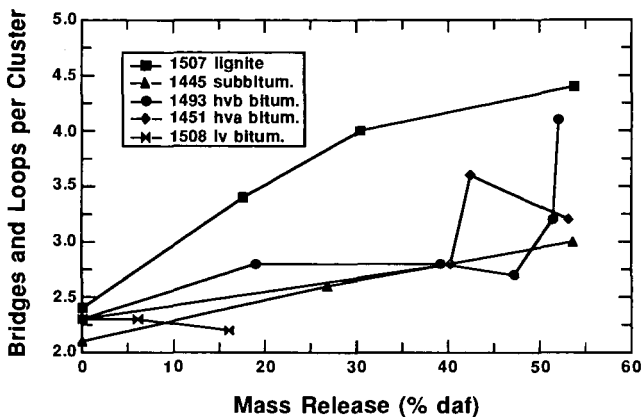


Figure 2. The number of bridges and loops per cluster vs. the extent of mass release due to devolatilization for chars collected at different residence times in the 1250 K gas temperature condition.

Coordination numbers for char samples obtained in the 1050 K gas condition in the CDL are shown as dashed lines and open symbols in Fig. 2. In the 1050 K gas condition, the coordination number determined for the chars from the subbituminous coal (PSOC-1445) does not decrease as much with mass release as indicated at 1250 K. The lower temperature condition does not permit the same degree of gas release as the higher temperature condition, and hence more side chains remain attached to the clusters. The coordination number data at 1050 K for the high rank coal (PSOC-1508) follow the data indicated at 1250 K. In general, the data at 1050 K support the conclusion inferred from the 1250 K data; no increases in the number of attachments per cluster are seen, indicating that crosslinking occurs only at existing side chain sites.

Carbon Aromaticity. The carbon aromaticities of the fully-devolatilized chars only range from 79% for the subbituminous coal to 88% for the Pittsburgh No. 8 and the Pocahontas coals, whereas f_a' in the parent coals range from 53% for the subbituminous coal to 77% for the Pocahontas coal. The carbon aromaticity measured for the subbituminous coal and char is uniformly lower than measured in the other four coals (and their chars). The carbon aromaticities of the fully-devolatilized chars from the other four coals lie in a narrow range from 84% to 88%.

Cluster and Attachment Molecular Weights. The average cluster molecular weight determined from the NMR analyses includes the aromatic carbons per cluster plus the attachments (bridges and side chains) to the cluster, i.e., the contributions from both the aromatic and aliphatic material in the vicinity of a cluster. Cluster molecular weights of chars collected in the CDL at the 1250 K gas condition as a function of residence time are shown in Fig. 3. The average cluster molecular weight for parent coals ranges from 270 amu for the Illinois No. 6 coal to 440 amu for the Zap lignite, as shown in Fig. 3 at a

residence time of 0 ms. However, as these coals are heated and the volatiles are released, average cluster molecular weights for the chars of these different coals become very similar.

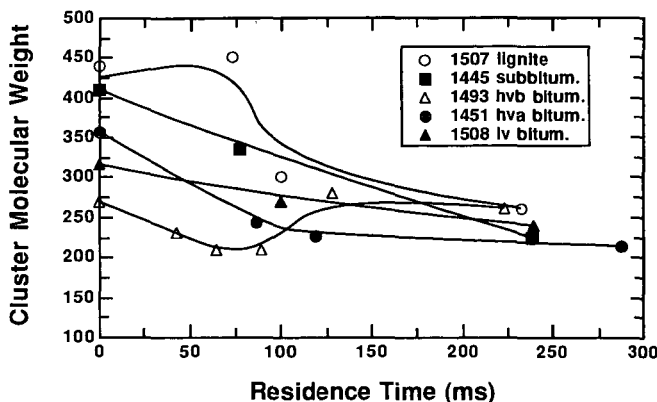


Figure 3. Average cluster molecular weights in coals and chars collected in the 1250 K gas condition in the CDL, determined from ^{13}C NMR analyses. Parent coals are represented at 0 ms residence time.

Another comparison of chemical structure as a function of coal rank is the average molecular weight of attachments to clusters in the parent coal. Attachments to clusters include labile bridges (ξ), char bridges (c), and side chains (δ). The molecular weight of attachments m_{att} can be calculated from the cluster molecular weight by subtracting the mass in the aromatic fused structure (the number of aromatic carbons per cluster multiplied by the molecular weight of carbon) and dividing by the number of attachments per cluster:

$$m_{att} = \frac{M_{clust} - C_{clust} M_C}{\sigma + 1} \quad (1)$$

The definition of the molecular weight per cluster (M_{clust}) used here includes the mass in the aromatic part of the cluster plus the surrounding aliphatic material. The cluster molecular weight therefore includes the mass of side chains, and one-half the molecular weights of labile bridges and char bridges attached to the cluster, as follows:

$$m_{att} = \frac{\xi \frac{m_b}{2} + c \frac{m_{char}}{2} + \delta m_\delta}{\xi + c + \delta} \quad (2)$$

where ξ , c , and δ represent the populations of labile bridges, char bridges, and side chains, respectively. The factor of 2 in the m_b and m_c terms reflects the fact the only one-half of an intact bridge is attributed to a cluster. Unreacted coals contain very few char bridges (i.e., $c = 0$), and hence Eq. 2 reduces to the relation $m_{att} = m_\delta$, assuming that $m_\delta = m_b/2$. For fully-devolatilized chars, $\xi = 0$.

Attachment molecular weights have been thus determined for all five coals examined in the Sandia devolatilization experiments, as well as for chars at different residence times, as shown in Fig. 4. Attachment molecular weights for other parent coals are also shown, as reported by Solum, et al.⁷ for the Argonne premium coals¹⁴ and for three coals examined at Advanced Fuel Research (AFR).¹⁵ The continuous lines in this figure represent linear correlations of the data. The oxygen content of the parent coal is an indicator of coal rank; the oxygen content of the parent coal decreases as coal rank increases. The attachment molecular weights of the parent coals exhibit a definite trend as a function of coal rank; values of m_{att} range from 52 amu in the lignite and subbituminous coal (25% daf oxygen) to 13 amu for the highest rank coal (Pocahontas #3 lv bituminous, Argonne sample).

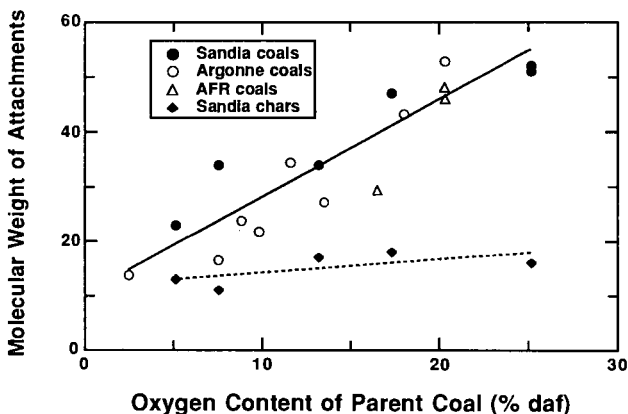


Figure 4. Average molecular weight of attachments to aromatic clusters in unreacted and fully-devolatilized coals as a function of coal type. Data for non-Sandia coals are taken from Solum, et al.⁷. Fully-devolatilized chars are from the longest residence time (~ 250 ms) in the 1250 K gas condition in the CDL.

The fully-devolatilized chars in Fig. 5 are from the longest residence time (~ 250 ms) in the 1250 K gas condition in the CDL (in 100% N₂). The molecular weights of attachments for the fully-devolatilized chars vary from 18 to 11 amu, which is not a significant dependence on coal rank. The fully-devolatilized chars do not contain any labile bridges, and hence the attachments to the cluster consist solely of char bridges and side chains. The fact that the average molecular weight of attachments to aromatic clusters in the fully-devolatilized chars is low enough (11 to 18 amu) to compare with bridges consisting of one atom (12 amu for carbon, 16 amu for oxygen) suggests that low molecular weight side chains may consist mainly of methyl groups (15 amu) and OH groups (17 amu), which are more stable than longer side chains such as COOH or ethyl groups (C₂H₅).

Stable char bridges are thought to mainly consist of three types: (a) biphenyl bridges, where a bridge is formed between neighboring carbons on different aromatic clusters (Ar-Ar); (b) ether-type bridges where a single oxygen atom forms a bridge between neighboring clusters (Ar-O-Ar); and (c) a carbon bridge, thought to mainly consist of single carbon atoms between clusters (Ar-C-Ar). The molecular weights of these three types of bridges are low enough to be consistent with the NMR data: 0 amu for the biphenyl bridge; 16 amu for the oxygen bridge; and 14 amu for the carbon bridge.

Discussion of CDL Data. It is well known that the physical structures (i.e., apparent densities and internal surface areas) of these chars vary significantly, causing a difference in the *apparent* reactivities of these chars (based on external surface area). However, the similarity in chemical structure of the fully-devolatilized chars from different coals may imply that the *intrinsic* chemical reactivities of these chars may be similar. The exact relationship between cluster molecular weight, carbon aromaticity, and intrinsic chemical reactivity is not yet clear. The fact that the chemical structure of these chars are similar is somewhat surprising because the chemical compositions of these chars are different. The carbon contents of the fully-devolatilized chars vary from 83% on a dry ash-free (daf) basis for the lignite char to 92% daf for the Pocahontas char. The oxygen contents of these chars range from 9.9% daf for the lignite char to 3.3% daf for the Pocahontas char. The NMR chemical structure data on chars should be compared in the future with physical structure and reactivity data.

B. Chemical Structure of Coal Chars in the CCL

Char samples from five coals collected at 47 ms residence time in the CCL with 0% post-flame oxygen were analyzed by ^{13}C NMR spectroscopy. The chars taken from the CCL-0 condition are very similar in chemical structure to the chars taken immediately after tar release in the CDL experiments at 1250 K (residence times of approximately 70 to 100 ms). In the CDL, these chars have finished releasing tar, and are beginning the slower gas release phase. The chars in the CCL-0 condition at 47 ms have just completed tar release as well, and hence should be followed by a slower light gas release region. The similarity in chemical structure of chars from the 1250 K gas condition in the CDL and from the CCL-0 condition is shown in Fig. 5. The solid lines in these figures represent the CDL data at different residence times, while the dashed line represents data from the CCL-0 experiments. Residence time for a given coal is in the vertically upward direction.

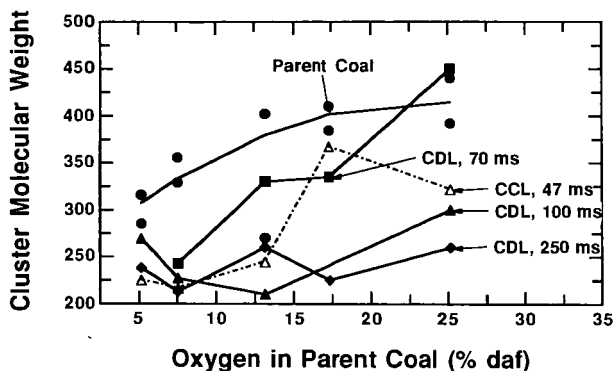


Figure 5. Comparison of cluster molecular weights in char samples from the CCL-0 condition and the 1250 K gas condition in the CDL (see caption to Fig. 6).

The cluster molecular weights (Fig. 5) in the CCL-0 chars from the low rank coals generally lie between the values observed in the chars collected at 70 and 100 ms in the CDL. In contrast, the cluster molecular weights in CCL-0 chars from the high rank coals are most similar to the CDL chars collected at 100 ms. Similar trends were observed in the carbon aromaticities of the chars from the CDL and CCL.

Quantitative measures of chemical structure (e.g., carbon aromaticities, cluster molecular weights) for the CCL-0 chars always lie close to the values observed in the chars collected at 70 or 100 ms in the CDL, and do not approach the values observed at 250 ms in the CDL. The chemical structure data for the CCL-0 chars therefore indicate that tar release in the CCL is complete at 47 ms, but that further release of light pyrolysis gases is still underway in the early stages of char combustion. Simultaneous char combustion and light gas evolution occur as the char ignites, and both must be considered in the determination of reactivities early in the char combustion process.

Conclusions

The chemical structures of chars from an electrically-heated laminar flow reactor (CDL) and a flame-driven flow reactor (CCL) show remarkable similarities. The CCL chars are similar to the chars that were collected in the CDL immediately after tar release, but before the further release of light gases. This indicates that char combustion occurs concurrently with the late degassing stage of devolatilization. The fully-devolatilized chars from the CDL exhibit similar chemical structure characteristics, such as molecular weight per cluster and attachment molecular weight, even though the parent coal structures are quite different. The similarity in chemical structure of the chars is in contrast to the general trend in char reactivity (in oxygen); low rank coals are generally more reactive than high rank coal chars. This implies that the principal cause of differences in char reactivity is physical structure (e.g., internal surface area, porosity) rather than chemical structure.

Acknowledgements

The pyrolysis work carried out at the Sandia Livermore Combustion Research Facility was supported by the DOE/PETC Direct Utilization AR&TD Program. NMR work was supported through the Advanced Combustion Engineering Research Center at Brigham Young University and the University of Utah which is supported by the NSF, 23 industrial firms and DOE/PETC. Additional support was provided through the Consortium for Fossil Fuel Liquefaction Science by DOE/PETC.

References

1. Grant, D. M., Pugmire, R. J., Fletcher, T. H., Kerstein, A. R.: *Energy and Fuel*, 3, 175 (1989).
2. Fletcher, T. H.: *Comb. Sci. & Tech.*, 63, 89 (1989).
3. Fletcher, T. H.: *Comb. & Flame*, 78, 223 (1989).
4. Niksa, S. and Kerstein, A. R.: *Energy and Fuels*, 5, 647 (1991).
5. Solomon, P. R., Hamblen, D. G., Carangelo, R. M., Serio, M. A. and Desphande, G. V.: *Energy and Fuel*, 2, 405 (1988).
6. Ko, G. H., Sanchez, D. M., Peters, W. A., and Howard, J. B.: 22nd Symp. (Int.) on Comb., The Comb. Inst., Pittsburgh, PA, 115 (1988).
7. Solum, M. S., Pugmire, R. J., and Grant, D. M.: *Energy and Fuels* 3, 187 (1989).
8. Fletcher, T. H., Solum, M. S., Grant, D. M., Critchfield, S., and Pugmire, R. J.: 23rd Symp. (Int.) Comb., The Comb. Inst., Pittsburgh, PA, 1231 (1990).
9. Pugmire, R. J., Solum, M. S., Grant, D. M., Critchfield, S., and Fletcher, T. H.: *Fuel*, 70, 414 (1991).
10. Mitchell, R. E.: 22nd Symp. (Int.) on Comb., The Comb. Inst., Pittsburgh, PA, 69 (1988).
11. Fletcher, T. H. and Hardesty, D. R.: Milestone Report for DOE's Pittsburgh Energy Technology Center, contract FWP 0709, in press (1991).
12. Suuberg, E. M., D. Lee, and Larsen, J. W.: *Fuel*, 64, 1668 (1985).
13. Solomon, P. R., Serio, M. A., Deshpande, G. V., and Kroo, E.: *Energy & Fuels*, 4, 42 (1990).
14. Vorres, K. S.: *ACS Div. Fuel Chem. prepr.*, 32:4, 221 (1987).
15. Serio, M. A., D. G. Hamblen, J. R. Markham, and Solomon, P. R.: *Energy & Fuels*, 1, 38 (1987).

CORRELATION OF STRUCTURE AND REACTIVITY IN ALKYLARENE THERMOLYSIS

C. Michael Smith, Minda M. McNally and Phillip E. Savage*
University of Michigan, Department of Chemical Engineering
Ann Arbor, MI 48109-2136

KEYWORDS: Alkylarenes, Bond Cleavage, Reactivity Indices, Pyrolysis, Hydrogenolysis

INTRODUCTION

There is an industrial trend toward developing molecular-level process models for the conversion of hydrocarbon-containing feedstocks. The development of such models has been motivated by a desire for more efficient processes and improved product quality, and to an extent by environmental regulations. Recent and continuing advances in analytical chemistry, which provide increasingly detailed structural descriptions of complex materials, and advances in computing have fueled the formulation of these increasingly complex models. An integral part of such models is a set of correlations that relates the reactivity (e.g., kinetics and product distributions) of a given portion of the feedstock to its chemical structure.

Polycyclic n-alkylaromatic moieties are important structural features of feedstocks such as crude oils, bituminous sands, kerogens, asphaltenes, and coals,¹⁻⁵ and recently the thermal chemistry of representative model compounds has been explored.⁶⁻¹¹ An interesting observation that arose from these pyrolysis experiments was that the very strong aryl-alkyl C-C bond was susceptible to hydrogenolytic cleavage. We developed a quantitative correlation that related the rate of this aryl-alkyl bond cleavage in long-chain n-alkylarenes to the respective localization energies through Dewar reactivity numbers calculated from perturbational molecular orbital (PMO) theory.⁸ In this paper we extend the previous analysis to develop a similar structure-reactivity correlation for methylarenes based on the set of methylaromatics displayed in Figure 1.

EXPERIMENTAL

1-Methylnaphthalene (1-MN), 1-methylanthracene (1-MA), 2-methylanthracene (2-MA), and 9-methylanthracene (9-MA) were pyrolyzed at temperatures between 350°C and 450°C. All chemicals were obtained from Aldrich. The pyrolyses were conducted in constant-volume, 316 stainless steel, micro-batch reactors. The reactors were constructed from one Swagelok port connector and two Swagelok end caps, and they had a nominal volume 0.6 ml. Previous work established that the reactor material did not alter the experimental results.¹⁰ As an additional test for catalytic activity by the reactor walls, we conducted several pyrolyses in the presence of stainless steel filings and saw no appreciable effect on conversion and product selectivities.

The batch reactors were typically loaded with 10 mg of the model compound and 10 mg of an internal standard and sealed in a nitrogen-filled glovebox. After being loaded and closed, the reactors were placed in an isothermal, fluidized sandbath. Upon reaching the desired holding time, the reactors were removed from the fluidized bath, and the reaction was quenched. The products were recovered by repeated extraction with benzene.

The reaction products were analyzed by gas chromatography (GC) and gas chromatography-mass spectrometry. The GC analysis used a Hewlett Packard 5890 instrument equipped with a flame ionization detector (FID). The reaction products were identified by comparing their GC retention times with those of authentic standards and by inspection of their mass spectra. Product molar yields, calculated as the number of moles of product formed divided by the number of moles of the reactant initially loaded in the reactor, were obtained from the GC analyses using experimentally determined FID response factors. We estimate the uncertainty in these yields to be about 20%. Further analytical details have been given previously.⁶⁻¹⁰

RESULTS

In the following section, we present the results from the pyrolysis of 1-MA, 2-MA, and 9-MA. Tables I-III give representative data for these compounds in terms of the yields of the major products and selected minor products.

1-Methylanthracene (1-MA): The neat pyrolysis of 1-MA was conducted at 400°C, 425°C, and 450°C for batch holding times up to 300 minutes. Table I provides representative experimental data obtained under different reaction conditions. The products from 1-MA pyrolysis were anthracene, 9,10-dihydroanthracene (DHA), 1,2,3,4-tetrahydroanthracene (THA), 1-methyl-9,10-dihydroanthracene (1-MDHA), 9-methylanthracene, 5 dimethylanthracene (DMA) isomers, and benzene-insoluble char. We were not able to determine the specific locations of the methyl groups in the dimethylanthracene isomers so we have simply identified these isomers as I, II, III, IV, and V.

Anthracene was the most abundant product at all reaction conditions, and its molar yield generally increased with batch holding time at all three temperatures. The highest anthracene yield was 31%, which was obtained at a batch holding time of 120 minutes for the pyrolysis at 450°C. At conversions less than 50%, 1-MDHA was the second most abundant product, but at higher conversions its yield was low. For example, at 425°C the molar yield for 1-MDHA reached a maximum value of 2.9% at a holding time of 60 minutes, and it subsequently decreased to 1.4% at 300 minutes. This same behavior (i.e., the presence of a maximum) was also observed for each of the dimethylanthracene isomers and 9-methylanthracene. Such behavior was not observed for the yields of the remaining minor products, DHA and THA. Rather, the molar yields of these products were very low at short batch holding times, but they increased steadily with time to become significant minor products. For example, at 425°C the molar yields of DHA and THA were 0.5% and 0.1%, respectively at 60 minutes, but these yields increased to 3.5% and 2.2%, respectively, at 300 minutes.

2-Methylanthracene (2-MA): Table II lists the products' molar yields obtained from the pyrolysis of 2-MA at 400, 425, and 450°C. The major products were anthracene and 2-methyl-9,10-dihydroanthracene (2-MDHA). The minor products included three dimethylanthracene isomers. A benzene-insoluble char was also observed. The highest conversion of 2-MA, 87%, occurred at the most severe reaction conditions employed (200 minutes at 450°C).

The molar yield of anthracene steadily increased with batch holding time. The highest molar yield (20%) for this compound was obtained at 450°C for a batch holding time of 200 minutes. The behavior of the 2-MDHA yield was analogous to that of the 1-MDHA yield in 1-MA pyrolysis. For example, at 450°C the molar yield of 2-MDHA increased to 5.8% at 75 minutes and subsequently decreased thereafter.

9-Methylanthracene (9-MA): The neat pyrolysis of 9-MA was conducted at 350, 375, and 400°C for batch holding times up to 180 minutes. Table III provides representative data from these experiments. The major product from 9-MA pyrolysis was always anthracene. The highest yield of anthracene, 42%, was obtained at the most severe conditions (90 minutes at 400°C), and the corresponding conversion of 9-MA was 85%. DHA and two dimethylanthracene isomers were observed as minor products. The molar yield of DHA increased with batch holding time until it reached a maximum, and then it subsequently decreased. At 400°C, for example, the maximum molar yield for this compound was 5.1% at 30 minutes.

PYROLYSIS PATHWAYS

We used the Delplot technique to deduce a general reaction network for the pyrolysis of the methylanthracenes studied.¹² This methodology determines the order of appearance of products in a reaction network through the examination of their initial selectivities, where the selectivity is calculated as the molar yield divided by the reactant conversion. These initial selectivities are determined as the y-intercept of the selectivity versus conversion curve for each product. Typically, products that have a non-zero initial selectivity are primary products (those that arise directly from the reactant), and they are the first to appear in the reaction network. Products that have zero initial selectivities are generally secondary and higher order products.

Figure 2 displays the Delplots for 1-MA pyrolysis. The discrete points are the experimental data, and the curves are drawn to convey the trends in these data. Figure 2a presents the selectivities to anthracene, DHA, and 1-MDHA as a function of conversion. Analysis of the y-intercepts for each of the products reveals that anthracene and 1-MDHA have initial selectivities of 0.19 and 0.14, respectively, and that the initial selectivity for DHA is essentially zero. This signifies that anthracene and 1-MDHA are primary products, and DHA is a secondary or higher order product. Figure 2a also shows that the selectivity to 1-MDHA decreases with conversion, which implies that 1-MDHA undergoes secondary decomposition at higher conversions. In this light, it is interesting to observe that the DHA selectivity increases with conversion, and that one possible route to its formation is dealkylation of 1-MDHA.

The Delplots for the five dimethylantracene isomers are displayed in Figure 2b. The initial selectivity for each of these compounds is non-zero, which indicates that each is a primary product. The selectivity to each of these compounds decreases with the 1-MA conversion, which may indicate that secondary decomposition occurs.

We conducted similar reaction pathway analyses using the pyrolysis product data for the other two methylantracenes to develop a general reaction network for the pyrolysis of methylantracenes. This pyrolysis network is shown in Figure 3. The network includes the primary conversion of each of the methylantracenes to anthracene and to dimethylantracene isomers. This portion of the pathway involves reversible steps. 1-MA and 2-MA can also undergo primary reaction to 1-MDHA and 2-MDHA, respectively, and DHA can form through the secondary reactions of 1-MDHA, 2-MDHA, and anthracene.

STRUCTURE AND REACTIVITY

Our development of a structure-reactivity correlation for the compounds in Figure 1 will focus on the pathway through which the aryl-alkyl C-C bonds are cleaved. The mechanism responsible for this cleavage involves a hydrogenolysis reaction in which the methyl substituent is displaced by hydrogen,^{6,7} but the mechanistic details remain unresolved. Possible mechanisms include hydrogen atom ipso-substitution,¹³ molecular disproportionation,^{14,15} and radical hydrogen transfer.^{16,17} Each of these mechanisms involves the transfer of a hydrogen atom from a donor to the *ipso* position of the methylantracene thereby engendering aryl-alkyl bond cleavage. Thus, in essence, this reaction involves a substitution reaction in which the methyl group is replaced by a hydrogen atom.

For aromatic substitution reactions involving a family of arenes, the differences in the activation energies are likely due to the changes in the differences between the energies of the delocalized electrons in the reactants and in the transition state (i.e., $\Delta E_{\pi}^{\ddagger}$, the delocalization energy of activation). From PMO theory and the Evans-Polanyi principle, we expect the differences in activation energies to be proportional to the differences in the energies of reaction, which in turn can be attributed to the change in energy of the delocalized electrons (π -energy of the system, ΔE_{π}) provided there is little or no change in energy of the localized bonds and in solvation.¹⁸⁻²⁰ The result of this analysis allows us to write Equation 1, where α is the Evans-Polanyi factor.

$$\Delta E_{\pi}^{\ddagger} \cong \Delta E_a = \text{constant} + \alpha \Delta E_{\pi} \quad (1)$$

For even alternant hydrocarbons, ΔE_{π} can be calculated readily from PMO theory as

$$\Delta E_{\pi} = 2\beta(a_{0r} + a_{0s}) = \beta N_t \quad (2)$$

where β is the resonance integral, and a_{0r} and a_{0s} are the coefficients of the non-bonding molecular orbitals at the positions adjacent to the position of substitution, which is denoted by the subscript t .^{18,19} The value of β should be the same for a given reaction family since the structures of the transition states should be similar. The quantity $2(a_{0r} + a_{0s})$ is defined as the Dewar reactivity number, N_t , and the values for the compounds used in the present study were given in Figure 1. These Dewar numbers are for the aromatic position bearing the methyl substituent.

Combining Equations 1 and 2 shows that

$$\Delta E_a = \text{constant} + \alpha \beta N_i \quad (3)$$

Equation 3 suggests that a semilog plot of the reaction rate constants for aromatic substitution reactions as a function of the Dewar reactivity number, N_i , should be linear. We desired to employ the Dewar reactivity number as a correlating parameter, but we could not calculate the value of the rate constant because the precise form of the hydrogenolysis rate law is unknown. Thus, we chose to employ initial rates in the correlation. These rates were calculated as the initial slope of the arene molar yield vs. time curve. Figure 4 displays the natural logarithm of this initial rate of aryl-alkyl bond cleavage at 400°C as a function of the Dewar reactivity number for the methylarenes used in this study and for 1-methylpyrene (1-MP).⁹

Two linear correlations exist for the data presented in Figure 4. The first is for the methylarenes in which the position bearing the methyl group and the position with the lowest Dewar number (i.e., most reactive position) coincide, and the second is for the three methylanthracenes, compounds in which these positions do not necessarily coincide. These two distinct lines emerge because there are two key features that principally control the rate of hydrogenolysis. The first is the rate at which hydrogen is added to and CH_3 removed from the substituted position in the methylarene. This rate should correlate with the Dewar number of the position bearing the substituent. The second feature is the rate at which hydrogen is added to any position on the methylarene to form potential radical hydrogen donors, which can subsequently engender hydrogenolysis. This rate, to a first approximation, should correlate with the Dewar number of the most reactive position in the methylarene. Thus, the two key Dewar numbers for a polycyclic alkylarene are the one for the substituted position and the one for the most reactive position (i.e., the lowest one). For compounds where these numbers coincide, a single line is expected. Thus, the data for 9-MA, 1-methylpyrene (1-MP), and 1-methylnaphthalene (1-MN) fall on a single line. For an alkylarene in which these Dewar numbers differ (i.e., 1-MA, 2-MA) a different correlation is expected. This expectation is realized by the methylanthracene data in Figure 4.

Each peripheral carbon atom in a polynuclear aromatic can accept hydrogen from a donor, and each carbon atom has its own susceptibility for hydrogen addition, which is dependent upon its intrinsic reactivity. The Dewar reactivity number provides a numerical measure of the ease of hydrogen addition to a given position. Positions with lower Dewar numbers accept hydrogen more readily than do positions with higher Dewar numbers. Thus, the rates of hydrogenolysis for methylarenes having the methyl group at the position possessing the highest reactivity (e.g., lowest Dewar number) should correlate with the Dewar number of that position because a majority of the hydrogen addition will be to the ipso-position. This correlation appears as line 1 in Figure 4.

For methylarenes in which the methyl group is not substituted on the position of highest reactivity, hydrogen adds more rapidly to non-ipso positions to form hydroaromatic radicals than it adds to the ipso position. These hydroaromatic radicals can engender subsequent hydrogenolysis through radical hydrogen transfer steps. Thus, methylarenes with highly reactive non-ipso positions can undergo hydrogenolysis at a rate that is higher than expected from the Dewar number of the ipso position. The presence of these more reactive non-ipso positions provides additional modes for engendering hydrogenolysis. This behavior is exhibited in the methylanthracenes because the 9-position is highly reactive, and it can readily accept hydrogen to form a 9-hydroanthracyl radical. These hydroaromatic radicals can then transfer hydrogen to the ipso position, via RHT for instance, and engender hydrogenolysis. This increase in the H-donor pool concentration increases the rate of demethylation above what it would be if the highly reactive 9 position were absent. Thus, the rates of aryl-alkyl C-C bond cleavage for 1-MA and 2-MA fall above line 1 in Figure 4.

The insight gained from Figure 4 can be used for predictive purposes. Consider two methylarenes that have identical Dewar numbers for the position bearing the methyl substituent. In the first compound the position of highest reactivity and the position bearing the substituent coincide, whereas in the second compound they do not. The rate of demethylation

will be greater in the second compound because additional modes of hydrogen transfer involving hydroaromatic radicals are available.

SUMMARY AND CONCLUSIONS

1. The pyrolysis of methylanthracenes leads to anthracene as the major product. Minor products include methyl-9,10-dihydroanthracenes, 9,10-dihydroanthracene, and dimethylanthracenes.
2. Anthracene, dimethylanthracenes, and methyl-9,10-dihydroanthracenes were primary products of methylanthracene pyrolysis. Dihydroanthracene and methylanthracene isomers were secondary products.
3. The rates of aryl-alkyl bond cleavage for methylanthracene pyrolyses were correlated with the Dewar reactivity numbers for the peripheral aromatic carbon bearing the methyl group. A second correlation was deduced for the rate of demethylation of 9-methylanthracene, 1-methylpyrene, and 1-methylnaphthalene. The existence of two distinct structure-reactivity correlations is consistent with the governing hydrogen transfer mechanisms.

ACKNOWLEDGEMENTS

This work was supported in part by the Link Foundation, the Shell Faculty Career Initiation Fund, and the National Science Foundation (CTS-8906859). Acknowledgement is also made to the donors of the Petroleum Research Fund (ACS-PRF # 23744-AC4), administered by the ACS, for the partial support of this research. We also thank Scott Schnieder for conducting the 1-methylnaphthalene experiments.

LITERATURE CITED

1. Ali, L. H.; Al-Ghannam, K. A. and Al-Rawi, J. M. *Fuel* **1990**, *69*, 519-521.
2. Kolandaisamy, M; Betts, B; Smith, J. *Fuel* **1990**, *69*, 1322-1325.
3. Strausz, O. *AIChE Symp-Ser* **1989**, *273*, 1-6.
4. Waller, P. R.; Williams, A.; Bartle, K.D. *Fuel* **1989**, *68*, 520-526.
5. Speight, J. G. *Prepr.-Am. Chem. Soc., Div. Pet. Chem.* **1989**, *34*, 321-328.
6. Smith, C. M.; Savage, P. E. *Ind. Eng. Chem. Res.* **1991**, *30*, 331-339.
7. Smith, C. M.; Savage, P. E. *Energy and Fuels*, **1991**, *5*, 146-155.
8. Smith, C. M.; Savage, P. E. *AIChE Journal* **1991**, *37*, 1614-1624.
9. Smith, C. M.; Savage, P. E. *Energy and Fuels* **1992**, *in press*
10. Savage, P.E.; Jacobs, G.E.; Javanmardian, M. *Ind. Eng. Chem. Res.* **1989**, *28*, 645-652.
11. Freund H.; Matturo, M. G.; Olmsted, W. N.; Reynolds, R. P.; Upton, T. H. *Energy & Fuels* **1991**, *5*, 840-846.
12. Bhole, N. A.; Klein, M. T.; Bischoff, K. B. *Ind. Eng. Chem. Res.* **1990**, *29*, 313-316.
13. Vernon, L. W. *Fuel* **1980**, *59*, 102-107.
14. Billmers, R.; Brown, R. L.; Stein, S. E. *Int. J. Chem. Kinet.* **1989**, *21*, 375-389.
15. Billmers, R.; Griffith, L. L.; Stein, S. E. *J. Phys. Chem.* **1986**, *90*, 517-523.
16. Malhotra, R.; McMillen, D. F., *Energy and Fuels*, **1990**, *4*, 184-193.
17. McMillen, D. F.; Malhotra, R.; Chang, S.J.; Olgier, W.C.; Nigenda, E; Fleming, R. H. *Fuel*, **1987**, *66*, 1611-1620.
18. Dewar, M. J. S.; Dougherty, R. C. "*The PMO Theory of Organic Chemistry*" Plenum Press, New York, **1975**.
19. Dewar, M. J. S. "*The Molecular Orbital Theory of Organic Chemistry*" McGraw Hill, New York, **1969**.
20. Streitwieser, A. "*Molecular Orbital Theory for Organic Chemists*" John Wiley & Sons, New York, **1961**.

Temp (°C)	400	400	400	400	400	425	425	425	425	425	450	450	450	450	450
Time (min)	60	150	200	240	300	30	60	150	300	425	30	90	120	150	300
Anthracene	2.9%	9.3%	4.8%	10.3%	16.7%	4.0%	10.8%	16.4%	23.8%	26.8%	14.7%	26.3%	30.9%	28.8%	23.3%
DHA	0.0%	0.6%	0.2%	0.7%	1.5%	0.0%	0.5%	1.2%	2.7%	3.5%	0.9%	2.6%	3.4%	3.2%	3.4%
THA	0.0%	0.2%	0.0%	0.3%	0.8%	0.0%	0.1%	0.5%	1.4%	2.2%	0.2%	1.1%	1.7%	1.6%	1.7%
DMA I	0.3%	0.9%	0.5%	1.0%	1.2%	0.4%	1.0%	1.2%	1.0%	0.5%	1.1%	1.0%	0.6%	0.9%	0.0%
DMA II	0.3%	1.1%	0.5%	1.2%	1.8%	0.4%	1.2%	1.7%	2.1%	1.3%	1.5%	2.1%	1.4%	0.9%	0.0%
DMA III	0.7%	2.0%	1.1%	2.2%	2.6%	0.9%	2.3%	2.5%	2.1%	0.7%	2.5%	2.0%	0.0%	0.0%	0.0%
DMA IV	0.1%	0.3%	0.1%	0.2%	0.3%	0.1%	0.2%	0.3%	0.3%	0.0%	0.4%	0.4%	0.3%	0.0%	0.0%
DMA V	1.0%	1.3%	1.4%	1.0%	0.7%	1.3%	1.5%	0.7%	0.4%	0.0%	0.9%	0.3%	0.0%	0.0%	0.0%
1-MDHA	2.3%	3.4%	2.7%	2.9%	3.3%	2.0%	2.9%	2.3%	2.2%	1.4%	2.3%	1.9%	1.4%	1.1%	0.1%
9-MA	0.0%	0.5%	0.1%	0.5%	0.9%	0.0%	0.6%	0.8%	0.9%	0.3%	0.6%	0.8%	0.3%	0.3%	0.0%
1-MA	74.9%	56.3%	75.6%	47.4%	36.6%	81.4%	66.1%	32.7%	22.1%	9.5%	43.3%	20.7%	9.5%	8.2%	2.7%

Temp (°C)	400	400	400	400	400	425	425	425	425	425	450	450	450	450	450
Time (min)	15	60	90	120	130	30	45	60	150	200	60	75	90	160	200
Anthracene	0.1%	0.2%	0.7%	1.0%	1.2%	2.5%	3.8%	4.3%	6.7%	8.9%	6.5%	9.5%	11.3%	14.6%	19.7%
DMA I	0.1%	0.4%	0.7%	0.9%	0.8%	0.7%	1.7%	2.1%	0.8%	1.2%	0.7%	1.1%	1.3%	0.0%	1.6%
DMA II	0.1%	0.1%	0.1%	0.1%	0.0%	0.1%	0.2%	0.0%	2.9%	3.3%	2.5%	3.1%	3.7%	0.0%	0.0%
DMA III	0.2%	0.4%	0.4%	0.5%	0.4%	0.4%	1.1%	1.4%	1.7%	1.4%	1.6%	0.0%	1.6%	0.0%	0.0%
2-MDHA	1.7%	2.5%	3.4%	3.8%	3.5%	1.3%	3.4%	4.7%	5.9%	4.7%	4.9%	5.8%	5.3%	4.6%	0.0%
2-MA	100.6%	95.0%	87.6%	82.3%	66.7%	81.8%	78.8%	70.2%	67.0%	53.5%	67.2%	61.2%	44.7%	37.0%	13.3%

Temp (°C)	350	350	350	350	350	375	375	375	375	375	400	400	400	400	400
Time (min)	15	30	60	100	180	15	30	45	60	90	15	30	45	60	90
Anthracene	7.2%	1.9%	2.9%	3.4%	4.6%	6.4%	11.6%	15.3%	20.9%	20.6%	9.0%	17.9%	34.5%	33.1%	42.0%
DHA	1.0%	0.0%	0.2%	0.6%	0.2%	0.5%	0.8%	1.1%	1.2%	1.1%	2.6%	5.1%	2.2%	2.3%	1.1%
DMA I	0.7%	0.0%	0.0%	0.4%	0.5%	0.8%	1.4%	2.0%	2.3%	1.9%	1.6%	2.5%	2.4%	1.4%	1.0%
DMA II	2.5%	0.7%	1.1%	1.1%	1.7%	0.7%	2.6%	2.5%	2.4%	0.8%	1.0%	1.4%	2.5%	1.9%	1.9%
9-MA	94.3%	122.0%	115.7%	106.0%	129.0%	84.0%	78.3%	78.3%	61.8%	39.9%	53.4%	34.8%	30.8%	18.1%	15.3%

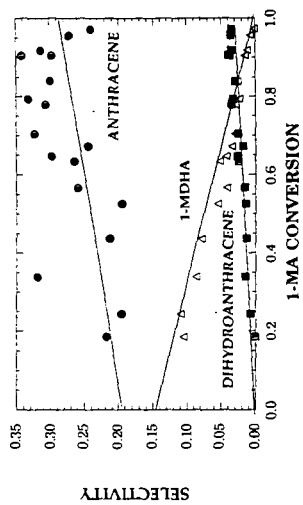


Figure 2a: 1-MA Selectivity to Anthracene, 9,10-Dihydroanthracene (DHA), and 1-Methyl-9,10-dihydroanthracene (1-MDHA).

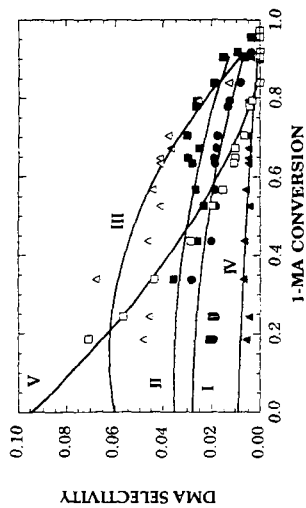


Figure 2b: 1-MA Selectivity to Dimethylanthracene (DMA) Isomers (I-V).

Model Compounds	Name	Dewar Number
	1-Methylnaphthalene (1-MN)	1.81
	1-Methylantracene (1-MA)	1.57
	2-Methylantracene (2-MA)	1.89
	9-Methylantracene (9-MA)	1.26
	1-Methylpyrene (1-MP)	1.51

Figure 1: Heavy Feedstock Model Compounds.

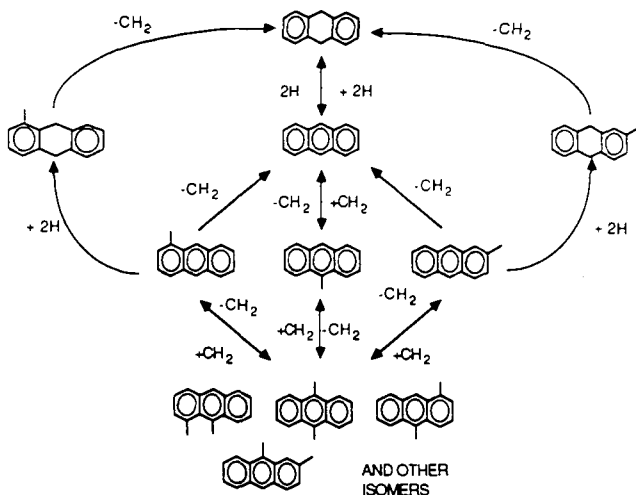


Figure 3: Pyrolysis Network for Methylanthracenes.

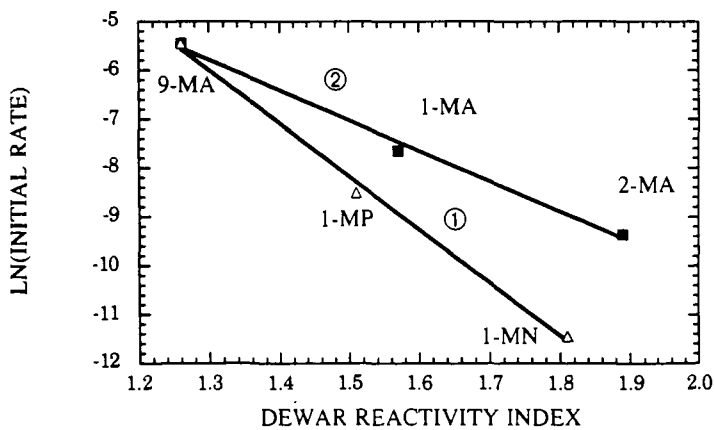


Figure 4: Correlation of Initial Rate of Demethylation in Methylarene Pyrolysis with Dewar Reactivity Numbers

CHARACTERIZATION OF COALS, OTHER KEROGENS, AND THEIR EXTRACTS BY THERMAL MASS SPECTROMETRY

R. E. Winans, P. E. Melnikov, and R. L. McBeth
Chemistry Division, Argonne National Laboratory
9700 S. Cass Avenue, Argonne, IL 60439

Keywords: DCI mass spectrometry, coal extracts, coal structure

INTRODUCTION

The objective of this study is to elucidate the nature of the medium size molecules derived from coals by a succession of stronger extraction conditions. The Argonne Premium Coals have been extracted with pyridine, binary solvents and with KOH/ethylene glycol at 250 °C. Thermal desorption and pyrolysis mass spectrometry were the major approaches chosen to provide detailed information on structure and heteroatom composition. Soft ionization techniques including desorption chemical ionization (DCI) and fast atom bombardment (FAB) were combined with high resolution and tandem MS techniques. This paper will focus on the comparison of the nature of the unextracted coals, the pyridine extract and the extracted coal residue. With this approach the desorption-pyrolysis yields of the extracts and residues combined were greater than the yields from the starting material. Although molecule weight distributions had a minor dependence on rank, the nature of molecules with the same nominal mass varied greatly with rank.

Pyrolysis combined with a variety of mass spectrometric techniques has been used extensively to study coals and separated coal macerals. High resolution mass spectrometry elucidated the distribution of heteroatoms in vacuum pyrolysis products resulting in the discovery of a large number of products containing multiple heteroatoms.¹ The more volatile pyrolysis products have been examined by PyGCMS and PyMS methods. Thermogravimetric MS techniques yield quantitative data with rather slow heating rates.² Field ionization MS (FIMS) is a technique widely used to provide molecular weight distributions of volatile tars.³ Data are available for all eight of the Argonne Premium coals^{4,5} and will be compared to the results by other MS techniques. In addition, Meuzelaar, Schulten and co-workers have compared the results of PyFIMS, low voltage PyMS and TGAMS and discovered similar patterns in the low mass regions.⁶ Recently, FABMS has been applied to the characterization of coal vacuum pyrolysis products yielding data similar to FIMS.⁷ Initial results using the DCIMS approach on demineralized and extracted Argonne coals have been presented⁸, and this paper will extend this study to include the pyridine extracts. Also, tandem MS is used to elucidate the structure of larger molecules. The problem of secondary reactions occurring due to the pyrolysis step is reduced by focussing on extracts.

EXPERIMENTAL

A complete discussion of the characteristics of the coals used in this study has been reported.⁹ Selected elemental analysis values and results from vacuum pyrolysis, and extractions are given in Table I. Details on how the coals were treated are shown on the flow diagram in Scheme I. A complete description of the KOH in ethylene glycol treatment has been reported.¹⁰

The DCIMS studies have been performed on a Kratos MS 50 triple analyzer with isobutane as the reagent gas. The solids and extracts were heated directly in the source of the mass spectrometer on a small platinum wire coil. The wire was heated from 200° C to 700° C at 100° C/min with the source body kept at 200° C.

In addition to the three-sector MS 50, tandem MS data have been obtained on a four-sector instrument located at the University of Manchester, Institute of Science and Technology (UMIST). The spectrometer is a combination of two Kratos Concept-H's, each with a 10,000 mass range. The sensitivity in MS-2 where the daughter spectra are obtained is enhanced by using an array detector.

Scheme 1

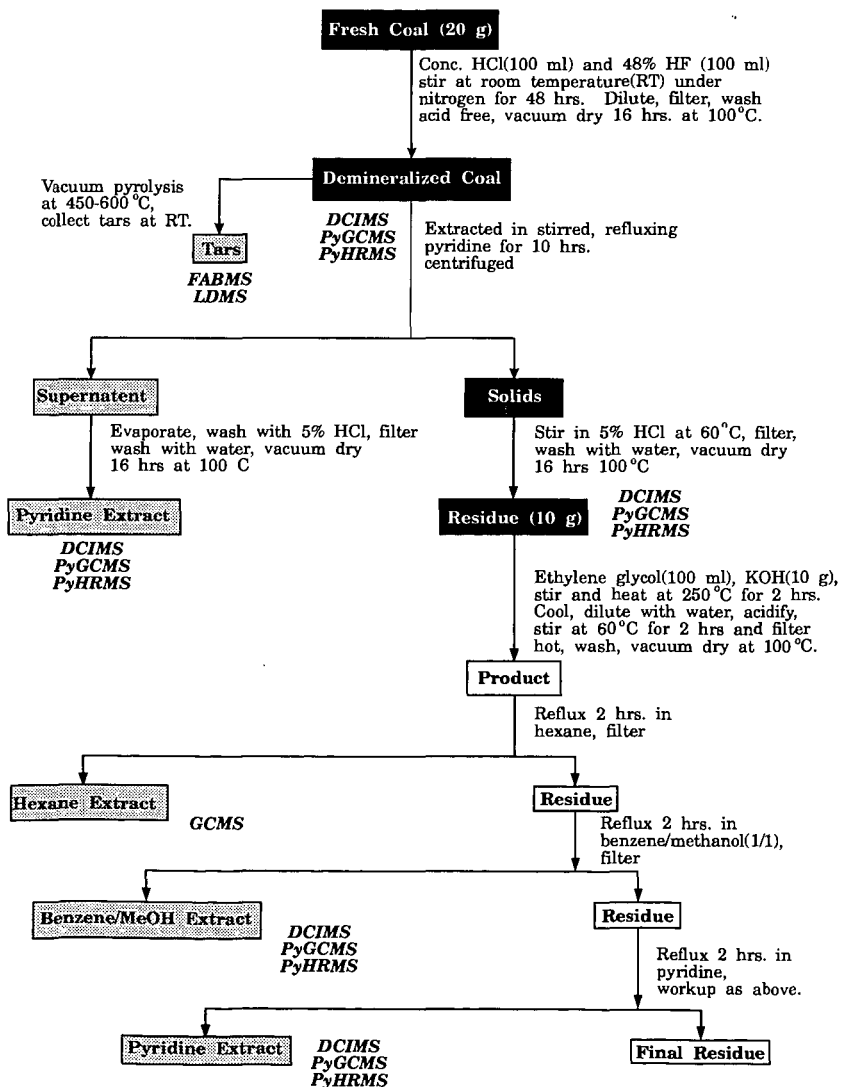


Table 1. Elemental Analysis and Yields for the Coal Samples, Ordered by Carbon Content.

Sample	Name	%C dmmf*	Per 100 Carbons		Yields (Wt%, dmmf*)		
			H	O	Pyrolysis	Pyridine Extract	KOH/Glycol Solubles
8	Beulah-Zap Lignite	74.1	79.5	20.9	23.6	17.9	84.1
2	Wyodak-Anderson SubB	76.0	85.6	18.0	39.3	29.3	79.0
3	Illinois No. 6	80.7	77.2	13.0	36.8	29.0	71.1
6	Blind Canyon hvBB	81.3	85.7	10.8	50.2	25.0	
4	Pittsburgh hvAB	85.0	76.7	7.96	16.2	24.4	
7	Lewiston-Stockton hvAB	85.5	76.3	8.93	22.9	16.9	
1	Upper Freeport mvB	88.1	66.0	6.59	14.3	3.6	
5	Pocahontas lvB	91.8	58.5	2.04	12.1	2.6	

dry mineral matter free

RESULTS AND DISCUSSION

From examination of Table 1 it is apparent that the batch pyrolysis yields and the pyridine extract yields parallel each other, except for the Blind Canyon coal (APCS 6). This coal is rich in liptinites which may account for the greater pyrolysis yield. However, the yields of products observed in the DCIMS experiments as a function of time and temperature for the coal and the extract differed significantly. This is shown for the Blind Canyon coal in Figure 1. The extract exhibits a much more bimodal character with a significant yield of volatiles at the lower temperature. In addition, the high temperature peak is shifted to higher temperatures for the extract compared to both the unextracted and extracted coal. This is a general phenomena for all the coals but becomes more pronounced with the higher rank coals. These data suggest that the thermally extractable material as discussed by Meuzelaar, et al.,⁹ may be a subset of the potentially extractable material. In addition, the extracts appear to be more thermally stable compared to the solids. This may be due to a transport problem of moving the volatiles through the pore structure where secondary reactions can occur. Also, it may be that there is more donatable hydrogen available in the extracts.¹¹

In some cases the extracts yielded higher molecular weight products and a different set of compounds compared to the whole coal. Figure 2 shows an example of this result for the Lewiston-Stockton coal

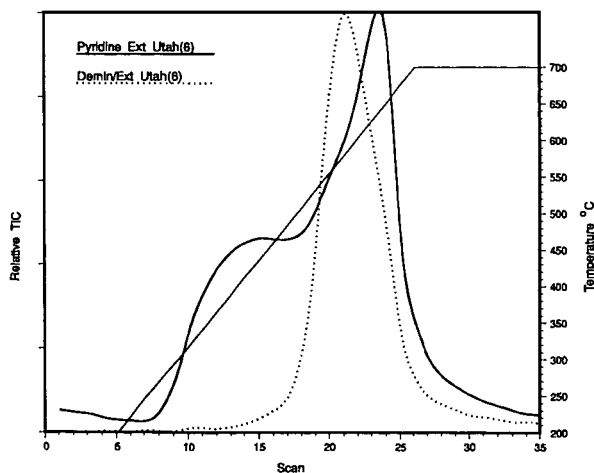


Figure 1. Total ion pyrograms from DCIMS of Blind Canyon (APCS 6) pyridine extract and demineralized and extracted residue.

(APCS 7). Note that the whole coal spectrum shows well defined series at $m/z < 250$ while the extract contains two sets of series of peaks at $m/z=250-400$ and $m/z=500-600$. The high mass set is expanded in Figure 2b. There are pairs of peaks separated by two mass units and repeating every 14 units (methylene). What is even more interesting is that these products appear across the whole temperature range as is shown in Figure 3. Initially, it was thought that these peaks could be a series of M+1 ions

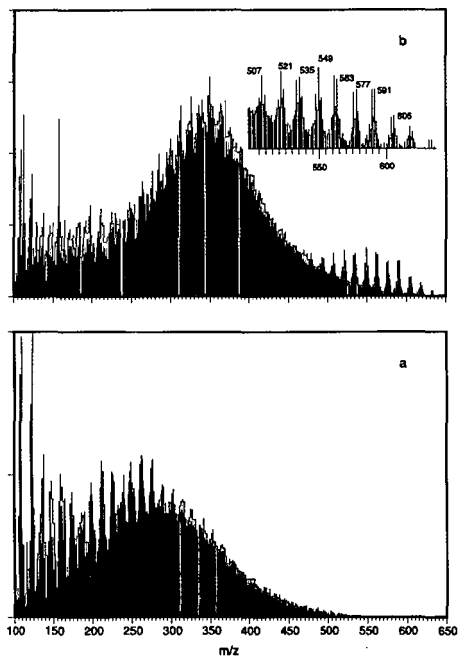


Figure 2. Averaged DCI mass spectra for (a) demineralized Lewiston-Stockton coal (APCS 7) and (b) pyridine extract of the same coal.

resulting from porphyrins. Because of the unusual nature of these ions, we felt it was worth further investigation by tandem MS. The daughter spectrum of $m/z=535$ is shown in Figure 4. It is a fairly complicated spectrum with a large number of aliphatic fragments. It is not a porphyrin or a very large ring number polycyclic aromatic compound. There is the possibility that it could be an aromatized terpenoid with the partial structure shown in Figure 4 for the fragment at $m/z=255$. A very different daughter spectrum is observed for parent ion $m/z=533$, demonstrating that these pairs of peaks are apparently not related.

The thermal stability of the extracts is seen also in the average molecular weight of the volatiles. An example is shown in Table 2 for the Lewiston-Stockton coal (APCS 7). The average molecular weight did not vary over a large temperature range for the coal while for the extract varied significantly. It started out high with the release of the large non-polar molecules, decreased at the start of the pyrolysis, and then increased with temperature.

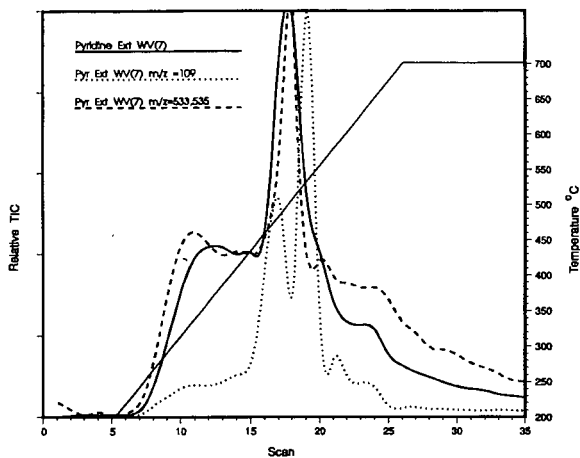


Figure 3. Total and selected ion pyrograms for DCI MS of pyridine extract of Lewiston-Stockton coal (APCS 7): solid - total ion, dotted - $m/z = 109$ and dashed - sum of $m/z = 533, 535$.

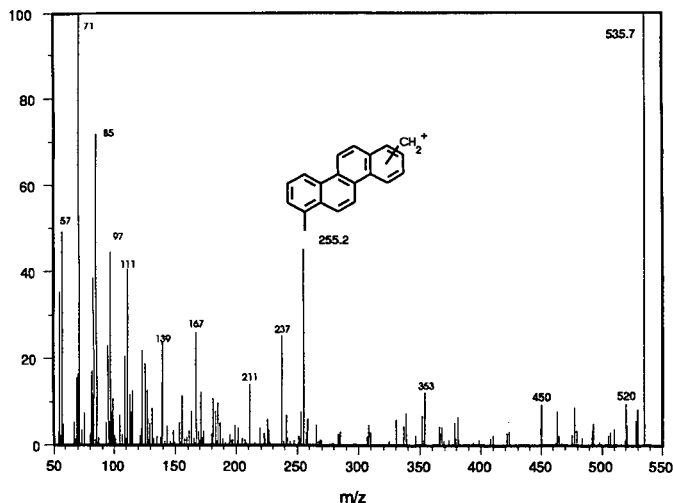


Figure 4. Daughter spectrum from parent $m/z = 535$ from CIMS of pyridine extract from Lewiston-Stockton coal (APCS 7) taken on UMIST four-sector instrument.

Table 2. Average Molecular Weights for Lewiston-Stockton (APCS 7) from DCIMS.

Sample	Temperature (°C)	M _n	M _w
Deminerized	475	240	283
	650	253	290
Pyridine Extract	375	316	345
	500	298	334
	650	319	356
	700	342	374

M_n= number average molecular weight; M_w= weight average molecular weight

Another interesting result is the suggestion from the extract data that large molecules derived from lignin sources are soluble in pyridine. In Figure 3, it is shown the selected ion ($m/z=109$) curve which would represent alkylphenol fragments. There is very little yield at the lower temperatures, but as soon as high temperature pyrolysis begins these fragments are observed. From some initial experiments with the base solubilized material, it is interesting to note that the most abundant products in the low rank coals are C₂ and C₃ alkylphenols derived from lignin. This helps to demonstrate the concept that coals are not a simple two phase system; however, they are more likely a continuum of increasing molecular weight species.

CONCLUSIONS

This work demonstrates that future work should place emphasis on the extracts and mild degradation products. Thermally extractable molecules and solvent extractable molecules are likely to be different with the former possibly a subset of the latter. Large lignin-derived fragments exist in the pyridine extractables which suggest that these extracts may be quite representative of the whole coal (vitrinite).

ACKNOWLEDGEMENTS

This work was performed under the auspices of the Office of Basic Energy Sciences, Division of Chemical Sciences, U.S. Department of Energy, under contract number W-31-109-ENG-38. Assistance of M. Morris (UMIST), D. W. Tudge and S. Evans (Kratos) in obtaining the 4-sector MSMS spectra is appreciated.

REFERENCES

1. Winans, R.E. and Neill, P.H. In *Geochemistry of Sulfur in Fossil Fuels*, W.L. Orr and C.M. White, Eds., ACS Symposium Series 429, ACS, Washington, D.C., 1990, Ch. 15, p. 249-259.
2. Szabo, P.; Varhegyi, G.; Till, F.; Szekely, T. *Thermochimica Acta*, 1990, 170, 167-177.
3. Schulten, H.-R. and Marzec, A. *Fuel*, 1986, 65, 855-860.
4. Solomon, P.R.; Serio, M.A.; Despanda, G.V.; Kroo, E. *Energy Fuels*, 1990, 4, 42-54.
5. Malhotra, R.; McMillen, D.F.; Huestis, D.L. *Preprint, Division Fuel Chem., ACS*, 1991, 36(3), 1252-1258.
6. Yun, Y.; Meuzelaar, H.L.C.; Simmler, N.; Schulten, H.-R. *Energy Fuels*, 1991, 5, 22-29.
7. Winans, R.E. *J. Anal. Appl. Pyrolysis*, 1991, 20, 1-14.
8. Winans, R.E.; McBeth, R.L.; Hunt, J.E.; Melnikov, P.E. *Proceedings, 1991 International Conf. Coal Sci.*, 1991, 44-47.
9. Vorres, K.S. *Energy Fuels*, 1990, 4, 420-425.
10. Winans, R.E.; Hayatsu, R.; McBeth, R.L.; Scott, R.G.; Moore, L.P.; Studier, M.H., In *Coal Structure*, Gorbaty, M.L., Ouchi, K. Eds.; Adv. Chem. Series 192, ACS, 1981, 161-178.
11. Solomon, P.R., private communication.

STRUCTURE/REACTIVITY STUDIES OF SINGLE COAL PARTICLES AT VERY HIGH HEATING RATES BY LASER PYROLYSIS GC/MS

Walced S. Maswadeh, Y. Fu, Joel Dubow and Henk L.C. Meuzelaar
Center for Micro Analysis & Reaction Chemistry
University of Utah, Salt Lake City, Utah 84112

KEYWORDS: high heating rate devolatilization, laser devolatilization/GC/MS technique, coal devolatilization kinetics

INTRODUCTION

Recently, Maswadeh et al. [1] reported on the design, construction and testing of a single particle levitation/laser devolatilization apparatus featuring an on-line gas chromatograph/mass spectrometer (GC/MS) system, enabling coal devolatilization experiments at heating rates in the 10^5 - 10^6 K s⁻¹ range. Analysis of bituminous coal particles revealed a high degree of qualitative correspondence with pyrolysis patterns obtained at much slower (10^2 - 10^0 K s⁻¹ range) TG/MS heating rates [1], thus providing mechanistic justification for extrapolating kinetic parameters obtained by slow pyrolysis techniques (e.g., TG/MS or TG/IR) to the high heating rates characteristic of full scale, suspension fired coal combustors.

A second observation made with the aid of laser pyrolysis GC/MS was that the distribution of devolatilization products observed at very high heating rates was not measurably influenced by the presence or absence of air [1]. A subsequent redesign of the system permitted the use of electron microscopy (EM) grids to support individual coal particles, thereby simplifying the experimental set up, improving collection efficiency of volatile products and facilitating optical alignment of the particles (microscopy, optical micropiprometry) as well as retrieval of residual char particles [2].

EXPERIMENTAL

Materials

Bculah Zap and Illinois #6 coal samples were obtained from the Argonne Premium Coal Sample Program. Minus 100 mesh samples were carefully sieved and the subfraction passing through a #170 mesh screen but retained by a #230 mesh screen was used for further analysis. Several coal particles were picked up by means of a glass rod and transferred over to the EM grid (see Figure 1). A single particle was then selected visually under the microscope and centered manually with the help of the two HeNe laser guide beams shown in Figure 1.

Two Color Micropiprometer

Since the temperature-time history of the particle is necessary for describing tar evolution kinetics, the two color micropiprometer depicted in Figure 1 was constructed. Light emitted from the hot particle is collimated in a Cassegrainian objective (Ealing x 15/.28) and subsequently chopped at 2 kHz (Stanford Research Systems chopper, model SR540, Palo Alto, CA). A 5.066-5.364 micron IR band pass filter transmits the 5 micron band to a 15x Cassegrainian objective focussed on the first IR detector and reflects the remainder of the beam through a 1.84-2.11 micron band pass filter (both filters from Optical Filter Corp. Natick, Mass.) to a 15 X Cassegrainian objective focussed on the second IR detector. The two detectors are dewar mounted, liquid nitrogen cooled InSb photodiodes (Barnes Engineering, Stamford Conn.). The flip mirror shown in Figure 1 is a manually controlled mirror inserted into the optical path when the video camera is employed.

Signal chopping is employed to eliminate and to take into account the d.c. drift in the measurements, to operate in the frequency region of maximum D^* for the detectors and facilitate an increase in the signal to noise ratio for the measurement system [3]. The detector current outputs are converted to voltages, fed to two filtered preamplifiers (Tektronix, model AM 502) and recorded by means of a Hewlett Packard Model 5183 dual channel, 4 Mhz storage oscilloscope. The filters eliminate spurious signals arising from pulsing the CO_2 laser.

Laser Py-GC/MS

Single, 60-120 μm dia. particles of Beulah Zap lignite were analyzed by means of CO_2 laser Py-GC/MS using single laser pulses ranging in duration from 2-20 msec. The particles were mounted on copper EM grids, as shown in Figure 1. Volatile products were sampled into a 6 ft long, 180 μm i.d. fused silica capillary GC column coated with DB5 (0.40 μm) using a valveless, automated vapor sampling (AVS) device (U.S. patent 4,970,905). In these experiments, the AVS was set to "inject" a 2 sec long vapor pulse into the capillary "transfer line" column 0.1 sec after the laser pulse. Subsequently, the capillary GC column was heated ballistically from ambient to 200 C over a 2 minute period while volatile pyrolysis products were being eluted directly into the high vacuum of the Finnigan MAT ion trap mass spectrometer (ITMS). Approximately 1,200 mass spectra were recorded at a rate of 4 spectra per second after each laser pyrolysis of a single coal particle.

RESULTS AND DISCUSSION

Two Color Micropyrometer Measurements

Following Spjut et al. [4] the single channel and two channel transient responses were calculated. These showed that the intrinsic 2-color pyrometer response time was on the order of 0.1 microsecond and that the 5 micron channel was nearly a factor of two faster than the 2 micron channel. However, parasitic impedances and impedance mismatches between the detectors and the preamplifiers slowed the response time considerably, so that chopping at frequencies of 1 Khz and above caused a degradation in response, especially in the 5 micron channel. This effect led to a small but systematic underestimation of the temperature in these data but has recently been eliminated using techniques to increase system electronic bandwidths. In order to minimize systematic errors, careful temperature calibration was performed over the 300-1100 K range using a specially constructed 0.88 mm dia. black body cavity radiator. This calibration is extrapolated to higher temperatures using standard radiation pyrometry theory. The results are shown in Figure 2.

As shown in Figure 3, two Beulah Zap lignite particles (63-90 μm) produced maximum temperature readings in the 1700-1850 K range, which is directly comparable to the characteristic operating temperatures of full scale pulverized coal combustors [5]. The temperature history profiles suggest a two step heating behavior with initial heating rates of approx. 2.10^5 K s^{-1} giving way to lower heating rates (approx. 4.10^4 K s^{-1}) after 6-7 milliseconds. Laser beam intensities are known to remain essentially constant ($\pm 5\%$) throughout the duration of the pulse (after an initial 1 millisecond stabilization period). Partial obscuration of the particle surface by the rapidly expanding and cooling cloud of volatiles, combined with evaporative surface cooling effects could be the source of the observed temperature variations in the 6-15 millisecond range. Similar temperature profiles were obtained for a series of Illinois #6 particles (not shown here).

Laser Py-GC/MS Analysis

A typical GC/MS profile of the volatile laser pyrolysis products of a single Beulah Zap coal particle is shown in Figure 4, illustrating the good signal to noise ratio obtained in spite of the small particle size and the relatively low tar yields (<10% daf coal) of lignites. The largest GC peaks seen in the

total ion chromatogram (TIC) profile after the initial "air peak" in Figure 4a consist of toluene ($M^+ = m/z$ 91), phenol (m/z 94), cresols (m/z 108), C2 phenols (m/z 122), naphthalene (m/z 128), and methyl guaiacol (m/z 138), as further detailed by the selected ion chromatogram (SIC) profiles in Figure 4b-d illustrating the useful degree of chromatographic pre-separation achieved by the short capillary "transfer line" GC column. All major isomers are readily identifiable, thus providing a sensitive way of comparing pyrolysis mechanisms at high heating rates with those observable at much lower heating rate, e.g., in TG/MS experiments, as reported previously [1,2]. It should be noted here that the observed pyrolysis profiles of most Beulah Zap lignite particles are quite similar to the profiles obtained from the much slower (10^2 - 10^3 K s⁻¹) Curie-point Py-GC/MS experiments (not shown here), e.g., with regard to the dominant (alkyl) phenol series. As discussed before [1], however, the highly polar and reactive dihydroxy benzenes tend to be absent or underrepresented in laser Py-GC/MS profiles of low rank coals, presumably as a result of mass transfer limitations resulting in condensation reactions of the dihydroxybenzenes inside the char particle. The less reactive methoxyphenols characteristic for lignites and thought to represent typical building blocks of fossilized lignin [7] are readily detected as shown by the prominent methyl guaiacol peaks in Figure 4a.

By performing laser Py-GC/MS analysis of Beulah Zap coal particles at 8 different laser pulse durations and summing the quantitative response of the dominant tar components at m/z 108 (C1 phenols) and m/z 122 (C2 phenols) for each laser experiment, it proved possible to construct the tar evolution profile shown in Figure 5. Note that each point represents the average of 3-4 laser Py-GC/MS analyses. From previous experience it was expected that 20 milliseconds would suffice to obtain complete devolatilization. As demonstrated in Figure 5, however, the tar yield still seems to be increasing at 20 milliseconds, probably due to a somewhat reduced laser power output. Unfortunately, we omitted to determine remaining volatile matter content at 20 milliseconds by subjecting each remaining char particle to a second laser pulse of ample long duration. From the shape of the profile and the intensities of the mass spectra obtained, the tar yield at 20 milliseconds is assumed to be 60-80% of the maximum tar yield obtainable.

Kinetic Considerations

The tar evolution profile in Figure 5 invites the question whether kinetic parameters can be extracted from these data. In view of the relatively small number of data points and the large number of potential sources of error in this type of experiment the authors decided not to attempt a direct extraction of kinetic parameters (which involves differentiation of the curve in Figure 5) but rather to compare the measured profile with predicted yield profiles derived from low heating rate data, using appropriate kinetic models. Beulah Zap tar evolution profiles obtained by three different laboratories (Advanced Fuels Research, using TG/FTIR at 30 K min⁻¹ [8] and 10 K min⁻¹; and Lawrence Livermore National Laboratory, using Py-MS/MS at 4 K min⁻¹ [9]) are represented in Arrhenius plot format (Figure 6). All profiles show excellent agreement (max. 25 K difference in temperatures, corresponding to less than a factor 2 in rate constant difference, when correcting for variations in heating rate) in spite of the very different experimental set-up. The two TG/MS curves (Nie et al., unpublished data) were recorded in our laboratory with a new system operating at ambient pressure and featuring a molecular leak type quartz probe positioned within 5 mm of the TG crucible. When ignoring the minor temperature offsets between the curves, the average slopes and curvatures are quite similar with the possible exception of the TG/FTIR curve. In other words, three of the four curves appear to represent the same set of activation energies.

This brings up the important question how to interpret the observed curvature of all four profiles in the Arrhenius plot. Three possible options are: (1) multiple parallel reactions characterized by a particular distribution of activation energies [10]; (2) a continuously variable (conversion dependent) activation energy (see appendix); and (3) a single, constant activation energy with a heat or mass transfer controlled reaction rate. Most likely, we are dealing with a combination of all three scenarios. There is little doubt that multiple parallel reactions are involved in coal pyrolysis, as can be readily observed by time-resolved pyrolysis MS experiments [11, 12]. Similarly, it is well understood that continuous chemical alteration of the coal matrix takes place throughout the pyrolysis process, gradually transforming the original coal particle into a fully developed char particle. In other words, the chemical structure and composition of the coal particle halfway through the pyrolysis reaction are fundamentally different from that of the unreacted particle as can be readily determined by interrupting the pyrolysis process [13]. Obviously, the activation energy (and its distribution) are unlikely to remain constant throughout the entire process. Finally, evidence of mass transfer limitations (e.g., caking!) is readily observable in TG experiments, especially at heating rates above $5-10 \text{ K min}^{-1}$, depending on coal type and rank. Although all three phenomena: distributed activation energy, continuously variable activation energy and mass transfer limitations can readily explain the observed curvatures in the Arrhenius plot, each assumption leads to different rate and yield predictions at very high heating rates, as illustrated for the DAE (distributed activation energy) and VAE (variable activation energy) models in Figure 7. The numerical procedures used to obtain Figures 6-8 will be explained in detail elsewhere [6]. No attempt was made to predict the effects of transfer limitations due to the particle size dependence and the lack of information on the exact particle size distribution in the various experiments.

Interestingly, the DAE and VAE assumptions each lead to quite different predicted rate constants at high heating rates, thus opening up the possibility of direct experimental verification! Figure 8 compares the DAE and VAE predictions to the observed tar evolution profile. Although our VAE prediction appears to produce a better fit with the observed data, the current lack of quantitative information on the effect of transport limitations on the results of the devolatilization experiments at slow as well as at fast heating rates precludes the possibility of reaching a firm conclusion. Figures 5-8 merely illustrate that the experimental and numerical tools are in hand to start answering some of these questions and that experimental results obtained with different techniques and in different laboratories are starting to converge in a highly promising manner. Foremost among the problems that remain to be addressed however, appears to be the need to conduct systematic studies on the effects of heat and mass transfer limitations under slow as well as rapid coal devolatilization conditions.

ACKNOWLEDGEMENTS

The authors wish to thank N. Rappaport, X. Nie and N.S. Arnold for their valuable help and advice. This work was supported by the Advanced Combustion Engineering Research Center. Funds for this Center are received from the National Science Foundation, the State of Utah, 23 industrial participants and the U.S. Department of Energy.

LITERATURE REFERENCES

1. Maswadeh, W.; Huai, H. and Meuzelaar, H.L.C.; *ACS Preprints, Div. of Fuel Chem.*, 36(2) 733-740, 1991.
2. Maswadeh, W.; Meuzelaar, H.L.C.; *Proc. 39th ASMS Conf. on Mass Spectrom. All. Top.*, 1991, 192-193.
3. Wolff, W., and Zissis, G., *The Infrared Handbook*, Office of Naval Research, Dept. of the Navy, Arlington, VA, 1978.

4. Spjut, R.E., and Balsaitis, P., *Mat. Res. Soc. Symp.* 87, 295-302, 1987.
5. Smoot, D., and Smith, P. in: *Coal Combustion and Gasification*, D. Luss (ed.) Plenum Press, NY, 37-75 (1985).
6. Maswadeh, W.; Meuzelaar, H.L.C.; Dubow, J.S to be submitted to *Energy & Fuels*.
7. Nip, M.; de Leeuw, J.W.; Schenck, P.A.; Meuzelaar, H.L.C.; Stout, S.A.; Given, P.H.; Boon, J.J., *J. Anal. Appl. Pyrol.*, 1985, 8, 221-239.
8. Solomon, P.R.; Serio, M.A.; Carangelo, R.M.; Bassilakis, R. *Energy & Fuels*, 1990, 4, 319-333.
9. Burnham, A.K.; Oh, M.S.; Crawford, R.W.; *Energy & Fuels*, 1989, 3, 42-55.
10. Braun, R.L.; Burnham, A.K.; *Energy & Fuels*, 1987, 1, 153-161.
11. Chakravarty, T.; Windig, W.; Hill, G.R.; Meuzelaar, H.L.C. *Energy & Fuels*, 1988, 2, 400-405.
12. Yun, Y.; Meuzelaar, H.L.C. *ACS Preprints, Div. Fuel Chem.*, 1988, 33(3), 75-84.
13. Pugmire, R.J.; Solum, M.S.; Grant, D.M.; Critchfield, S.; Fletcher, T.H. *Fuel*, 1988, 2., 1991, 70, 414-423.

Appendix - VAE Calculation

1. From experimental rate $\left(\frac{dX}{dT}\right)$ versus temperature (T), integration is performed from $T_0 \rightarrow T$ to obtain conversion $X(T)$.
2. An Arrhenius plot is made which is a plot of $\ln \left(\frac{dX/dT}{1-X}\right)$ versus $\left(\frac{1}{T}\right)$.
3. The first derivative of this Arrhenius plot at different temperatures yields $(-Ea/R)$ and the intercept is equal to $\ln(A_0)$. These are plotted versus T.
4. From the plots of $-Ea/R$ versus T and X versus T a plot of (Ea) versus X is made.
5. A polynomial fit is made for the apparent activation energy (Ea) versus conversion X in Step 4.

$$Ea(X) = a_0 + a_1x^1 + a_2x^2 + a_3x^3 + \dots$$
 and the resulting frequency factor determined ($Ea = a \ln A_0 + b$).
6. The relationship from step 5 is matched with the experimental rate using the standard equation below:

$$\frac{dX}{dT} = \left(\frac{Ea(X)-b}{a m}\right) e^{-\frac{Ea(X)}{RT}} (1-X)$$
7. The above equation is plotted for high heating rates using the Ea(X) function obtained at low heating rates and compared to the high heating rate experimental data.

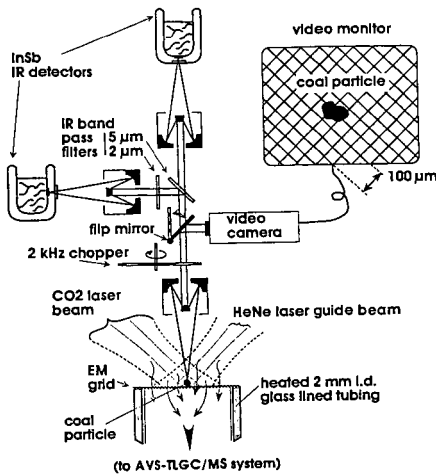


Figure 1. Schematic overview of two-color micropyrometer module with grid supported coal particle, incident dual CO₂ and HeNe laser beams, and inlet to AVS-TLGC/MS system.

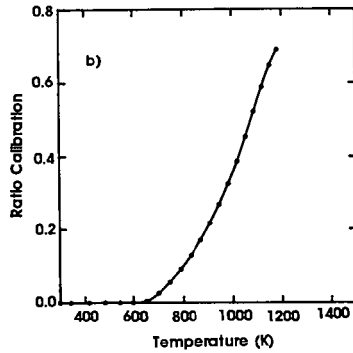
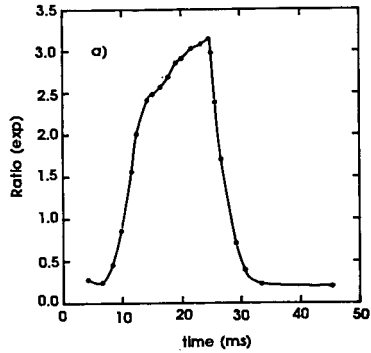


Figure 2. Pyrometer Calibration. The ratio of the outputs from the signal channels at 2.0 microns and 5.2 microns, as shown in (a), is converted to temperature using black body calibration, as depicted in (b). Above 1100 K, temperature is extrapolated using calibration and two channel pyrometry theory.

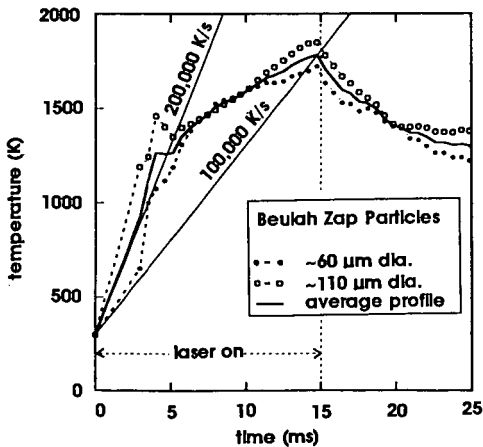


Figure 3. Temperature/time profiles of 2 Beulah Zap lignite particles during 15 millisecond CO₂ laser heating pulse and subsequent 10 millisecond passive cooling period.

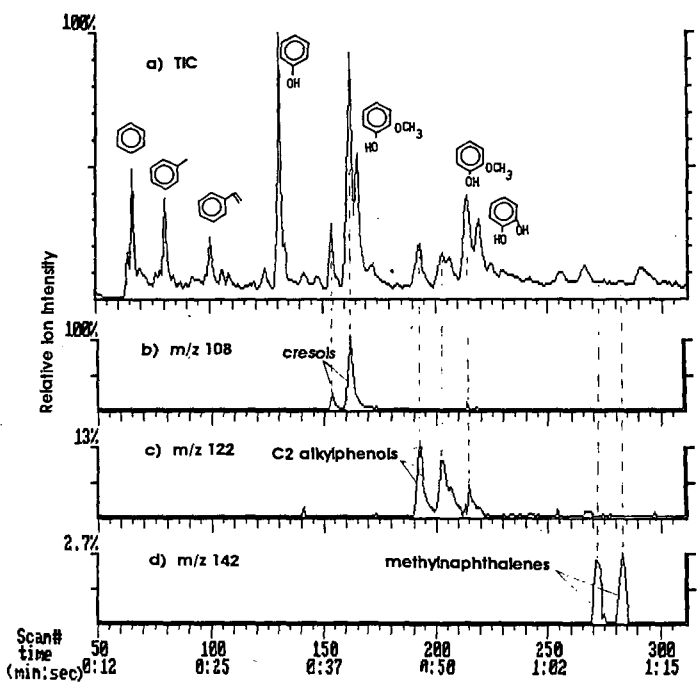


Figure 4. Typical laser Py-GC/MS profile of a 100 μm dia. Beulah Zap particle at 20 msec pulse duration. Note highly useful GC separation within approx. 70 seconds as well as dominant hydroxyaromatic signals (in agreement with low coal rank). Integrated area signals at m/z 108 and 122 were used to calculate "tar yields" shown in Figures 5 and 8.

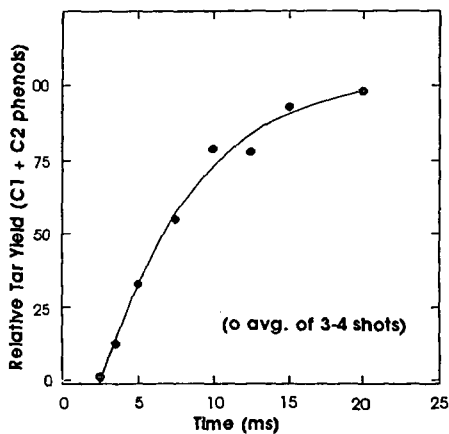


Figure 5. Relative tar yields (normalized to 20 ms yields) of 60-100 μm dia. Beulah Zap lignite particles at 8 different laser pulse times. Note that devolatilization still appears incomplete at 20 ms. Compare with Figures 3 and 4.

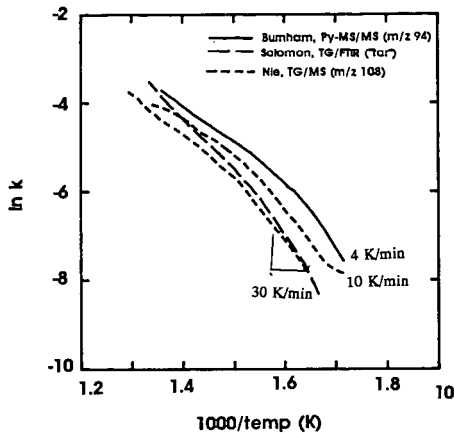


Figure 7. Comparison of VAE and DAE predictions of tar evolution kinetics at typical laser heating rates based on the 30 K min⁻¹ TG/MS profile shown in Figure 6. Note DAE model fit (42 ± 4 kcal/mol). For details of VAE prediction calculation, see Appendix.

Figure 6. Arrhenius plots showing very good agreement of literature data (Burnham, Solomon) on Beulah Zap tar evolution kinetics with our TG/MS data in spite of marked differences in experimental technique (and some variation in "tar" definition), especially when correcting for variations in heating rate. Note that entire tar evolution profiles were plotted (see Appendix).

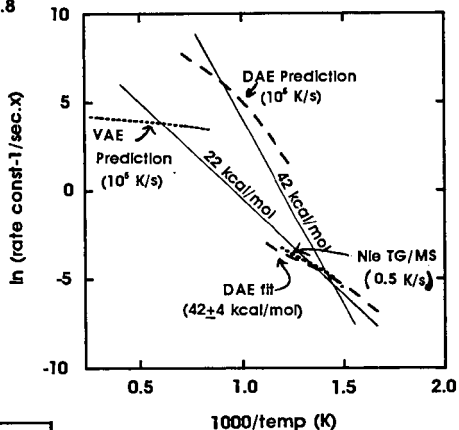
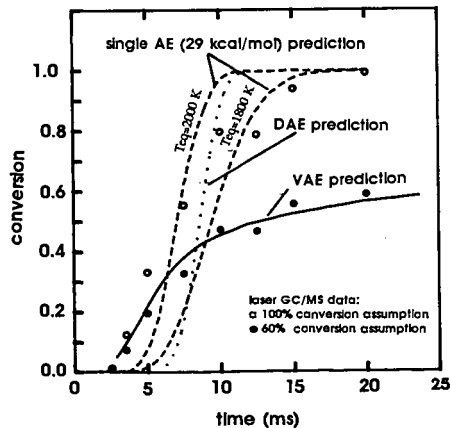


Figure 8. Measured and predicted relative tar yields of Beulah Zap coal particles. Note that VAE prediction indicates only 60% relative tar yield within 25 milliseconds. Measured points (o, o) represent averages of 3 or 4 laser shots. Single Ea (SAE) and Variable Ea (VAE) predictions use measured temp profiles (see Figure 3), DAA prediction uses linear heating rate (10^5 K s⁻¹).



Analysis of Coals from the San Juan Basin by Programmed Temperature Micropyrolysis

John G. Reynolds and Alan K. Burnham

Lawrence Livermore National Laboratory
University of California
Livermore, CA 94551

Abstract

Eighteen coals from the San Juan Basin of the southwestern U.S. were analyzed by micropyrolysis at constant heating rates for temperatures of maximum evolution (T_{max}) and pyrolysis yields. T_{max} values increased with maturity (as measured by vitrinite reflectance [% R_m]). The pyrolysis yields increased with increasing maturity until approximately R_m of 0.9% after which the yield declined rapidly.

A subgroup of coals from the Fruitland seam of the San Juan basin was also analyzed by micropyrolysis at several constant heating rates to determine laboratory pyrolysis kinetics. The kinetic calculations yielded the energy of activation by the approximate method (E_{approx}) and the principal energy of activation by the discrete method (principal $E_{discrete}$) in the range of 55 to 57 kcal/mol for the coals in the R_m range of 0.4 to 0.9%. However, the coal with the highest R_m (1.30%) had E_{approx} and principal $E_{discrete}$ around 63 kcal/mol.

These Fruitland seam coals were also extracted with organic solvents and the residual coals were analyzed to determine laboratory pyrolysis kinetics. The results were within experimental error of the kinetic values calculated for the corresponding unextracted coals.

Key words: San Juan Coals, Pyrolysis Kinetics, and Yield

Introduction

The San Juan Basin in the southwestern U. S. (Four Corners area) is a major producer of natural gas. Recently, there has been activity in the exploration for gas in the upper cretaceous Fruitland seam, which is the major deposit of coal in the basin. The Fruitland seam is considered to have the potential of 50-56 tcf of gas production, as well coal reserves of approximately 200 billion tons.¹

Most of the production is probably due to the thermal maturation over geological time. To assist in the understanding of this hydrocarbon production, we have been studying thermal maturation of source materials in the laboratory by pyrolysis techniques,² such as the Pyromat II micropyrolyzer.³ With this technique, the pyrolysis kinetics are measured, and through selected models, these kinetic

parameters measured have been extrapolated to produce relevant maturation parameters.

This report summarizes pyrolysis kinetic analysis of selected coals from the San Juan Basin by the Pyromat II micropyrolyzer. A more complete listing and analyses of this data will be reported elsewhere.⁴

Experimental

Kinetic Analysis. The method of kinetic analysis using the Pyromat II has been described in detail elsewhere.³ Briefly, the kinetics were determined from multiple runs at constant heating rates on approximately 4 to 10 mg samples. Generally three - 50°C/min, one - 7°C/min, and two - 1°C/min runs were performed. If T_{max} values and profile shapes were not in agreement, more runs at these heating rates were performed.

Yield Analysis. Yield analysis was performed on all samples by comparing to the yield of AP22 oil shale. This yield has been determined from Fisher Assay to be 88 mg of pyrolysate/gram oil shale. Two furnaces were used for these measurements. The yields were determined by two methods: 1) the yield was determined for the coal from two or three runs at the nominal heating rate of 25°C/min, from 250°C to 700°C using the old furnace. The AP22 standard was run twice daily and a single calibration factor was determined for the entire set of runs (over a period of four days). 2) For the four samples used in the kinetic analyses, several determinations were performed using the new furnace. To assure more accurate yields, the standard was run immediately before each coal sample. The standard values were then averaged each day, providing a daily calibration factor.

Samples. All samples were received run-of-mine condition, sealed in plastic bags. The whole allotment (5 to 10 grams) was ground with mortar and pestle in a nitrogen purge glove bag to inhibit oxidation. Homogeneity problems were encountered with some samples and these were reground.

Eighteen samples were received from various parts of the San Juan Basin - Fruitland formation, 12; Menefee formation, 4; Hog mountain tongue, 2. Table 1 shows the formation, the sample identification symbols, the well and depth (feet), and the vitrinite reflectance values (mean random reflectance values). The samples range from essentially subbituminous rank to medium-volatile bituminous. The depths of the Fruitland samples vary considerably and are not directly correlated with rank because of non-uniform heating due to an intrusion in the formation and the different well locations through out the field. For Henry AGC Fed #1, the shallower samples are from the Fruitland formation, and the deeper samples are from the Menefee formation (the well probably passes through the Pictured Cliffs and Cliff House sandstone formations). For Champ #5, the shallower sample is from the Fruitland formation, probably more north than the Henry AGC Fed #1 well, the intermediate samples are from the Hog Mountain tongue, and the deepest

samples are from the Menefee formation. The maturity of the Menefee formation samples from these two wells is only slightly higher than that of the shallower Fruitland samples.

Extraction. 0.2 to 0.5 g of the coal sample were extracted in a micro-soxhlet extractor for 36 hours using either the 92% CH₂Cl₂/8% MeOH azeotrope or 100% tetrahydrofuran (THF) as the extraction media. After the extraction was complete, the extracted coal was dried *in vacuo* and the solvent with the extracted bitumen was removed under a stream of N₂ gas. Mass balances exhibited over 98% recovery for the CH₂Cl₂/MeOH extractions. The THF extraction exhibited over 100% recovery after extensive drying, indicating some permanent incorporation of the solvent into the sample.

Elemental Analyses. Table 2 lists the C, H, N, CO₂, and TOC (total organic carbon) analyses (there was not enough CH₅D sample to analyze). Most of the coals have TOC levels which fall in the range of 30 to above 60 wt%, with KB5B being the richest. Two are less than 30 wt% and one, CU2A, is extremely lean in organic matter. This coal exhibits anomalous evolution behavior (see below). The coals are also very low in carbonate content (%CO₂).

T_{max} and Yield Data

Relationship between T_{max} and vitrinite reflectance. Figure 1 shows the T_{max} values at the nominal heating rate of 25°C/min measured directly on the coal samples from the San Juan Basin as a function of maturity (measured by vitrinite reflectance). Included are not only the Fruitland seam coals, but also coals from the other seams.

Except for the two coals with the lowest R_m values, all the T_{max} values fall nicely on a slightly curved line which has a positive slope with increasing R_m values. This behavior includes coals from the Fruitland, Menefee, and Hog Mountain seams. Generally two runs were performed on each coal and both runs were in good agreement, except for CU2A. The T_{max} of this coal was particularly susceptible to sample size.⁵ Ten runs were made to obtain reasonably reproducible data. This coal has a very low TOC (see Table 2), and mineral matter, sample inhomogeneity, as well as a high percentage of the TOC being bitumen, could be causes for variations in the pyrolysis behavior.⁶

The coals with the lowest R_m, CH5A and HAFA, have T_{max} values which do not fall in line with the rest of the T_{max} values. Measurements on these coals and GR3A and KBSA were repeated to check reproducibility, and the results were found to be comparable to the original data. (The latter data was taken on the Pyromat II after the furnace was replaced) No reason for the outlying behavior of CH5A and HAFA is obvious from the little data we have on other properties of the coals. However, both these coals are found at the shallowest depth (300 ft above the others). In addition, the CH5A sample was from above the Hog Mountain tongue, and both

HAFa and CH5A samples are from above the Menefee formation (see Table 1). It is important to note that Michael et al.⁷ found a linear relationship between R_m and T_{max} for Rock Eval measurements on coals from the San Juan basin. This result would suggest CH5A and HAFa as being well behaved and that the Menefee and Hog Mountain coals (see Figure 1) do not follow the trend.

Relationship between yield and vitrinite reflectance. The yields were also measured at the nominal heating rate of 25°C/min on the coals from the San Juan Basin, and are shown in Figure 1 as the open symbols (corresponding to the closed symbols for the T_{max} values). Because the Pyromat II has no direct method of measuring yield, these values were measured by using an AP22 standard (see experimental). For most of the data shown in Figure 1, the calibration factor from the AP22 standard was an overall average (yield method 1). For selected coals, the yields were checked more carefully, particularly if the value appeared to not follow the trend in Figure 1 (yield method 2).

The yield data shown in Figure 1 exhibits scatter, particularly for the low R_m coals. However, the yields appear to decrease with increasing R_m , with a noticeable change in the curvature around R_m of 0.9%. This is even more noticeable when considering only the Fruitland formation coals. (GR3B does not really follow this trend as well as one determination for CU2A. We had significant problems with every aspect of CU2A, and have little confidence in the reproducibility. Alternatively, it may contain primarily migrated bitumen.) The trend of decreasing yield above R_m of 0.9% has been seen for the Fruitland seam previously.⁶

Effect of bitumen extraction on pyrolysis yields. Four Fruitland coals, CH5A, MOAB, KB5B, and CU5A, were extracted with organic solvents to remove native bitumen and the pyrolysis yields were determined. Table 3 shows a summary of these data and compares them with the data on the corresponding unextracted coal. In all cases, the extraction reduces the pyrolysis yield. The magnitude depends upon the coal and the extraction solvent. The extracted pyrolysis yields as percentage of unextracted pyrolysis yield are: CH5A, 79; CH5A (THF extraction), 82; MOAB, 92; KB5B, 95; CU5A, 65. The extraction appears to have less effect with increasing R_m except for CU5A, which has the highest R_m of the samples studied. This behavior is opposite to the pyrolysate yields themselves which exhibit a decrease around R_m of 0.9%.

Because we had no previous experience with these coals, we selected 92% CH_2Cl_2 /8% MeOH as the extraction solvent because of its: effectiveness in extracting shales, the reduced likelihood of coal structure damage due to swelling, and minimal irreversible binding. The extraction yields using this solvent calculated from the weight of extracted bitumen were: CH5A, 4.4%; MOAB, 4.1%; KB5B, 4.8%; CU5A, 4.2%. However, these yields seem relatively low compared to bitumen yields for other coals, so THF was selected as an alternate. This solvent has a higher solubility parameter, and could possibly extract more native bitumen. The yield for CH5A using 100% THF as the extraction solvent was 6.9%, which is not a

significantly higher to cause re-extraction of the samples. Solvents such as pyridine were ruled out because of their destructive interactions with the coal structure and the noted irreversible binding.⁷

Qualitatively, the native-bitumen extraction yields are consistent with the amount the pyrolysis yields are reduced upon extraction for all the coals except CU5A. For this coal, the pyrolysis yield is reduced substantially more than would be expected from the extraction yield. The reasons for this are not clear. CU5A is the most mature sample of the group and has one of the lowest pyrolysis yield based on bitumen recovery. In addition, all the extractions of CU5A (four) showed a mass balance of over 100%, unlike the other samples, indicating solvent was incorporated into the coal structure, and suggesting the coal network was being much more affected by the extractions than the other coals.

Kinetics of Evolution of Organic Materials by Pyrolysis

Fruitland Coals. Four Fruitland coals, CH5A, MOAB, KB5B, CU5A, were examined to determine their kinetic parameters for hydrocarbon evolution. These coals were picked because their range in R_m covers from the least to most mature of the samples (see Table 1). Figure 2 shows the kinetic parameters for the discrete and approximate analyses from the best kinetic sets for each coal. The best kinetic set was chosen from multiple runs and multiple determinations, primarily from the agreement of the approximate and the discrete parameters, as well as the least squares analysis of the fits.

The best kinetic sets show some interesting trends. The parameters for the lower rank coals are all very similar. CH5A has E_{approx} and principal E_{discrete} slightly higher than MOAB and KB5B. CU5A stands out as having the highest R_m of the samples studied and distinctly different kinetic parameters (higher E_{approx} and principal E_{discrete}). This appears to follow the behavior seen before in the kinetic studies of Argonne premium coals,⁸ which show a decrease in activation energy with increasing rank for the lower rank coals, and an increase in activation energy with increasing rank for the higher rank coals.

Figure 2 also shows the fits of the evolution data using the discrete distribution model. The fits for CH5A, MOAB, and KB5B look very good. However, the fits for CU5A look significantly poorer. This will be discussed below.

Extracted Fruitland Coals. To understand the effects of native bitumen on the kinetics parameters of these coals, CH5A, KB5B, MOAB, and CU5A were extracted with organic solvents and the pyrolysis kinetics were determined from multiple-heating rate experiments. The best kinetic sets are listed in Table 4.

As in the case for the unextracted coals, the lower rank coals all have very similar kinetic parameters. E_{approx} and principal E_{discrete} are slightly higher for CH5X. As the rank increases, E_{approx} and principal E_{discrete} are slightly lower for both MOAX

and KB5X, and then is significantly higher for CU5X. This behavior is almost identical to the behavior of the unextracted coals.

Comparing the parameters in Figure 2 and Table 4 shows the kinetics for the unextracted and corresponding extracted coals are within experimental error. CH5X and CH5A show the most difference. Noting the possibility of compensating A values for the lower activation energy values for CH5X, the discrete kinetic parameters were recalculated for CH5X holding the A value fixed at 1.74×10^{15} . Table 5 shows these results. Although the least squares fits were not as good as for the CH5X kinetic set, the resulting discrete parameters were almost identical to those of the unextracted CH5A coal.

The similarity of the parameters for the unextracted coals and the corresponding extracted coals indicates the extraction does little to effect the kinetic parameters. The biggest differences are seen in the calculated T_{max} values at the heating rate of $25^{\circ}\text{C}/\text{min}$. The extracted coals yield values which are slightly higher for the lower ranks, and essentially identical for the higher rank coals. However, this difference is probably not significant enough to confidently say the extraction affects laboratory pyrolysis evolution kinetics, or that extraction is necessary in these cases to obtain valid kinetics.

This was not the case for CU5A, where the kinetic determinations were not as easy to interpret. The choice for the best kinetic set required several determinations, as well as considering the extracted data also. Figure 3 shows a comparison of extracted and unextracted CU5A at the nominal heating rate of $25^{\circ}\text{C}/\text{min}$. Obvious is the removal of the low temperature evolving material in the extracted sample. This had a significant effect on discrete kinetic parameters. Also, the σ values in Figure 2 and Table 4 show this extraction affects the peak width of evolving materials in the kerogen pyrolysis range.

As stated in the yield section, CH5A was also extracted with THF. The best kinetic set is shown in Table 5, which shows that the THF extraction had little effect on the kinetic parameters, where the values are within experimental error of the $\text{CH}_2\text{Cl}_2/\text{MeOH}$ extraction parameters.

Conclusions

For the San Juan Basin coals in this study:

- 1) T_{max} increases systematically with increasing maturity (as measured by vitrinite reflectance).
- 2) Total pyrolysate yield increases with increasing maturity until a R_m of approximately 0.9%. After this, the yield begins to decrease rapidly.

For the Fruitland seam coals in this study:

- 1) Extraction with 92% CH₂Cl₂/8% MeOH removes approximately 4% by weight of total sample. This qualitatively agrees with the reduction of pyrolysis yield upon extraction, except for CU5A.
- 2) Extraction of CH5A with 100% THF showed modest increase in bitumen yield over the 92% CH₂Cl₂/8% MeOH extraction, but showed no decrease in pyrolysis yield. This suggests THF is being incorporated into the coal.
- 3) Kinetic calculations of CH5A, MOAB, and KB5B, showed similar kinetic parameters. CU5A, however, had much higher activation energies.
- 4) Kinetic calculations of the extracted CH5A, MOAB, and KB5B showed similar kinetic parameters. Extracted CU5A, however, had much higher activation energies.
- 5) Kinetic parameters of the extracted CH5A, MOAB, and KB5B coals were almost identical to the parameters of the corresponding unextracted coal indicating extraction does little to effect the coal structure and is probably not necessary for these determinations.
- 6) Kinetic calculations for CU5A showed large differences between approximate and discrete parameters. The kinetic parameters of the extracted data set were used to resolve these discrepancies which suggests extraction is necessary for this coal.

Acknowledgments

We thank Edward L. Jones and Ann M. Murray for experimental assistance and Vido Nuccio of the U. S. Geological survey for the samples and the corresponding vitrinite reflectance data. This work was performed under the auspices of the U. S. Department of Energy by the Lawrence Livermore National Laboratory under contract number W-7405-ENG-48.

References

1. D. D. Rice, C. N. Threlkeld, A. V. Vuletich, and M. J. Pawlewicz, *Oil and Gas J.*, Aug 13, 60-61 (1990).
2. R. L. Braun and A. K. Burnham, *Energy and Fuels*, 4, 132-146 (1990).
3. R. L. Braun, A. K. Burnham, J. G. Reynolds, and J. E. Clarkson, *Energy and Fuels*, 5, 192-204 (1991).
4. J. G. Reynolds, LLNL Report UCRL-ID-XXXXXX (1992).
5. J. G. Reynolds and A. M. Murray, LLNL Report UCRL-ID-106505 (1991).

6. H. Dembicki, Jr., B. Horsfield, and T. T. Y. Ho, A.A.P.G. Bulletin, 67(7), 1094-1103 (1983).
7. G. E. Michael, D. E. Anders, and B. E. Law, manuscript to be published.
8. D. D. Whitehurst, T. O. Mitchell, and M. Farcasiu, Coal Liquefaction, (1980), Academic Press, New York.
9. A. K. Burnham, M. S. Oh, R. W. Crawford, and A. M. Samoun, Energy and Fuels, 3, 42-55 (1989).

Table 1. Selected information on coals from the San Juan Basin.

Sample ID	Formation	Depth (feet)	Vitrinite Reflectance (%R _m)
HAFa ^a	Fruitland	1528-1534	0.46
HAFB ^a	Menefee	3049-3054	0.57
HAFC ^a	Menefee	3800-3810	0.58
CH5A ^b	Fruitland	950-960	0.44
CH5B ^b	Hog Mountain	1880-1890	0.52
CH5C ^b	Hog Mountain	1910-1920	0.49
CH5D ^b	Menefee	3170-3180	0.54
CH5E ^b	Menefee	3210-3220	0.54
MOAA ^c	Fruitland	2927-2937	0.76
MOAB ^c	Fruitland	3085-3106	0.82
KB5A ^d	Fruitland	3046-3056	0.82
KB5B ^d	Fruitland	3169-3184	0.93
GR3A ^e	Fruitland	2520-2540	0.62
GR3B ^e	Fruitland	2540-2550	0.66
CU2A ^f	Fruitland	3960-3990	1.08
SJ8A ^g	Fruitland	3150-3160	1.22
SJ8B ^g	Fruitland	3148-3158	1.24
CU5A ^h	Fruitland	4180-4200	1.30

Wells:

a. Henry AGC Fed #1 (Yates Petroleum Co.). b. Champ #5 (Dugan Petroleum Co.). c. Moore A #8 (Amoco Production Co.). d. Kernaghan B #5 (Amoco Production Co.). e. Grenier #103 (Meridian Oil). f. Carracas Unit 23A #2 (Nassau Resources). g. San Juan 32-5 #108 (Meridian Oil). h. Carracas Unit 17B #15 (Nassau Resources).

Table 2. Selected elemental analyses for coals from the San Juan Basin.

Sample	%C	%H	%N	%CO ₂	TOC
HAF A	41.81 (0.35)	3.78 (0.14)	1.26 (0.10)	0.96	41.55
HAF B	40.22 (0.09)	3.63 (0.03)	1.26 (0.22)	0.53	40.08
HAF C	59.74 (1.33)	4.69 (0.06)	1.43 (0.22)	0.47	59.61
CH5 A	51.88 (0.20)	3.99 (0.06)	1.12 (0.09)	2.65	51.15
CH5 B	61.86 (0.06)	4.83 (0.19)	1.49 (0.24)	0.62	61.69
CH5 C	46.08 (1.19)	3.73 (0.12)	1.08 (0.01)	0.72	45.88
CH5 D	na	na	na	na	na
CH5 E	26.11 (31.7)	2.30 (0.10)	2.19 (0.09)	0.63	25.94
MO A A	38.27 (3.83)	3.10 (0.06)	1.10 (0.16)	2.31	37.64
MO A B	63.21 (1.93)	4.12 (0.07)	1.53 (0.04)	0.88	62.97
KB5 A	60.23 (1.67)	4.41 (0.26)	1.43 (0.19)	1.41	59.85
KB5 B	64.09 (1.08)	4.48 (0.14)	1.89 (0.27)	1.35	63.72
GR3 A	18.41 (0.34)	1.95 (0.01)	0.63 (0.04)	1.76	17.93
GR3 B	55.69 (2.28)	4.96 (0.89)	1.62 (0.06)	1.65	55.24
CU2 A	1.93 (0.06)	0.52 (0.08)	nd	2.91	1.14
SJ8 A	36.35 (0.56)	2.65 (0.13)	1.17 (0.09)	0.95	36.09
SJ8 B	33.42 (1.29)	2.37 (0.06)	0.88 (0.03)	1.33	33.06
CU5 A	56.29 (0.58)	3.26 (0.06)	1.19 (0.07)	0.12	55.75

na. Not enough sample to analyze. nd. Analyzer problem with N determination

Table 3. Summary of yield data by Pyromat II micropyrolysis for selected coals and bitumen-extracted coals from the San Juan Basin at the nominal heating rate of 25°C/min.

Coal	Extraction Solvent	Yield, mg pyrolysate/ g coal	Yield, mg pyrolysate/ g TOC
CH5A	none	131	255
CH5A	92% CH ₂ Cl ₂ /8% MeOH	104	na
CH5A	100% THF	108	na
MOAB	none	191	303
MOAB	92% CH ₂ Cl ₂ /8% MeOH	175	na
KB5B	none	192	303
KB5B	92% CH ₂ Cl ₂ /8% MeOH	182	na
CU5A	none	91	163
CU5A	92% CH ₂ Cl ₂ /8% MeOH	59	na

na = not enough sample to measure TOC

Table 4. Approximate and discrete kinetic parameters from the best kinetic sets selected for extracted CH5A (CH5X), MOAB (MOAX), KB5B (KB5X), and CU5A (CU5X) coals.

Sample	CH5X	MOAX	KB5X	CU5X
Approximate E, ^a kcal/mol	55.9 (0.05)	55.2 (0.09)	55.2 (0.09)	63.2 (0.20)
Approximate A, 1/sec	4.83 X 10 ¹⁴	9.7 X 10 ¹³	8.64 X 10 ¹³	5.52 X 10 ¹⁵
Approximate σ , % of E	3.14	2.34	2.40	3.16
Discrete E, % of Total				
41 kcal/mol			0.09	
42 kcal/mol	0.49			
43 kcal/mol	0.33		0.25	
44 kcal/mol	0.66	0.11	0.67	
45 kcal/mol		0.01	0.63	
46 kcal/mol	0.24	0.44	1.00	
47 kcal/mol	0.29	0.19	1.07	0.80
48 kcal/mol	0.42	1.41	1.31	
49 kcal/mol	0.05	0.23	1.44	0.56
50 kcal/mol	1.03	1.86	1.84	0.74
51 kcal/mol	0.38	0.40	1.02	0.80
52 kcal/mol	1.74	0.89	1.71	0.78
53 kcal/mol	3.65	3.42	1.13	0.68
54 kcal/mol	5.26	0.35	8.15	1.78
55 kcal/mol	16.70	26.26	25.63	0.39
56 kcal/mol	21.12	22.30	20.77	2.72
57 kcal/mol	16.08	17.21	12.04	0.18
58 kcal/mol	11.98	5.17	4.56	1.67
59 kcal/mol	4.91	5.79	6.54	0.89
60 kcal/mol	3.41	3.17		10.45
61 kcal/mol	3.17	1.77	4.83	15.21
62 kcal/mol	2.03	2.10	0.10	16.02
63 kcal/mol	1.36	0.43		11.71
64 kcal/mol	2.55	3.02	4.74	8.99
65 kcal/mol				5.99
66 kcal/mol	0.89			3.03
67 kcal/mol	1.73	3.47		2.86
68 kcal/mol				6.11
69 kcal/mol				
70 kcal/mol				
71 kcal/mol				7.65
Discrete A, 1/sec	6.47 X 10 ¹⁴	1.65 X 10 ¹⁴	1.13 X 10 ¹⁴	2.40 X 10 ¹⁵
T _{max} , °C, at 25°C/min	468.06	491.78	494.94	514.51

a \pm error in kcal/mol in parentheses

Table 5. Approximate and discrete kinetic parameters from the best kinetic sets selected for CH5A, CH5X (92% CH₂Cl₂/8% MeOH extracted CH5A), CH5X with fixed A (from CH5A determination), and CH5T (THF extracted CH5A).

Sample	CH5A	CH5X	CH5X fixed A	CH5T THF extracted
Approximate E, ^a kcal/mol	56.7 (0.07)	55.9 (0.05)	55.9 (0.05)	55.7 (0.03)
Approximate A, 1/sec	9.99 X 10 ¹⁴	4.83 X 10 ¹⁴	4.83 X 10 ¹⁴	4.06 X 10 ¹⁴
Approximate σ, % of E	3.58	3.14	3.14	3.05
Discrete E, % of Total				
42 kcal/mol		0.49		1.14
43 kcal/mol		0.33		0.85
44 kcal/mol		0.44	0.28	0.18
45 kcal/mol			0.66	1.95
46 kcal/mol		0.46		0.68
47 kcal/mol		0.29	0.24	
48 kcal/mol		0.42	0.23	0.99
49 kcal/mol		0.05	0.39	
50 kcal/mol	2.41	1.03	0.15	1.65
51 kcal/mol	1.42	0.38	0.68	0.13
52 kcal/mol	2.76	1.74	0.79	3.32
53 kcal/mol	1.53	3.65	1.02	3.34
54 kcal/mol	5.92	5.26	3.48	10.56
55 kcal/mol	5.87	16.70	4.28	23.76
56 kcal/mol	12.80	21.12	11.59	15.41
57 kcal/mol	19.60	16.08	20.41	16.20
58 kcal/mol	14.07	11.98	17.40	4.57
59 kcal/mol	16.02	4.91	13.97	4.90
60 kcal/mol		3.41	7.40	3.51
61 kcal/mol	7.72	3.17	3.97	0.98
62 kcal/mol	0.40	2.03	2.79	2.62
63 kcal/mol	3.52	1.36	3.49	0.87
64 kcal/mol	0.04	2.55		
65 kcal/mol	2.39		3.88	2.38
66 kcal/mol		0.89	0.03	4.71
67 kcal/mol	1.85	1.73		0.82
68 kcal/mol	0.21		2.84	7.97
69 kcal/mol				
70 kcal/mol	1.48			
71 kcal/mol				7.27
Discrete A, 1/sec	1.74 X 10 ¹⁵	6.47 X 10 ¹⁴	1.75 X 10 ¹⁵	4.06 X 10 ¹⁴
T _{max} °C, at 25°C/min	464.48	468.06	468.06	468.87

a ± error in kcal/mol in parentheses

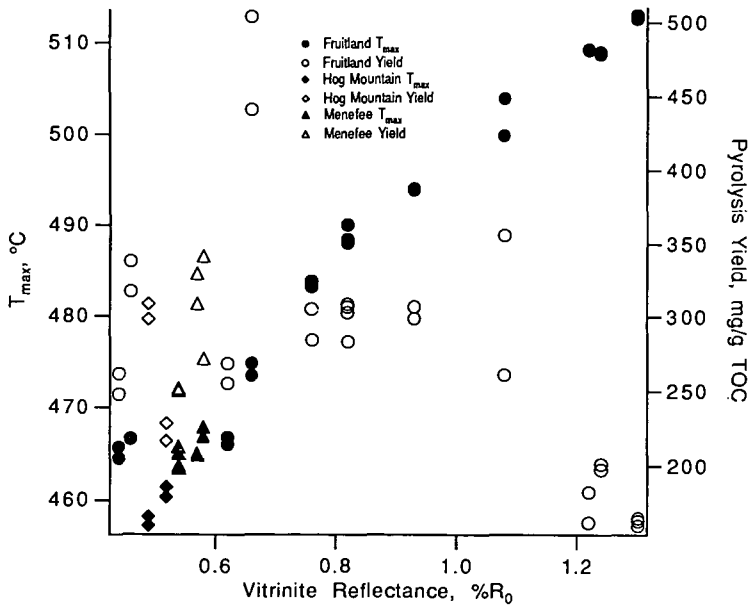


Figure 1. Relationship of maximum rate of evolution (T_{max}) and pyrolysis yield (mg/g TOC) with vitrinite reflectance ($\%R_m$) at the nominal heating rate of 25°C/min for selected coals from the San Juan Basin.

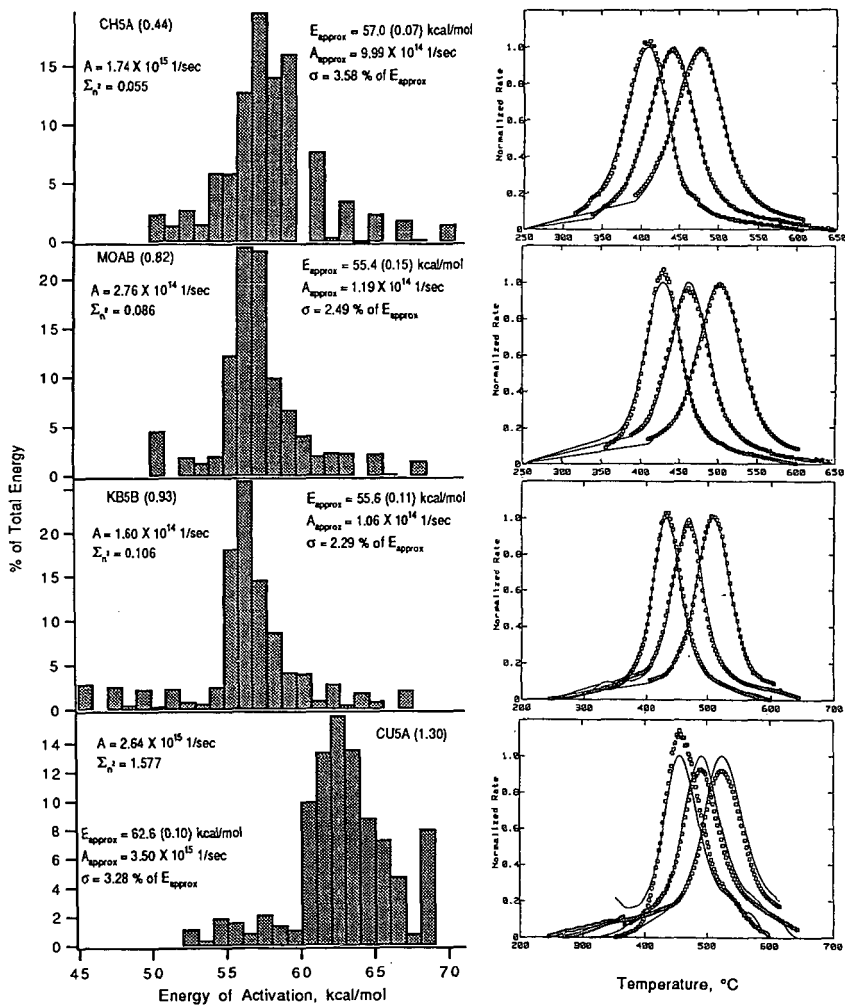


Figure 2. Approximate and discrete kinetic parameters for CH5A, MOAB, KB5B, and CU5A coals (left side) and corresponding evolution data fits from the discrete kinetic analysis (right side).

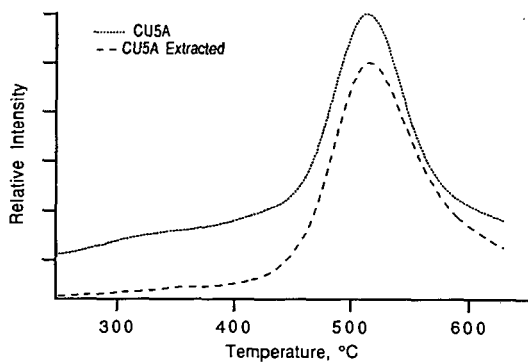


Figure 3. Evolution profiles for CU5A and extracted CU5A coals at the nominal heating rate of 25°C/min.

CURIE-POINT PYROLYSIS MASS SPECTROMETRY OF SHANXI COALS

Huaying Huai, Alec F. Gaines+ and Peter J.J. Tromp++
Center for Micro Analysis and Reaction Chemistry, University of Utah,
Salt Lake City, Utah 84112

+ Middle East Technical University, Institute of Marine Science, P.O. Box 28,
33731 Erdemli - ICEL, TURKEY

++ Institute of Chemical Engineering, University of Amsterdam,
Nieuwe Achtergracht 166, 1018 WV Amsterdam, The Netherlands

Keywords: pyrolysis mass spectrometry, coal structure, Chinese coal

ABSTRACT

Seven Shanxi (PRC) coals, having carbon contents from 80.5% to 94.2%wt (daf), have been studied by the Curie-point pyrolysis mass spectrometry technique. Markham Main (British) coal, 83.5 %C and Bulli (Australian) coal, 89.3 %C, have been used as references. As reported by other workers [1,2] studying very different depositions, three major groups of compounds, aliphatic hydrocarbons (e.g. alkenes), aromatic hydrocarbons (e.g. alkylbenzenes, alkylnaphthalenes, alkylpolyaromatics) and oxygen containing aromatics (e.g. alkylphenols, dihydroxybenzenes), were prominent amongst the pyrolysis products. The relative proportions of oxygen containing compounds and aromatic hydrocarbons, illustrated by the ratio of the intensities of the m/z 156/108 peaks, change with rank. The spectra are consistent with the low lignite content and the moderately low sulfur contents of Shanxi coals.

INTRODUCTION

Pyrolysis-mass spectrometry (Py-MS) was first introduced as a promising technique for the study of polymers in 1948 [3,4]. In 1973, Meuzelaar et al. [5] designed a Py-MS system in which products from a Curie-point pyrolyzer were ionized by low energy electrons so that molecular, rather than fragment, ions were formed and passed directly into a quadrupole mass spectrometer. Since then many studies of solid fuels have been reported [1,6,7,12-18]. These studies have shown coal pyrograms to be dominated by series of ions representing several groups of aromatic and aliphatic hydrocarbons as well as heteroaromatic compounds. Differences between the spectra were shown to correlate with rank (maturity) [1,3], maceral composition [12,14] and reactivity towards liquefaction [10,11].

Thus, the method gives detailed, and at least semiquantitative information about the structures of the complex but volatile products obtained from the pyrolysis of solid fuels at rather fast rates of heating. Moreover, there is a sufficient bank of existing data in the literature that the nature of the products from any individual coal can be related to such parameters as its maceral group composition, its deposition and its rank.

The North China Block (tectonic plate), approximately coincident with Shanxi Province, gives rise to about one third of China's current production of coal. As part of a study to delineate the organic geochemistry of Shanxi coals and to relate the chemistry of these coals to their present and potential use, seven Shanxi bituminous coals, covering a range of rank from 80.5 to 94.2 %C (daf) have been studied by means of Curie-point Py-MS. The results have been compared with those from well characterized coal deposited in Euramerica (Markham Main coal, Britain) and another deposited in Gondwanaland (Bulli coal, New South Wales, Australia).

EXPERIMENTAL

Sample Preparation

Nine coals were sampled for this study. Seven of these were mined from six coalfields of Shanxi Province, PRC [19]. Markham Main and Bulli coals were mined in Yorkshire (Britain) and in New South Wales (Australia), respectively. The elemental composition of the coals is given in table 1. The samples were ground in a nitrogen - filled glove box to a particle size smaller than 63 μm , dried in a vacuum oven at 70 C for 3 hours, sealed under nitrogen and kept in a deep freeze until needed. The samples for each experiment were taken from a coal/water slurry, prepared by impregnation of the ground coal sample with deionized water until the pore volume was filled. Aliquots ($\sim 50 \mu\text{m}$) from these slurries were applied with a spatula to ferromagnetic pyrolysis wires on which they were air-dried.

Pyrolysis Mass Spectrometry Analysis

The Curie-point Py-MS technique has been described elsewhere [2]. Within 1 hour of coating, the wire samples were pyrolyzed at a Curie-point temperature of 770 K (pure iron wires), previously found to be optimal for the pyrolysis of coal samples. The pyrolysis conditions were: vacuum, $\sim 10^{-4}$ Pa; heating time, 0.1 sec; and heating rate, ~ 7000 C/sec. The mass spectrometer conditions were: temperature of the expansion chamber, 200 C; electron energy, 15 eV; mass range scanned, m/z 25-225; scan speed, 10 scans/sec; and total number of spectra averaged, 200. Each coal slurry was analyzed in triplicate.

RESULTS AND DISCUSSION

The pyrolysis mass spectra of the coals, including the Markham Main and Bulli coals, are shown in Figure 1 in order of increasing rank of coal. The spectra include peak sequences apparently representing suites of limited numbers of homologous compounds. The chemical structures and corresponding mass numbers of the most important species are given in table 2.

The differences between the spectra in Figure 1 appear to be related primarily to rank. In agreement with the known effects of rank on the chemical composition of coals, the relative intensities of aromatic compounds which do not contain oxygen functional groups, such as alkylbenzenes (m/z: 78, 92, 106, etc.), alkyl-naphthalenes (m/z: 128, 142, 156, etc.), and alkylphenanthrenes/anthracenes (m/z: 178, 192, 206, etc.) increase with rank, whereas the intensities of such oxygen containing aromatic hydrocarbons as alkylphenols (m/z: 94, 108, 122, etc.) decrease. Since relatively few samples were used in this study, factor and/or discriminant analysis were not applied. However, the ratio of the relative intensities of the m/z 156 (C2-naphthalenes) and the m/z 108 (C1-phenols) peaks as functions of the carbon content and the atomic ratio of oxygen/carbon (Figure 2 and 3, respectively) illustrates the rank dependence. Due to very low absolute amounts of ions generated, the results from the anthracite, Fenghuang Shan coal, are not included in the Figures 2 and 3. It is to be noted that the results from Bulli coal differ from those of Shanxi coals of similar rank. Bulli coal contained 74.5% of inertinite with a rather large amount of fusinite [19]. Consequently, the spectra of Bulli coal, containing prominent alkylbenzenes, resemble the fusinite spectra obtained by Larter [6]. Other features of the mass spectra derived from Shanxi coals are: (1) low H_2S formation (m/z 34) consistent with the moderately low sulfur content indicated by the elemental analyses (Table 1), and (2) low formation of alkanes (m/z: 58, 72, 86, etc.) consistent with the low liptinite content of these coals [19].

Finally, the coherence of the pyrolysis mass spectra of coals from depositions on different tectonic plates and in different climatic conditions is part of the evidence that the whole coal family, which may now be taken to include the Shanxi coals, shares a common system of structural chemistry [2]. Differences in pyrolysis mass spectra are caused by variations in the rank of the coal (that is, by differences in the geochemical temperatures to which the coals were subjected [20]) and, to a lesser extent, by differences in their maceral group composition (that is, by variations in the original flora and the degree to which it was preserved by the deposition). That being written, it should be understood that the volatile products examined by Py-MS may have structures which are the result of secondary, retrogressive reactions as well as of the structures in the original coals. Relatively few of the mass spectra generated by the Shanxi coals contained hydroaromatic structures characteristic of vitrinite [21] and the presence of alkanes is direct evidence of cracking.

CONCLUSIONS

Curie-point pyrolysis of seven coals from the North China Block generated volatiles in which alkenes, alkylaromatics, alkylphenols and dihydroxylbenzenes were prominent. The ratio of the C2-naphthalenes to the C1-phenols produced by the pyrolyses increased with the rank of the coals. The pyrolysis products, though they may have suffered retrogressive, secondary reactions, are nevertheless consistent with the coals from the North China Block having the structures expected of lipinite poor, bituminous coals.

ACKNOWLEDGEMENTS

This work was conducted in the FOM Institute for Atomic and Molecular Physics (The Netherlands) and partially funded by Taiyuan University of Technology (PRC) and the SEDC (UK). The authors would like to thank Professors Colin D. Flint and Jacob A. Moulijn for their encouragement.

REFERENCES

1. Meuzelaar, H.L.C.; Harper, A.M.; Hill, G.R.; Given, P.H. *Fuel*, 1984, 63, 640.
2. Tromp, P.J.J. *Ph.D. Thesis*, 1987, University of Amsterdam, The Netherlands.
3. Madorsky, S.L.; Strauss, S. *Ind. Eng. Chem.*, 1948, 40, 848.
4. Wall, L.A. *J. Res. Nat. Bur. Stand.*, 1948, 41, 315.
5. Meuzelaar, H.L.C.; Kistemaker, P.G. *Anal. Chem.*, 1973, 45, 587.
6. Larter, S.R. *Ph. D. Thesis*, 1978, University of Newcastle upon Tyne, U.K.
7. Meuzelaar, H.L.C.; Harper, A.M.; Pugmire, R.J. *ACS Preprints, Div. Fuel Chem.*, 1983, 28(1), 97.
8. Meuzelaar, H.L.C.; Hoesterey, B.L.; Windig, W.; Hill, G.R. *Fuel Proc. Tech.*, 1986, 15, 59.
9. Huai, H.; Lo, R.; Yun, Y.; Meuzelaar, H.L.C. *ACS Preprints, Div. Fuel Chem.*, 1990, 35(3), 816.
10. Meuzelaar, H.L.C.; Wood, R.W.; Futrell, J.H.; Wojcik, L.H. *Proc. 28th Ann. Conf. Mass Spectrom. All Topics*, New York City, 1980, 460.
11. Meuzelaar, H.L.C.; McClennen, W.H.; Tomlinson, J.H.; Pope, D.L. *Proc. Int. Conf. Coal Sci.*, Dusseldorf, 1981, 816.
12. Meuzelaar, H.L.C.; Harper, A.M.; Pugmire, R.J.; Karas, J. *Intl. J. Coal Geol.*, 1984, 4, 143.
13. van Graas, G.; De Leeuw, J.W.; Schenck, P.A. *J. Anal. Appl. Pyrol.*, 1980, 2, 265.
14. Nip, M.; De Leeuw, J.W.; Schenck, P.A. *Geochim. Cosmochim. Acta*, 1988, 52, 637.
15. Nip, M. *J. Anal. Appl. Pyrol.*, 1987, 11, 125.
16. Nip, M.; De Leeuw, J.W.; Schenck, P.A.; Windig, W.; Meuzelaar, H.L.C. *Geochim. Cosmochim. Acta*, 1989, 53, 671.
17. Chaffec, A.L.; Johns, R.B.; Baerken, M.J.; De Leeuw, J.W.; Schenck, P.A.; Boon, J.J. In: *"Advances in Organic Geochemistry, Org. Geochem."* (Schenck, P.A.; De Leeuw, J.W.; Lijmbach, G.W.M. Eds.), 1983, 6, 409.

18. Eglinton, T.I.; Larter, S.R.; Boon, J.J. *J. Anal. Appl. Pyrol.*, 1991, 20, 25.
19. Huai, H. *Ph.D. Thesis*, 1989, University of London, U.K.
20. Teichmuller, M.; Teichmuller, R. In: "*Stach's Textbook of Coal Petrology.*" (Stach, E.; Taylor, G.H.; Mackowsky, M-Th.; Chandra, D.; Teichmuller, M.; Teichmuller, R. Eds.), Gebruder Borntraeger, Berlin, 3rd Edition, 1982, pp. 5-86.
21. Davis, M.R.; Abbott, J.M.; Cudby, M.; Gaines, A.F. *Fuel*, 1988, 67, 960.

Table 1. Elemental Composition of Coal Samples

Sample	Weight % daf					
	C	H	N	S	O(diff)	O/C
Pinglu Erpu coal	80.5	4.9	1.3	0.6	12.7	0.118
Markham Main coal	83.5	5.1	1.4	1.0	9.0	0.081
Datong Jueqiang Buxiang coal	83.9	5.2	0.9	0.9	9.1	0.083
Xuangang Jiaojia Zhai coal	86.2	5.2	1.7	1.8	5.1	0.044
Xishan Gujiao coal	86.9	5.0	1.6	1.4	5.1	0.044
Fenxi coal	89.9	5.1	1.5	0.5	3.0	0.025
Bulli coal	89.3	4.9	1.7	0.5	3.6	0.030
Jishuigou coal	89.6	4.8	1.2	1.2	3.2	0.027
Fenghuang Shan coal	94.2	2.9	0.9	0.9	1.1	0.009

Table 2. Chemical Structures and Corresponding Mass Numbers of the Most Important Compounds and Groups of Homologous Compounds, Present in the Mass Spectra of the Coals

Groups of homologous compounds	Chemical Structures with corresponding mass numbers
Alkenes	$C_2H_4(28)$; $C_3H_6(42)$; $C_4H_8(56)$; $C_5H_{10}(70)$; etc.
Benzenes	 (78);  (92);  (106);  (120); etc.
Naphthalenes	 (128);  (142);  (156); etc.
Phenanthrenes &	 (178);  (192);  (206); etc.
Anthracenes	 (178);  (192);  (206); etc.
Phenols	 (94);  (108);  (122); etc.
dihydroxybenzenes	 (110);
Sulfur compounds	$H_2S(34)$; $CH_3SH(48)$;

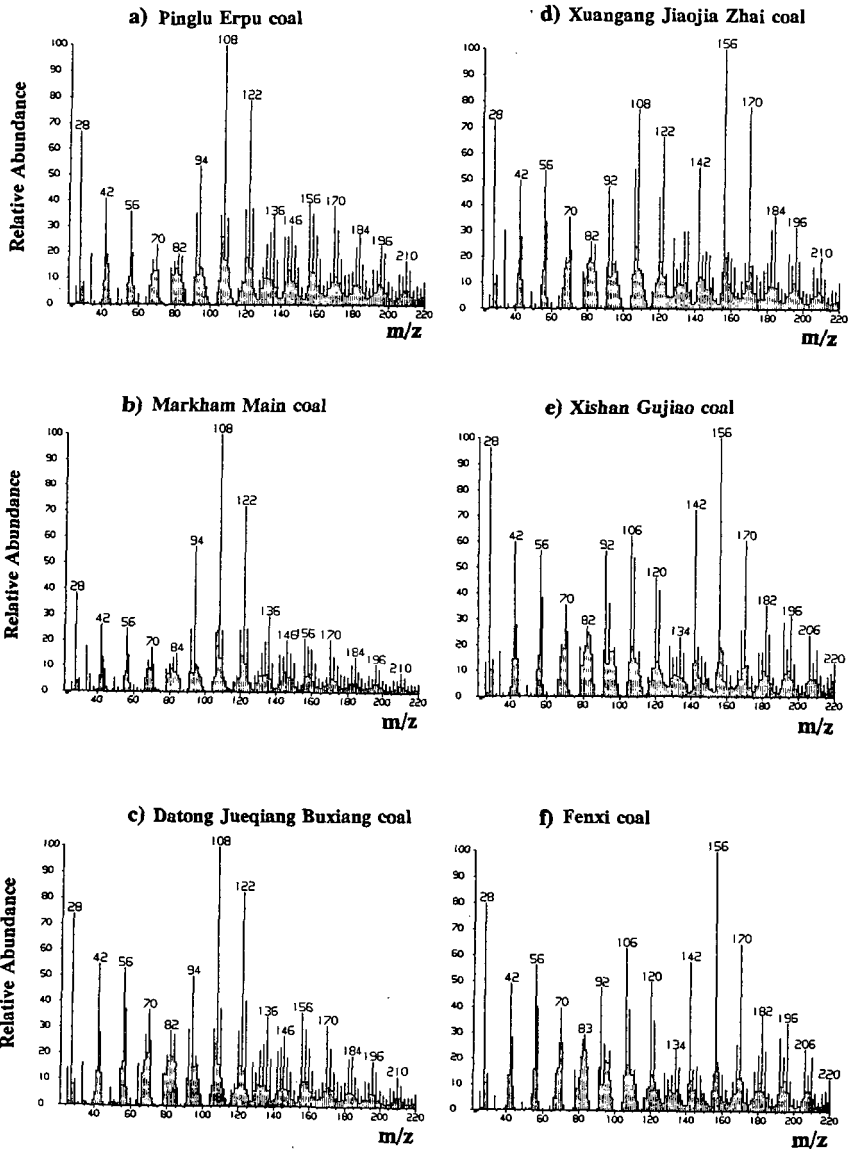


Figure 1. Average mass spectra of coals.

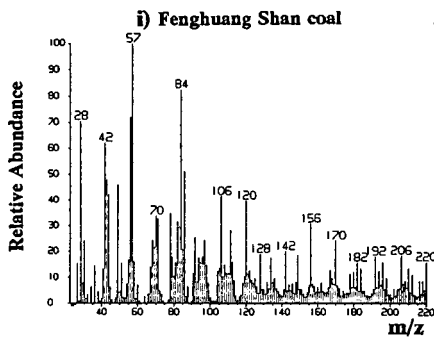
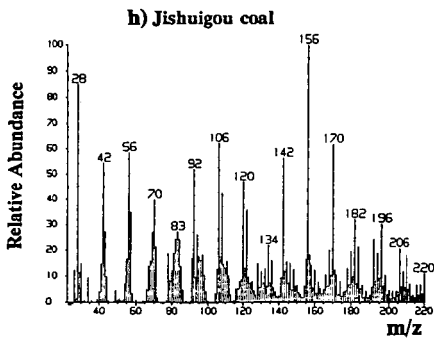
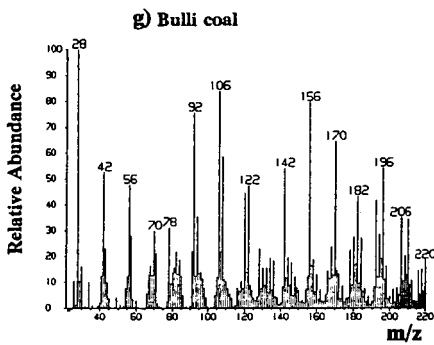


Figure 1. (continued).

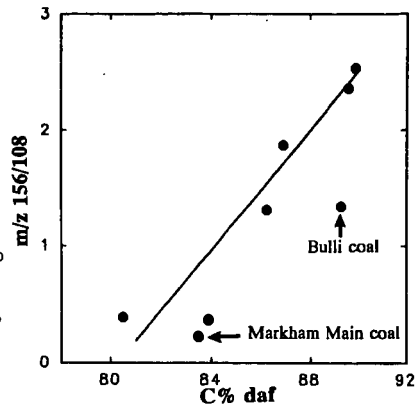


Figure 2. Variation of the ratio of m/z 156/108 from Py-MS with carbon content of coals.

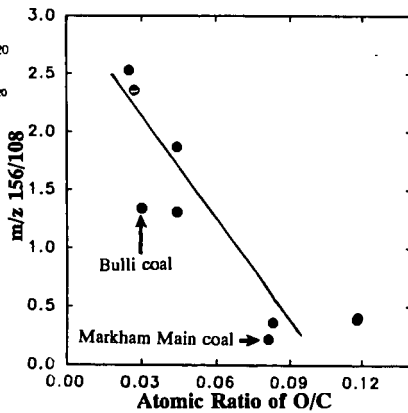


Figure 3. Variation of the ratio of m/z 156/108 from Py-MS with atomic ratio of O/C of coals.

FT-I.R. STUDY OF OXYGENATED FUNCTIONAL GROUPS DISTRIBUTION
DURING DRY-PHASE OXIDATION OF COALS.

V. Calemma, P. Iwanski, R. Rausa and E. Girardi
Eniricerche SpA, 20097 San Donato Mil.se, Milan, Italy

Keywords: coal, oxidation, FT-i.r.

INTRODUCTION

When coal is oxidized with air in dry-phase conditions at temperatures higher than 150 °C, besides the well known alteration of several coal properties [1], a mixture of base extractable substances is formed in considerable yields after a few hours [2]. These substances are generally referred to as regenerated humic acids (RHA). Although details of chemical changes in coal "molecule" caused by air oxidation are only partially understood, the results of spectroscopic and chemical studies on dry oxidized coals are consistent with a preferential oxidation of the aliphatic part of coal structure, leading to a more aromatic product and to a concomitant formation of various oxygenated functional groups (-COOH, C=O, CO-O-CO, etc.) [3,4]. In a previous FT-ir study [4], performed on a subbituminous B coal oxidized between 175 and 275 °C, only the overall trend of carbonyl groups was presented and no considerations about the behavior of hydroxyl groups were made owing to the complexity of regions where oxygenated functional groups absorb. The objective of this work was to detect and determine, the formation and relative changes in concentration of various oxygenated functional groups as a function of oxidation time by applying the curve-resolving procedure and acetylation of coal samples. The aim was to gain a better understanding of the structural modification which occur during the formation of RHA.

EXPERIMENTAL

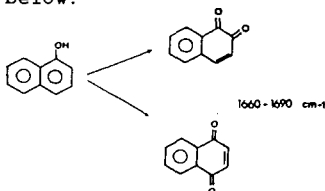
Two U.S coals (M. Rosebud and a subbituminous B) were used in this study. Their ultimate and proximate analyses are given in table 1. The as received coals were crushed, sieved and the fraction 106-250 µm was used throughout this investigation. Oxidation tests were performed in a steel fluid bed reactor, at 200 °C, with air pressure of 0.2 MPa and reaction times up to 4 hours. For each run the reactor was charged with 30 g of dried coal heated (in flowing N₂) and pressurized. Subsequently the coal sample was reacted switching over the nitrogen flow with a controlled flowrate of preheated air. For all runs the gas superficial velocity was 5.1 cm/sec. After reaction, oxidation was stopped by feeding nitrogen and after that the reactor was depressurized and cooled to room temperature. Finally, the oxidized coal samples were subjected to elemental analysis, characterized by FT-ir spectroscopy and selected samples were acetylated to determine hydroxyl groups. Experimental procedures used for preparing KBr pellets and obtaining FT-ir spectra of coal samples have been described elsewhere [4]. The latter were obtained on a Digilab ETS/15 FT-ir spectrometer. The

characterization of region between 1900 and 1450 cm^{-1} , was achieved through curve-fitting procedure, performed using the software supplied with the Data General processing system. The parameters requested in deconvolution procedure are mainly the number of bands, their positions, the gaussian coefficient and the base line intercepts. The gaussian coefficient was fixed at 0.3. The number of bands was determined after a critical examination of the second derivative of the spectra. Their position was recalculated iterating the fitting procedure. For each spectrum the base line was drawn between two points where no absorption occurs, namely around 1800 and 730 cm^{-1} . Acetylation of raw and oxidized coal samples was conducted following the procedure set up by Blom et al.[5]. No attempt was made to demineralize the coal samples prior acetylation.

RESULTS AND DISCUSSION

Figure 1 shows FT-ir spectra of Montana Rosebud coal at various oxidation degrees. From a general point of view the evolution is similar for both coals and as observed by other investigators [6] the most remarkable changes are those occurring in the regions 3000-2700 cm^{-1} (aliphatic C-H₁ stretching), 1800-1600 cm^{-1} (C=O stretching) and 1300-1000 cm^{-1} (-C-O-C- stretching, phenolic and alcoholic C-O stretching, OH bending, etc.). As the reaction time increases the absorption due to aliphatic groups decreases while the absorption bands due to C=O stretching and present in the region 1300-1000 cm^{-1} display a noteworthy increase. Figure 2 shows the FT-ir spectrum of subbituminous B coal between 1870 and 1450 cm^{-1} and its second derivative. Upon examination, fig.2 reveals the presence of three well defined maxima (1770, 1718 and 1608 cm^{-1}) and shoulders or secondary maxima to be distinguished from possible artifacts. This situation was verified to be valid for each spectrum of coal samples examined. As an example of the results obtained through curve fitting procedure, fig. 3 shows the infrared spectrum of a oxidized coal sample curve-resolved into nine bands. The choice of number and position of component bands was made on the basis of the second derivative of spectrum, FT-ir measurements on ion exchanged and acetylated coal samples and results obtained by other investigators in similar works [7,8,9]. Assignments of component bands are given in table 2. In this connection it is important to stress that owing to unavoidable interference of adjoining bands, the presence of different molecular situations and its modifications caused by oxidation, the absorption frequency of bands resulting from the curve fitting procedure have undergone slight shifts (generally $\pm 5 \text{ cm}^{-1}$) during reaction. The structural changes observed were similar for both coals examined and the most remarkable concerned the bands at 1771, 1734, 1711, 1684 and 1648 cm^{-1} whose evolution is reported in figures 4 and 5. On the contrary bands located at 1608, 1585, 1568 and 1542 cm^{-1} as expected did not display significant variations. The results presented in the figures 4 and 5 show that the evolution of different functional group containing C=O is qualitatively similar for both coals and as the reaction proceeds the concentration of each group increases. However significant differences exist between the two coals as regards the formation rates and relative concentration of various C=O groups during reaction. Previous results obtained by FT-ir and ¹³C-NMR [4,10] showed that at 200 °C the oxidation occurs almost exclusively on the aliphatic part

of coal structure. Therefore the formation of different oxygenated functional groups detected by I.R. spectroscopy can be explained in terms of oxidative destruction of aliphatic structures. Considering the Wisser model of coal structure [11], where polyaromatic and hydroaromatic units are joined by short aliphatic chains and various ether linkages to form a three-dimensional network, it is possible to single out some structural units, which through the oxidation of aliphatic part, can give rise to the formation of detected oxygenated functional groups. Some possible reaction pathways, worked out on the basis of the results obtained, and considering the different reactivity of various structures towards the oxygen, are given in figure 6. The changes in hydroxyl groups content (alcoholic and phenolic) upon oxidation at 200 °C was determined by measuring the area of the peaks centred at 1367 cm^{-1} (CH_2 bending) and 1187 cm^{-1} (-C-O- stretching) of acetylated coal samples. Before discussing the data it is important to stress that the bands used to follow the hydroxyl behavior are due to phenolic and alcoholic group. However literature data[9] show that the content of the latter is much lower than that of phenolic group. In addition, some results of curve fitting procedure of the complex spectral band due to the C=O stretching of acetyl group indicate that the R-OH/Ar-OH ratio remains almost constant during reaction at 200 °C. Therefore the trend observed should reflect the behavior of phenolic group. The trend reported in figure 7 shows a noteworthy decrease of hydroxyl groups contents in the first hour of oxidation followed by a levelling off at longer reaction times. It is known that the presence of hydroxyl groups activate the aromatic ring towards oxidation and that phenols are easily oxidized to quinones, which subsequently can evolve to carboxyl through rupture of benzenic ring [12]. Therefore the observed trend can be interpreted by the reaction scheme given below:



Furthermore, the disappearance of hydroxyl groups can also be a result of condensation reactions between hydroxyl and carboxyl or hydroxyl groups to form esters and ethers bonds respectively. The latter might have a negative effect on RHA formation for the alkaline hydrolysis of ether bond occurs with difficulty and demands more drastic conditions than those used to determine the alkali solubility of oxidized coal [2,13].

CONCLUSIONS

The changes of coal structure caused by molecular oxygen at 200 °C have been evaluated by FT-ir spectroscopy and acetylation of coal samples. The results indicate that the oxidative process leads to the formation of different oxygenated functional groups such as carboxyls, ketones, conjugated carbonyls and various type of esters. Their evolution with time as well as the trend of hydroxyl groups

has been determined. On these grounds some reaction pathways which explain the oxygenated functional group formation in terms of oxidative attack of aliphatic structure have been presented. Keeping in mind the coal structure proposed by Wiser [11], a major conclusion of this work is that formation of RHA should be mainly associated with the break-down of aliphatic structure which lead to smaller fragments (through oxidation of links between aromatic and hydroaromatic clusters) and to a concomitant increase of oxygenated functional groups which make these substances soluble in alkali solution.

REFERENCES

1. M.Rashid Khan and R.G. Jenkins in "Chemistry of coal weathering" Ed. by C.R. Nelson, Elsevier, Amsterdam, 1989, chapter 5.
2. V. Calemma, R. Rausa and E. Girardi, Proc. of the 1989 Int. Conf. on Coal Science, Tokyo, Japan, vol.1, pg. 233.
3. J.R. Havens, J.L. Koenig, D. Kuehn, C. Rhoads A. Davis and P.C. Painter, Fuel 62, 936, (1983).
4. V. Calemma, R. Rausa, R. Margarit and E. Girardi, Fuel 67, 764, (1988)
5. L. Blom, L. Edelhausen and D.W. van Krevelen, Fuel 38, 537, (1959)
6. J.K. Kister, M. Guiliano, G. Mille and H. Dou, Fuel 67, 1076, (1988).
7. C.A. Rhoads, J.T. Senftle, M.M. Coleman, A. Davis and P.C. Painter, Fuel 62, 1387, (1983)
8. P. Painter and C. Rhoads, ACS., Fuel Chem. Div. Prep. 26(1), 35, (1981)
9. P. Painter, M. Starsinic and M. Coleman, in "Fourier Transform Infrared Spectroscopy", Ed. by J.R. Ferraro and L.J. Basile, Academic Press, 1985, vol. 4, chapter 5.
10. R. Rausa, V. Calemma, S. Ghelli and E. Girardi, Fuel 68, 1168, (1989)
11. W.H. Wiser, ACS Symp. Ser. 71, 29, (1978)
12. M. Lj. Mihailovic and Z. Cekovic in " The Chemistry of Hydroxyl Group", Ed. by S. Patai, John Wiley & Sons (Interscience), 1971, part 1, chapter 10, pg.505
13. E. Staude and F. Patat in " the Chemistry of ether linkage", Ed. by S. Patai, John Wiley & Sons (Interscience), 1969, chapter 2, pg. 46.

	Sub.B*	M. Rosebud*	Wavenumber (cm^{-1})	Assignment
%C	63.5	63.0	1770	Ar-O-CO-R (1775-1765)
%H	4.7	4.1	1734	R-O-CO-R (1750-1735)
%N	1.1	1.0		Ar-CO-OR; Ar-O-CO-Ar (1740-1715)
%S	0.9	0.7		
%O (by diff.)	20.5	14.7	1711	-COOH (1720-1705)
%Ash	9.6	16.5	1684	Ar-CO-R (1700-1670)
%V.M.	44.1	39.4	1648	Ar-CO-Ar (1680-1640)
				Quinones as: 2 C=O in two rings (1655-1635)
			1608	aromatic stretching
			1585	aromatic band [9]
			1562	$-\text{COO}^- \text{M}^+$
			1541	$-\text{COO}^- \text{M}^+$

* moisture free basis

Table 1. Characteristics of utilized coals

Table 2. Band Assignments

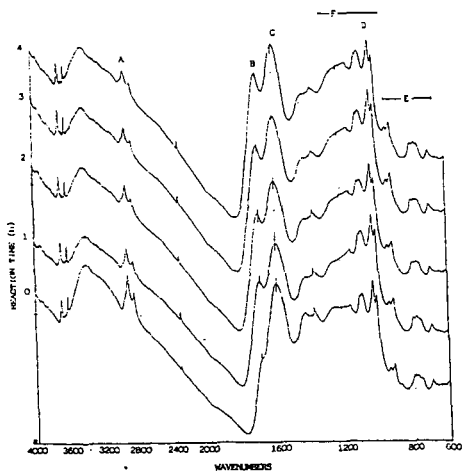


Figure 1. FT-ir spectra of Montana Rosebud coal at various oxidation degrees. A: aliphatic; B: C=O stretching; C: aromatic stretching; D: mineral matter; E: aromatic C-H out of plane bending; F: C-O stretch., C-C stretch., OH bending, etc.

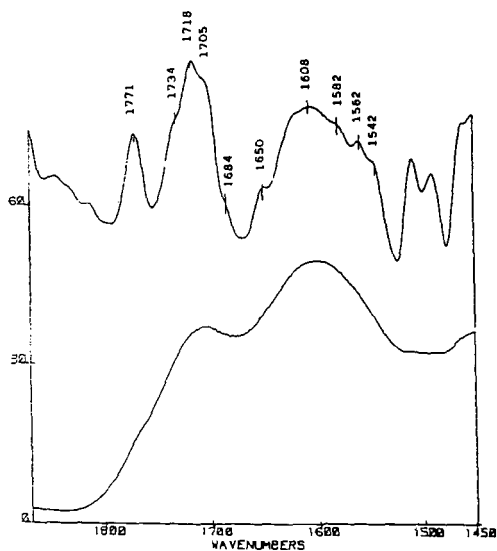


Figure 2. Bottom : FT-ir spectrum of oxidized subbituminous B coal between 1850 and 1450 cm^{-1}
 Top: Second derivative of spectrum

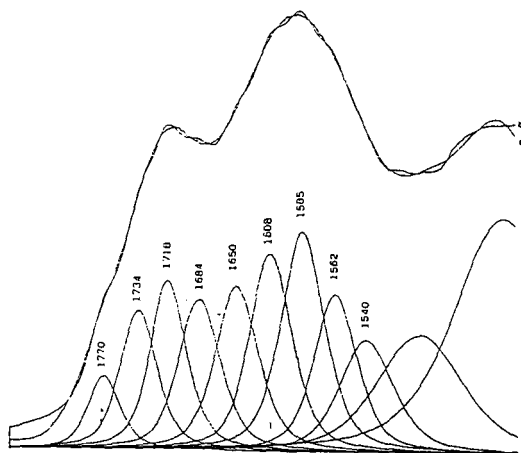


Figure 3. FT-ir spectrum of oxidized Montana Rosebud coal between 1850 and 1450 cm^{-1} and component bands from curve fitting procedure.

Figure 4. M. Rosebud coal, evolution of various oxygenated functional groups containing C=O

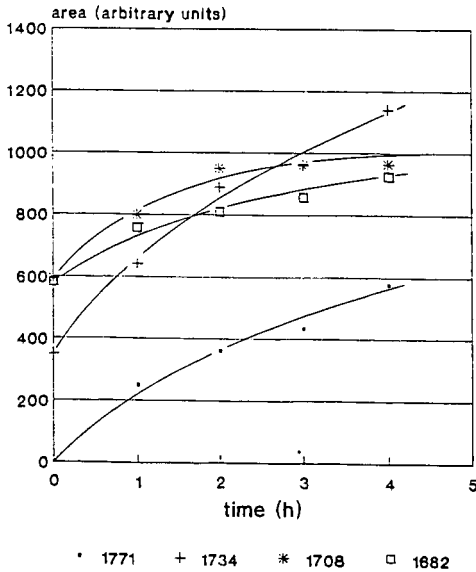
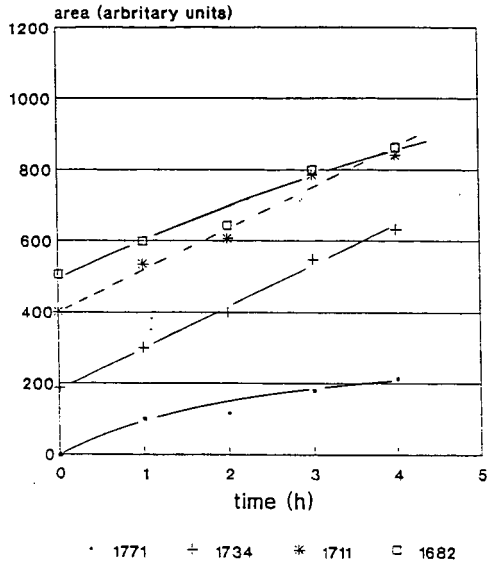


Figure 5. Subbituminous B coal, evolution of various oxygenated functional groups containing C=O

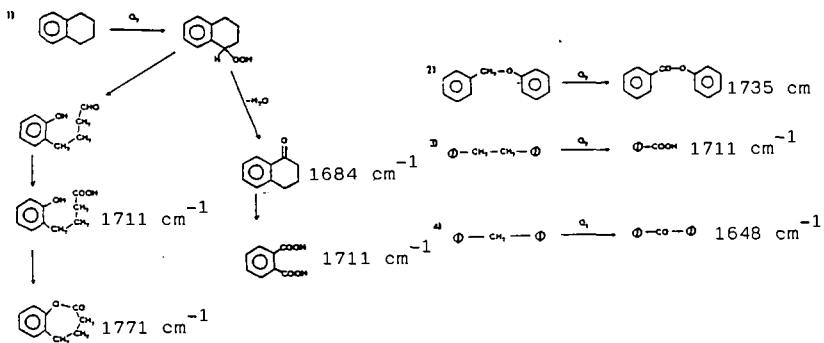


Figure 6. Scheme depicting the proposed reaction pathways that may occur during the oxidation on the grounds of FT-ir results.

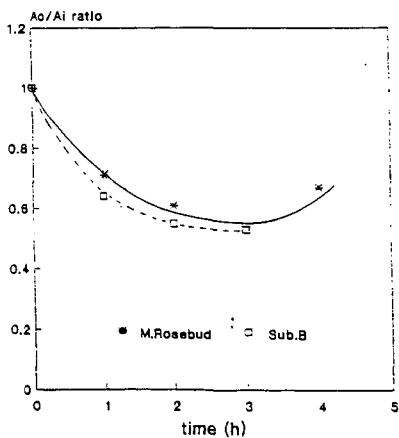


Figure 7. Graph of the fractional change in the peak area (1187 cm^{-1}) of hydroxyl groups versus oxidation time.

EVOLUTION OF VOLATILE SULFUR COMPOUNDS DURING TEMPERATURE-PROGRAMMED
PYROLYSIS-COMBUSTION WITH A QUADRUPOLE GAS ANALYZER

K.C. Hackley and C.-L. Chou
Illinois State Geological Survey
615 East Peabody Drive
Champaign, IL 61820

Keywords: coal pyrolysis-combustion, volatile sulfur species, quadrupole gas analyzer

The evolution of sulfur species during combustion of pyrolysis volatiles from coal IBC-109 (1.13% sulfur, 0.42% chlorine) of the Illinois Basin Coal Sample Program has been studied using a pyrolysis-combustion apparatus in conjunction with a quadrupole gas analyzer (QGA). This work is part of an on-going project which investigates the role of sulfur and chlorine in coal in boiler corrosion. A better understanding of the behavior of these elements in coal during combustion may help elucidate the mechanism of boiler corrosion. The experimental conditions are designed to simulate the formation of sulfur compounds during coal combustion.

The pyrolysis-combustion apparatus used with the QGA to study the release of gases from coal is capable of heating the coal sample from the ambient to about 850°C at different heating rates. Major components include a quartz tube reactor, a gas flow controller, two split-tube furnaces, a programmable temperature controller, 50- μ m capillary tubing connecting a Dycor QGA to the pyrolysis system, and a microcomputer (Fig. 1). Approximately 0.5 gram of coal is heated nonisothermally under a controlled atmosphere (air, nitrogen, oxygen, or other gases) in the quartz-tube reactor which consists of two consecutive chambers. The coal is pyrolyzed in the first chamber under a nitrogen atmosphere and the volatile products are carried to the second chamber where they are combusted at 850°C under a constant flow of oxygen. The gaseous products are sampled through the capillary tube and monitored with a quadrupole gas analyzer. The different gaseous species are determined in the QGA by monitoring the atomic mass associated with different species, such as mass 64 for SO₂ and 44 for CO₂. The data from the QGA and temperature controller are transmitted to a microcomputer and stored as ASCII files on the hard disk.

The release of sulfur compounds from the coal was monitored as the temperature was increased from the ambient to 850°C at a heating rate of 50°C/min. Sulfur dioxide (SO₂) was released from coal IBC-109 primarily between 250° and 650°C (Fig. 2). The SO₂ profile showed a small initial release of sulfur between 250° and 400°C followed by a main peak between 400° and 550°C with a maximum at 510°C, and then by a small peak close to 625°C. The main SO₂ peak is associated with the release of volatile matter from the coal. The smaller higher temperature peak is probably associated with the release of pyritic sulfur^{1,2}. The initial small broad peak of SO₂ is unusual relative to other SO₂ profiles from Illinois coals² but may be characteristic of this sample. Perhaps there is a significant amount of weakly bonded organic sulfur compounds which are released in the initial volatilization of IBC-109.

When the combustion atmosphere was changed to a reducing condition, gaseous COS and H₂S were detected. Figure 3 compares the profiles for SO₂ and COS under an oxidizing condition where the excess oxygen concentration in the combustion chamber never fell below 5 percent (Run 3) to where a reducing condition occurred in the combustion chamber during the major release of volatiles (Run 4). An

obvious peak was obtained for COS in Run 4. The H₂S profile is more difficult to comprehend because of the presence of oxygen isotope ¹⁸O in the oxygen flow. The combination of ¹⁸O and ¹⁶O gives a mass of 34 for oxygen (¹⁶O¹⁸O), the same as H₂S. Thus the profile of mass-34 will mimic that of O₂ (mass 32). When O₂ is consumed, the oxygen (mass 32) will drop to background levels as will the ¹⁶O¹⁸O profile (mass 34). Figure 4 shows this effect for masses 32 and 34 of a blank run where the oxygen flow was shut off between 400° and 625°C. If H₂S is present under a reducing condition, a peak should occur in the mass-34 profile during the period of O₂ depletion. Figure 5 shows typical profiles of sulfur species, including mass 34, obtained when the O₂ was consumed during the experiment. The H₂S peak is observed in the trough of the mass-34 profile. As the rate of volatile gases released from the coal sample decreases, the O₂ concentration is no longer completely consumed and the reduced gas species disappear.

For this high-chlorine coal, we also attempted to monitor the evolution of HCl gas (mass 36) with QGA. Only a very weak peak was obtained for mass 36 during complete combustion with sufficient oxygen however, when the combustion atmosphere was under a reducing condition, a better gas release profile was obtained for the species of mass 36. This improved profile of mass-36 is probably not due to HCl. With the occurrence of H₂S under the reducing condition, the enlarged peak of mass-36 (Fig. 5) is most probably a result of the presence of the naturally occurring heavy sulfur isotope ³⁴S in the hydrogen sulfide (H₂³⁴S, total mass = 36).

Thus, the sulfur species formed in the combustion gas are controlled by the oxidizing condition in the combustion chamber. The experiments indicate that sulfur dioxide (SO₂) is the predominant sulfur species observed during combustion of pyrolysis volatiles. In some of the experiments, during the major release of volatiles, between 450° and 550°C, all oxygen in the pyrolysis system was consumed and a reducing condition occurred which resulted in the detection of additional sulfur species (COS and H₂S).

This work has been sponsored by the Illinois Department of Energy and Natural Resources through its Coal Development Board and Center for Research on Sulfur in Coal, and the U.S. DOE.

References

1. Oh M.S., Burnham A.K. and Crawford R.W., ACS Fuel Chemistry Division Preprints 33 (1), 274 (1988).
2. Hackley K.C., Frost R.R., Liu C.-L., Hawk S.J. and Coleman D.D., Illinois State Geological Survey Circular 545, 33 p. (1990).

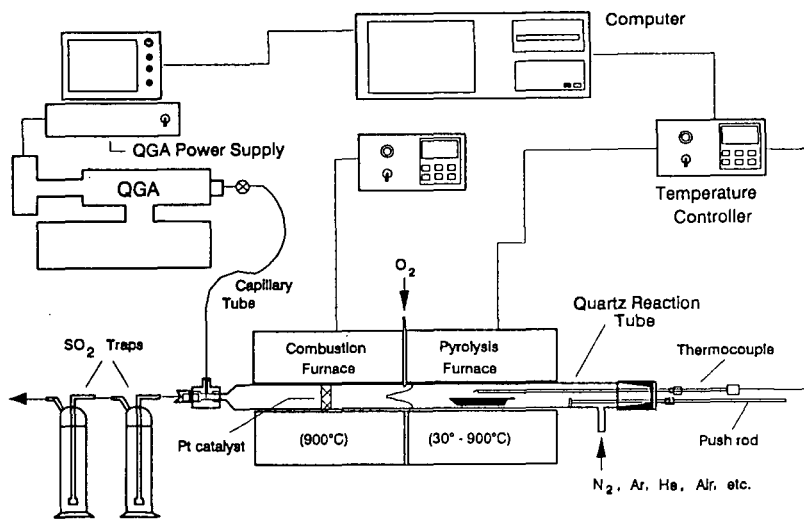


Figure 1. The experimental setup of a temperature-programmed pyrolysis-combustion system in conjunction with a quadrupole gas analyzer.

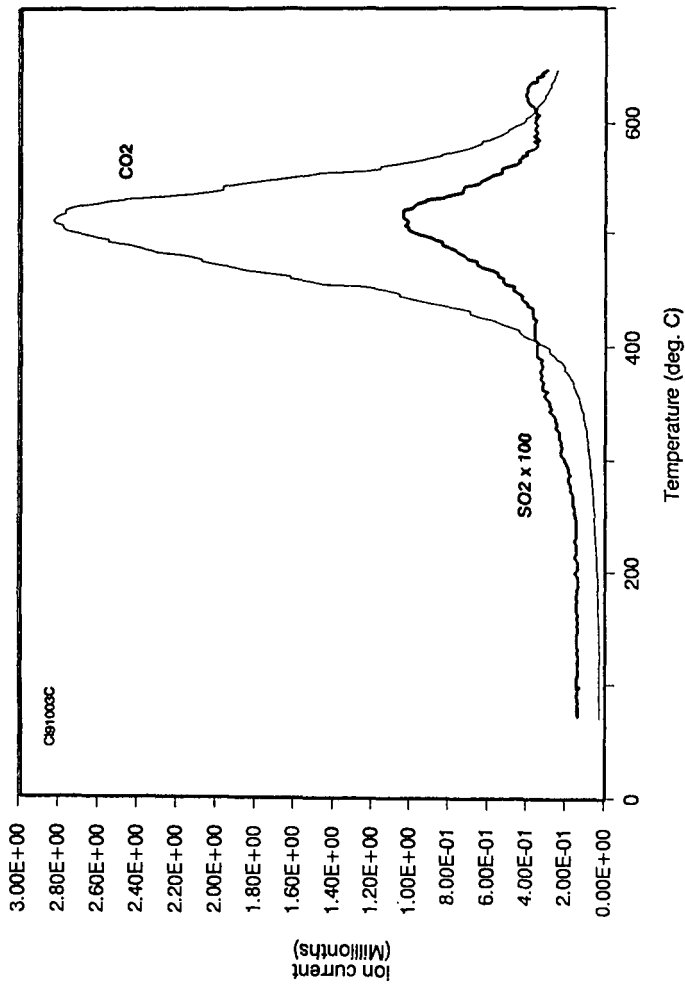


Figure 2. Profiles of CO₂ and SO₂ (X100) in combustion gas under an oxidizing condition at a heating rate of 50°C/min.

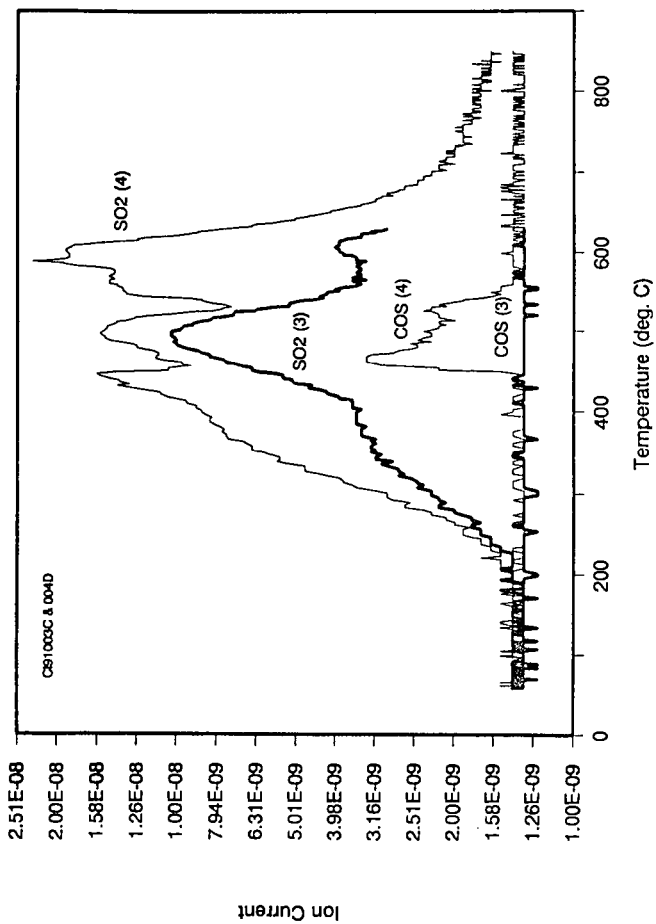


Figure 3. SO₂ and COS profiles when combustion chamber was under oxidizing (Run 3) and reducing (Run 4) conditions.

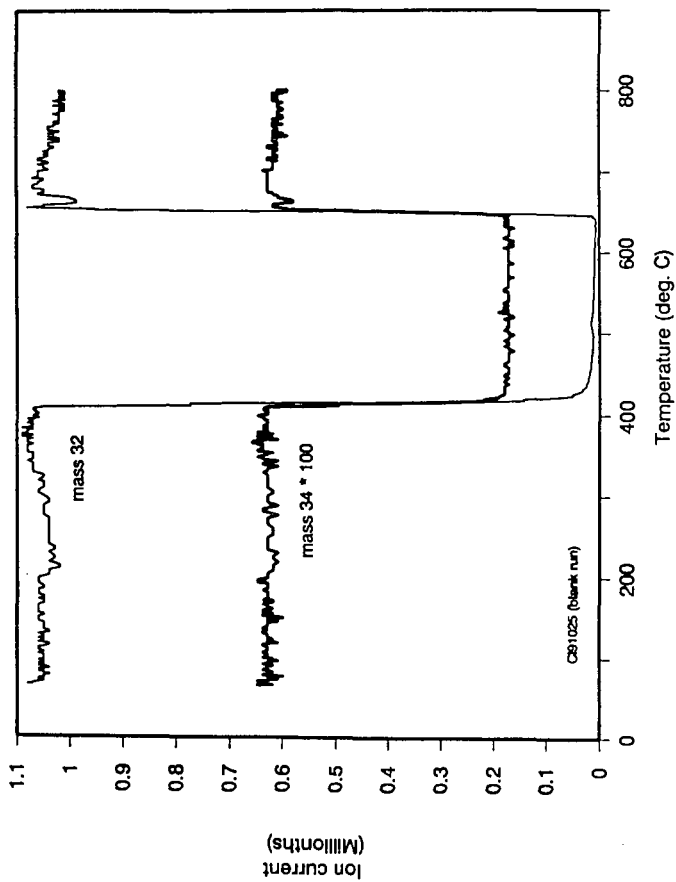


Figure 4. Profiles of masses 32 and 34 ($\times 100$) during a blank run where O_2 flow was shut off between 400° and $625^\circ C$.

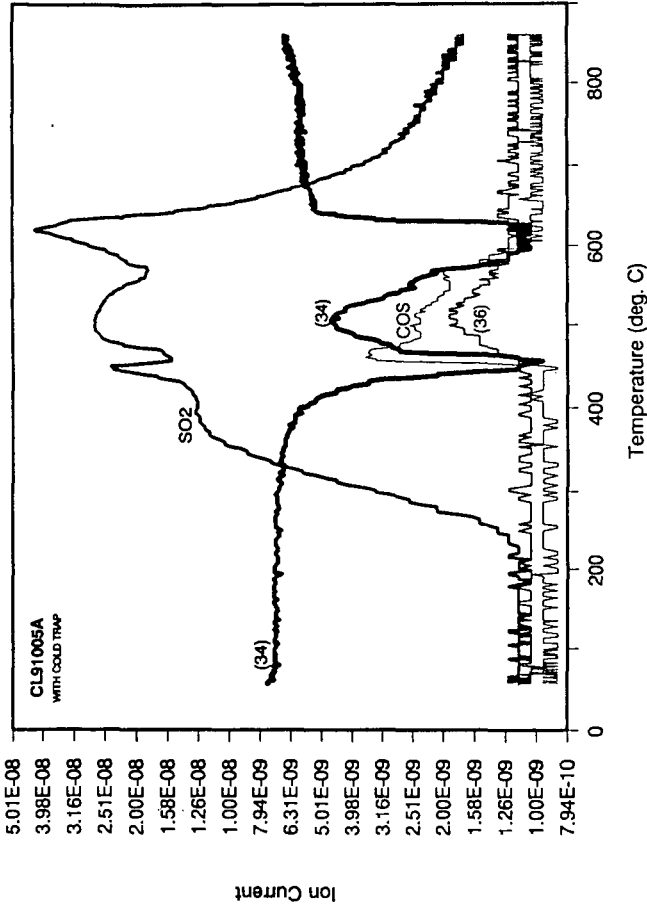


Figure 5. Gas release profiles obtained when combustion chamber was under a reducing condition. Mass numbers in parentheses are used for profiles that possibly represent more than one gaseous species.

SECONDARY PYROLYSIS AND COMBUSTION OF COAL VOLATILES

D. Marlow, S. Niksa, and C. H. Kruger
High Temperature Gasdynamics Laboratory
Stanford University
Stanford, CA 94305

Keywords: Coal Volatiles, Combustion, Burning Velocity

INTRODUCTION

During the initial stages of pulverized fuel (p. f.) firing devolatilization converts about half of the injected coal mass into gases, including many fuel compounds. The subsequent secondary pyrolysis and combustion of these volatile compounds accounts for large portions of the heat release, pollutant formation, and soot evolution during coal combustion. This study focuses on the combustion of the volatiles. Noncondensable volatiles, without tar or soot, from the pyrolysis of a bituminous coal were mixed with O_2 and N_2 and burned in a constant volume combustion bomb. The resulting laminar burning velocity determinations provide a means of estimating global combustion rates. Laminar burning velocities are reported as a function of equivalence ratio and unburned gas temperature for a single pyrolysis condition, in which most of the tar had converted to soot.

APPARATUS

As seen in Fig. 1, the volatiles are generated by entraining pulverized coal particles in N_2 , and passing the suspension through an induction furnace. At the exit of the furnace, a fraction of the N_2 /volatiles stream is diverted from the main stream of gas and char, and drawn through a heated filter to an evacuated storage tank. The stored gas is then pumped to the combustion bomb, where it is mixed with O_2 and N_2 , and ignited by an electric spark.

Design details and performance characteristics of the radiant coal flow reactor are given elsewhere.^{1,2} Briefly, the coal suspension passes through a quartz tube within an inductively heated cylinder of graphite maintained at temperatures from 1000 K to 1850 K. Radiation from the graphite heats the coal particles at $10^4 - 10^5$ K/sec. The N_2 carrier gas is transparent to radiation, and can only be heated by convection from the coal suspension and the quartz tube. Since the coal suspension supplies much of the heat to the carrier gas, the gas temperature can be kept low to minimize secondary reactions among the volatiles by operating with very dilute suspensions (about 100 particles/cc). However, to obtain the flammable mixtures for this study the coal loading was increased to 2400 particles/cc. At this condition, secondary pyrolysis of the volatiles is virtually complete.

Gas concentrations were determined with gas chromatography (for H_2 , CO, CH_4 , C_2H_6 , C_2H_4 , C_2H_2 , C_3H_6 , and light oils) and non-dispersive infrared analysis (for CO_2 and H_2O). Hydrogen and CO were sampled with a gas-tight syringe and measured with a thermal conductivity detector after separation on Molecular Sieve 5A. Chromatography for these compounds was conducted immediately after sampling to avoid diffusive loss of H_2 . Methane, C_2H_6 , C_2H_4 , C_2H_2 , and C_3H_6 were sampled into a multiposition valve and measured with a flame ionization detector (FID) after separation on Silicalite. The remaining hydrocarbons in the gas stream were grouped as light oils and measured by direct injection of the gas stream into the FID. The resulting total signal included the signals from $C_1 - C_3$ hydrocarbons, which were subtracted out; the remainder was then converted to a light oil concentration using the conversion factor for pentane, which has a molecular weight similar to the oils'.

The combustion bomb is a spherical pressure vessel (15.24 cm diam.) constructed from 316 stainless steel, and equipped with 10 access ports. Copper electrodes form a 1 mm spark gap at the center of the spherical chamber. Three ionization gages spaced about the chamber wall monitor the arrival time of the flame to check for flame sphericity (an assumption in the data reduction). The transient

pressure rise from combustion is monitored by a water-cooled piezoelectric pressure transducer mounted at the bomb wall. Laminar burning velocities are determined from the transient pressure trace. But this determination is complicated by the fact that the pressure rise is related both to the rate at which volatiles enter the flame, and the rate at which the unburned gas is compressed by the expansion of the products behind the flame. A computational procedure has been adapted to separate these two effects, and is explained elsewhere.³

EXPERIMENTAL

An HVA bituminous coal (Illinois #6, IBCSP 105) distributed by the Illinois Basin Coal Sample Program was used. The coal was ground under liquid nitrogen and dry-sieved to produce a 75-106 micron size fraction. The 75 micron cutoff was then improved by sedimentation of the coal in water. An ultimate analysis of the sized coal gave 64.8 % C, 4.9 % H, and 1.4 % N on a moisture free basis. Before each use, the coal was dried overnight at 330 K under 15 kPa of N₂.

The radiant coal flow reactor was operated at 1640 K and a nominal residence time of 200 msec. The large amounts of soot observed at the furnace exit confirmed extensive secondary pyrolysis of the volatiles. Soot and condensed volatiles were removed on a glass fiber filter maintained at 330 K. The filtered noncondensable volatiles were stored at 450 K, and pumped to the combustion bomb through lines heated to 380 K.

The combustion bomb was operated at an initial pressure of 0.07 MPa, which is sufficiently low to keep inordinate uncertainties in the initial section of the pressure trace from obscuring the behaviour at 0.1 MPa. The bomb was preheated to the two initial temperatures of 493 K (5 runs) and 579 K (4 runs). Compression heats the unburned gases to 540 K and 635 K, respectively, by the time the bomb pressure has reached 0.1 MPa. Oxygen was added to the volatiles to obtain fuel lean equivalence ratios (defined in terms of fuel/O₂ ratios) from 0.5 to 0.9, where the fuel comprises H₂, CH₄, C₂H₆, C₂H₄, C₂H₂, C₃H₆, light oils, and CO. Nitrogen was also added to maintain a constant diluent/O₂ ratio of 4.3 +/- 0.25 on a mole/mole basis; N₂, CO₂, and H₂O are the diluents.

RESULTS

Table I gives the measured species concentrations for two fills of the storage tank. The first mixture provided the results at 540 K, while the second mixture was used at 635 K. While H₂, CH₄, and CO are the most abundant fuel species, the remaining hydrocarbons contribute about half of the heat release of combustion. In fact, the light oils alone contribute about a quarter of the heat release. Because of their higher molecular weights, very small mole fractions of these higher hydrocarbons contribute significant amounts of energy release.

Fig. 2 shows the volatiles burning velocities measured for two unburned gas temperatures. The magnitude of the measured velocities is much smaller than that for H₂/air combustion at similar conditions ($S_u = 720$ cm/sec in air at an equivalence ratio of 0.9 and an unburned gas temperature of 635 K), but similar to that for CH₄/air (see correlations in Fig. 2).⁴ Note, however, that the correlations are for air, which has a diluent/O₂ ratio of 3.76, while the volatiles measurements are for a diluent/O₂ ratio of 4.3; CH₄ burning velocities for the same diluent ratio would tend to be 10 to 20 % lower. While CH₄ and volatiles burning velocities compare favorably for the conditions of this study, this result cannot be generalized. Further secondary pyrolysis leads to higher levels of H₂ and CO than observed here and lower levels of heavy hydrocarbons,² so that such volatiles mixtures might be expected to burn faster. Also, lower rank coals produce more H₂O, CO₂, and CO than observed here, and these species can be expected to play more important roles in the combustion of volatiles from these coals. Finally, the condensable tars absent from this study can contribute more than half of the heat release of combustion, and can be expected to introduce additional rank effects into the combustion rates of volatiles.

SUMMARY

A facility has been constructed to study the effects of primary and secondary pyrolysis on the combustion rates of the volatiles from coal. Concentration measurements for an HVA bituminous coal show that under significant secondary pyrolysis H₂, CH₄, and CO are the most abundant noncondensable fuel species; but other hydrocarbons, especially light oils, contribute significantly to the heat release. For the conditions of this study, the measured burning velocities are similar to those of methane. However, we do not anticipate this similarity in subsequent studies in which coal rank and extent of secondary pyrolysis are varied, and tar is left in the volatile fuel mixture.

ACKNOWLEDGEMENT

Support for this program is provided by the United States Department of Energy's Morgantown Energy Technology Center under Grant DE-FG22-86PC90511.

REFERENCES

1. Chen, J. C., Chang, Y. Cleo, and Niksa, S., Proc. 1989 Int'l Coal Science Conf., IEA, Tokyo, p. 503.
2. Chen, J. C., Castagnoli, C., and Niksa, S., Paper No. 90-48, WSS/CI Fall 1990 Mtg., San Diego, CA, October 1990.
3. Metghalchi, M., and Keck, J. C., Combust. Flame, 1980, **38**, 143.
4. Iijima, T., and Takeno, T., Combust. Flame, 1986, **65**, 35.

Table I: Measured Species Concentrations of Stored Volatiles.

		Mole % of Stored Volatiles									
	H ₂	CH ₄	C ₂ H ₆	C ₂ H ₄	C ₂ H ₂	C ₃ H ₆	Light Oil	CO	CO ₂	H ₂ O	N ₂ [#]
1	4.9	2.3	0.079	0.61	0.61	0.16	0.84	2.28	0.34	3.0	84.9
2	4.6	1.9	0.050	0.49	0.55	0.16	0.50	1.88	0.32	3.0*	86.6

* Estimated. Not measured.

By difference.

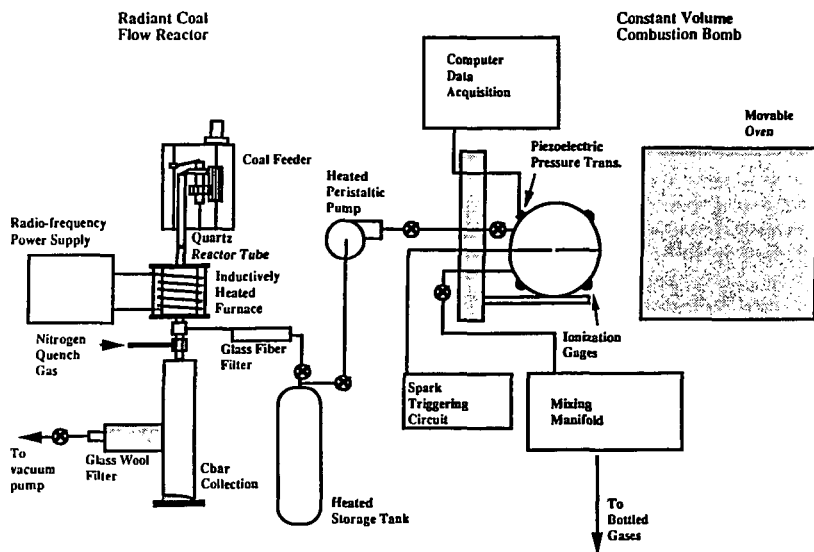


Fig 1: Schematic of the radiant coal flow reactor, the means of transporting volatiles, and the constant volume combustion bomb.

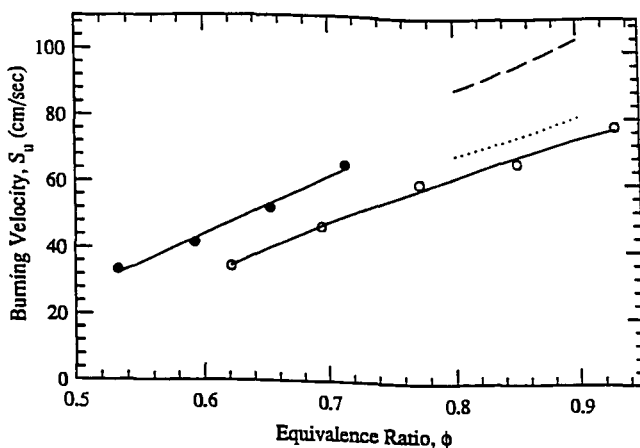


Fig 2: Burning Velocities, S_u , for the noncondensable volatiles of Table 1 as a function of stoichiometry for unburned gas temperatures of 540 K (○), and 635 K (●). The burning velocities for CH_4/air combustion are indicated by 540 K, and — — 635 K. Schematic of the radiant coal flow reactor, the means of transporting volatiles, and the constant volume combustion bomb.

Microscopic Studies on the Dispersion of Iron/Molybdenum Bimetallic Catalysts in Argonne Coals

David A. Sommerfeld, Jumpol Jaturapitpornsakul,
Larry Anderson and Edward M. Eyring
Dept. of Chemistry and Dept. of Fuels Engineering
University of Utah
Salt Lake City, UT 84112

Keywords: catalyst dispersion, bimetallic catalysts, EPMA

Abstract

The dispersion and reactivity of an iron/molybdenum coal liquefaction catalyst was investigated in three Argonne coals. Three coals (Blind Canyon, Wyodak and Pittsburgh #8) were impregnated with a 1 wt% Fe and 1 wt% Mo liquefaction catalyst using both ultrasonic and incipient wetness techniques. The yields of THF solubles in demineralized Blind Canyon coal indicate no significant advantage in the use of ultrasound as the impregnation technique. Results of electron probe microanalysis (EPMA) reveal that the catalyst is coated on the surface of the particles prior to hydrolysis at 350 °C and 2000 psig H₂. EPMA micrographs indicate that the catalyst occupies the interior of the coal particles after hydrolysis. Our results suggest that coal catalyst mobility occurs during hydrolysis and may be due to the liquid phase present in the coal and the amount of porosity.

Introduction

Catalyst dispersion remains an area in coal liquefaction research requiring a more thorough understanding.¹ Common sense suggests that the more evenly dispersed and the finer the size of the catalyst the more efficient the coal liquefaction. In other words, both the form of the catalyst and the manner in which it is introduced into the coal affect the coal liquids yields.

In this study we examine the role of the catalyst impregnation technique upon coal hydrolysis by comparing the incipient wetness technique with ultrasonic impregnation. A series of bimetallic catalysts were studied in three coals from the Argonne Premium Coal Sample Program. The dispersion of the catalyst was followed with electron probe microanalysis (EPMA) as in previous studies.² Electron probe microanalysis is a microscopic technique that allows one to examine on the micron scale the distribution of elemental species by detecting characteristic X-rays (Fig. 1).^{3,4}

Experimental

Samples of 100 mesh Blind Canyon, Wyodak and Pittsburgh #8 coals were obtained from the Argonne Premium Coal Sample Program

and stored at 0 °C until impregnation. In some studies involving Blind Canyon coal the coal samples were demineralized. The demineralization process occurred under nitrogen using warm (about 60 °C) solutions of concentrated HCl followed by concentrated HF and then concentrated HCl.

The following catalyst systems were studied: 0.05% Mo, 1% and 0.01% Fe, 1% and 0.01% Ni, 1% and 0.01% Fe/0.05% Mo and 1% and 0.01% Ni/0.05% Mo (note: these are all in wt%). Two methods of catalyst impregnation were compared: incipient wetness and ultrasound. For bimetallic catalysts the impregnation was done sequentially from aqueous solutions using first the ammonium tetrathiomolybdate, followed by the iron(III) chloride hexahydrate or nickel(II) nitrate hexahydrate. Hydropyrolysis was done in a shaken tubing bomb reactor in which samples were reacted for one hour at 350 °C and 2000 psig of H₂. In order to determine the product yields, the samples were Soxhlet extracted with tetrahydrofuran (THF) after hydropyrolysis.

Samples for electron probe microanalysis were prepared with Petropoxy, polished to a smoothness suitable for EPMA, and sputter coated with carbon to reduce point charging of the surface. Visual images of the samples were obtained from the secondary electron and back-scattered electron images with a CAMECA Model SX-50 detector (Courbevoie Cedex, France). The catalyst dispersion in the samples was determined by collecting the characteristic X-rays for iron, nickel, molybdenum and sulfur with an energy dispersive spectrometer detector. X-ray analysis was done using a Digimap program. Sample magnification was x1000 or x1500.

Results

The resulting yields are summarized in Tables 1 and 2. The first set of experiments involved the use of demineralized Blind Canyon coal. These first experiments were run in order to determine which method of impregnation was better, incipient wetness or ultrasound, and whether preextracting the coal with THF improved the yields. As seen in Table 1 no significant advantage exists for either impregnation technique and preextraction with THF actually decreases the yields of THF solubles upon hydropyrolysis. The rest of the experiments were all done with coals that had not been preextracted and had been impregnated by the incipient wetness technique and were performed in order to determine the efficiency for producing THF solubles of various Fe/Mo and Ni/Mo bimetallic catalysts. The results show that the bimetallic catalysts are much more efficient than either metal alone (Table 1). More importantly, even when the loading of the Fe/Ni promoters is decreased by two orders of magnitude significant amounts of THF solubles are still produced.

These images are of samples that have been impregnated with 1 wt% Mo because the 0.05 wt% loading of Mo results in a Mo concentration too close to the detection limits of the EPMA for accurate micrographs. The EPMA images for iron, nickel and molybdenum show that all three of the cationic species behave in

a similar manner. Before hydropyrolysis the catalyst species are located on the surface of the coal particles (Fig. 2). After reaction the catalyst species occupy the interior of the coal particles (Fig. 3). This is true for the iron, nickel and molybdenum catalytic species.

The second set of experiments involved three different Argonne coals: Wyodak, Pittsburgh #8 and Blind Canyon and were done in order to determine whether the choice of catalyst impregnation technique seriously affected the yields of THF solubles. The coals were used as received from the Argonne Premium Coal Sample Program. The catalyst system used was 1 wt% Fe/1 wt% Mo with the same reaction conditions as given previously. For the Pittsburgh #8 and Blind Canyon coal samples there was no significant difference in the yields of THF solubles between samples impregnated by incipient wetness or by ultrasound (Table 2). A significant difference occurs for Wyodak coal. The samples impregnated by incipient wetness exhibit a 13% higher yield of THF solubles. As described in the case above, before hydropyrolysis the catalytic species are found on the surface of the coal particles. After hydropyrolysis these species are found in the interior of the coal particles.

Discussion

Sulfided molybdenum can provide a reasonably efficient coal liquefaction catalyst.^{5,6} Recently, Li and coworkers,⁷ using a fixed-bed reactor, found that a MoS₂ loading of 0.5% produces a 35% oil yield under hydropyrolysis conditions of 3 M Pa and 798 K for 30 minutes. As they note in their conclusion, a Mo loading of 0.5% is commercially unrealistic due to its high cost and the sulfur added to the hydropyrolysis products.⁷

The yields reported in the present study (Tables 1 and 2) result from a procedure using lower Mo loadings (0.05%) and mild hydropyrolysis conditions. The presence of the iron/nickel promoters appears to increase the efficiency of hydropyrolysis (Table 1). These results seem to indicate that one of the most promising routes to commercially feasible coal liquefaction involves the use of bimetallic catalyst systems with loadings of less than 1% and the use of mild hydropyrolysis conditions. The mild conditions would permit a catalytic rather than thermal breakdown of the coal structure.

The EPMA experiments lead to two main conclusions: First, catalyst mobility occurs during hydropyrolysis for these coals and catalytic species. Second, because these catalysts are mobile species during hydropyrolysis, the choice of catalyst impregnation technique probably will not significantly affect the coal liquefaction yield.

What does affect the liquefaction yield is the rank of the coal. The best yields were obtained from a subbituminous coal, Wyodak coal, which is 75% C.⁸ Blind Canyon coal, a high volatility bituminous coal which is 81% C, provided the next best yield of THF solubles. Pittsburgh #8 with a carbon content of 83% provided the lowest yields of THF solubles (Table 2). As has been pointed out

by Derbyshire,⁹ the rank of a coal and its carbon content correlate with the porosity of the coal structure. Upon heat treatment the open pore structure of low rank coals is preserved whereas higher rank coals undergo increasing degrees of graphitization. We believe this effect helps to explain our results. If, as we surmise, catalyst mobility occurs during hydroxyprolysis then a more efficient catalyst dispersion process will occur in the low rank coals resulting in a higher yield of THF solubles. Higher rank coals will have less efficient catalyst dispersion during hydroxyprolysis and hence lower THF soluble yields. This is precisely what we find for the yields of Wyodak versus Blind Canyon and Pittsburgh #8 coals (Table 2).

Acknowledgment

Financial support by the U.S. Department of Energy, Fossil Energy Division, through the Consortium for Fossil Fuel Liquefaction Science, Contract No. UKRF-4-21033-86-24, is gratefully acknowledged. Ray Lambert provided generous technical assistance.

References

1. Derbyshire, F.J. Catalysis in Coal Liquefaction, IEA Coal Research: London, 1988, p. 17.
2. Wang, H.P.; Lo, R.; Sommerfeld, D.A.; Huai, H.; Pugmire, R.J.; Shabtai, J.; Eyring, E.M. Fuel, in press.
3. Newbury, D.E.; Fiori, C.E.; Marinenko, R.B.; Myklebust, R.L.; Swyt, C.R.; Bright, D.S. Anal. Chem. (1990), 62, 1159 A.
4. Newbury, D.E.; Fiori, C.E.; Marinenko, R.B.; Myklebust, R.L.; Swyt, C.R.; Bright, D.S. Anal. Chem. (1990), 62, 1245 A.
5. Derbyshire, F.J.; Davis, A.; Lin, R.; Stansberry, P.G.; Terrer, M.-T. Fuel Proc. Technol. (1986), 12, 127.
6. Snape, C.E.; Bolton, C.; Dosch, R.G.; Stephen, H.P. ACS Div. Fuel Chem., prep. (1988), 33, 351.
7. Li, B.-Q.; Braekman-Danheux, C.; Cypres, R. Fuel (1991), 70, 254.
8. Vorres, K.S. Energy & Fuels (1990), 4, 420.
9. Derbyshire, F.J. Fuel (1991), 70, 276.

Table 1. Catalytic Hydropyrolysis of Blind Canyon Coal
THF^c

Catalyst ^a	Impregnation ^b	Sol.	Insol.
0.05% Mo	U	40	52
0.05% Mo	I	42	52
1% Fe + 0.05% Mo	I	55	41
0.01% Fe + 0.05% Mo	I	50	43
1% Ni + 0.05% Mo	I	50	46
0.01% Ni + 0.05% Mo	I	52	45

^aCatalyst loadings are given in wt%

^bImpregnation: U=ultrasound, I=incipient wetness

^cYields are given as % of maf coal

Table 2. Comparison of Yields and Impregnation Technique
THF^b

Coal	Impregnation ^a	Sol.	Insol.
Wyodak	U	55	36
Wyodak	I	68	20
Pittsburgh #8	U	53	45
Pittsburgh #8	I	56	42
Blind Canyon	U	62	36
Blind Canyon	I	63	38

^aImpregnation: U=ultrasound, I=incipient wetness

^bYields are given as % of maf coal

Electron Probe Microanalysis Schematic

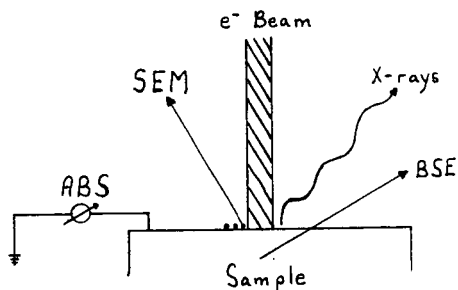


Figure 1. This illustration portrays the various signals generated by EPMA. An e^- beam of 10-30 keV impinges upon the sample surface resulting in three "visual" signals and characteristic X-rays. The secondary electron image (SEM) results when the incoming electron beam causes the loosely bound surface electrons to leave the sample. Back-scattered electrons (BSE) have entered the sample and through atomic interactions are emitted from the sample. The absorption image (ABS) is read as a current from the sample and accounts for those electrons of the incoming electron beam that are not back-scattered.

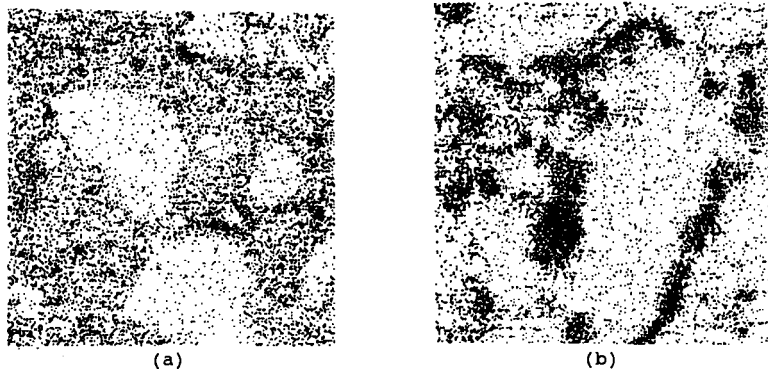
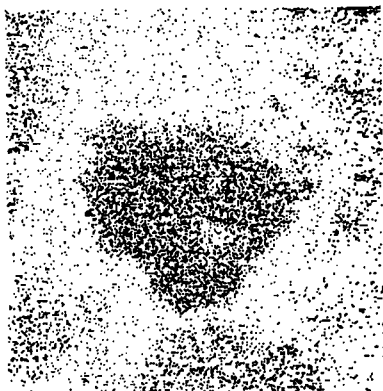


Figure 2. These EPMA micrographs are 97 x 97 microns. Figure 2a is of 1 wt% Fe impregnated Blind Canyon coal before reaction. Figure 2b is of 1 wt% Ni impregnated Blind Canyon coal before reaction. The cationic species have not entered the particles, they are located on the surfaces of the coal particles as seen by the rings and ghost images of particles.



(a)



(b)

Figure 3. The EPMA images here are 97×97 microns. Figure 2a is an image of Blind Canyon coal after impregnation with 1 wt% Fe and hydrolysis. The iron is now evenly dispersed throughout the coal particle in the center of the image. Figure 2b is an image of Blind Canyon coal after impregnation with 1 wt% Ni and hydrolysis. The nickel species has entered the coal particle in the lower-right corner of the image and is less evenly dispersed.

XPS STUDY OF CATALYSTS AND CATALYST IMPREGNATED COAL

P.J. Reucroft and J.Y. Kim

Dept. of Material Science & Engineering,
University of Kentucky, Lexington, KY 40506

INTRODUCTION

The highly dispersed forms of certain catalysts are believed to be very active in the conversion of coal to liquids via direct liquefaction.¹⁻³ A catalyst with a higher specific surface area and fine particulate size can be utilized at small concentrations to achieve better performance in terms of overall coal conversion and selectivity to lighter products (oils) in direct coal liquefaction.⁴

X-ray photoelectron spectroscopy (XPS) has been used to study the surface characteristics of six catalysts and a catalyst impregnated Illinois #6 coal. This technique provides the surface elemental distribution and chemical information about the outermost 3-4 nm of the exposed solid surface. This characterization has shown that the concentration of elements at the outermost layer measured by XPS is different from that in the bulk determined by chemical analysis. The oxygen concentration was enriched in the surface regions of all the samples. The oxidation states of these elements were generally identified.

XPS depth profiling studies also have been carried out to determine if there are any differences in the distribution of the major components in catalyst II (Mo/FeOOH/SO₄²⁻) and catalyst I (FeOOH/SO₄²⁻) impregnated Illinois #6 coal. A systematic trend towards lower weight concentrations of both oxygen and sulfur was observed for both samples as the sputtering time increased (i.e. when going from surface to the bulk).

EXPERIMENTAL

Six catalysts and catalyst I (FeOOH/SO₄²⁻) impregnated Illinois #6 coal were investigated in the surface characterization studies. These samples were obtained from the Univ. of Pittsburgh⁵ and are shown in Table 1. The powdered samples were examined in their as-received form and their particle sizes were less than -100 mesh.

The powdered samples were mounted on the spectrometer probe tip by means of double-sided adhesive Scotch insulating tape. The samples were pressed with the aid of a metal spatula and the excess that had not adhered was tapped off. To exclude the possibility of recording contaminants associated with the tape, the tape was also analyzed separately. It was found that the constituents of tape were not detected by XPS, and that the photoionization signals are characteristic of the catalyst and coal samples alone.

The samples were examined by XPS on a Kratos XSAM 800 spectrometer using Mg K α (1253.6 eV) radiation. The spectrometer was run in fixed retarding ratio (FRR) mode at a pass energy of 13 kV and 15 mA. Under these conditions, the full width at half maximum (FWHM) of the Ag (3d_{5/2}) peak is ≈ 1.1 eV. Spectra were recorded at $< 5 \times 10^{-7}$ torr.

Radiation damage to the sample from long-term exposure to the X-ray beam was not observed. All binding energies were referred to carbon (1s) at 285 eV to compensate for

sample charging. Elemental concentrations were obtained from peak areas and corrected for atomic sensitivity factors.

The peak was deconvoluted using a peak synthesis procedure which employed a Gaussian line shape at fixed binding energies determined from model compound studies.⁶ The data system permitted the intensity of the components and their FWHM to be varied in order to obtain the best fit between the experimental and the synthesized spectra.

Ar⁺ sputtering of the powdered sample was carried out with the Ar⁺ gun operating at 3.5 kV (estimated etching rate of ca. 20 Å/min, as determined from a SiO₂ standard film). Each charge compensation was referred to the C 1s peak at 285 eV.

RESULTS AND DISCUSSIONS

Surface Compositions

The XPS spectra showed a distinct peak for major elements, oxygen, iron, and tin, as well as the minor component, sulfur, in each catalyst sample. The C 1s peak was observed in all catalysts and can be ascribed to carbon contamination. Cl 2p was only observed in the tin oxide catalyst (III). This occurs because chlorine was introduced as SnCl₄·5H₂O in the starting materials that were used for the preparation of the tin oxide catalysts. This excess chlorine was left at the surface after sample preparation. The quantitative analysis results are shown in Table 2.

To determine the oxidation states of Fe, Mo, and Sn, narrow survey scans were carried out. The binding energies of the Fe 2p, Mo 3d and Sn 3d levels showed the expected values for the most stable oxidation states of these elements. Multiple splitting was observed in the transition elements, such as Fe and Mo. Figures 1a and b show the results for Fe 2p and Mo 3d, respectively. This is the result of spin interaction between an unpaired electron from the photoionization process and other unpaired electrons present in the system. The point of real interest is that the separation between the two peaks varies depending upon the environment of the atom concerned. In Fig. 1a, the Fe 2p peak shows the 13.6 ± 0.05 eV splitting between the 2p_{1/2} and 2p_{3/2} peaks. This was observed in all iron oxide containing catalysts. The observed splitting corresponds well with the Fe 2p peaks of Fe₂O₃ and/or FeOOH (Goethite) in model compound studies.⁶ The Fe compound shown in the surface of the catalyst samples can thus be ascribed to either Fe₂O₃ or FeOOH.

Mo 3d showed the 3.2 eV splitting between the 3d_{3/2} and 3d_{5/2} peaks in the catalyst II, IV, and V samples. Molybdate (MoO₄²⁻) was used as a starting material in the preparation of these catalysts. This anion is readily oxidized at the surface and produces the stable oxidation state MoO₃ at the catalyst surface. Sn 3d also showed the multiple splitting of 8.45 eV. This can be ascribed to SnO₂ and is shown in Fig. 1c. Emphasis has been focused on the S 2p peaks of raw coal samples in earlier reports.⁷ It was shown that the S 2p peak always displays two photolines with a separation of 5.6 eV in raw coal samples. However, the XPS spectrum of S 2p in the catalyst samples showed only one S 2p peak at 168.8 eV, corresponding to SO₄²⁻. This result is shown in Fig. 1d where a catalyst spectrum is compared with that of catalyst impregnated coal. In the upper spectrum, the peak at 164 eV can be ascribed to sulfide in the coal.

From the above results, it was concluded that all major elements showed the most stable oxidation states at the surface of all catalysts and catalyst impregnated coal samples.

Depth Profile Studies

In order to show if there is any difference in the distribution of the elements and chemical changes between the surface and bulk, the samples have been analyzed by combining Ar^+ sputtering with XPS measurements. Due to the edge effect associated with the unetched sample surface, the depth profiles for materials in powder form were difficult to obtain. Preferred areal sputtering was carried out to reduce this effect. Although different features such as preferential sputtering, atomic mixing, particle size effects, etc., can effect the etching profiles, sputtering was performed in the present studies for comparative purposes on samples where such effects were expected to be very similar.

Figures 2a and b show depth concentration profiles for the most abundant elements in catalyst I and catalyst I impregnated Illinois #6 coal samples, respectively. A systematic trend towards lower weight concentrations of both oxygen and sulfur was observed for both samples as sputtering time increased. A relatively high oxygen concentration was determined initially at the surface by XPS before etching, but a sharp drop in oxygen concentration was subsequently observed as shown in Fig. 2a. This surface enrichment of oxygen can be ascribed to air oxidation and the oxidized layer thickness was estimated to be 40-50 Å. In Fig. 2a, Fe shows an enrichment as the etching proceeds from the surface to the bulk of catalyst I. This was also observed in catalyst II. From these results, which show a decrease in oxygen and an increase in iron concentrations with increased etching, it can be concluded that the surface iron particles are covered with an oxide layer. However, no change was observed in the iron concentration in the case of the catalyst impregnated coal sample shown in Fig. 2b. It can thus be concluded that the iron particles, in catalyst I impregnated Illinois #6 coal, are encapsulated by organic materials from the coal.

Chemical state changes for sulfur were observed as the etching proceeded in both samples. The surface sulfur showed a binding energy of 168.8 eV, indicating sulfate (SO_4^{2-}) and no peaks were observed in the sulfide region (164 eV) in the case of the catalyst I sample. As sputtering time increased, however, the sulfate peak decreased and finally disappeared. A sulfide or elemental sulfur peak was then observed. These results are shown in Figs. 3a and b. This can be ascribed to the removal of oxidized sulfur at the surface by the etching procedure. No chemical state changes were observed for Fe and Mo states as a result of etching.

SUMMARY AND CONCLUSIONS

It is apparent from this study that XPS can be used to obtain surface chemistry information and elemental identifications on the exposed solid surface. The major elements showed the most stable oxidation states. Sputtering with Ar^+ is a useful tool in determining depth concentration profiles along the outermost sample surfaces. However, in the case of chemical state changes during etching procedures, the interpretations tend to be inconclusive, unless extensive, time-consuming data accumulation can be performed.

ACKNOWLEDGEMENT

We gratefully acknowledge financial support from the Consortium for Fossil Fuel Liquefaction Science, Univ. of Kentucky under Dept. of Energy Contract no. DE-FC22-90 PC 90029. We also thank Dr. G.P. Huffman for his interest in this work.

REFERENCES

1. F.J. Derbyshire, Catalyst in Coal Liquefaction: New Direction for Research, IEA Coal Research, London, 1988, IEA CR-08
2. A.V. Cugini, R.G. Lett, I. Wender, Energy & Fuels, 3, 1989, 120-126
3. S. Weller, M.G. Pelipetz, Ind. Eng. Chem., 43, 1951, 1243-1246
4. T. Suzuki, H. Yamada, P. Sears, Y. Wadanabe, Energy & Fuels, 3, 1989, 707-713
5. Catalyst samples were supplied by V.R. Pradham and I. Wender, Univ. of Pittsburgh
6. C.D. Wagner, W.M. Riggs, L.E. Davis, J.F. Moulder, and G.E. Muilenberg, Handbook of X-ray Photoelectron Spectroscopy, Perkin Elmer Corp. Phys. Elec. Div., Norwalk, CT, 1979
7. P.J. Reucroft, J.Y. Kim, Annual report for CFFLS, 1989-1990

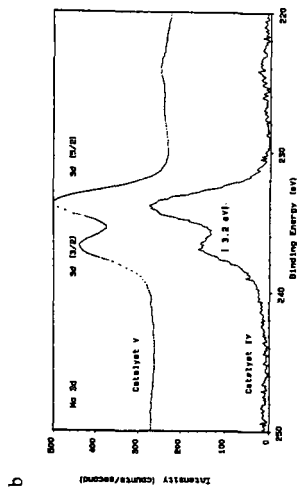
Table 1. Summary of Materials

Catalyst	Symbol	Elemental Analysis
FeOOH/ SO ₄ ²⁻	I	3.0 wt% Sulfur
Mo/FeOOH/ SO ₄ ²⁻	II	1.0 wt% Mo and 2.0 wt% Sulfur
FeOOH/SnO(OH) ₂ / SO ₄ ²⁻	III	
Mo/ Fe ₂ O ₃ / SO ₄ ²⁻	IV	0.5 wt% Mo and 1.3 wt% Sulfur
Fe ₂ O ₃ / MoO ₄ ²⁻	V	2.0 wt% Mo
SnO ₂ / SO ₄ ²⁻	VI	
FeOOH/ SO ₄ ²⁻ on Ill. #6		10.0 wt% Fe and 2.0 wt% Sulfur

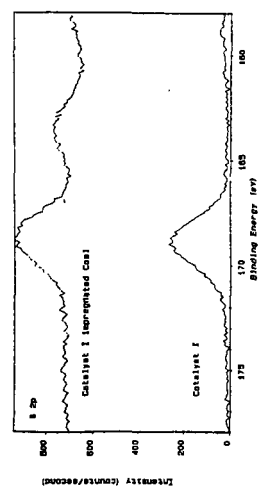
Table 2. Bulk and Surface Concentrations (wt%) for Catalysts

Element	I		II		IV		V		III	VI
	Bulk	XPS	Bulk	XPS	Bulk	XPS	Bulk	XPS	XPS	XPS
Fe	57.85	40.79	59.12	40.43	68.87	40.71	67.61	34.69	27.09	
O	34.15	52.24	37.88	48.65	31.34	46.22	30.09	39.97	30.55	19.07
S	3.00	6.97	2.00	4.51	1.30	6.34			0.46	2.05
Mo			1.00	6.40	0.50	6.74	2.00	25.94		
Sn									41.89	78.88

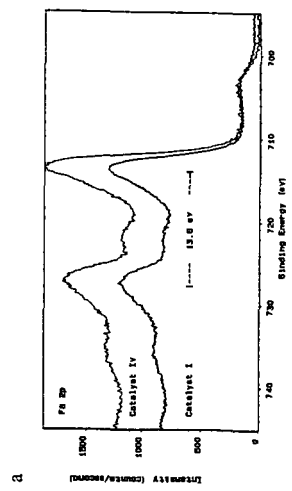
FeOOH/ SO₄²⁻ on Ill. #6 --- C:43.46, O:38.54, Fe:6.67, S:1.87, Al:3.48, Si:3.97
 Raw Coal (Illinois #6) ----- C:66.58, O:22.53, S:1.52, Al:3.99, Si 4.3



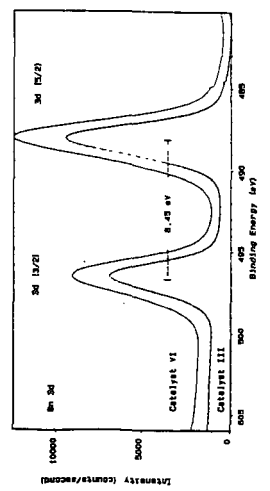
b



d



c



c

Figure 1. Typical XPS narrow scan spectra for (a) Fe 2p for catalysts I & IV, (b) Mo 3d for IV & V, (c) Sn 3d for III & VI, and (d) S 2p for catalyst I and catalyst I impregnated on Illinois #6 coal

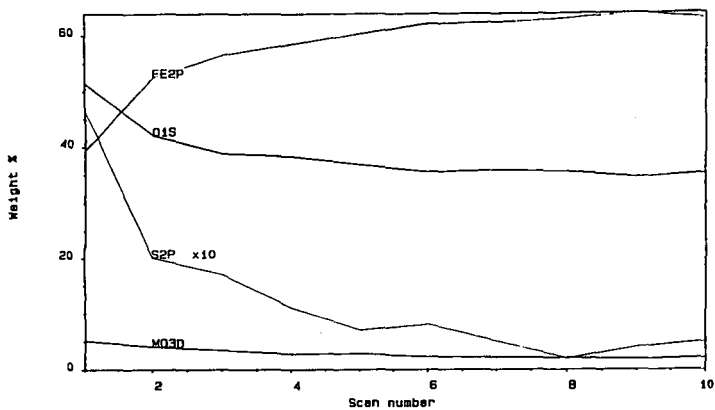


Figure 2-a. XPS depth profile of Catalyst I

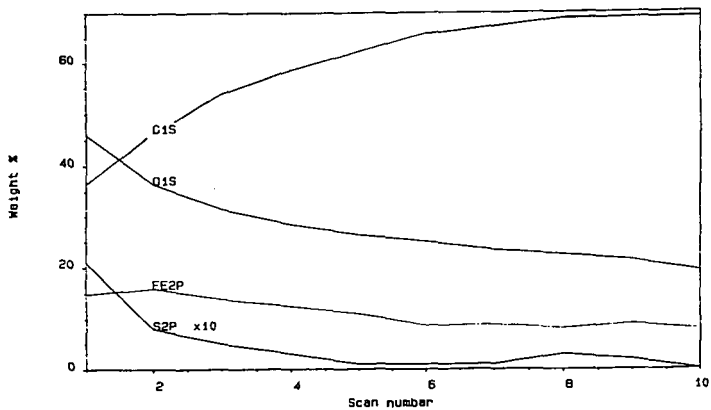


Figure 2-b. XPS depth profile of Catalyst I impregnated on Illinois #6 coal

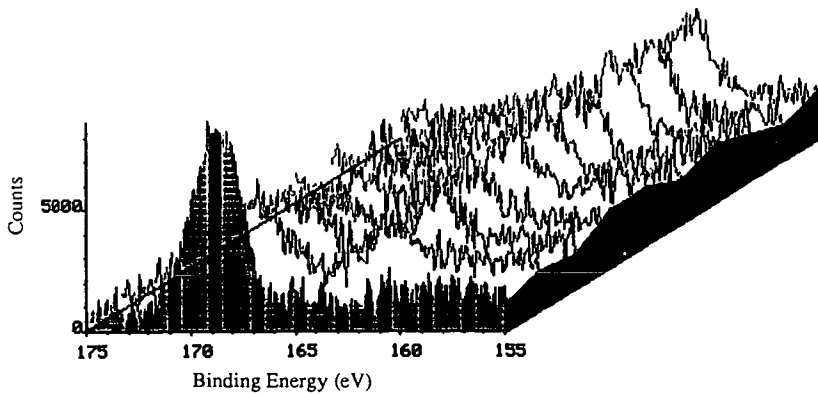


Figure 3-a. XPS depth profile of Sulfur in Catalyst II

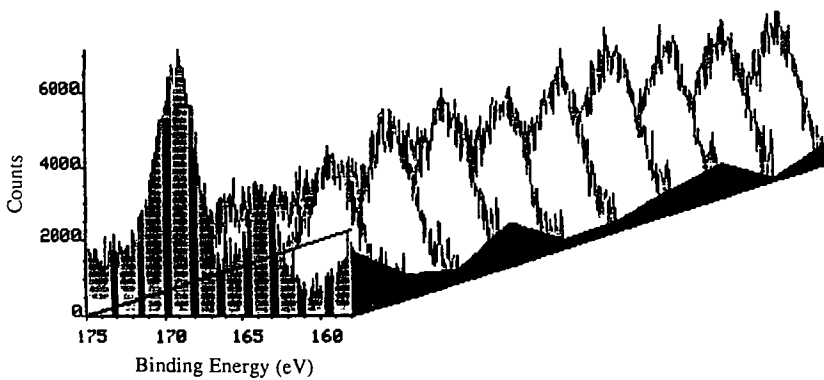


Figure 3-b. XPS depth profile of Sulfur in Catalyst I impregnated Illinois #6 coal

THE EFFECTS OF CHLOROBENZENE PRE-TREATMENT ON THE LOW-SEVERITY LIQUEFACTION BEHAVIOUR OF PITTSBURGH No.8 COAL

C.A. McArthur, A.J. Mackinnon, P.J. Hall and C.E. Snape

University of Strathclyde, Dept. of Pure & Applied Chemistry, Thomas Graham Building, 295 Cathedral Street, Glasgow G1 1XL

Keywords: Conformational changes, macromolecular structure, tetralin extraction, hydrogenation.

ABSTRACT

Recent work has demonstrated that pre-treating coals, particularly with polar solvents, can give rise to significantly improved yields under relatively low-severity liquefaction conditions. Although accessibility is undoubtedly improved, interpretation of these phenomena in terms of changes in the macromolecular structure of coals is complicated by the fact some organic matter is being removed at the same time that conformational changes may be occurring. Chlorobenzene has the advantage of extracting virtually no organic matter from coals and, in this study, the effects of chlorobenzene treatment on short contact time tetralin extraction and dry hydrogenation with and without a dispersed sulphided molybdenum (Mo) catalyst for the Pittsburgh No. 8 Argonne Premium Coal Sample have been investigated. While the chlorobenzene treatment significantly improved the yields from tetralin extraction and non-catalytic hydrogenation due to improved accessibility of solvent and hydrogen gas respectively, reduced yields were obtained in catalytic hydrogenation presumably due to the oil diffusing more effectively out of the remaining macromolecular framework and reducing the effectiveness of hydrogen atom transport from the catalyst.

INTRODUCTION

It was established by Brown and Waters⁽¹⁾ during the 1960s that chloroform-extractable material within the macromolecular structure of coking coals markedly affects their ability to swell during carbonisation. A close correspondence was found between the release of chloroform-soluble material and pore accessibility with increasing temperature. More recently, the effect of pre-swelling and pre-extracting coals in both polar and non-polar solvents on conversions in direct liquefaction has begun to receive considerable attention⁽²⁻⁷⁾ as it is particularly important to overcome mass transfer limitations to maximise yields. For extraction in hydrogen-donor^(2,5) and non-donor^(5,7) solvents and for dry (solvent-free) hydrogenation⁽⁸⁾, significant improvements in overall conversions to pyridine/tetrahydrofuran (THF)-soluble material and in oil yields have been achieved. The study by Joseph⁽⁴⁾ in which tetrabutylammonium hydroxide (TBAH) was the most effective swelling solvent used has demonstrated that the beneficial effect is evident in hydroliquefaction both with and without a dispersed catalyst. As well as pre-swelling or pre-extracting coals in polar solvents, contacting coals at elevated temperatures with non-polar liquefaction solvents including 1-methylnaphthalene⁽⁷⁾ and 9,10-dihydrophenanthrene⁽⁵⁾ has given rise to significant improvements in conversion in short contact time liquefaction and in fluidised-bed pyrolysis⁽⁹⁾. In contrast, removal of chloroform-extractable material has resulted in lower conversions in fluidised-bed pyrolysis⁽¹⁰⁾ and in high temperature extraction with phenol⁽¹¹⁾.

Clearly in the above cases where improved liquefaction yields have been achieved, the accessibility of solvents within the highly porous macromolecular structure of coals has been improved, particularly during the initial stages of liquefaction where retrogressive reactions need to be avoided. However, interpretation of the above phenomena in terms of changes in the macromolecular structure of coals is complicated by the fact some organic matter is being removed at the same time that conformational changes may be occurring and, in the case of polar solvents and pre-treatments at elevated temperatures, hydrogen bonds are being disrupted. Chlorobenzene has the advantage of extracting virtually no organic matter from coals⁽¹²⁾ but it is non-polar and does not significantly disrupt hydrogen bonds at relatively low temperatures (<150°C). Therefore, in principle, it is possible to decouple the effects of conformational changes and extraction for this non-polar solvent. Indeed, it has already been demonstrated that chlorobenzene treatment markedly affects mass transfer phenomena in Upper Freeport coal⁽¹³⁾ (Argonne Premium Coal Sample). Although the

CO₂ surface area remained constant at 180 m² g⁻¹, the time to reach equilibrium decreased from about 6 hours to only 5 minutes. Moreover, there was a significant change in the fractal dimension derived from SAXS. This parameter is a measure of the overall smoothness of the pores and varies between D=2 for a flat plane and D=3.0 for a surface so convoluted that it effectively fills a three dimensional volume. The change in D from 2.8 to 2.5 indicates that the chlorobenzene treatment is smoothing the pores and, as the CO₂ equilibration times demonstrate, this has a significant effect on mass transport within the macromolecular structure.

If the effect of chlorobenzene for Upper Freeport coal is general for most bituminous coals, significant changes in liquefaction behaviour can be anticipated due to the improved accessibility of solvents into the microporous structure and also the ability of coal-derived oil to possibly diffuse more effectively out of the remaining macromolecular framework. In this study, the effects of chlorobenzene treatment on short contact time tetralin extraction and dry hydrogenation with and without a dispersed sulphided molybdenum (Mo) catalyst for the Pittsburgh No. 8 Argonne Premium Coal Sample are reported and the results are discussed in light of the recent work on solvent pre-treatments (2-8).

EXPERIMENTAL

Pittsburgh No.8 coal was treated in chlorobenzene under nitrogen for 1 week in a Soxhlet apparatus. The extracted coal was then dried *in vacuo* at 50°C.

The following liquefaction experiments were conducted in duplicate on the original and chlorobenzene treated samples. For extractions in a hydrogen-donor solvent, 1 g of sample used and 2 g of tetralin were loaded into a microreactor which was submerged in a fluidised sandbath at 400°C for 15 minutes and was agitated using a flask shaker. The heat-up period for the thin-walled 1/2" O.D. microreactors was less than 2 minutes. After extraction, the reactor contents were recovered by filling the microreactor with dichloromethane (DCM) and placing it in an ultrasonic bath. The DCM washings were refluxed and filtered using phase separating paper and the DCM-solubles were recovered by evaporating the filtrate to dryness. The DCM-insolubles were weighed after drying *in vacuo* and were then refluxed in pyridine and filtered to determine the yield of pyridine-insolubles.

The dry or solvent-free hydrogenations were carried out with and without a sulphided Mo catalyst in a 9/16" O.D. microautoclave (*ca* 10 cm³) constructed of Autoclave Engineer high pressure fittings. For the catalytic experiments, the samples were loaded with 1% Mo (daf basis) by impregnation with a methanolic/water solution of ammonium dioxodithiomolybdate (14). 0.3 g of sample was loaded into the microautoclave which was pressurised to 70 bar with hydrogen. A sandbath at 400°C was raised to fully submerge the microautoclave for 60 min., the heat-up period being *ca* 5 min. The reactor contents were recovered and fractionated as described above for the tetralin extractions.

RESULTS AND DISCUSSION

Tables 1 and 2 list the yields of DCM-solubles, pyridine-solubles/DCM-insolubles and pyridine-insolubles from the duplicate tetralin and hydrogenation experiments, respectively, carried out on the initial and chlorobenzene-treated coal, the repeatability being *ca* ± 1% daf coal. The mean values are presented in Figures 1 and 2.

Tetralin Extractions

To highlight mass transfer effects during the initial stages of coal dissolution, tetralin was chosen as the solvent because it is largely in the vapour phase at 400°C and a relatively short contact time of 15 minutes was selected. Table 1 and Figure 1 indicate that chlorobenzene treatment has significantly improved the yield of DCM-solubles or oil. The fact that the total conversions to pyridine-solubles are extremely high would suggest that, for Pittsburgh No.8 coal which will undoubtedly soften to a considerable extent at 400°C, given that the free swelling index is 8, solvent accessibility is not too critical a factor affecting the initial dissolution. However, the vast increase of 20% daf coal in the yield of DCM-solubles clearly indicates improved solvent transport has been achieved with more hydrogen being available to promote the thermal breakdown of pyridine-soluble/DCM-insoluble material into oil.

The increase in oil yield is broadly comparable to that of 14% reported by Joseph ⁽⁴⁾ for tetralin extraction (with a hydrogen over-pressure) of an Illinois No.6 pre-treated with TBAH. Increases of only 5% were obtained for THF and methanol, but, nonetheless, pre-swelling with both these weakly-basic solvents increased the overall conversions to THF-solubles more than with TBAH. However, their boiling points are considerably lower than that of 132°C for chlorobenzene and, although some disruption of the hydrogen-bonding network in coals would undoubtedly have occurred as the coal swells to a significant extent, it is uncertain whether the glass transition temperature would have been lowered sufficiently to allow the coal to adopt a lower energy configuration. It is likely that the chlorobenzene treatment will also lead to significant improvements in primary conversions for non-hydrogen-donor polynuclear aromatic compounds in light of the fact THF extraction achieved this for a UK bituminous coal ⁽⁵⁾.

Hydrogenation

It is well-established that dispersed catalysts, such as sulphided Mo, significantly improve oil yields in solvent-free hydrogenation. At 400°C, yields of chloroform-solubles have been found to increase from 10-20% to 50-60% (daf basis) for bituminous and sub-bituminous coals upon catalyst addition ⁽⁵⁾. Interestingly, opposite conversion trends have been found after chlorobenzene treatment with and without catalyst for Pittsburgh No.8 coal (Table 2 and Figure 2). Without catalyst, the treatment increased the DCM-soluble yield from 19 and 31% and reduced the pyridine-insoluble yield from 40 to 20% indicating that transport of hydrogen gas into the depolymerising coal has been improved. Perhaps surprisingly at first sight, catalytic hydrogenation of the treated coal gave 25% less oil (DCM-solubles) and 12-13% more pyridine-solubles/DCM-insolubles and pyridine-insolubles (Table 2 and Figure 2).

The results with catalyst would appear to be contrary to both those of Joseph ⁽⁴⁾ and Artok *et al* ⁽⁸⁾ who both achieved increased yields in catalytic hydroliquefaction after pre-swelling in polar solvents. However, the experiments by Joseph were carried out in the presence of tetralin and the dominant effect could be the improved transport of the solvent into the macromolecular framework resulting in both more effective hydrogen donation and the transfer of dissociated hydrogen atoms from the catalyst particles. Further, the use of polar solvents which swell the coal considerably may have improved the dispersion of the Mo catalyst, although there is little evidence from hydropyrolysis studies on THF-extracted coals that this is the case ⁽¹⁵⁾. Without solvent, the transfer of hydrogen atoms is dependent on the bitumen or the oil generated by hydrogenation. However, it is likely that the transport of the oil out of the remaining macromolecular structure has also been improved by chlorobenzene treatment and, therefore, the effectiveness of the catalyst is reduced due to the less bitumen remaining in the pore structure to transport hydrogen atoms to reaction sites. Although Artok *et al* ⁽⁸⁾ found improved conversions in catalytic hydrogenation of Blind Canyon coal and two lignites, the experiments were conducted at 275°C and, not surprisingly at this low temperature, total conversions were less than 30% meaning that the amounts of oil available to transfer hydrogen atoms were small. Therefore, it is probable that the principal effect of pre-swelling in TBAH was to improve access of hydrogen gas into the macromolecular structure and thus limit retrogressive reactions.

General discussion

This investigation has reinforced other recent work ⁽²⁻⁸⁾ which indicated that pre-treatments can greatly enhance liquefaction yields, particularly in relatively low-severity regimes. However, much of the other work was concerned with pre-swelling coals in polar solvents where the dominant effect is undoubtedly the disruption of hydrogen bonding. Conversely, chlorobenzene is a low-swelling solvent and does not disrupt coal hydrogen bonding. However, as mentioned earlier, it acts as a plasticizer and, as such, lowers the glass transition temperature thus inducing conformational changes in the coal macromolecule during treatment. The nature of the conformational changes have yet to be elucidated but they are different to those induced by polar solvents and could well involve the disruption of non-covalent bonding between aromatic moieties. Indeed, our continuing research will investigate whether the conformational changes are general or occur to vastly differing extents for coals of varying rank and whether similar changes occur for other non-polar solvents, particularly polynuclear aromatic and hydroaromatic compounds found in vehicle solvents used in coal liquefaction. Circumstantial evidence discussed earlier would indeed suggest that this is the case ^(5,7) and more suitable contact between solvent and coal prior to liquefaction could prove to be extremely beneficial from a processing standpoint.

ACKNOWLEDGEMENT

The authors thank the British Coal Utilisation Research Association and the Science & Engineering Research Council for financial support.

REFERENCES

1. H.R. Brown and P.L. Waters, *Fuel*, 1966, **45**, 17.
2. R.M. Wham, *Fuel*, 1987, **66**, 283.
3. N.R. Pollack, G.D. Holder and R.P. Warzinski, *Prepr. Am. Chem. Soc. Div. Fuel Chem.*, 1991, **36**(1), 15.
4. J.T. Joseph, *Fuel*, 1991, **70**, 139 and 459.
5. C.E. Snape, F.J. Derbyshire, H.P. Stephens, R.J. Kottenstette and N.W. Smith, *Fuel Process. Technol.*, 1990, **24**, 119.
6. J.M. Rincon and S. Cruz, *Fuel*, 1988, **67**, 1162.
7. N.K. Narain, H.R. Appell and B.R. Utz, *Prepr. Am. Chem. Soc. Div. Fuel Chem.*, 1983, **28**(1), 161.
8. L. Artok, H.H. Schobert, G.D. Mitchell and A. Davis, *Prepr. Am. Chem. Soc. Div. Fuel Chem.*, 1991, **36**(1), 36.
9. C. Riemer and C.E. Snape *GB Patent No. 2,204,877A*, 1988.
10. J.W. Larsen, T.L. Sams and B.R. Rogers, *Fuel*, 1980, **59**, 666.
11. R.J. O'Brien, J.R. Gibbons and R. Kandiyoti, *Fuel Process. Technol.*, 1987, **15**, 71.
12. M. Nishioka and J.W. Larsen, *Energy and Fuels*, 1990, **4**, 100.
13. P.J. Hall and J.W. Larsen, *Energy and Fuels*, 1991, **5**, 228.
14. C.E. Snape and C.J. Lafferty, *Prepr. Am. Chem. Soc. Div. Fuel Chem.*, 1990, **35**(1), 1.
15. C.E. Snape, C. McArthur and S. Mitchell, unpublished results in *Final Report to EC on Project No. EN3V-0048-UK(H)*, 1992.

Table 1 Tetralin Extraction Results

	DCM sols	% daf coal Pyr sols/DCM insols	Pyr sols
Initial coal	43.0	54.1	2.6
	42.7	55.1	1.7
CB Treated coal	62.9	32.0	3.0
	62.7	30.0	2.7

CB Treated coal is chlorobenzene extracted coal

Table 2 Hydrogenation Results

	DCM conv*	% daf coal DCM sols	Pyr sols/DCM insols	Pyr insols
Non-catalysed Initial	22.0	17.5	30.7	40.5
	23.7	19.9	31.1	40.8
CB Treated	30.1	26.3	45.8	17.4
	29.7	27.9	46.2	19.1
Catalysed Initial	62.4	58.2	29.4	5.1
	62.1	57.9	30.9	5.4
CB Treated	36.0	31.5	44.0	18.1
	35.5	31.4	42.6	17.4

* DCM sols + gas + water

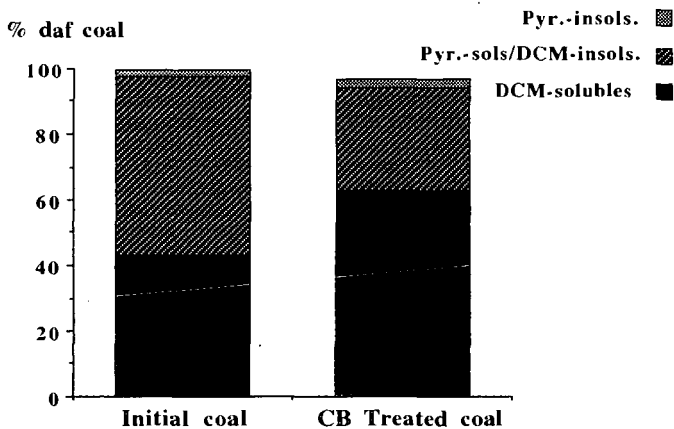


FIGURE 1 YIELDS FROM TETRALIN EXTRACTIONS

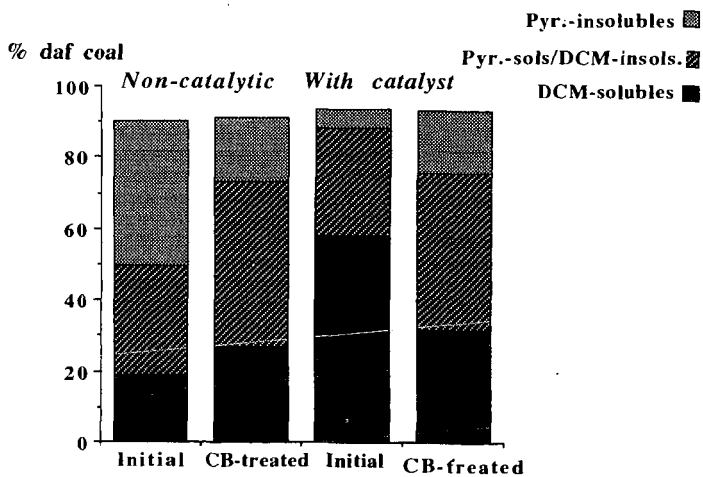


FIGURE 2 HYDROGENATION YIELDS

REACTIVITY OF COALS UNDER COPROCESSING CONDITIONS

Jasna Tomić and Harold H. Schobert
Fuel Science Program,
Department of Materials Science and Engineering,
The Pennsylvania State University,
University Park, PA 16802

Key words: coprocessing, coal reactivity, thermoplastic properties

INTRODUCTION

In the recent years greater interest has developed for processes involving coal and petroleum fractions to produce distillate fuels. Coprocessing is especially attractive as a direct liquefaction process because it involves the use of heavy petroleum fractions, so both coal and heavy petroleum resids are upgraded simultaneously. The main distinction of coprocessing from other direct liquefaction processes is that coprocessing is more complex from a chemical standpoint than direct liquefaction processes which use traditional solvents, due to the greater variety of hydrocarbons (aromatics from the coal and aliphatics from the petroleum) present in the system. Therefore, need arises for better understanding of the chemical and physical interactions during coprocessing (1).

The aim of the present study is to examine the influence of reaction conditions, coal and petroleum resid properties as well as the compatibility of the coal/petroleum resid pairs in terms of structural components on total coal conversion. Special focus will be given to the reactivity of coals and interactions of the coal and resid which lead to anisotropic coke.

EXPERIMENTAL

Five coal samples, ranging in rank from subbituminous B through high volatile A bituminous, from the Penn State Coal Sample Bank were used in this project. The coals were ground to -100 mesh and stored under nitrogen. Three petroleum resid samples were used. The West Texas (FHC-470) and Blend (FHC-571) resids were obtained from Amoco Co. and Hondo resid was obtained from Unocal. Analytical data for the coal and petroleum feedstocks are shown in Tables 1 and 2.

Prior to the reaction, the coal samples were dried to a 1% moisture under vacuum. The petroleum resid samples were used as received. A mixture of resid and coal (2.5g coal + 5g resid) was placed in a 20ml stainless steel vertical tubing bomb (microautoclave) reactor. The air was evacuated from the reactor by carefully flushing with nitrogen before pressurizing with nitrogen or hydrogen gas. The starting cold gas pressure was approximately 3.5 MPa. Reactor vessels were immersed in a fluidized sand bath which was previously preheated to 350°, 400° or 450°C and was vigorously shaken during the reaction. The reaction time was usually 30 min but some additional reactions were carried out at 15, 45, and 60 min. At the end of the reactions the microautoclave was cooled nearly instantaneously by immersing it in water.

The products were washed out from the reactor with tetrahydrofuran (THF) and separated into THF-solubles and THF-insolubles. The insoluble matter was transferred to a Soxhlet thimble and was extracted under a nitrogen atmosphere for 24 h. The THF was removed from the soluble portion in a rotary evaporator and the solid residue rinsed with acetone and pentane to remove any residual THF. Both the soluble and insoluble portions were dried under vacuum for 12 h. Total coal conversion was defined on basis of the final weight of THF-insoluble matter.

In addition to coprocessing reactions, a series of baseline experiments were performed. Thermal stability tests of the petroleum resids were carried out in order to assess the amount of THF-insoluble matter resulting from the petroleum resids directly and similarly coal was reacted alone (in the absence of a solvent) under the same reactions conditions. Unreacted (raw) coal was also extracted with THF to determine the extractable amount of coal. The amount of THF-insoluble was corrected for the amount produced from resid thermal stressing before calculating the coal conversion.

The petroleum resids were fractionated into pentane-soluble and pentane-insoluble. The pentane-solubles were analyzed by GC and, when possible, with GC-MS. The coal and the solid residue were characterized by CPMAS. The insoluble residue samples were embedded in an epoxy resin and their surfaces were polished for optical microscopy. An optical microscope with reflected polarized light was used to identify anisotropic structures in the produced solid residues.

RESULTS AND DISCUSSION

Reactions were conducted in nitrogen and hydrogen atmospheres in order to determine the influence of molecular hydrogen on coal conversion. The increase in coal conversion due to hydrogen gas was estimated by the difference of the results of coal blank (no solvent) experiments under hydrogen and nitrogen at a given temperature of reaction. These results are shown in Table 3. The first observation is that presence of hydrogen increased the conversion of the two lower rank coals more than the conversion of the higher rank coals, especially at 450° C. The lower rank coals also seem to be least sensitive to molecular hydrogen at 400° C. These results agree with the observations reported by Mochida et al. (2) that higher rank coals prefer lower temperatures, while the lower rank coals prefer higher reaction temperatures. The authors relate this to the structure of the coals and the strengths of the bonds which are inversely proportionate to the preferred reaction temperature.

We previously reported (3) the results of reactions of coal with model compound solvents. For all coals, the conversions were highest at 400° C with the exception of reactions involving pyrene. Reactions with pyrene gave the highest conversion compared to the alkylated benzenes and n-alkanes, but overall, the conversions with any solvent were better than in the absence of a solvent. Also we observed that different coals reacted differently in a hydrogen and nitrogen atmosphere in the presence of a solvent. The lower rank coals actually gave higher conversions at 400° C (and in some cases at 450° C) under nitrogen, while the higher rank coals benefited from the presence of hydrogen gas. These observations indicate that coals of different rank react differently and have different response to hydrogenation and solvation conditions. Non-donor solvents under H₂ overpressure decreased the conversion for the lower rank coals compared to the blank runs and compared to the reactions under N₂. It has been reported in the literature that lower rank coals require a better hydrogen donor especially at elevated temperatures, due to the greater number of reactive species resulting from the broken crosslinks (2) and because of the smaller size of the polyaromatic structures in these coals (4).

The results of coal conversion for the coal/resid reactions based on solubility in THF are presented in Table 4. Similarly as in the model compound studies, the coprocessing experiments yielded highest conversions at 400° C. The reactions at this temperature seem to be governed by the nature of the coal, because there is little influence of the different petroleum resids. Even between the different coals there is not significant difference at 400° C. This fact is emphasized because of the great range in results when the reaction temperature is increased to 450° C. In this case the influence of the resid feedstock is evident as well as the interactions between the coal/resid pairs. The conversions at 450° C decrease compared to the previous temperature for all coal/resid pairs

but there is obviously an influence of the resids as shown by the differences between the values in Table 4 for one coal compared to those between different coals. Figures 1 and 2 show the variation of coal conversion with temperature and coal/resid feedstock pairs.

The interactions in a coprocessing system are both physical and chemical. At 350° and 400° C the dominant effect is the dissolution of the coal particles in the solvent. At these temperatures it is predominantly a physical process because no effect of the petroleum resid (solvent) is noticed and the range of coal conversion values is small. Whether the solvent (resid) acts as a donor or a non-donor is still not a significant effect at these temperatures (5). As the temperature increases the physical dissolution of coal particles reaches a limit, and the petroleum resid undergoes chemical changes at the elevated temperature. (Note that the resids produced significant amounts of THF-insolubles only at 450° C.)

We had reported earlier (3) that the coal conversion results of the coal/resid reactions were similar to those when pyrene was in the system. This would imply that the resids act as hydrogen shuttlers. Other reported investigations indicate that indeed petroleum resids act as shuttlers rather than donors (6). The aromatic compounds present in petroleum resids can act as hydrogen shuttlers. The aromaticities of the petroleum resids used in this project, determined by NMR are shown in Table 2.

In addition to following the degree of conversion by solubility of the products in THF, optical microscopy was used to study the morphology of the solid residues. The polarized light enabled identification of isotropic versus anisotropic material. Optical microscopy of the THF-insoluble residue show that the solids are in most part isotropic when the temperature of reaction is 350° and 400° C. Anisotropic structures are detected in the solid residue from coal/resid reactions that has seen temperatures of 450° C. A closer examination of the anisotropic structures indicates that anisotropy occurs at the contact between the coal and petroleum resid particles. The resid particles surround the coal particles, which later fuse. Figure 3 shows the optical micrograph of the THF-insoluble residue obtained from reaction of PSOC 1488 subbituminous coal with Blend resid at 450° C. The lighter spots represent the anisotropic structures surrounding isotropic coal particles which are fused together. Anisotropic structures formed solely from petroleum the resid are present also. Davis et al (7) compared the THF-insoluble residue of a high volatile A and high volatile C coal and found anisotropy only in the case of the high volatile A coal. Therefore, the anisotropic structures found in the residue of the coprocessing reactions, regardless of the coal rank are attributed to the presence of the petroleum resids in the system and the coal/resid interactions.

The optical textures of the solids exhibit differences depending on the coal used in the reaction. Differences observed can be correlated to the thermoplastic properties of the coals. The higher rank coal (PSOC 1504) with a FSI of 5.5 produced solids which had pores as a result of swelling. Figure 4 shows the optical micrograph of the THF-insoluble residue obtained from reactions of PSOC 1504 with Blend resid at 400° C. The isotropic coal particles contain pores which are a result of swelling. The lower rank coal (PSOC 1488) has a FSI of 0 and does not pass through a plastic range so the solid particles under the microscope showed mostly sharp cracks as a result of devolatilization. This can be correlated with the degree of coal conversion. Namely, the coal exhibiting strong thermoplastic properties (PSOC 1504) under same reaction conditions achieves higher coal conversion than the coal that does not pass through a plastic range. These result again indicate that the structural components of the coals play an important role in the interactions during coprocessing and ultimately enhance or reduce the formation of undesirable semi-coke structures.

CONCLUSIONS

The results from coprocessing of five coals of different rank with three petroleum resids indicate that the degree of coal conversion depends on the nature of the coal as well as the nature of the resids. The conversions were optimum at 400° C where the reactions seem to be governed strongly by the coal. At temperatures up to 400° C the results indicate that the dominant effect is the dissolution of the coal particles in the solvent. The nature of the resid and especially its donor abilities, effect the conversion at temperatures higher than 400° C. The petroleum resid has undergone chemical changes above this temperature and the interactions of the coal and petroleum resids become an important factor in the conversion to light weight products. This is evident under an optical microscope where anisotropic structures were detected especially at the contact between the coal and petroleum resid particles. The morphology of the particles in the insoluble residue also indicate that thermoplastic properties of coals can be related to their reactivity under coprocessing conditions. The coal exhibiting stronger thermoplastic behavior also showed to be more reactive for coprocessing. Higher thermoplasticity is an indicator of greater mobility of structural fragments leading to higher coal conversions.

ACKNOWLEDGEMENTS

The authors are pleased to acknowledge the financial support for this research provided by the U.S. Department of Energy. The assistance of Dr. Semih Eser with optical microscopy results is greatly appreciated. We are also grateful for the assistance of Dr. O.P. Mahajan of Amoco Corporation and Dr. G.E. Dolbear of Unocal in obtaining the resid samples. We have also enjoyed useful discussions with Drs. Bruce Utz and Karl Schroeder of the Pittsburgh Energy Technology Center (DOE).

LITERATURE CITED

1. Curtis, C. W., and R. A. Winschel, in "Coal Liquefaction : A Research Needs Assessment Technical Background" DOE/ER-0400, Final Report, Vol II, February 1989.
2. Mochida, I., Kishino, M., Sakanishi, K. Korai, Y., and Takahashi, R., *Energy & Fuels*, 1987, 1, 343.
3. Tomic, J., and H. H. Schobert, *Am.Chem.Soc.,Div. Fuel. Chem. Preprints*, 1991, 36(2), 617.
4. Malhotra, R., and D. McMillen, *Energy & Fuels*, 1990, 4, 184.
5. Neavel, R., *Fuel*, 1976, 55, 237.
6. Rahimi, P. M., W. H. Dawson, and J. F. Kelly, *Fuel*, 1991, 70, 95.
7. Davis, A., Mitchell, F. J., Derbyshire, F. J., Rathbone, R. F., and R. Lin, *Fuel*, 1991, 70, 352.

Table 1. Analyses of Project Coals.

Coal (rank)	PSOC 1488 subB	PSOC 1498 hvCb	PSOC 1501 hvBb	PSOC 1504 hvAb	PSOC 1448 hvAb
%C (dmmf)	76.56	78.24	81.17	82.88	85.20
%H	5.27	5.50	5.32	5.86	6.12
%N	0.95	1.83	1.56	1.77	1.86
%O	17.22	14.43	11.95	9.49	6.81
FSI	0.0	0.5	2.0	5.5	8.0
max fluid, T°C	n/a	n/a	421	433	438

Table 2. Analyses of Petroleum Feedstock.

	Hondo	W. Texas FHC-470	Blend FHC-571
Oils (wt.%)	43.9	39.4	21.4
Resins	40.2	59.1	62.8
Asphaltenes	15.9	0.5	14.8
%C	83.40	86.39	83.91
%H	11.80	11.23	10.26
%S	5.10	0.68	4.8
C _{ar} (%) ^a	25.4	28.5	32.3
H _{ar} (%) ^a	8.1	8.2	9.3

^a determined by NMR

Table 3. Increase in coal conversion (wt%) by hydrogenation at three temperatures.

Coal	350°	400°	450°
PSOC 1488	5.49	5.11	11.7
PSOC 1498	4.06	1.9	7.9
PSOC 1501	1.81	3.26	1.92
PSOC 1504	2.75	1.11	3.59
PSOC 1448	4.5	3.58	2.26

Table 4. Total coal conversion for coal/resid reactions at 30 minutes.

Resids	350°	400°	450°	350°	400°	450°
	N ₂			H ₂		
	PSOC 1488					
Hondo	17.61	28.63	6.86	5.46	27.29	9.93
Blend	17.73	28.46	3.45	17.35	31.32	-13.54
W.Texas	14.81	28.87	19.31	19.95	33.03	16.99
	PSOC 1498					
Hondo	12.41	22.53	3.21	7.88	22.79	48.68
Blend	11.41	24.83	0.17	11.56	27.93	-2.7
W.Texas	9.92	23.61	21.08	16.5	26.82	12.83
	PSOC 1501					
Hondo	14.99	29.92	13.4	13.36	28.89	12.41
Blend	12.36	29.5	-0.39	14.75	31.75	20.99
W.Texas	15.2	29.51	26.91	20.89	31	25.85
	PSOC 1504					
Hondo	19.14	36.54	16.53	17.38	31.3	16.66
Blend	13.73	31.94	2.54	16.48	33.94	0.52
W.Texas	13.36	33.66	26.99	14.73	31.98	28.91
	PSOC 1448					
Hondo	17.33	31.87	14.37	16.45	36.2	15.26
Blend	16.24	33.85	-0.46	14.07	32.78	6.88
W.Texas	17.5	32.35	25.99	15.26	36.39	29.05

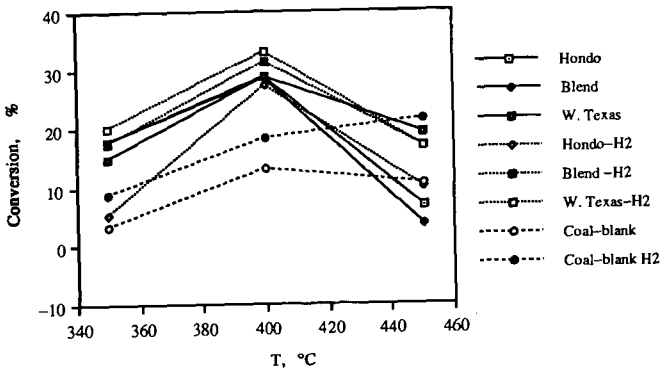


Figure 1. Coal conversion of subB coal (PSOC 1488) at three reaction temperatures under hydrogen and nitrogen atmospheres with three petroleum resid.

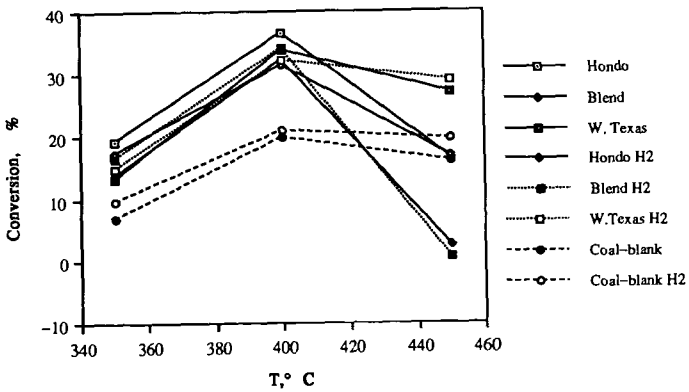


Figure 2. Coal conversion of hvAb coal (PSOC 1504) at three reaction temperatures under hydrogen and nitrogen atmospheres with three petroleum resid.

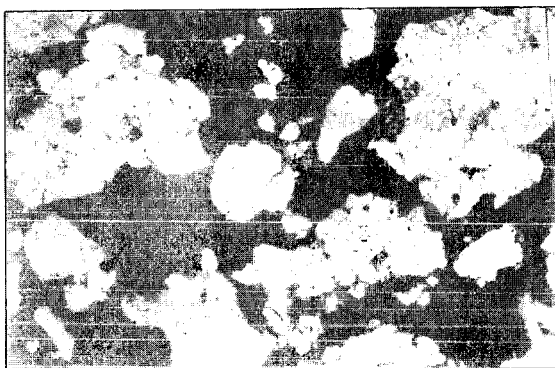


Figure 3. Optical micrograph of the THF-insoluble residue obtained from PSOC 1488 (subB) with Blend resid at 450° C.



Figure 4. Optical micrograph of the THF-insoluble residue obtained from PSOC 1504 (hVCb) with Blend resid at 450° C.

THE FLUIDIZED BED PYROLYSIS CHARACTERISTICS OF MOROCCAN OIL SHALE

U. M. Graham¹, O. Bekri² and T. L. Robl¹.

¹Center for Applied Energy Research, University of Kentucky,
3572 Iron Works Pike Lexington, KY 40511;

²Office National De Recherches Et D'Exploitations
Petrolieres, Rabat, Morocco.

Keywords: Fluidized bed, oil yields, material balances.

ABSTRACT. Pyrolysis characteristics of oil shales from the Timahdit and Tarfaya deposits were investigated in fixed bed, nitrogen swept fixed bed and fluidized bed pyrolysis. The objectives of this work were to determine the effects of pyrolysis conditions on product yields and distribution of the pyrolysed shales. Samples representative of two lithologic units (M_1 and T_4), which comprise part of the richest zone of the Timahdit oil shale formation and samples representative of five zones (R_0 , R_1 , R_2 , R_3 and R_4) of Tarfaya deposit were examined. The shales are primarily carbonates, averaging 12.9 (Timahdit) and 11.3 (Tarfaya) percent organic carbon. Modified Fischer assay for the shales resulted in oil yields ranging between 13.2 and 20.4 gal/ton. Fluidization resulted in shale oil yields ranging from 133 - 157 percent of modified Fischer Assays.

INTRODUCTION. Large deposits of oil shales exist in Morocco. Extensive exploration and processing research has been conducted over the past decades (1). Moroccan oil shale deposits, discovered in the 1960's (1) include those at Guir, Ganntour, Mescala, Oulad Abdoun, Tanger, Tarfaya and Timahdit (1-6). Because oil shales are the only abundant indigenous source of fossil fuel in Morocco an extensive resource assessment program has been conducted by Office National de Recherches et D'Exploitations Petroliers (ONAREP). The entire shale oil resources were estimated to amount to 50 billion barrels (2).

Organic carbon contents for Moroccan shales, averaging between 11 and 13 percent, are very similar to both western and eastern US oil shales (2). When western US oil shale technologies are applied to Moroccan shales, a significant amount of carbon is left on the spent shales (2, 4) and large amounts of off-gases are generated. This is similar to the case for eastern US oil shale, where coking and cracking reactions result in high residual carbon and large off-gas volume (7, 8). Fluidized bed retorting has been shown to enhance oil yields when applied to eastern US oil shale by minimizing retrograde oil reactions. This is accomplished by providing rapid heat up and product sweep.

Thus, the objectives of this study are to determine if fluidized bed retorting will enhance oil yields from Moroccan shale and to determine the nature of products produced from the shale. Oil shales from the Timahdit and Tarfaya deposits were selected and the pyrolysis characteristics were investigated using fixed bed, nitrogen swept fixed bed and fluidized bed conditions.

CHARACTERIZATION OF TIMAHDIT AND TARFAYA OIL SHALE DEPOSITS. The Cretaceous Timahdit and Tarfaya oil shale have been under intensive study since 1974 as potential sources of domestic oil (1 - 6). The Timahdit and Tarfaya deposits are among the largest of the

Moroccan oil shales, and are located strategically relative to major cities, potential ports and mining configuration (2). The Timahdit deposit is situated in the Middle Atlas region in the north central part of Morocco, 155 miles southeast of Rabat and 22 miles south of Azrou, and occur in two northeast-southwest trending geosynclines (2). The Tarfaya deposit is located in the south west region along the Atlantic Coast of the Moroccan Sahara. The coastal location is a significant factor in the potential development of this deposit. A comprehensive summary of the previous research relative to the Tarfaya and Timahdit oil shale activities is presented elsewhere (1, 2, 5).

Marlstones, silicious marlstones and limestones comprise the bituminous rocks of the Tarfaya and Timahdit oil shale regions (1, 2). Representative samples from Tarfaya and Timahdit deposits utilized in this study are derived from seven oil shale zones which are further distinguished in 21 sub-zones (Table 1). A considerable variation in zone thickness occurs among the individual beds (Table 1). Samples representative of two lithologic units (M_1 and T_4 , see Table 1), which comprise only part of the hydrocarbon section of the Timahdit deposit (2), were available for study. These two shale beds contain predominantly argillaceous marls. In contrast, the Tarfaya oil shales consist mainly of chalks with varying kerogen contents and are characterized by higher moisture contents compared to those of Timahdit (2). The richest Tarfaya oil shale zone, R-zone, is subdivided into 5 lithologic units (R_0 , R_1 , R_2 , R_3 and R_4), all of which were available in this study (see Table 1).

The seven oil shale samples under investigation were obtained from master batches which were produced from bulk samples derived from individual shale beds. The shales were crushed, blended and screened to 18 x 20 mesh for the pyrolysis study. The shale was stored under argon to retard oxidation. Fixed bed, N_2 -swept fixed bed and fluidized bed runs were conducted using representative sample aliquotes with the same grain size to allow for more precise comparison of the oil yields.

EXPERIMENTAL.

Modified Fischer Assay

A single fixed bed retorting system was used to determine the Fischer Assay pyrolysis characteristics of the seven oil shale zones. A single retort was utilized to eliminate unaccountable systematic errors and to obtain an unbiased base for comparison. Modifications to standard Fischer Assay procedures were employed because it had been previously shown that these running conditions provide for more reproducible results for eastern US oil shales (9, 12). This study's operating conditions included a linear heating rate of 12 °C/min during oil evolution and a 30 minute soak time at maximum retort temperature of 550 °C. The purpose of the modified Fischer Assay experiments was to establish oil yield data for the shale samples that will be used in the fluid bed retort experiments.

N_2 -Swept Fixed Bed Experiments

The fixed bed retorting system is described in detail elsewhere (9). Operationally, a continuous stream of N_2 -gas was allowed to enter the pyrolysis zone after being heated to run temperature (550°C). Preheating of the purge-gas was achieved while passing it through a spiral coil that was encased in the reactor furnace. The N_2 -stream swept oil vapors and a small amount of fines into the product collection system. The purpose of the N_2 -swept fixed bed runs was to determine variations in oil yields caused when the contact time between oil vapors and shale particles was reduced.

Bench Scale Fluidized Bed Experiments

Apparatus: A 1.5 inch diameter reactor as used for fluid bed pyrolysis of Eastern Shales was used in this study. The apparatus has also been described in detail elsewhere (9) and only a brief description is offered here. The retort itself was constructed of 316 stainless steel and has a 100 micron stainless steel filter at the bottom which serves as distributor plate. A stand pipe controlled the spent shale overflow from the bed. To closely monitor the retort conditions three thermocouples were located above the distributor plate at lower, medium and upper bed heights. The retort was enclosed in an electrically heated furnace which further accommodates a gas preheater and a fines trap. The preheater served to heat the fluidizing gas to bed temperature before entering the shale zone. The baffled fines trap helped to remove shale particulates from the oil vapor to diminish coke formation before vapors exit the high temperature zone provided by the furnace. A screw feeder was calibrated to add raw shale at a feeding rate of 2.0 ± 0.1 g/min into the reactor. N_2 purge-gas was passed down from the feed bin and up through the spent shale reservoir into the reactor. A purge-gas flow rate of 0.25 - 0.30 STP L/min was sufficient to prevent oil vapors from escaping through either inlet or exit pipes. Helium gas was used as fluidizing medium. The volumetric He-flow rate at bed temperature (550°C) and pressure (1 atmosphere) was adjusted to 28 L/min and in combination with a shale feed rate of 2.0 g/min provided for a shale residence time of approximately 20 minutes.

The above fluidized bed pyrolyser provides all of the following: good mixing of the shale solids including both raw shale and pyrolysed ash particles; excellent heat transfer; rapid heating rates of the shale particles; and, a uniform pyrolysis temperature of 550°C . In addition, short residence time of oil vapor in the hot zones favors low oil cracking.

Product Collection Traps: The same configuration of product traps used for eastern US oil shales was employed in this study and the reader is referred to the original work (9). Four traps were used to condense the products generated in the fluidized bed retort. The trap closest to the reactor exit pipe, an air-cooled stainless steel tube, condensed a tarry product. The second trap, an Ice/bath, is designed to remove both oil and H_2O from the vapor phase and consists of a closed pyrex tube with gas in- and outlet openings. The third trap, was developed to condense large amounts of products and utilizes thermal wells and densely coiled stainless steel wire spirals for increased precipitation surface (10, 11). The trap itself was immersed in a Dry Ice/isopropanol bath (-78°C). The final trapping system consists of a 50 ml pyrex tube, sealed with a rubber stopper and was immersed in a Dry/Ice isopropanol bath. The exit tube is connected into a hood system and allows non-condensable vapors to be removed. A gas sample can be drawn for analysis of the vapor phase. Gases leaving the product collection apparatus were monitored on a Carle Gas analyser (Series SX-AGC) to determine off-gas weight.

RESULTS AND DISCUSSION. Operating parameters employed in this study are not necessarily optimum running conditions. They were chosen as a basis for this investigation because a large data base is available from previous bench scale fluidized bed retorting on similar materials.

Ultimate and proximate analyses indicate major differences in moisture, ash and sulfur contents between the Timahdit and Tarfaya oil shales under investigation (Table 2). Results of material balances for modified Fischer Assay runs (Table 3) and N_2 -swept fixed bed experiments (Table 4) demonstrate that the latter pyrolysis method caused a slight enhancement in oil recovery. Modified Fischer assay for the shales resulted in oil yields ranging between 13.2 and 20.4 gal/ton and oil yields obtained in the N_2 -swept fixed bed retorting experiments were in the range of 15.7 - 21.6 gal/ton. Therefore, a maximum oil yield increase of 21 percent was achieved by

mobilizing oil vapors with a continuous flow of N_2 gas which reduced the overall residence time of the oil vapors on the shale particles. Also, a decrease in off-gas emission was recorded when N_2 gas mobilized the oil vapors (Table 3, 4), suggesting that vapor phase cracking was reduced. In general, a slightly greater reduction in off-gas emission was recorded for the Tarfaya oil shale samples compared to those of Timahdit. The difference may be related to the higher carbonate and moisture and lower sulfur contents of Tarfaya shales. The results further indicate that oil densities increase for the N_2 -swept fixed bed runs (0.956 - 0.971 g/cm³, Table 4) compared to modified Fischer Assay (0.944 - 0.968 g/cm³, Table 3).

Fluidized bed pyrolysis resulted in oil yields in excess of the modified Fischer Assay and N_2 -swept fixed bed pyrolysis (Table 6 and Figure 1). At this point of study, fluidized bed retorting was performed for three of the seven shale samples. Oil yields obtained from the bench scale fluid bed retort (Table 6) were based on oil collected in the trapping system. The moisture collected simultaneously with the oil was resolved during Karl Fischer water analysis. The C_5^+ hydrocarbon fraction in the off-gas phase was not accounted for in the mass-balance calculations at this time. The C_5^+ concentration was determined to be insignificantly small in the off-gas for either of the fixed bed retort methods employed.

Using the 1.5 inch diameter fluid bed retort, at 550°C operating temperatures 55 to 60 percent of the carbon was removed from the Timahdit shale samples (M_1 and T_4) and 65 percent of the carbon was removed from the Tarfaya shale (R_4). Material balances indicated oil yields for the Timahdit and Tarfaya shale samples to vary between 133 to 157% of those of the Fischer Assay runs (Table 6). A comparison with Eastern shale fluidized bed retorting shows great similarities with respect to overall oil yield and processing behavior.

The fluidized bed retorting of Moroccan oil shales appears very promising from a view point of oil yields. Fluidized beds provide not only enhanced oil yields under relatively non-severe conditions (moderate temperatures of 550°C at atmospheric pressures), but also leave the pyrolysed shale with much less remaining sulfur. This has two potential advantages. The first is lower environmental risks do to lower acid release after exposure to atmosphere. A second is the potential recovery of elemental sulfur, a needed raw material in Morocco.

ACKNOWLEDGEMENTS

The authors gratefully acknowledge the work of D. Thomas and M. Moore for analytical support and D. McLean for sample preparation.

REFERENCES

- 1 Russell P.L., (1990). Oil shales of the world. Their Origin, Occurrence and Exploitation, Chap. 3, Pergamon Press, Oxford, p. 15-30.
- 2 Bekri, O. and Ziad, M.,(1992). Proceedings of the 1991 Eastern Oil Shale Symposium, Lexington, KY (in press).
- 3 Bouchta, R. and Marcil, A., (1981). Moroccan oil shale development program, 6th IIASA Resources Conference, Golden Colorado, pp. 24.
- 4 Bouchta, R., (1985). Oil shale programme in Morocco, Office National de Recherches et d'Exploitations Pétrolières, Oil shale Division, Rabat, Morocco, pp. 21
- 5 Bouchta, R. and Bekri, O., (1981). Oil shale activities in Morocco, Office National de Recherches et d'Exploitations, Rabat, Morocco, pp. 24.
- 6 Anon, (1986). Oil shale in Morocco, research and development activities. A brochure by Office National de Recherche et d'Exploitations Pétrolières, Rabat, Morocco.

- 7 Rubel, A.M. and Carter, S.D., (1984). Symposium on Characterization and Chemistry of Oil Shales, American Chemical Society, St. Louis, 202.
- 8 Margolis M.J., (1982). Proceedings of the 1981 Eastern Oil Shale Symposium, Lexington KY.
- 9 Rubel A.M., Margolis M.J., Haley J.K. and Davis B.H., (1983). Proceedings of Eastern Oil Shale Symposium, IMMR, 89.
- 10 Wallman P.H., Tamm P.W. and Spars B.G., (1981). Oil shale retorting kinetics. Symposium on Oil Shale, Tar Sands, and Related Materials, American Chemical Society, Washington D.C., 163.
- 11 Richardson J.H., Nuss E.B., Ott L.L., Clarkson J.E., Bishop M.O., Gregory L.J., and Morris C.J.,(1982). Fluidized bed pyrolysis of oil shale, oil yield, composition and kinetics. UCID-195648, Lawrence Livermore National Laboratory.
- 12 Coburn T.T., Rubel A.M. and Henson T.S.,(1981). Eastern oil shale retorting: Pyrolysis of the Sunbury shales of Kentucky. IMMR Reprint no. IMMR 81/062, University of Kentucky, Lexington, KY.

TABLE 1 OIL SHALE ZONES FROM TARFAYA AND TIMAHDIT DEPOSITS

DEPOSIT TYPE	SAMPLE ID [sub-zone]	OIL- SHALE ZONES	ZONE THICKNESS [meter]
TARFAYA OIL SHALE DEPOSITS	RON	I RO	1.1
	R-1A	II R1	7.45
	R-1B		
	R-1C		
	R-1D		
	R-1E		
	R-1F		
	R-1G		
	R-2A1	III R2	4.4
	R-2A3		
	R-2B1		
	R-2B2		
	R-2C	IV R3	4.85
	R-3A1		
	R-3A2		
R-3A3			
R-3A4			
R-3A5			
R-4B1	V R4	2.2	
TIMAHDIT OIL SHALE DEPOSITS	T-4	VI T	42.15
	M1-COUCH	VII M	67.35

TABLE 2 PROXIMATE AND ULTIMATE ANALYSES OF MOROCCAN OIL SHALE DEPOSITS

SAMPLE ID	MOISTURE	VOLATILES	ASH	FIXED CARBON	1*		N	2*
	wt %	wt %	wt %	wt %	C	H	wt %	S
TARFAYA OIL SHALE DEPOSIT								
RON	2.39	40.3	56.33	1.1	16.88	1.41	0.63	0.19
R-1A	2.77	41.8	54.86	0.6	18.88	1.92	0.84	0.98
R-1B	3.91	39.4	55.87	0.8	14.82	1.29	0.62	0.15
R-1C	4.67	41.8	52.86	0.7	19.02	2.07	0.83	0.35
R-1D	6.61	42.3	49.76	1.3	19.06	2.44	0.76	0.39
R-1E	4.44	44.1	51.73		19.93	2.14	0.83	0.48
R-1F	2.47	47.7	49.62	0.2	21.84	2.01	0.82	0.47
R-1G	7.04	43.2	49.96	0	19.14	2.23	0.79	0.46
R-2A1	1.98	41.5	55.38	1.2	14.7	0.94	0.52	0.17
R-2A3	4.68	39.7	53.37	2.2	17.4	1.74	0.7	0.32
R-2B1	8.12	40.7	49.71	1.5	15.44	1.8	0.52	0.08
R-2B2	5.45	42.9	51.31	0.3	15.43	1.46	0.54	0.19
R-2C	3.01	42.2	53.77	1.1	13.9	1.03	0.57	0.13
R-3A1	6.47	43.6	49.71	0.2	18.31	1.95	0.76	0.29
R-3A2	5.15	40.9	52.83	1.1	17.6	1.78	0.7	0.37
R-3A3	3.54	48.1	48.14	0.3	22.23	2.27	0.31	0.52
R-3A4	5.91	47.1	46.13	0.9	20.98	2.36	0.81	0.39
R-3A5	7.75	38.9	52.36	1.1	15.16	1.8	0.53	0.23
R-4B1	7.05	44.1	48.59	0.3	19.16	2.19	0.67	0.39
TIMAHDIT OIL SHALE DEPOSIT								
T-4	2.79	29.5	65.31	2.4	15.65	1.63	0.78	1.44
M1-COUCH	1.8	36.4	60.94	0.9	19.77	1.85	0.77	1.9

1* organic + inorganic C

2* organic + inorganic S

TABLE 3 MATERIAL RECOVERY FROM MODIFIED FISCHER ASSAY

SHALE MATERIAL	R0	R1	R2	R3	R4	M	T
	wt %	wt %	wt %	wt %	wt %	wt %	wt %
SPEND SHALE	81.4	76.55	89.57	77.08	75.11	85.07	83.16
H2O	9.26	12.08	4.11	14.02	13.01	4.44	7.27
OIL	6.72	7.94	5.33	8.22	8.19	7.09	6.19
GAS	1.82	3.45	1.02		3.75	3.33	3.41

TABLE 4 MATERIAL RECOVERY FROM N2-SWEPT FIXED BED

MATERIAL	R0 wt %	R1 wt %	R2 wt %	R3 wt %	R4 wt %	M wt %	T wt %
SPEND SHALE	81.45	76.21	88.89	77.52	75.05	83.17	81.74
H2O	9.35	12.99	3.99	14.29	14.11	4.97	7.31
OIL	7.41	8.27	6.31	8.41	8.25	8.69	7.88
GAS	1.77	2.56	0.77		2.61	3.12	3.06

TABLE 5 OIL YIELD AND OIL DENSITY OF PYROLOYSED SHALES

ZONE	FA OIL DENSITY		N2-FA OIL DENSITY	
	[gal/ton]		[gal/ton]	
R0	16.97	0.949	18.57	0.956
R1	19.92	0.955	20.66	0.959
R2	13.29	0.959	15.68	0.964
R3	20.39	0.966	20.79	0.969
R4	20.27	0.968	20.38	0.971
T	15.71	0.944	19.66	0.61
M	17.92	0.948	21.58	0.965

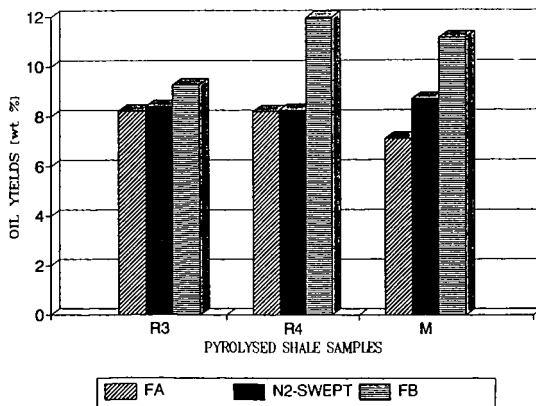
TABLE 6

YIELDS FOR FLUID BED RETORT

ZONE	OIL wt %	1* FB vs. FA %
R3	9.28	133
R4	11.96	146
M	11.13	157

1* percent oil yields of Fischer Assays

FIGURE 1 COMPARISON OF OIL YIELDS



**THE OXIDATION OF THE KEROGEN OF CHATTANOOGA SHALE
WITH ALKALINE PERMANGANATE AND CHROMIC ACID**

Melissa Rogers and Chris W. McGowan

Department of Chemistry, Tennessee Technological University
Cookeville Tennessee 38505

Keywords: oil shale, kerogen, oxidation

INTRODUCTION

The majority of the organic material in oil shales is present in the form of kerogen. Kerogen is a high molecular weight heteropolymer which is insoluble in common organic solvents. Due to the interferences inherent in the analysis of such material, data obtained from raw kerogen concentrates is somewhat limited and valid only on a statistical basis. One method used to more thoroughly characterize the kerogen structure is to break down the polymeric matrix by controlled oxidation followed by analysis of the oxidation products.

Several methods have previously been used to oxidize Chattanooga Shale and kerogen concentrates derived from the shale. Leonard (1) used 3.5 percent ozone to oxidize shale samples and a kerogen concentrate. Water and ether soluble acids were extracted from the oxidized material. Products consisted primarily of aliphatic hydroxy acids. A later study by Kinney and Leonard (2) produced highly oxygenated ether and water soluble acids. Kinney and Schwartz (3) oxidized Chattanooga Shale with air at 200°C for 200 hours in order to maximize the production of humic acids. The acids obtained were quinoid in nature and similar to those obtained from coal. Stanton and co-workers (4,5,6) utilized a stepwise oxidation with perchloric acid to oxidize Chattanooga Shale. The primary products were highly polar, unsaturated carboxylic acids. A model for the structure of the kerogen in Chattanooga Shale was proposed by Stanton et al. (6). The model consisted of highly condensed aromatic material with alkyl side chains. Ether oxygen was a major crosslink in the kerogen matrix.

This paper describes the characterization of two kerogen samples derived from Chattanooga Shale by oxidative degradation with alkaline potassium permanganate and chromic acid. The oxidation products were separated into acidic and basic fractions. Samples were analyzed by fourier transform infrared spectrophotometry (FTIR) and gas chromatography (GC). Selected samples were analyzed by gas chromatography coupled to mass spectrometry (GC-MS).

EXPERIMENTAL

A sample of the Gassaway member of the Chattanooga Shale was obtained from the Eastern Highland Rim area of Tennessee. The sample was ground to minus 60 mesh in preparation for demineralization and bitumen extraction. A 1000-g sample was demineralized using a combination of hydrochloric and hydrofluoric acids (5). Bitumens were removed by soxhlet extractions with benzene and methanol. The kerogen concentrate obtained had a mass of 235.1 g. A kerogen concentrate previously prepared by Stanton (4,5) was also used in this study.

Both kerogen samples were oxidized with alkaline permanganate solution. Samples having a mass of approximately two grams were oxidized in a stepwise manner using 100-mL aliquots of a 0.06 molar potassium permanganate solution in 1.6 percent potassium hydroxide. The solution was heated to 90°C until complete permanganate consumption was indicated by the loss of purple and green colors in the reaction flask. The mixture was filtered at the end of each reaction step and the residue washed with 1.6 percent potassium hydroxide to insure complete product removal. Neutral and basic molecules were separated from the aqueous product mixture by ether extractions. The remaining aqueous phase was then acidified and extracted with ether to remove the ether soluble acids. Precipitated acids which formed at this stage were also collected. All extractions were performed in three steps with one hour allowed for partitioning between the phases in each step. The remaining aqueous solution was essentially colorless, indicating a low concentration of water soluble acids. No effort was made to recover these compounds. The residue from alkaline permanganate oxidation contained large amounts of manganese dioxide, which was removed by treatment with oxalic acid in order to determine the mass of the remaining organic material. The residue from one sample dissolved completely, indicating that the kerogen sample had been entirely converted to soluble species.

A 14-g sample of the kerogen concentrate was also oxidized in a stepwise manner using 3.0 M chromic acid solution and successively longer oxidation steps. The time periods of the oxidation steps were 3, 6, 12, 24, and 48 hours. The oxidation products were separated at the end of each step by a series of extractions. Heptane and ether extractions removed the oxidation products from the aqueous solution. These extracts were then extracted with 6.0 M sodium hydroxide in order to separate the basic fraction of the products. The sodium hydroxide solutions were then back-extracted with heptane or ether to isolate the basic products.

The raw kerogen concentrate was analyzed by X-ray diffraction (XRD) and scanning electron microscopy using energy dispersive X-rays (SEM-EDX) in order to determine the identity of any resistant mineral material. Oxidation products obtained from alkaline permanganate and chromic acid oxidations were analyzed using FTIR, GC, and GC-MS. Infrared spectra were obtained by

using thin films and potassium bromide pellets with a Nicolet 20 DXB FTIR Spectrometer. Gas chromatograms of the neutral and basic fractions, and of the methyl esters of the ether and heptane soluble acids were obtained on a Perkin-Elmer 8500 Gas Chromatograph with an SGE SPB-5 capillary column. Selected samples were analyzed by GC-MS using a Hewlett Packard 5987 gas chromatograph/mass spectrometer with a similar column.

RESULTS AND DISCUSSION

The kerogen concentrate was 17.1 percent ash. The ash was brick red in color. After dissolution, iron was determined spectrophotometrically with 1,10-phenanthroline (7). The ash was found to be 55.4 percent iron(III) oxide. Scanning electron microscopy of the kerogen concentrate indicated the presence of iron and sulfur. X-ray diffraction confirmed these findings and indicated that the mineral material consisted almost exclusively of pyrite. This was expected as pyrite is not removed by the demineralization procedure. By comparison, inorganic ash made up 33.8 percent of the kerogen concentrate prepared by Stanton. The difference is due mainly to the somewhat irregular distribution of pyrite in the Chattanooga Shale.

The oxidation products obtained from both alkaline permanganate and chromic acid oxidations were separated into basic and acidic fractions. Chromic acid oxidation products were further separated into heptane and ether soluble fractions. Alkaline permanganate oxidation also produced considerable high molecular weight acids which precipitated from solution. These precipitated acids remained complex enough to make analysis difficult. Therefore, 50-mg samples of precipitated acids from several steps were further oxidized with 10-mL portions of 0.06 alkaline permanganate. These reactions were carried out using microscale apparatus. Products were separated in a manner similar to the original permanganate oxidations, the exception being that any precipitated acids formed were returned to the reaction flask.

Product mass data for the alkaline permanganate oxidations reveal some interesting differences between the two samples. While the recovery of basic material and soluble acids is very similar, that of precipitated acids and residual material is quite distinct. The kerogen concentrate with 33.8 percent ash (Table 1) produced only moderate amounts of precipitated material and left no residue. Slightly less than 30 percent of the original sample weight was recovered as oxidation products. This suggests that large amounts of the structure were oxidized to carbon dioxide and other light molecules which would be lost. The kerogen concentrate with 17.1 percent ash (Table 2) produced large amounts of precipitated acids as well as considerable residual material. One hundred thirty percent of the initial sample weight was recovered as oxidation products and residual material. This represents not only the retention of much of the initial structure but also the incorporation of large amounts of oxygen. This data appears to indicate some significant

heterogeneities in the kerogen of the Chattanooga Shale, although no definite conclusions may be drawn on the basis of two samples. Chromic acid oxidation of the 17.1 percent ash sample (Table 3) produced generally low product recovery. This is consistent with oxidation of only the more reactive sites of this resistant material.

Infrared spectra were obtained for all fractions. Spectra for both acidic and basic fractions indicated the presence of both aromatic and aliphatic material. Basic fractions were found to contain hydroxyl and amide groups, as well as various substituted benzenes. The presence of ether functionalities and both aromatic and aliphatic ester groups was indicated, as were quinone structures. Spectra of acidic fractions were dominated by peaks attributable to carboxylic acid groups. Aromatic ethers, alcohols, phenols, and thiols were also present. The spectra of precipitated acids were similar to those of soluble acids. The major difference between the two was that oxygen containing functional groups were more dominant in the precipitated acid fraction and aliphatic material was greatly reduced.

Gas chromatograms were obtained for all basic fractions. The acidic fractions were converted to methyl esters using boron trifluoride in methanol (8). Gas chromatograms were then recorded for the methyl esters of all acidic fractions with the exception of the precipitated acids produced by alkaline permanganate oxidation. Chromatograms were obtained for the degradation products of the precipitated acids. Gas chromatography data indicated a broad diversity of products.

Selected samples from each product type were analyzed by gas chromatography-mass spectrometry. Preliminary analysis of the mass spectra obtained has confirmed the presence of both aromatic and aliphatic material. Both acidic and basic fractions contained multisubstituted benzenes, saturated and unsaturated cyclic structural units, and long alkyl chains. n-Alkane chains containing up to thirty carbons have been identified. The basic fractions were found to contain amines, alcohols, thiols, and esters. Hydrocarbons and alcohol functionalities were dominant. Carbon skeletons consist primarily of disubstituted benzenes, multisubstituted cyclohexanes, and n-alkyl chains. Molecular sizes range from sixteen to twenty-seven carbons. The acidic fractions were esterified prior to analysis, and the spectra of these samples were characterized by peaks attributable to the ester functionality. The compounds were interpreted as originally being mono- and poly-carboxylic acids. Carbon skeletons consisted of mono-, di-, and tri-substituted benzenes, phenols, cyclic groups, and n-alkyl chains. Molecular sizes range from ten to thirty carbons.

CONCLUSIONS

A kerogen concentrate derived from the Chattanooga Shale was oxidized in a stepwise manner with alkaline potassium permanganate and chromic acid. Infrared analysis of the oxidation products indicated the presence of aromatic and aliphatic material. Functionalities included alcohols, thiols, phenols, ethers, esters, quinones, and carboxylic acid groups. Gas chromatography-mass spectrometry analysis of selected oxidation products confirmed that both aromatic and aliphatic material was present in the oxidation products. Carbon skeletons of the products were found to consist of substituted benzenes, saturated and unsaturated cyclic structures, and n-alkyl chains. Molecular sizes ranged from ten to thirty carbons. The largest molecules were interpreted as n-alkanes and n-saturated monocarboxylic acids. Aromatic material was typically multifunctional, and was probably responsible for most of the cross-linking within the kerogen. This data will be used to suggest modifications to the structure of Chattanooga Shale kerogen proposed by Stanton (6). Several basic modifications to the structure are in order. Sulfur and nitrogen containing compounds are confirmed in the oxidation products and amine, amide, and thiol groups should be introduced into the model. Alkyl chains of up to thirty carbons should also be included, essentially doubling the length of those in the present model. Other groups which should be accommodated include carbon chains with multiple double bonds, phenols, quinones, and disubstituted benzene rings.

ACKNOWLEDGEMENTS

This work was supported by a Tennessee Tech Faculty Research Grant. The authors would like to thank Scott Schlorholtz, Glenn Oren and Warren Straszheim of Iowa State University for the XRD and SEM-EDX analyses. The authors appreciate the efforts of Robin Bright at Tennessee Tech University for developing some of the GC methods. The authors would also like to thank Susana Harwood of the Water Center at Tennessee Tech University for running the GC-MS system. Donation of the samples of Chattanooga Shale by H. Wayne Leimer of the Earth Sciences Department at Tennessee Tech is gratefully acknowledged.

REFERENCES

1. Leonard, J.T., "Ozonolysis of the Organic Matter of Chattanooga Black Shale," Univ. Microfilms (Ann Harbor), L.C. Card No: Mic 59-2987, 1288 (1959).
2. Kinney, C.R. and J.T. Leonard, "Ozonization of Chattanooga Uraniferous Black Shale," J. Chem. Eng. Data, **6**, 474 (1961).
3. Kinney, C.R. and D. Schwartz, "Partial air Oxidation of Chattanooga Uraniferous Shale," Ind. Eng. Chem., **49**, 1125 (1957).

4. Stanton, B.J. and C.W. McGowan, " The Analysis of the Organic Matter in Chattanooga Shale by Oxidation with Perchloric Acid," Prepr. Pap.-Am. Chem. Soc., Div. Fuel Chem., **33**, 449 (1988).
5. Stanton, B.J., R.M. Morris and C.W. McGowan, "The Characterization of the Kerogen of Chattanooga Shale, Part I - the Oxidation of the Chattanooga Shale with Boiling Perchloric Acid," Fuel Process. Technol., **29**, 85 (1991).
6. Stanton, B.J., D.J. Davidson and C.W. McGowan, "The Characterization of the Kerogen of Chattanooga Shale, Part II - Analysis of Oxidation Products and Proposal of a Model of the Structure of Kerogen in Chattanooga Shale," Fuel Process. Technol., **29**, 97 (1991).
7. Diehl, H. and G.F. Smith, Quantitative Analysis, John Wiley and Sons, Inc., New York, 368 (1952).
8. McGowan, C.W. and H. Diehl, "The Oxidation of Green River Oil Shale with Perchloric Acid. Part II - The Analysis of Oxidation Products," Fuel Process. Technol., **10**, 181 (1985).

TABLES

TABLE 1. Product masses (in mg) resulting from the alkaline permanganate oxidation of the kerogen concentrate with 33.8 percent ash

	Basic Fraction	Soluble Acids	Precipitated Acids	Total Product
Step 1	10.2	12.6	8.6	31.4
Step 2	7.0	14.9	69.3	91.2
Step 3	5.0	19.0	33.9	57.9
Step 4	4.0	19.1	43.5	66.6
Step 5	10.6	31.6	55.1	97.3
Step 6	13.5	23.5	61.4	98.4
Step 7	3.7	32.3	48.5	84.5
Step 8	3.3	25.3	35.4	64.0
Step 9	3.4	24.1	19.7	47.2
Step 10	4.4	11.1	0	15.5
Residue				0
Total	65.1mg	213.5mg	375.4mg	654.0mg
Initial sample: 2.2106g				

TABLE 2. Product masses (in mg) resulting from the alkaline permanganate oxidation of the kerogen concentrate with 17.1 percent ash

	Basic Fraction	Soluble Acids	Precipitated Acids	Total Product
Step 1	7.5	22.0	27.1	56.6
Step 2	12.1	21.0	185.2	218.3
Step 3	6.9	21.1	78.9	106.9
Step 4	5.9	32.0	555.7	593.6
Step 5	3.9	32.6	30.8	67.3
Step 6	10.5	29.9	37.2	77.6
Step 7	11.9	29.1	54.5	95.5
Step 8	3.2	31.0	32.4	66.6
Step 9	3.6	14.0	0	17.6
Step 10	8.8	6.0	0	14.8
Residue				1380.3mg
Total	66.8mg	216.7mg	974.7	2638.5mg

Initial sample: 2.0164g

TABLE 3. Product masses (in mg) resulting from the chromic acid oxidation of the kerogen concentrate with 17.1 percent ash

Oxidation Step	Water Soluble Bases	Ether Soluble Bases	Heptane Soluble Bases	Ether Soluble Acids	Heptane Soluble Acids
3 hour	1.0	2.5	0.4	2.3	4.3
6 hour	2.0	41.1	1.1	5.8	3.5
12 hour	43.2	43.3	40.5	6.2	35.2
24 hour	8.4	11.6	7.7	10.4	10.1
48 hour	9.1	8.9	6.9	14.5	6.0
Total	63.7mg	107.4mg	56.6mg	39.2mg	59.1mg

Total product: 326.0mg Residue: 14.1458g
Initial sample: 14.4139g

COKING AND CRACKING REACTIONS OF OIL VAPOR OVER HOT OXIDIZED OIL SHALE

M. F. SINGLETON, C. J. MORRIS, P. H. WALLMAN, and C. B. THORSNESS
Lawrence Livermore National Laboratory, Livermore, California 94550

Keywords: coking, cracking, mineral surfaces, shale oil

ABSTRACT

The investigation of cracking and coking reactions of shale oil vapor in the presence of hot oxidized oil shale is conducted both for its intrinsic importance and in support of the modeling effort on the oil shale process. The model includes mass transfer of vapor through the gas film surrounding the shale particles with countercurrent flow of cracked low-molecular weight products, diffusion through the pore system, adsorption onto the internal surfaces, chemical reaction of the adsorbate, and desorption of oil and light gas. Results from two experimental configurations are related to the model calculations, and the application of coking and cracking in the retort process to upgrade oil product are discussed.

INTRODUCTION

Hot-Recycle-Solids (HRS) oil shale processes^(1,2) provide the heat for reaching pyrolysis temperatures through recycle of a burned shale stream. The intimate contact between primary oil vapors and recycled burned solids results in oil property changes that are mostly favorable but can also result in oil yield loss to coke and noncondensable gases. Previous work at LLNL^(3,4) and at CSIRO in Australia^(5,6) has shown that partial coking of shale oil vapors over oxidized shale minerals can have a favorable oil upgrading effect due to cracking of heavy oil to lighter components. Hence the degree of coking in HRS oil shale processes may provide an opportunity to improve oil quality and at the same time control the undesirable loss of product to excess coking and cracking. As a guide to this optimization we have developed a coking model that is based on the HRS pilot plant process developed at LLNL.

The coking process is quite complex because of its heterogeneous character coupled with its dependence on both oil properties and surface properties⁽³⁾. In many respects it resembles catalytic petroleum crackers in that both processes involve the contact of oil vapors with a hot porous solid. Similar to the deactivation of many solid catalyst, the surface reactions on oxidized shale have been shown⁽⁴⁾ to change with coke buildup leading to a slowdown of the overall coking rate with time.

In the model we assume that the oil is a mixture of three pseudocomponents each with a different boiling point. The diffusion rates and the adsorption equilibria are different for the three components, but the intrinsic coking kinetics are assumed to be the same since experimental data on intrinsic coking rates of specific oil components are not available. We also assume that the three oil components undergo the same coking reaction on the surface to produce coke and light gas with the same stoichiometry (2/3 coke and 1/3 gas). No production of lighter oil components from adsorbed heavy oil has been included since basic kinetic data do not exist. Even with these simplifying assumptions the current model has several adjustable parameters which are determined by matching the model to experimental results.

In our previous study⁽⁴⁾ we used a simple packed-bed reactor with a constant oil feed. With that apparatus, the oil upgrading effect was established: Fig. 1 shows a sample result that compares the boiling point distribution of the feed oil with the product oil distribution after 27% of the oil is coked. The partially coked oil is considerably lighter, and hence more valuable, than the starting oil. In modeling this effect, we make use of the fact that the result in Fig. 1 can be predicted by postulating that coke originates from the heavy end of the boiling point distribution without production of any light oil components. Such an explanation is no doubt a simplification of the real coking/cracking reactions that probably both produce and remove light oil. Nevertheless, this result provides a basis for the simple reaction stoichiometry adopted for the model. In the same study⁽⁴⁾ we determined the intrinsic coking rate of shale oil adsorbed on a non-porous quartz surface. This coking rate was determined on a well-

coked surface, because the fresh surface is covered with coke in a fraction of the total elapsed time of each experiment. For this same reason, the apparatus used in Ref. 4 did not allow determination of coking kinetics over fresh-oxidized porous shale surfaces. In order to relax this limitation we took a different experimental approach in our current work.

EXPERIMENTAL APPROACH

The apparatus shown schematically in Fig.2 consists of a fluidized bed for pyrolyzing a small shale sample followed by a packed bed of oxidized shale where coking reactions occur. An oil-vapor pulse from the fluidized bed enters the packed bed at the inlet and emerges as an altered oil pulse from the outlet. The hydrocarbon concentrations of both of these pulses are determined in separate experiments by oxidizing the oil pulse to $\text{CO}_2 + \text{H}_2\text{O}$ in a combustion tube and monitoring the combustion products by a rapid mass spectrometer. Coke deposited in the packed bed is quantitatively determined by subsequent oxygen addition and burnoff with quantification of the combustion products. A disadvantage of this apparatus relative to the apparatus of Ref. 4 is that the products are destroyed and cannot be used for studying oil property changes. Another experimental limitation is that only dilute vapors (i.e., low oil concentrations) can be studied.

The system was standardized on an Anvil Points, Green River Formation oil shale with a grade of about 24 gallons/ton. Shale sample drops varied from 0.5 to 1.6 grams each. Most of the experiments included a series of sample drops into the fluidized bed with the resulting oil pulses passing through the packed bed followed by burnoff of both beds at the end of each series of drops. Consequently the first oil pulse in each series encountered a freshly oxidized shale surface whereas subsequent oil pulses saw an increasingly coked surface. The size of the packed bed was varied, so that the coke yield would differ relative to the oil pulse. Shorter beds were used for small particles because small particles showed a greater overall coking tendency than did large particles.

COKING MODEL

The basis for the current coking model is a computer code developed at LLNL⁽⁷⁾ for heterogeneous reactions in a porous sphere. This code is quite rigorous; i.e., it incorporates the Stefan-Maxwell relationships for describing diffusion of gas species in the multi-component system. The code also allows for a film resistance around the particle, but this resistance proved to be insignificant for the cases studied here. This general code and the numerical scheme employed for its solution are not discussed in this paper. Rather the emphasis here is on the relationship of the experimental data to the results obtained from the code.

Table 1. Oil Component Properties Used in Model

Component	Boiling Point °C	Molecular Weight	Fraction Wt%	Diffusivity @ 500° C cm ² /s
1	200	155	50	0.27
2	400	338	25	0.17
3	500	451	25	0.15

Properties of the three oil pseudocomponents are specified in Table 1. This selection of components implies a three-point discretization of the continuous boiling-point curve of the shale oil. More components could easily be added. Molecular diffusivities predicted by theory⁽⁸⁾ are also given in Table 1. The effective diffusivities for porous shale are based on the ϵ^2 model⁽⁹⁾. A typical porosity (ϵ) and total surface area of oxidized Green River formation oil shale are 0.3 and 5 m²/g, respectively.

The adsorption equilibrium relationships are based on the Langmuir isotherm⁽⁹⁾ and are given by:

$$K_i \cdot P_i^* = \frac{\theta_i}{1 - (\theta_1 + \theta_2 + \theta_3)}, \quad i = 1, 2, 3 \quad (1)$$

where

K_i = Equilibrium constant of component i (kPa^{-1} , function of temperature)

P_i^* = Equilibrium vapor pressure of component i (kPa)

θ_i = Surface coverage factor for component i ($[\text{Oil}_i, \text{ads}] / [\text{Oil}_{\text{max,ads}}]$)

K_i correlates to the heat of adsorption ΔH_i according to the van't Hoff relationship:

$$K_i = k_0 \exp\left(\frac{\Delta H_i}{RT}\right) \quad (2)$$

where

$$\frac{\Delta H_i}{R} = 10 \cdot T_{\text{boiling point}} \quad (\text{Trouton's rule for heat of condensation})$$

The equilibrium relationships, Eqs. 1 and 2, contain two adjustable parameters: the pre-exponential factor k_0 in Eq. 2 and the total number of sites for adsorption $[\text{Oil}_{\text{max,ads}}]$ appearing in the definition of θ_i .

A third adjustable parameter is the preexponential factor A appearing in the first-order coking rate, Eq. 3, for the intrinsic coking rate on a freshly oxidized surface. The activation energy is assumed to be the same as for the coking rate on a coked surface from Ref. 4 shown for reference in Eq. 4:

$$\frac{d[\text{Oil}_i, \text{ads}]}{dt} = -A \cdot \exp\left(-\frac{19270 \text{ K}}{T}\right) \cdot [\text{Oil}_i, \text{ads}] \quad (\text{mineral surface}) \quad (3)$$

$$\frac{d[\text{Oil}_i, \text{ads}]}{dt} = -10^9 \cdot \exp\left(-\frac{19270 \text{ K}}{T}\right) \cdot [\text{Oil}_i, \text{ads}] \quad (\text{coked surface}) \quad (4)$$

The model uses a weighted average of Eqs. 3 and 4 for the case of a partially coked surface.

RESULTS

The fitted parameters are: $k_0 = 3 \cdot 10^{-7} \text{ kPa}^{-1}$, $[\text{Oil}_{\text{max,ads}}] = 0.6 \text{ mg/m}^2$, and $A = 10^{10} \text{ s}^{-1}$. This set of parameters produces the match of model results (shown as drawn curves) to experimental results (shown as individual points) in Figs. 3 and 4. For plotting the exposure time in these figures, the actual oil pulses have been approximated by assuming rectangular oil pulses instead of the true pyrolysis-kinetic pulses used in both experiment and model calculations.

Figure 3 shows that oxidized shale particle size has a strong effect on overall coking rate and that the overall coking rate declines significantly at a coke coverage of approximately 3 mg/g. The slowdown is particularly strong for the 1-mm particles because the initial overall coking rate for this small particle size is not dominated by pore diffusion. The model matches the slowdown by switching from a combination of Eq. 3 and Eq. 4 to Eq. 4 kinetics only at a coke coverage of 3 mg/g. (There is an order of magnitude change in intrinsic coking rate between the two equations.) The coke coverage of 3 mg/g is equivalent to 0.6 mg/m^2 and corresponds approximately to a monolayer. It is significant that the matching of the model produced the same monolayer limit for the maximum adsorbed oil concentration on the surface.

The two sets of 5-mm particle data in Fig. 3 show the importance of differential reactor conditions. The diamond series used a larger bed than the triangle series, and the consequence is a significant

depletion of cokable reactants across the bed (hence less coke per g of oxidized shale) for this series of experiments.

Figure 4 shows the results of varying the temperature of the oxidized-shale bed. Increasing temperature increases the overall coking rate but not in proportion to the increase in intrinsic coking rate that Eqs. 3 and 4 predict. Pore diffusion is only partially responsible for limiting the overall coking rate increase with temperature; another effect particularly important at low oil coverage of the surface is the reduced adsorbate equilibrium concentration on the surface which is modeled by the equilibrium constant in Eq. 2. (The surface is assumed to be in equilibrium with the local oil vapor within the pore system.)

Figure 4 also shows a result of varying oil concentration at a constant temperature of 502 °C. Oil concentration is seen to have a significant effect on the overall coking rate for the 5-mm particles.

Figure 5 contains model results that address the question of coking at higher oil concentrations. The maximum oil concentration expected in HRS oil shale processes is a few hundred mg oil/l. (The exact concentration depends on the amount of stripping gas.) Fig. 5 shows that increasing oil concentration increases the coke yield but with a proportionality much less than first-order; this result has also been confirmed by experiment. Comparison of Fig. 5(a) and Fig. 5(b) reveals that the increased coke yield with higher oil concentration is due mostly to increased coking in the large particles. This is explained by pore diffusion responding to a higher driving force. The pore-diffusion effect is also evident in the coke profiles of the larger particle sizes: a coke wave penetrates gradually into the 5- and 7.5-mm particles. A distinct coke layer extending from the surface partway into the particle has also been observed visually in partially coked shale bed samples.

CONCLUSIONS AND FUTURE PLANS

We compared experimental data with a model based on physical and chemical phenomena that govern coking of oil vapors over a porous medium. We conclude that mass transfer, phase equilibria and intrinsic chemical kinetics are all important in determining the overall coking rates for oil shale processes where the product-oil vapor contacts an oxidized recycle solid stream. We have used our model to extrapolate the experimental data to higher oil concentrations typical of the HRS processes and to larger particle sizes. Although these extrapolations remain to be confirmed in a newly constructed laboratory apparatus, we are relatively confident that oil losses to coke in the HRS process can be kept to a level of 10-15% of primary oil produced (assuming recycle ratios of 2 to 3). We have also concluded that the physical adsorption step is at least partially responsible for the observed selectivity toward high-boiling components in the heterogeneous coking process. It is likely that the high-boiling components also have higher reactivities than the low-boiling components, and we intend to study possible differences in reactivity as a function of molecular structure. Different reactivities also lead to the question of reaction products: adsorbed oil will no doubt produce lighter oil, not just coke and noncondensable gas. Hence cracking reactions for oil adsorbed on the surface should be added to the two competing processes, coking and desorption, included in this study.

ACKNOWLEDGEMENTS

We wish to thank our colleagues who provided support throughout this project: Bob Cena for his technical and supervisory support, Doug Fields for technical skills and practical advice, Bob Taylor and Bruce Watkins for technical insight and discussion, Roz Swansiger for analytical support. Special thanks to Sharon Crowder for preparing this document and for taking care of a myriad of administrative details. This work performed under the auspices of the U.S. Department of Energy by the Lawrence Livermore National Laboratory under contract number W-7405-Eng-48.

REFERENCES

1. P. W. Tamm, C. A. Bertelsen, G. M. Handel, B. G. Spars and P. H. Wallman "The Chevron STB Oil Shale Retort," *Energy Progress* 2, 37 (1982).

2. A. E. Lewis and R. J. Cena "LLNL Pilot Plant Development – Part I," *Proc. of the Oil Shale and Tar Sand Contractor's Review Meeting*, pp. 72-85, T. C. Bartke, Ed., DOE/METC-90/6111, Morgantown, West Virginia (1990).
3. M. F. Singleton, P. H. Wallman, and R. Mallon, "Oil Cracking and Coking Experiments," *Proc. of the Sixth Briefing on Oil Shale Research*, Lawrence Livermore National Laboratory, Livermore, California, pp. 103-140 (1989).
4. P. H. Wallman, M. F. Singleton, and R. W. Taylor, "Cracking and Coking of Shale Oil Vapors," *23rd Oil Shale Symposium Proc.*, Colorado School of Mines, Golden, Colorado, pp.125-132 (1990).
5. G. C. Wall and P. Udaja, *Fuel* 67, 1340-1343 (1988).
6. P. Udaja and G.J. Duffy, Chensee, M.D. *Fuel* 69, pp. 1150-1154 (1990).
7. S. H. Johnson and A. C. Hindmarsh, "MSRS: A Fortran Code for the Numerical Solution of Solid/Fluid Reactions in Nonisothermal Multispecies Porous Spheres with Stefan-Maxwell Diffusion," *UCRL-21002*, Lawrence Livermore National Laboratory, Livermore, California (1988).
8. R. C. Reid, J. M. Prausnitz, and T. K. Sherwood, *The Properties of Gases and Liquids*, McGraw-Hill, New York (1977).
9. M. Suzuki, *Adsorption Engineering* (Chemical Engineering Monograph 25), Elsevier, Amsterdam (1990).

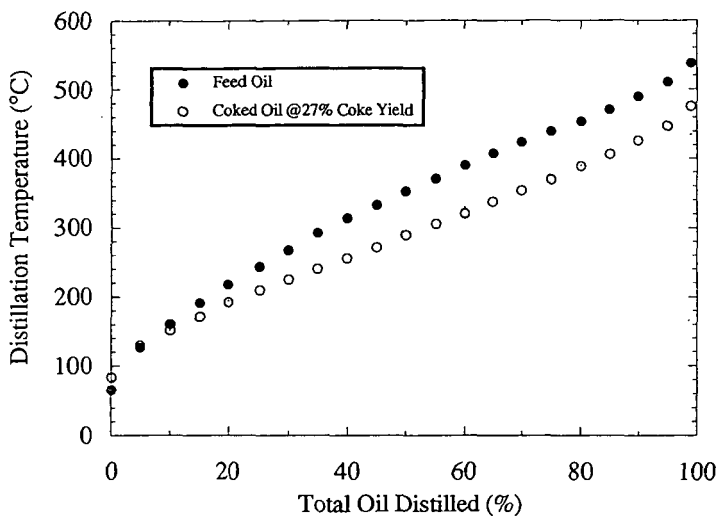


Figure 1 Effect of coking on shale oil boiling point distribution.

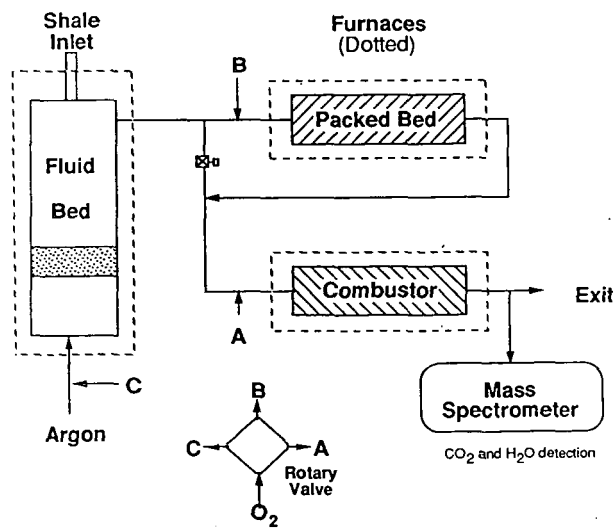


Figure 2 Apparatus for studying coking kinetics.

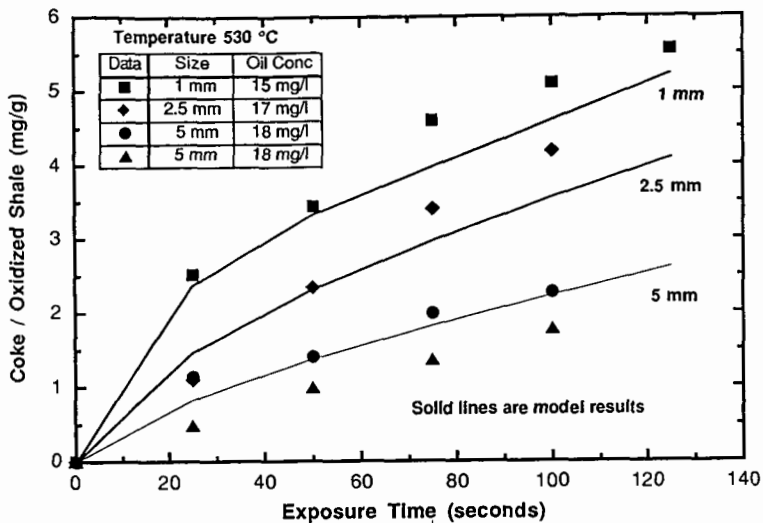


Figure 3 Particle-size effect on coke buildup.

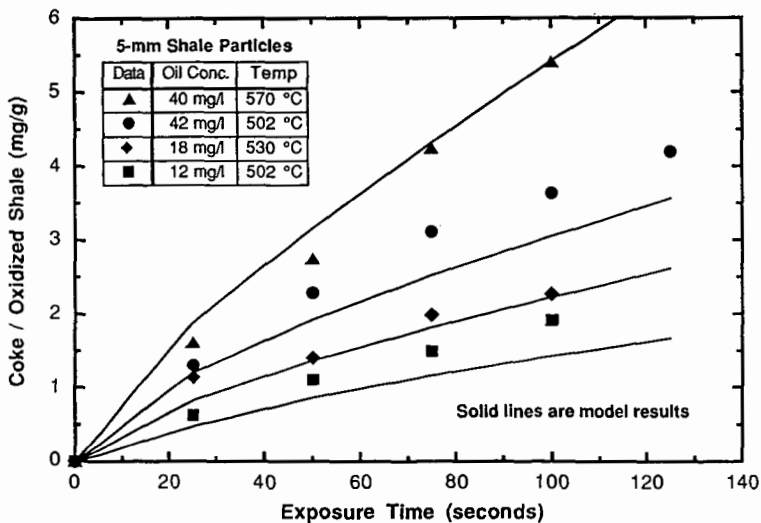


Figure 4 Temperature and oil-concentration effects on coke buildup.

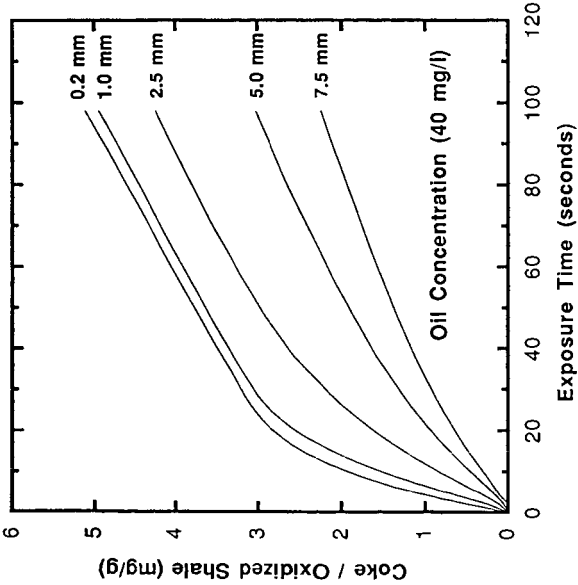


Figure 5 (a)

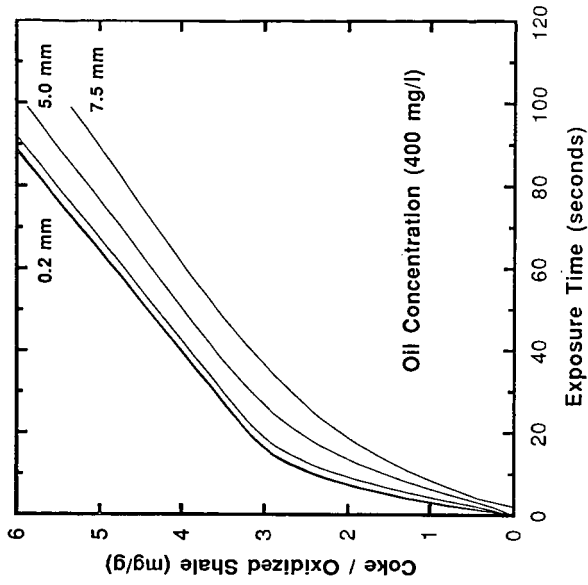


Figure 5 (b)

Figure 5 Model-predicted coke buildup with constant oil vapor concentration at (a) 40 mg oil/l, (b) 400 mg oil/l.

Investigation of product coking induced by hot recycle solids
in the KENTORT II fluidized bed retort.

D.N. Taulbee and S.D. Carter
University of Kentucky-Center for Applied Energy Research
Lexington, KY 40511

Keywords: coke, shale oil coke, fluidized bed.

ABSTRACT. The mechanism and extent to which oil shale pyrolysis products undergo secondary coking reactions is governed to a large degree by the nature and temperature of the surfaces with which these products interact. Since the composition and temperature of the solids utilized to transfer heat in the KENTORT II fluidized-bed reactor can, to some extent, be controlled, it is important to determine the relative coke forming activity of these solids at process temperature in order to maximize product yield. With this objective, an apparatus has been constructed that permits shale oil vapors generated in one fluidized bed to pass over selected substrates in a second fluidized bed. The reactivity of the solid as a function of exposure time is monitored with an on-line mass spectrometer while total carbon deposition is determined post-run by ultimate analysis of the substrate. Over the temperature range of 530-660^o C, the order of substrate reactivity was determined to be kaolinite > combusted shale > illite > gasified shale > pyrolyzed shale > sand. Surface area/pore volume data for the various substrates will be presented and discussed in terms of coking activity.

INTRODUCTION. One of the factors that ultimately controls oil yield during oil shale pyrolysis is the extent of secondary reactions, i.e., cracking and coking, that occur within the reactor¹. These reactions in turn, are governed by several factors including reactor temperature, product residence time, resource properties, and the types of solid surfaces which the vapor phase hydrocarbons contact at elevated temperature. For a given resource, short of resorting to high H₂ partial pressures, the simplest means of enhancing liquid yield is to reduce the product residence time. For this reason, among others, fluidized bed retorting is regarded as an attractive technology for processing the eastern US oil shales, and consequently, has been under continuing development at the UK-CAER since about 1982² in a process termed KENTORT II.

Since one of the more effective means to transfer heat in a fluidized bed reactor is through direct addition of heat carrying solids, solids recycle is thought to be the most practical approach for a large scale operation. Accordingly, a KENTORT II prototype operated at the CAER was designed to simulate commercial operation by recycling hot solids to the pyrolyzer from both a fluidized bed gasifier and combustor. However, delivery of hot solids to the pyrolyzer promotes secondary cracking and coking reactions resulting in lower oil yield. Therefore, since the temperature, concentration, and composition of the heat transfer solids can, to some extent, be controlled in the KENTORT design, it is vital that the reactivity of the heat-carrying solids be characterized at process temperature in order to minimize these detrimental reactions.

Several, often ingenious, strategies have been used to investigate the cracking and coking of shale oil over a solids substrate bed. However, all these techniques have suffered from an inability to closely simulate the solids/H₂C product interactions that take place in a continuous, solids recycle operation. For example, Levy et al.³ continuously injected Fischer assay shale oil into a reactor where the shale oil was vaporized then passed through a bed of solids. Though informative, the H₂C stream does not have the same composition or tendency toward coke formation as freshly generated

shale oil vapors, particularly for shale oils that contain significant amounts of non-volatile components. In an investigation reported by Coburn et al.,⁴ a pulse of oil shale was dropped into a fluidized bed pyrolyzer with the resulting vapors passed through a packed bed of solids. While this technique lends itself well to kinetic measurements, it suffers from the fact that the pyrolysis products differ in nature and concentration (and therefore reactivity) as a function of time. Rubel et al.⁵ connected a packed bed pyrolyzer in series with a packed bed of solids in the same furnace then subjected both beds to the same heating profile. While this technique provides information on the relative substrate reactivity, its transient nature is unsuitable for kinetic measurements, nor does it simulate fluidized bed conditions.

To realistically examine both the kinetics and reaction mechanisms, an apparatus has been constructed which permits shale oil vapors generated in one fluidized bed to pass over selected substrates in a second bed. Since the oil product is at no time cooled or removed from the reactor and the time for non-catalyzed secondary reaction to occur is minimal, product loss reactions are thought to closely simulate those that occur within a circulating solids fluid bed reactor. Substrates can be fed in either a batch or continuous mode. In the batch mode, a given substrate is heated to reaction temperature then exposed to shale oil vapors for a selected time period. Carbon deposition onto the solid is monitored in real-time using an on-line mass spectrometer and total deposition verified by elemental analysis of the substrate following exposure.

Because the KENTORT concept utilizes a combination of gasified and combusted shale particles as the heat transfer medium, examination of these materials is emphasized.

EXPERIMENTAL. The oil shale used in this study was the CLE003 master sample from Fleming County, Ky.⁶ The solid substrates examined and reactor conditions used are given in Tables 1 and 2. In addition to examining all of the substrates without pretreatment, aliquots of the gasified and combusted shale were placed in a solution of either 0.005 N NaOH or HCl overnight, thoroughly rinsed with deionized H₂O, then dried prior to testing.

The coking apparatus and procedures used are described in detail elsewhere.⁷ Following is a condensed description.

Apparatus. The apparatus consists of two vertically aligned fluidized beds (7.6 cm i.d.) that share a common fluidizing medium and are heated externally by two dual-zone electrical furnaces (Figure 1). The fluidizing gas, N₂ in this study, is preheated then routed to the lower fluidized bed maintained at 530^o C for all runs. Raw oil shale is metered by a N₂-purged screwfeeder into the lower fluidized bed where the level of solids is maintained at 7.6 cm by an exit standpipe.

In the upper portion of the apparatus, a vertical baffle divides the pipe into two unequal sections (73% and 27% of the cross sectional area). The larger section contains a fluidized bed of solids, and the smaller section provides a bypass-path for the fluidizing stream. A semi-butterfly valve beneath the baffled section selects the upward path for the pyrolysis product stream and is coupled to a three-way valve that routes a balancing gas to injection ports on either side of the baffle such that gas flows through both chambers regardless of the butterfly valve position. The balancing gas flow serves to maintain a constant total N₂ flow from the reactor, fluidize the upper bed, provide a gas seal for the semi-butterfly valve, and in some experiments, is used as a pretreatment gas for the substrate. A purge gas, argon, is introduced into the seal assembly of the semi-butterfly valve to inhibit coke formation and serve as a tracer gas to facilitate mass spectrometer analyses by correcting for pressure surges, changing flowrates, and instrumental fluctuations.

The balancing gas and the pyrolysis/fluidization stream are joined in the uppermost portion of the reactor. A split of this stream is drawn through a heated combustion tube (600^o C) filled with a Pt/Al₂O₃ catalyst to expedite combustion. Downstream from the combustion tube, a heated

(280°C), 0.3 mm fused silica capillary continually samples the combustion gases and routes them directly to the inlet of a VG model EGA 300MM quadrupole mass spectrometer (QMS) operating in the multiple ion monitoring (MIM) mode. The masses selected for continuous monitoring include 40 (Ar); 12 (C-to confirm mass 44); 18 (H₂O); 28 (N₂); 32 (excess O₂ from combustion); 44 (CO₂); 46 (NO₂); 64 (SO₂); and 42 (C₂H₆-to verify combustor performance). All selected masses were sampled at approximately 1.5 second intervals. Total product transit time from the reactor to the QMS detector was roughly 1 second.

Procedure. Following system heat-up, raw shale feed is initiated with the semi-butterfly valve positioned so that pyrolysis products bypass the upper, substrate bed (i.e. "bypass" position). At this point, the QMS is used to verify combustor operation and check overall system performance.

Next, ~100 g of substrate is loaded to the upper bed which is fluidized by the balancing N₂ gas. When the substrate reaches reaction temperature, QMS data collection is initiated and a baseline established. After approximately 3 minutes (>100 QMS scans), the semi-butterfly valve is rotated so that the upper bed is now fluidized by the pyrolysis stream from the lower bed and maintained in the 'fluidize' position for a selected time interval (5-15 minutes is typical). The valve is then returned to the bypass position and the substrate solids are immediately drained from the bed into a purged collection flask. QMS data collection is continued for at least 3 minutes to re-establish the baseline. The solids receiver flask is removed and replaced with an empty one and the procedure repeated.

Following exposure and recovery, each batch of substrate is weighed and ultimate analyses are performed using standard methods. Surface area and pore volume measurements by N₂ adsorption and Hg porosimetry are conducted on selected substrates. Total surface area data shown in this report represent the sum of meso and macro surface area from Hg porosimetry and BET micro surface area from N₂ adsorption. Pore volume data are from Hg porosimetry.

Part of the post-run data manipulation involves taking the ratio of the combustion gas the tracer gas intensity. By doing so, changes in selected elemental concentrations, particularly carbon, could be observed with minimal interference from changing measurement conditions that frequently occur during a run. These uncontrolled measurement variations include pressure fluctuations, changing combustor or capillary transfer tube flowrates, QMS drift, etc., and result in variations in the absolute level of combustion gases reported by the QMS that are not related to coking loss.

Results and Discussion. The method as described in this manuscript detects only those coking losses resulting from interaction between HC pyrolysis products and the solid substrate to which they are exposed. The apparatus was not configured to probe cracking reactions which will be examined in future experiments involving continuous substrate feed and model compound investigations. Nevertheless, because coking losses account for a significant reduction in oil yield in solid recycle systems and carbon deposition can affect the solids reactivity, the study of coking kinetics is crucial to yield optimization.

Two independent measures of carbon deposition were obtained. The first was calculated from ultimate analysis of the substrate prior to and following HC exposure. The main disadvantage with this approach is that numerous runs are required to establish the deactivation rate for a particular solid under a given set of conditions. Further, at low carbon concentrations, the analytical scatter of the ultimate analysis becomes significant and trace O₂ in the fluidizing gas is a potential problem. Therefore, a complementary measure of carbon deposition is required to provide an on-line determination of coke formation that is less prone to error at low conversion.

In the system described, the rate of carbon deposition onto a solid substrate can be inferred by measuring the total vapor phase carbon that exits the reactor in the by-pass mode (pyrolysis stream by-passes substrate bed) and comparing to the carbon that exits in the coking mode (pyrolysis stream

passes through substrate bed). However, accurately measuring total vapor phase carbon in a pyrolysis stream is not trivial. Collecting the product oil with the required precision is impractical in a fluid bed process due to numerous parameters that affect collection efficiency, i.e. HC concentration, fluidizing velocity, compositional changes due to cracking, etc. Attempts to measure the total HC product with a flame ionization detector (FID) have been reported.^{8,9,10} However, FID measurement suffers from a variety of quantitative flaws including a small, nonlinear response to HC's of differing size or type, insensitivity to heteroatoms, and problems with aerosol formation and condensation of larger components prior to measurement. In comparison, the combustion/QMS approach utilized in this work, rapidly combusts the product stream before condensation or aerosol formation can occur and avoids non-linearity problems by monitoring a single species (CO₂) over a reasonably narrow concentration range. In addition, total N and S deposition can potentially be measured as NO₂ and SO₂ though problems with apparent reaction between H₂S and substrate iron have been encountered.

A typical coking sequence is illustrated by the QMS CO₂/Ar ratio in Figure 2b. With the semi-butterfly valve in the initial bypass position, the CO₂/Ar ratio is near constant. Upon switching the valve to 'fluidize', the ratio immediately drops to a minimum then makes an asymptotic approach to a new constant ratio. The initial plunge in the CO₂/Ar ratio is apparently due to rapid transport of oil vapor into the substrate pores. The ratio rises as the concentration within the pores nears the extraparticle concentration. When the valve is returned to bypass, the original baseline is restored.

There is a good deal of scatter apparent in the CO₂/Ar ratio of Figure 2b (likewise for NO₂ and SO₂). However, the measured fluctuations are real and due to rapid changes in the CO₂ concentration since the absolute intensity of Ar tracer, fluidizing N₂, and excess combustion O₂ remain relatively constant. This rapid change in CO₂ intensity is assigned to a number of sources including fluctuations in the shale feed rate over short time intervals, the chaotic nature of a bubbling fluid bed reactor, fines carryover to the combustor, and perhaps particle-to-particle kerogen content variations. The first two are believed to account for the bulk of the observed scatter.

Although the QMS baseline scatter is pronounced, conversion of shale oil vapor to coke was higher than the scatter under all study conditions. However, due to the data scatter, instead of directly integrating the raw data, a least-squares curve was first fitted to the data and the area between the fitted curve and a least-squares line fitted to the baseline data was determined. The 2-parameter functional form (excluding the intercept) that best fit the response curves for all runs was a decaying exponential form (Eq. 1).

$$C_{solid} = a + b(1 - \exp(-ct)) \quad (1)$$

The area between the region described by this curve and the CO₂/Ar baseline was then integrated and related to the increase in carbon content of the substrate through a proportionality constant. This constant was calculated by taking the ratio of the rate of volatile carbon production from the pyrolysis zone (determined by elemental analysis of the pyrolyzed shale) to the baseline CO₂/Ar ratio.

The coke formation data from integration of Equation 1 was then averaged with the substrate ultimate analysis. These average values are shown plotted in Figures 3 as a function of exposure time and substrate bed temperature. With the possible exception of sand, all substrates showed a higher coking rate with temperature. However, this change was small enough to suggest that coke formation was, for the most part, mass transfer limited.

Also shown in Figure 3, are coke deposition data for combusted and gasified shales that were pretreated in either NaOH or HCl (0.005 N). In all cases, coking onto the treated substrates was not significantly different than coking onto the untreated substrate. This suggests that the rate of coke

formation on the combusted or gasified shale substrates was not dominated by ionic surface sites.

The plots of Figure 3 indicate the relative coking activity to follow the order of Sand < pyrolysed < gasified < illite < combusted < coarse kaolinite < fine kaolinite. In an attempt to relate coking activity to substrate properties, total surface area data are shown in Figure 4a plotted in the above order. With the exception of sand, it is apparent that coking activity does not follow the total surface area series of Figure 4a. However, the macro pore surface area shown in Figure 4b does appear to track coke formation with the exception of illite.

Figure 5a shows the sum of meso and macro pore volume (pores > 2 nm) for each substrate. With two exceptions, illite and course-grained kaolinite, this plots also tracks the order of relative coking activity from Figure 3. The course-grained kaolinite had a greater pore volume than did the fine-grained kaolinite but showed relatively less coking activity. The reason for this anomaly may be due to the substantial difference in surface area between these two samples (Figure 4). That is, even though the course-grained kaolinite had a larger pore volume, the substantially lower surface area perhaps countered the larger pore volume. In the case of illite, the relatively high coking rate cannot be explained by either surface area or pore volume. We cannot explain the relatively high coke formation rate for illite though we suspect there may be a significant difference in active surface site concentration (or perhaps the absence of a carbon coating) relative to the other substrates.

Finally, Figure 5b shows the changes in the combusted shale pore volume as a function of exposure time at 620° C. As might be expected, this value steadily declines with increasing exposure time suggesting that the rate of coke formation may be decreasing as well. Such a decline was not detected by curve fitting the QMS data though data scatter could easily have obscured a small effect. Longer exposure times planned for future experiments should help clarify this point.

Acknowledgments. The authors gratefully acknowledge the work of D. Smith and J. Fannin for assisting with the experiments and data reduction, and M. Stewart, G. Thomas and M. Moore for analytical support. This work was supported in part by the Morgantown Energy Tech. Ctr., USDOE, under Coop. Agreement DE-FC21-90MC27286 (such support does not constitute an endorsement by the USDOE of the views expressed in this manuscript).

References

1. Taulbee, D.N. and Carter, S.D., *Fuel*, **70**, 1991, p. 1245-51.
2. Carter, S.D., Robl, T.L., Rubel, A.M., and Taulbee, D.N., *Fuel*, 1990, **69**, p 1124.
3. Levy, J.H., Mallon, R.G., and Wall, G.C., *Proc. 3rd Australian Workshop on Oil Shale*, Lucas Heights, NSW, 1986, p. 133.
4. Coburn, T.T., Taylor, R.W., Morris, C.J., and Duval, C., *Proc.: Int. Conf. on Oil Shale and Shale Oil*, Beijing, China, 1988, Colorado Sch. Mines Press.
5. Rubel, A.M., Rimmer, S.M., Keogh, R., Robl, T.L., Carter, S.D., and Derbyshire, F.J., *Fuel*, 1991, **70**, 1352.
6. Carter, S.D., Taulbee, D.N., Rubel, A.R., Abner, R.T., *Proc.: 1988 Eastern Oil Shale Symp.*, **IMMR88/101**, Inst. Min. & Minerals Res., Lexington, Ky., May., 1989, p. 333-340.
7. Carter, S.D., and Taulbee, D.N., submitted to *Fuel*, Jan. 1992.
8. Richardson, J.H., Huss, E.B., Ott, L.L., Clarkson, J.E., Bishop, M.O., Taylor, J.R., Gregory, L.J., and Morris, C.J., **Report UCID-19548**, 1982, LLNL, Livermore, Ca.
9. Wallman, P.H., Tamm, P.W., and Spars, B.G., *ACS Symp. Ser. 163*, 1981, p. 93.
10. Carter, S.D., *ACS Div. of Pet. Chem. Prep.*, 1987, **32**, #1, p. 133.

Table 1. Substrate properties. Substrates are 20X60 mesh unless otherwise noted.

<u>Substrate</u>	<u>Origin</u>	<u>Preparation/comment</u>
Pyrolyzed Shale	Cleveland oil shale	530C in N ₂ /10 min
Gasified Shale	Cleveland oil shale	800C in Steam/20 min
Combusted Shale	Cleveland oil shale	700C in air/10 min
Sand	Ottawa, Canada	20X30 mesh
Illite	Carbon deficient Huron Shale (Three Lick Member), Rowan Co, KY	
Kaolinite-F	Fine grained, Georgia, USA	
Kaolinite-C	Course grained, Georgia, USA	

Acid/base treated substrates were placed in an excess of .005 N NaOH or HCl overnight, exhaustively rinsed with distilled H₂O, and dried prior to exposure.

Table 2. Reactor Conditions.

PYROLYZER:

Shale Feedrate	12 g/min
Superficial gas velocity	0.46 m/s
Temperature	530°C
Bed Height	7.6 cm

SUBSTRATE BED:

Substrate load	100 g (~3 cm depth)
Temperature	530-660°C
Solid Residence Time	5, 10, 15 min

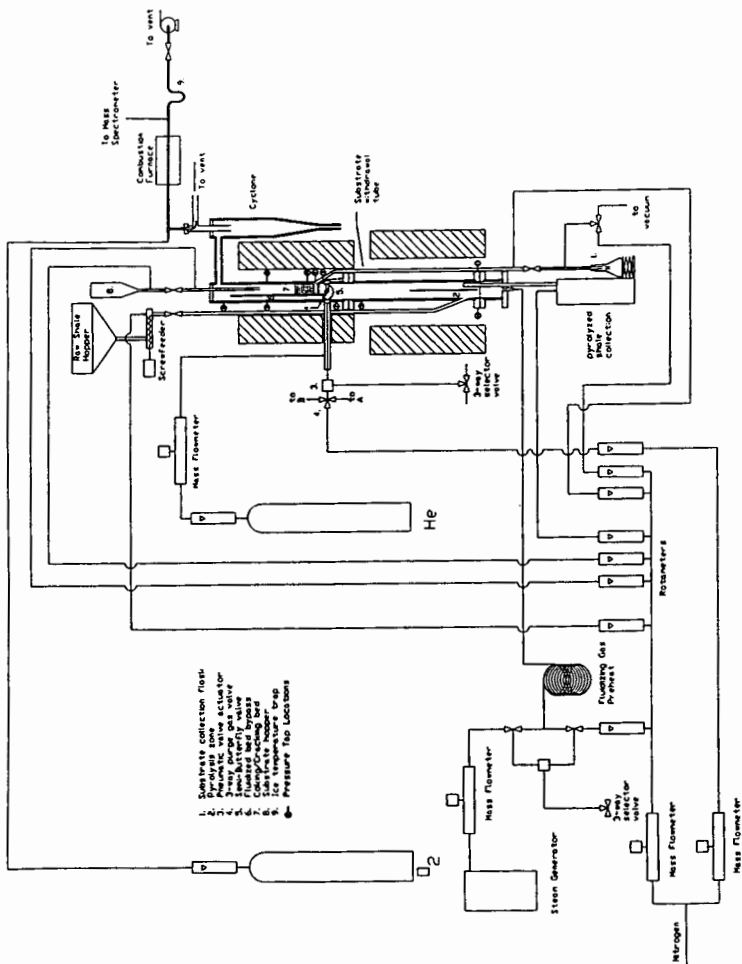


Figure 1. Flow diagram of the valved fluidized bed system for investigating the coking kinetics of shale oil vapors over solid materials.

Figure 2. Schematic of reactor configuration during coking sequence-Top.
 CO_2/Ar ratio (44/40 m/e) during typical coking sequence-Bottom.

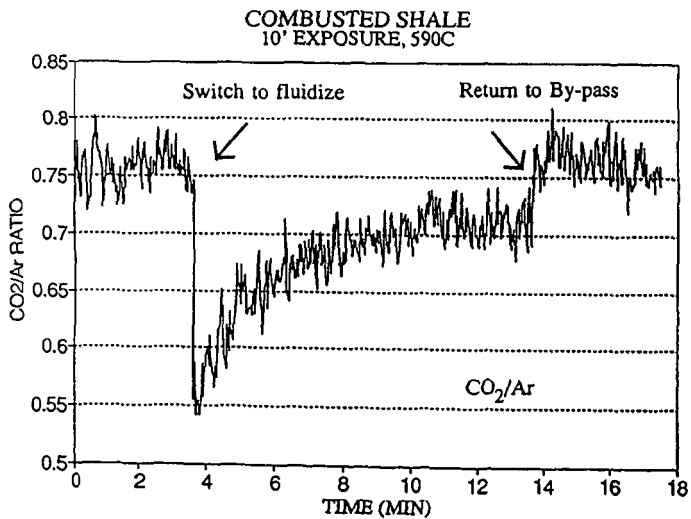
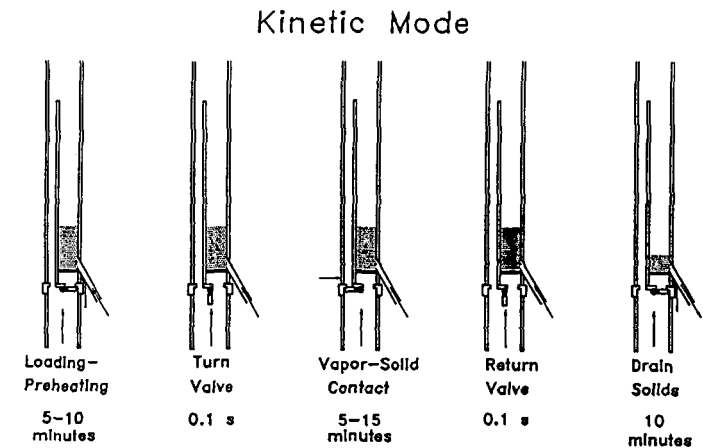
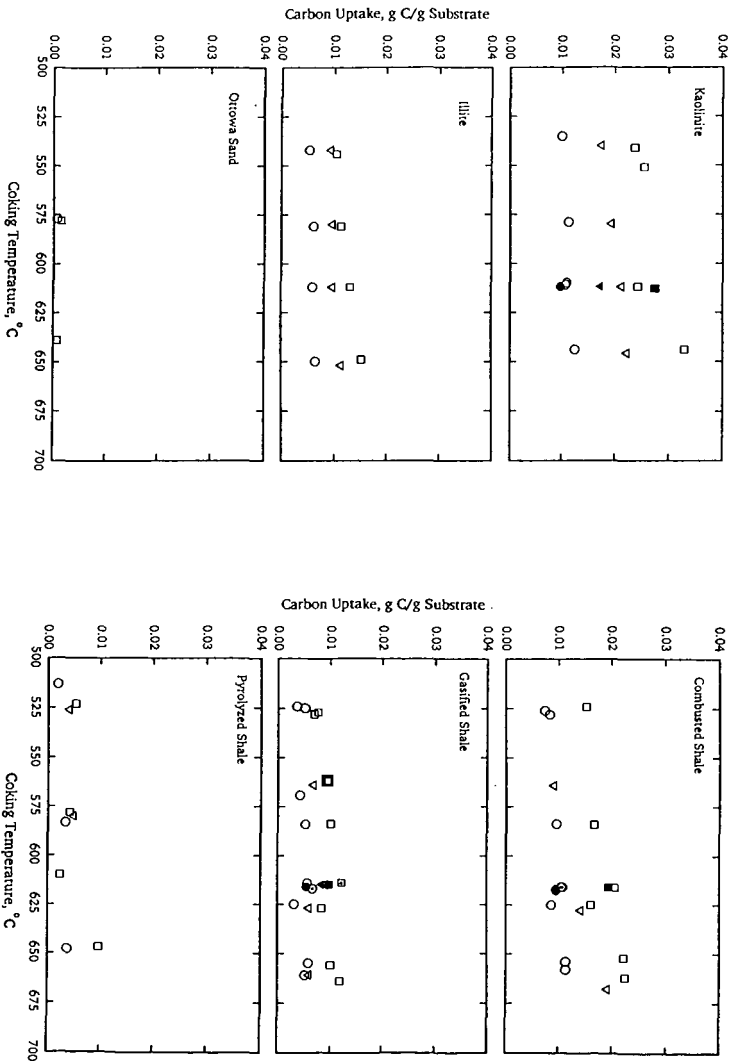


Figure 3. Average coke deposition as a function of exposure time and substrate temperature. \circ -5 min, ∇ -10 min, \square -15 min. Filled symbols represent either coarse-grained kaolinite (kaolinite plot) or base treated combusted or gasified substrate, symbols with \cdot represent acid treatment.



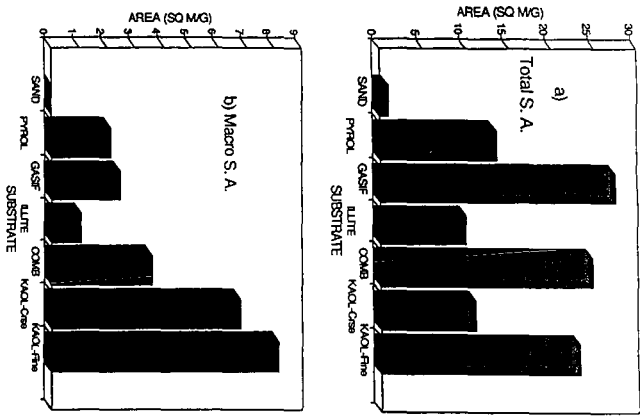


Figure 4. a) Total surface area. b) Surface area within macro pores. Substrates shown in order of increasing coking activity.

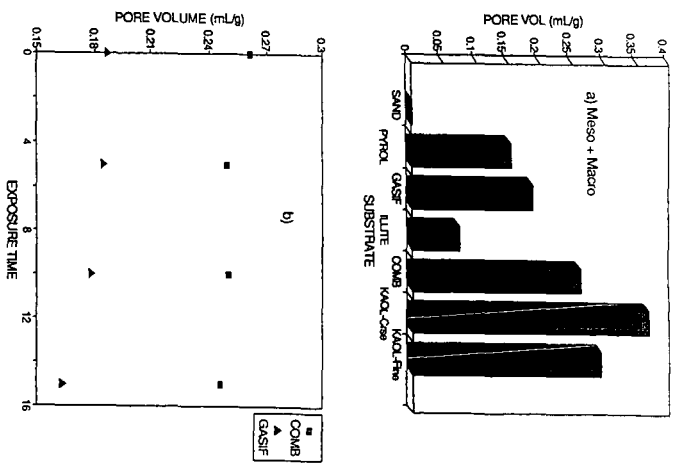


Figure 5. a) Meso + macro pore volume (mL/g substrate). b) Changes in the meso + macro pore volume for combusted and gasified substrates as a function of exposure time at 620°C.

Molecular Transformations in the Processing Sequence
Pyrolysis-Hydrotreating with Utah Oil Sands

by

F.V. Hanson, M.D. Deo, D.C. Longstaff and C.H. Tsai
Department of Fuels Engineering
University of Utah

INTRODUCTION

The utilization of Utah's Uinta Basin oil sands resource will most likely involve a combination of in-situ and mining-surface recovery techniques. It has been reported that 15-30% of Utah's oil sands are amenable to mining-surface recovery processes.⁽¹⁾ The mining-surface recovery processes include aqueous separation,⁽²⁻⁴⁾ solvent extraction^(5,6) and pyrolysis.⁽⁷⁻¹⁹⁾ The production of refinery feedstocks from mined oil sands can be accomplished by a number of processing sequences: aqueous separation or solvent extraction followed by coking or hydrotreating of the full range bitumen and rotary kiln or fluidized bed pyrolysis followed by hydrotreating of the bitumen-derived liquid.

The objective of this investigation was to explore the molecular transformations that occurred in the processing sequence pyrolysis of the mined oil sand ore in a fluidized bed⁽¹⁵⁾ followed by hydrotreating of the bitumen-derived liquid⁽²⁰⁾.

EXPERIMENTAL METHODS AND MEANS

Fluidized Bed Pyrolysis System

The bitumen-derived liquid used in the hydrotreating studies was produced from the Whiterocks tar sand ore in a large diameter fluidized bed pyrolysis reactor. The reactor temperature ranged from 773 to 813 K, and the average feed sand retention time was 17.2 minutes during the course of the production run.

The production of the bitumen-derived hydrocarbon liquid from the Whiterocks tar sand has been described in detail by Sung⁽¹⁵⁾.

Hydrotreater Process Unit

Process studies were conducted in a fixed bed reactor which operated in an upflow mode to minimize thermal gradients in the catalyst bed and to ensure complete wetting of the catalyst. A schematic of the hydrotreater system is presented in Figure 1. The reactor was designed for operation at a maximum pressure of 34.5 MPa at 773 K. The catalyst was diluted with quartz sand (50% by volume) in the inlet region of the bed (~20%) to trim the exotherm caused by olefin hydrogenation reactions.

The base case operating conditions for the hydrotreating study were as follows: reaction temperature, 619 K (653 °F); liquid hourly space velocity (LHSV), 0.5 h⁻¹; total reactor-pressure, 13.7 MPa (1980 psia) and hydrogen-to-hydrocarbon feed ratio, 890 m³/m³ (5000 scf/bbl). The API gravity of the total liquid product was constant at 23.2 °API after the reactor was on-stream for 94 hours at the base case conditions. At this point, it was assumed that the catalyst had attained a stationary state and that 95% of the coke deposition had occurred. A series of experiments were conducted in which the system was operated in a cyclic mode (base case condition/desired reaction condition/base case condition) for approximately 1000 hours. The total liquid product from each experiment was collected for analyses. The analytical test procedures conformed to those outlined in the ASTM manuals.

Mass balances were taken for 3 hours at the end of a 16-hour line-out period after the system had attained a stationary state at the new reaction conditions. The mass balances were conducted by monitoring the liquid fed to the reactor system for discrete time periods. At the conclusion of each mass

balance the collected gas and liquid samples were weighed and the gas sample was weathered into a vapor collector and analyzed by gas chromatography. All the mass balances were greater than 97.5 wt%.

The extent of nitrogen removal was the key reactivity parameter followed during the course of the study; however, the key operating parameter followed on the catalyst testing unit during the run was the specific and/or API gravity of the total liquid product.

Catalyst

A UNOCAL quadralobe Ni/Mo/Al₂O₃ hydrodenitrogenation (HDN) catalyst was used in this study. The catalyst contained 3.3 wt.% NiO, 12.8 wt.% MoO₃, and 0.8 wt.% P₂O₅. It had a surface area of 241 M²/g and a pore volume (Hg porosimetry) of 0.55 cm³/g. The sulfiding conditions were specified by the catalyst manufacturer. A solution of dimethyl disulfide in kerosene (~ 2 wt% sulfur) was used to sulfide the catalyst at a LHSV of 1.0 h⁻¹. The hydrogen-to-sulfiding solution ratio was 890 m³/m³ (5000 scf/bbl). The reactor temperature was adjusted to the initial run temperature after sulfur breakthrough at which point the sulfiding solution was discontinued.

A description of the experimental apparatus and operating procedures; a description of the catalyst and the catalyst activation procedures; and a summary of the process variable study have been reported by Longstaff, et al²¹. The design, construction and operation of the hydrotreater catalyst testing unit have been discussed in detail by Longstaff²⁰.

Analysis of Liquid Products

Simulated Distillation The boiling point distributions of the hydrotreated products were determined by simulated distillation. The samples were dissolved in dichloromethane and the analyses were performed on a programmed Hewlett-

Packard Model 5730 A gas chromatograph: the oven temperature was programmed from 243 to 623 K at 11°C/minute and was held at 623 K for 16 minutes; the injector temperature was initially set at 523 K and raised to 633 K after 12 minutes and the FID detector temperature was 673 K. The boiling point temperatures were calibrated with a standard mixture of normal paraffins (C₅ - C₄₄).

Gas Chromatography-Mass Spectrometry Analysis The bitumen-derived liquid feed and the hydrotreated total liquid products were analyzed with a gas chromatograph (Hewlett-Packard Model 5890 A) using a fused silica capillary column coated with 5% phenyl methyl silicone bonded stationary phase (30m x 0.25mm ID, DB-5, J & W scientific). The temperature program was ranged from 323 K to 573 K at 3°C min⁻¹, with a hold at 573 K for 20 minutes.

Gas chromatography - mass spectrometry analyses were performed on a Finnigan MAT95 high resolution gas chromatograph/mass spectrometer (Finnigan MAT ICIS II operating system) fitted with a DB-5 gas chromatographic column (30m x 0.25mm ID).

RESULTS AND DISCUSSION

The bitumen-derived liquid was significantly upgraded relative to the native bitumen (Table 1): 19.1 °API versus 11.9 °API; a viscosity of 85.4 cps @ 289 K, versus 2665 cps @ 358 K; a volatility (<811 K) of 82.2 wt.% versus 40.5 wt.%; a Conradson carbon residue of 4.7 wt% versus 8.1 wt%; etc., respectively. The atomic hydrogen-to-carbon (H/C) ratio of the bitumen-derived liquid was lower than that of the native bitumen. This reduction was related to dealkylation reactions during pyrolysis which resulted in the production of a more aromatic hydrocarbon liquid and consequently a lower H/C ratio. Furthermore, the asphaltene fraction in the native bitumen was assumed to be the primary precursor of the carbonaceous residue deposited on the spent sand thus the coking tendency

of the bitumen-derived liquid during hydrotreating was expected to be less than that of the native bitumen.

Identification of individual compounds in the volatile fractions (811 K) of the Whiterocks bitumen, the bitumen-derived liquid and the hydrotreated total liquid was based on the comparison to known spectra from the literature or were tentatively assigned based on interpretation of the mass spectrum.²²⁻³⁴ Major compound types found in the 1000°F minus fraction of the native Whiterocks bitumen were substituted and unsubstituted cyclohexanes, benzenes, decalins, tetralins, naphthalenes perhydrophenanthrenes (tricyclic terpanes), octahydrophenanthrenes, tetrahydrophenanthrenes, phenanthrenes, phenyl (cyclohexyl) alkanes, indan (cyclohexyl) alkanes, perhydrochrysenes (17,21-secohopanes), steranes (C₂₇ - C₂₉), hopanes (C₂₇ - C₃₅) and traces of paraffins. Heterocyclics such as benzofuran, indoles, quinolines, carbazoles and tricyclic and pentacyclic carboxylic acids were also detected.

Basically, the compounds types identified in the Whiterocks bitumen-derived liquid were similar to those identified in the volatile fraction of the bitumen. Several additional compound types were also identified: normal alkanes (C₇ - C₃₀) and α -alkenes, branched alkanes (C₇ - C₂₈) and alkenes, cyclopentanes, styrenes, indenenes, dihydronaphthalenes, dihydrophenanthrenes, and the olefin related to perhydro- β -carotane. The amounts of alkyl naphthalenes and alkylphenanthrenes increased in the bitumen-derived liquid compared with the bitumen. The hydrotreated bitumen-derived liquid consisted primarily of saturated compounds, such as alkanes (normal and branched) and cycloalkanes (1-5 rings). It also contained low concentrations of aromatic compounds which were predominantly monoaromatics.

The task of identifying the thermal reactions pathways in bitumen pyrolysis

was difficult due to the complexity of the native bitumen. However, several pathways were rationalized through the structural identifications of these three samples. These reactions included cleavage of long side chain, dehydrogenation, polymerization and condensation, and decarboxylation.

The normal and branched (mostly isoprenoid) alkanes and normal and branched-1-alkenes generated in the pyrolysis reactions probably originated as alkyl groups attached to aromatic rings in multi-ringed aromatics and naphenoaromatics and/or from alkyl bridges between two aromatic clusters, two naphenic clusters, and/or an ermoatic cluster and a naphenoaromatic cluster. Since these types of compounds were not found in the 811 K minus fraction of the bitumen, it was presumed that they were present in the high boiling, residual fraction of the bitumen.

The speculation regarding the pyrolysis reaction pathways was confirmed by gradient elution chromatography⁽³⁵⁻³⁷⁾ analysis of the native bitumen and the bitumen-derived liquids produced during the rotary kiln pyrolysis⁽¹⁸⁾ of the Whiterocks tar sand (Table 2). The breaking of alkyl linkages between clusters followed by dealkylation led to a reduction in the asphaltene content of the bitumen-derived liquid and to a large increase in the mono-, and dinuclear aromatic contents of these liquids.

The presence of alkyl indenenes, dihydronapthalenes, dihydrophenathrenes and the increased amounts of the alkyl naphthenes and phenanthrenes suggested that step-wise dehydrogenation of hydroaromatics occurred. The hydroaromatics present in the bitumen could have acted as hydrogen donors during pyrolysis.

Hydrogen was produced during the pyrolysis of oil sand. The formation of hydrogen was believed to have occurred via a gas phase reaction, coincident with light oils production and a solid reaction, associated with the formation of the

carbonaceous residue on the sand grains.⁽³⁸⁾ The clays in the solid substrate may have been activated at pyrolysis conditions and may have catalyzed polymerization and condensation of aromatics and hydroaromatics during pyrolysis. These reactions would be expected to be accompanied by the formation of hydrogen.

Small amounts of carbon dioxide were detected in the produced gases during pyrolysis of the Whiterocks oil sand. It was presumed that the CO₂ was produced by thermal decomposition of carboxylic acid functional groups present in the native bitumen. The decomposition of the R-COOH bonds readily occurred at the pyrolysis temperatures (723-823 K).⁽³⁸⁾ It was presumed that the CO₂ concentration would have been higher if the source of CO₂ had been related to the decomposition of mineral carbonates which were present in the reservoir rock.

Hydrogenation, hydrogenolysis and heteroatom removal were the principal reactions which occurred in the hydrotreater. The absence of olefins in the hydrotreated products and the heat released in the inlet region of the catalyst bed, suggested that hydrogenation of olefinic bonds occurred readily during hydroprocessing. The predominance of hydroaromatic species in the total liquid product indicated that polycyclic aromatics underwent partial hydrogenation. The naphtha and middle distillate fractions were formed via thermal and catalytic reactions at hydrotreating conditions.

ACKNOWLEDGEMENTS

John E. Fausett is thanked for providing the ore from the Whiterocks tar sand deposit. Dr. K.R. Chen is thanked for his contribution to the preliminary design and fabrication of the hydrotreating catalyst testing unit. The Wright Aeronautical Laboratories at the Wright-Patterson Air Force Base are acknowledged for the sponsorship of the work which led to the initial design of the hydrotreating unit. The financial support of the U.S. Department of Energy

through the Laramie Projects Office of the Morgantown Energy Technology Center is gratefully acknowledged. Dr. John Ward of UNOCAL, Inc., is gratefully acknowledged for providing the catalyst and for numerous, helpful discussions.

REFERENCES

1. Resnick, B.S., Dike, D.H., English, L.M., and Lewis, A.G., "Evaluation of Tar Sand Mining; Vol. 1. An Assessment of Resources Amenable to Mine Production," DOE/ET/30201-1 (DE82010249).
2. Miller, J.D. and Misra, M., "Hot Water Process Development for Utah Tar Sands," Fuel Proc. Technol. 6, 27-59 (1982).
3. Miller, J.D. and Misra, M., "Concentration of Utah Tar Sands by an Ambient Flotation Process," Internat. J. Miner. Proc. 2, 269-287 (1982).
4. Rendall, J.S., "Hot Water Bitumen Extraction Process" U.S. Patent No. 4,875,998 (October 24, 1989).
5. Rendall, J.S., "Solvent Extraction Process," U.S. Patent No. 4,160,718 (July 10, 1979).
6. Rendall, J.S. "Method and Apparatus for Solvent Extraction," U.S. Patent No. 4,424,112 (January 3, 1984).
7. Taciuk, W., Turner, L.R., and Wright, B.C., "Oil Shale Processing with the AOSTRA Taciuk Processor," Proc. 4th UNITAR/UNDP Intern. Conf. on Heavy Crude and Tar Sands, 5(237), 439-447. (1989).
8. Taciuk, W., "Process for Thermal Cracking a Heavy Hydrocarbon," U.S. Patent 4,180,455 (1977).
9. Boyer, L.D., Sooter, M.C., and Sage, F.E. "Method for Production of Distillable Hydrocarbonaceous Fuels and Carbonaceous Agglomerates from Heavy Crude Oil," "U.S. Patent 4,473,464 (1984).
10. Zimmermann, K.F., "Rotary Kiln for Drying and Deoiling Oil Sands and Oil Shales," Germany Patent DE 3,042,146 (1980).
11. Cha, C.Y. and Guffey, F.D., "Recycle Oil Pyrolysis and Extraction of Tar Sand," Proc. of 4th UNITAR/UNDP Intern. Conf. on Heavy Crude and Tar Sands, 5(106), 449-456 (1987).
12. Venkatesan, V.N. Fluidized-bed thermal recovery of synthetic crude from bituminous sands of Utah. Ph.D. dissertation. University of Utah, Salt Lake City, Utah. (1979).

13. Wang, J. The production of hydrocarbon liquids from a bitumen-impregnated sandstone in a fluidized bed pyrolysis reactor. M.S. thesis. University of Utah, Salt Lake City, Utah. (1983).
14. Dorius, J.C. The pyrolysis of bitumen impregnated sandstone from the P.R. Spring (Utah) deposit in a fluidized bed. Ph.D. dissertation. University of Utah, Salt Lake City, Utah, (1985).
15. Sung, S.H. The fluidized bed pyrolysis of bitumen-impregnated sandstone in a large diameter reactor. M.S. Thesis, University of Utah, Salt Lake City, Utah. (1988).
16. Shun, D. Fluidized Bed Pyrolysis of The Bitumen-Impregnated Sandstone from the Circle Cliff Deposit. Ph.D. Dissertation, University of Utah, Salt Lake City, Utah. (1990)
17. Cha, S., Hanson, F.V., Longstaff, D.C. and Oblad, A.G., "Pyrolysis of Bitumen Impregnated Sandstones: A Comparison of Fluidized Bed and Rotary Kiln Reactors." Proc. 1990 Eastern Oil Shale Conf., 136-145 (1991); Fuel 70, 1357 (1991).
18. Cha, S., "Pyrolysis of Oil Sands from the Whiterocks Tar Sands Deposit in a Rotary Kiln", Ph.D. Dissertation. University of Utah, Salt Lake City, Utah (1991).
19. Hanson, F.V. and Oblad, A.G., (1989), "The Fluidized Bed Pyrolysis of Bitumen-Impregnated Sandstone from the Tar Sand Deposits of Utah," Proc. Fourth UNITAR/UNP Internat. Conf. on Heavy Crude and Tar Sands, Vol. 5, 421-438.
20. Longstaff, D.C., (1992)., "Hydrotreating the Bitumen and Bitumen-Derived Liquid from the Whiterocks Oil Sand Deposit" Ph.D. Dissertation, University of Utah, Salt Lake City, Utah.
21. Longstaff, D.C., Deo, M.D., Hanson, F.V., and Oblad, A.G., (1992) "Hydrotreating the Bitumen-Derived Hydrocarbon Liquid Produced in a Fluidized-Bed Pyrolysis Reactor", Proc. 1991 Eastern Oil Shale Symp.
22. Philp, R.P., (1985)., "Fossil Fuel Biomarkers - Applications and Spectra," Methods in Geochemistry and Geophysics, 23, Elsevier, Amsterdam.
23. Henderson, W., Wollrab, V. and Eglinton, G., (1968)., "Identification of Steroids and Triterpenes from a Geological Source by Capillary Gas-Liquid Chromatography," Chem. Commun., 710.
24. Anderson, P.C., Gardner, P.M. and Whitehead, E.V., (1969)., "The Isolation of Steranes from Green River Shale," Geochim. Cosmochim. Acta, 33, 1304.
25. Anders, D.E. and Robinson, W.E., (1971)., "Cycloalkanes Constituents of the Bitumen from Green River Shale," Geochim. Cosmochim. Acta, 35, 661.

26. Gallegos, E.J., (1971)., "Identification of New Steranes, Terpanes and Branched Paraffins in Green River Shale by Combined Capillary Gas Chromatography and Mass Spectrometry," Anal. Chem., 43(10), 1151.
27. Gallegos, E.J., (1973)., "Identification of Phenylcycloparaffin Alkanes and Other Monoaromatics in Green River Shale by Gas Chromatography-Mass Spectrometry," Anal. Chem., 45(8), 1399.
28. Reed, W.E., (1977)., "Molecular Compositions of Weathered Petroleum and Comparison with its Possible Sources," Geochim. Cosmochim. Acta, 41 237.
29. Trendel, J.M., Restle, A., Connan, J. and Albrecht, P., (1982)., "Identification of Novel Series of Tetracyclic Terpene Hydrocarbons (C₂₄-C₂₇) in Sediments and Petroleum," J. Chem. Soc., Chem. Commun., 304.
30. Ekweozor, C.M. and Strausz, O.P., (1982)., "18,19-Bisnor-13 β H, 14 α H-Cheilanthane: A Novel Degraded Tricyclic Sesquiterpenoid-Type Hydrocarbon from the Athabasca Oil Sands," Tetrahedron Letters, 23(27), 2711.
31. Whitehead, E.V., (1974)., "The Structure of Petroleum Pentacyclanes," in Advances in Geochemistry.(eds. B. Tissot and F. Bienner), Editions, Technip, Paris, 225.
32. Bendoraitis, J.G., (1974)., "Hydrocarbons of Biogenic Origin in Petroleum - Aromatic Triterpanes and Bicyclic Sesquiterpenes," Advanced in Geochemistry, (eds. B. Tissot and F. Bienner), Editions, Technip, Paris, 209.
33. Kimble, B.J., Maxwell, J.R., Philp, R. P. and Eglinton, G., (1974)., "Identification of Steranes and Triterpanes in Geolipid Extracts by High-Resolution Gas Chromatography and Mass Spectrometry," Chem. Geology, 14, 173.
34. Aquino Neto, F.R., Restle, J., Connan, J., Albrecht, P. and Ourisson, G., (1982)., "Novel Tricyclic Terpanes (C₁₉-C₂₀) in Sediments and Petroleum," Tetrahedron Letters, 23(19), 2027.
35. Middleton, W.R., 1967, Gradient Elution Chromatography Using Ultraviolet Monitors in the Analytical Fractionation of Heavy Petroleum, Analytical Chemistry. 39 (14), 1839-1846.
36. Callen, R.B., Benderatis, J.G., Simpson, C.H., and Voltz, S.E., 1976. "Upgrading Coal Liquids to Gas Turbine Fuels I. Analytical Characterization of Coal Liquids," Ind. Eng. Chem., Prod. Res. Dev., 15 (4) 22.
37. Utley, J.K. 1980, The Adaptation of Gradient Elution Chromatography to the Analysis of the Bitumen and Synthetic Liquids Derived from Bituminous Sand, Senior Project Report, Department of Mining and Fuels Engineering, University of Utah, Salt Lake City, Utah.
38. Ritchie, R.G.S., Roche, R.S., and Steedman, W. "Non-Isothermal Programmed Pyrolysis Studies of Oil Sand Bitumens and Bitumen Fractions," Fuel, 1985, 64 391.

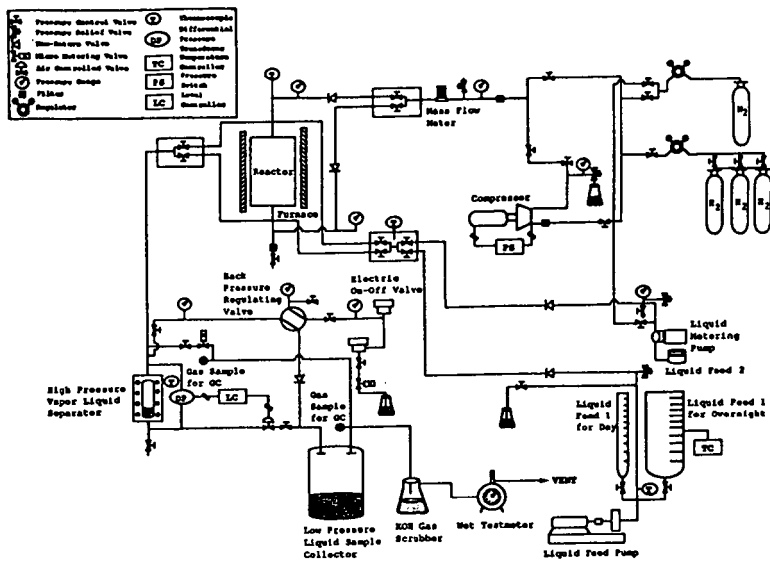


Figure 1 Flow diagram for a hydrotreating/hydrocracking unit

Table 1
Properties of Bitumen and Bitumen-Derived Liquids
from the Whitecourt Deposit Tar Sand

	Native Bitumen	Bitumen-Derived Liquid	Hydrotreated Bitumen-Derived Liquid
API Gravity	11.9	18.3	33
Conradson Carbon, wt%	8.1	4.7	NA
Pour Point, °C	330	378	219
Distillation			
Refluxivity, wt%	40.3	62.2	67.6
133 °C	513	434	318
178 - 227 °C, wt%	8.9	6.7	12.5
217 - 218 °C, wt%	4.9	10.3	46
218 - 219 °C, wt%	33.6	39.8	34.9
>219 °C, wt%	39.3	17.8	2.6
Elemental Analysis			
C, wt%	85.1	81.0	86.7
H, wt%	12.3	12.1	13.3
N, wt%/ppm	3.0	5.1	63 ppm
O, wt%/ppm	0.4	0.4	18 ppm
S, wt%	1.1	1.5	0
Wt, ppm	63	0	NA
V, ppm	0	0	NA

Table 2
Chemical Composition of the Bitumen-Derived Liquids from the Whitecourt Tar Sands

Run ID	Native Bitumen	WH-02-1	WH-02-2	WH-02-3	WH-02-4
Reactor Temperature, °C		395	395	395	395
Reactor Retention Time, min.		31	31	15	9
H ₂ Gas Flow Rate, SCFH		37.5	37.5	37.5	37.6
Reaction Station Characteristics					
Conversion, wt%	10.3	10.3	11.7	9.4	13.5
Wt%/ppm					
Oil, wt%	3.3	39.7	41.7	41.4	39.7
PM, wt%	31.3	18.1	18.6	11.9	11.5
Resid, wt%	15.0	11.4	12.5	13.0	13.3
Resid, wt%	3.0	0.9	1.5	1.2	1.3
Polys, wt%	1.6	1.3	1.7	1.7	1.3
Asphaltenes, wt%	12.4	12.9	12.9	13.1	9.3
Numbered Asphaltenes, wt%	10.9	0.4	2.2	9.3	7.9

The Effect of Cosolubilizing Lighter Components on the Asphaltene Content of Heavy Oils

Milind D. Deo, Jonsic Hwang and Francis V. Hanson
Department of Fuels Engineering
University of Utah, Salt Lake City, Utah, 84112.

Introduction

Asphaltenes are precipitates that separate from petroleum, petroleum residua or bituminous materials on treatment with low-boiling liquid hydrocarbons¹. The solvents for effecting this separation are n-pentane and n-heptane, although other light hydrocarbon solvents have also been used². The amount and composition of asphaltene fractions are important from processing considerations. In petroleum refining, asphaltene fractions can precipitate in heat exchangers and/or can deposit on catalysts causing excessive coke formation. A number of physical properties of the crude oils are also determined by the asphaltenes. In petroleum production operations, asphaltenes can precipitate and cause extensive formation damage. Asphaltene precipitation in oil reservoirs has proved to be a difficult problem to define and study^{3,4}.

Speight¹ provided a detailed discussion on the influence of solvent type on asphaltene separation. Yields of precipitate using various solvents and a western Canadian bitumen indicated that when the solvent carbon number was increased, the yields (wt% bitumen) decreased. This was particularly true for the n-alkane homologous series and was applicable to a lesser degree to naphthenic and aromatic compounds. The amount of precipitate correlated well with two types of solubility parameters defined by the following equations:

$$\delta_i = \gamma V^{-1/3} \quad (1)$$

$$\delta_2 = \left(\frac{\Delta H^v - RT}{V} \right)^{1/2} \quad (2)$$

where, γ is the solvent surface tension, V is the molar volume, ΔH^v is the heat of vaporization, R is the universal gas constant and T is the absolute temperature. Burke et al.³ used Equation 1 to define solubility parameters.

Fractionation of asphaltenes using solvent mixtures also exhibited varying yields depending on the ratio of the solvents used². This data suggests that the amount of asphaltene precipitate will be influenced by the lighter cosolubilizing components in the petroleum or bitumen. The work reported in this paper on the continuous supercritical fluid extraction (SFE) of an oil sands bitumen with propane provides direct evidence on the influence the lighter components have in keeping the asphaltene fractions in solution.

Experimental

The SFE system was custom-built for the University of Utah by Autoclave Engineers, Inc. A schematic of the apparatus is shown in Figure 1. Central to the system was a temperature controlled extractor with a capacity of 300 cc and rated to a pressure of 37 MPa at 615 K. The extractor was equipped with a magnetic-drive packer-less stirring device. Propane was charged into the extractor and the system was brought to the desired pressure using a high-pressure liquid pump. Pressure control is achieved by incorporating a back pressure regulator in parallel with the pump. The pump-head was cooled by a circulating cooling bath to ensure that the propane was maintained in a liquid state at the pump-head.

Initially 50 g of Whiterocks native bitumen was charged into the extractor. Selected properties of the bitumen are presented in Table 1. Once the initial equilibrium state was attained, propane was continuously pumped into the extractor. Commercial grade propane containing about 96% propane and

4% of other C₁ - C₄ hydrocarbon gases was used in this work. A heated metering valve was used to transfer the extracted phase from the extractor to the separator. The separator was held at ambient pressure. The solvent separated from the extract phase in the separator was vented through a flow totalizer which measured the cumulative volume of solvent withdrawn from the separator. The oil in the separator was collected and weighed. In all the experiments, a known amount of bitumen was charged into the extractor and the continuous extraction process was started. After about 25 liters of solvent (at room temperature) had passed through the totalizer, the amount of oil accumulated in the separator was collected and weighed. When the amounts of oil extracted became small relative to the amount extracted in the first 25 liters, the extraction was stopped. The extractor was depressurized and the residue was weighed and analyzed for maltenes and asphaltenes. In each extraction sequence, seven to eight extract samples were collected, each sample corresponding to an *extraction window* of 25 liters of propane vented through the totalizer or about 20 minutes of extraction time.

Asphaltene contents of the residual fractions produced during the propane extraction of the native bitumen were measured by the analytical method developed by AOSTRA⁵. Two grams of the residual oil sample were dissolved in an equal volume of toluene. Forty volumes of n-pentane were added for each volume of toluene. The AOSTRA method recommends benzene as the diluent; however, toluene was used in place of benzene for safety reasons. The precipitate was filtered from the solution, dried and weighed.

Results and Discussion

Experiments were performed at three different pressures (5.5 MPa, 10.3 MPa and 17.2 MPa) at a constant temperature of 380 K and at three different temperatures (339 K, 380 K and 422 K) at a constant pressure of 10.3 MPa. The critical temperature of propane is 369.8 K and its critical

pressure is 4.25 MPa. The effect of pressure on the extraction yields at 380 K is presented in Figure 2 and the effect of temperature on the extraction yields at 10.3 MPa is shown in Figure 3. Attempts have been made to link the extraction performance of dense gases to solvent density^{6,7}. The densities of pure propane at the experimental conditions, as calculated by the Peng-Robinson equation of state⁸ is presented in Table 2. It can be observed from Figures 2 and 3, and Table 2 that density did affect the extraction yields. However, pure solvent density was not the only parameter that governed the extraction process. The density variations for an increase in pressure from 5.5 MPa to 17.2 MPa at a temperature of 380 K and for an increase in temperature from 339 K to 422 K at a pressure of 10.3 MPa were almost identical (44%). However, Figures 2 and 3 indicated that pressure appeared to have a stronger influence on the extraction yields than temperature. The highest extraction yield was obtained at 380 K and 17.2 MPa.

The compositional variation in the extracted material as a function of time can be determined by examining the carbon number distributions of the first, middle and the last extracts for the experiments at 10.3 MPa and 380 K (Figure 4). The middle and the last extracts contained compounds heavier than the first fraction. The carbon number distributions of the middle extracts as a function of pressure (Figure 5) indicated that heavier compounds are extracted at higher pressure. No significant compositional changes in the middle extracts were observed as a function of temperature (Figure 6). This behavior appeared to be consistent with the extraction yield information, where it was observed that pressure had a stronger influence on the extraction process than temperature in the range of pressures and temperatures examined in this work.

Residual oils from all the extraction experiments were dark black solids. The asphaltene contents of the residual oils are listed in Tables 3 and 4 along with the elemental analyses of the residual oils. It should be noted

that the asphaltene content of the feed material was 5.9%. The asphaltene contents of all the residual oils were significantly higher than the original heavy oil. The asphaltene content of the residual oils increased with pressure. This was consistent with the observation that increased extraction of heavier compounds occurred as the extraction pressure was increased. The highest asphaltene content was found in the residual oil from the extraction at 380 K and 17.2 MPa where the extraction yield was also the highest. The asphaltene contents of the extracts were not measured in this study. The percentage of asphaltenes as a fraction of the original oil feed are also listed in Tables 3 and 4. These values were also considerably higher than the asphaltene content of the original oil. Obviously, compounds that did not precipitate from the original oil as pentane insolubles were precipitating from the residual oils.

These experiments established the fact that asphaltenes, as defined in this study (pentane insolubles), are not a definite compound class but were a collection of compounds specific to a given mixture. Lighter compounds in these mixtures helped keep the asphaltene fraction in solution when a pentane solubility test was performed on the mixture. During the extraction process, these lighter compounds were stripped from the original mixture, thus decreasing the tendency of the heavier molecules to be in solution. As a result of this, the pentane insolubles fraction increased in the residual oils. It is apparent from this reasoning that the asphaltene content of the residual oils would be higher for the residuals produced at conditions that led to more efficient extraction of the lighter components. The data demonstrated this with the exception of the extraction at 5.5 MPa and 380 K. In this experiment, despite an extraction of only about 20% of the material which consisted of relatively lighter compounds (Figures 2 and 5), an asphaltene fraction of 14% was observed in the residual oil. Extractions in the vicinity of the critical temperature of propane (T_c for 380 K is 1.03) and the quality of the compounds extracted may explain this data point. However, detailed

compositional information on the extracts (possibly by gas chromatography - mass spectrometry), their asphaltene contents, etc. would be required to evaluate this.

The elemental analysis of the residual oils reported in Tables 3 and 4 indicated that the H/C ratio of the residual oils decreased relative to the H/C ratio of the original bitumen. This suggested that saturated compounds are preferentially extracted by propane and that the heavier portion of the bitumen is relatively more unsaturated than the bitumen as a whole. It was also seen from the data that the nitrogen and sulfur contents of residual oils were higher than the original bitumen. This indicated that the heteroatomic species are concentrated in the unextractable heavier portion of the bitumen.

The solubility parameters (Equations 1 and 2) increase with carbon number¹. As the extraction pressure increased more of the heavier hydrocarbons are extracted (Figures 2 and 5). Thus the increase in the asphaltene content of the residual oils for increased extraction pressures was expected. The effect of solubilizing co-solvents² led us to presume that as lighter components are extracted, more of the heavier components ought to precipitate. Thus the data reported in this work were intuitive. However, the data did point out that it would be misleading to perform material balances on the asphaltene portions of the fractionated oils (as reported by Burke et al.³) since the type and amounts of asphaltenes in different fractions would depend on the solubility character of the specific fractions. Since residual oils recovered in the extractions were dark black solids, it may be wrong to presume that only the pentane insolubles asphaltene fraction of the original oil is susceptible to precipitate in any given recovery or refining process. The solubility parameter approach would also have to be modified to account for the different compound types that precipitate depending on the state of the mixture.

Conclusions

1. When an oil sand bitumen was subjected to supercritical extraction with propane, the residual oils left in the extractor exhibited significantly higher values of asphaltene fractions than the original oil (bitumen). The loss of cosolubilizing lighter components from the original oil during the extraction process caused more of the heavier components to precipitate thus increasing the apparent asphaltene content. This established that pentane-insoluble asphaltenes were not a definite compound class and that their nature and quantity in a given mixture was determined by the overall solubility character of the mixture.
2. As the extraction pressure increased at a constant temperature of 380 K, the asphaltene content of the residual oil also increased. This was consistent with the observation that the extraction yields increased with pressure and that heavier compounds were extracted at higher pressures.
3. The H/C ratio in the residual oils was lower than the original oil establishing that saturated compounds were preferentially extracted leaving the residual oils richer in unsaturated compounds than the original oil. The nitrogen and sulfur contents of the residual oils were also higher which indicated that heteroatomic compounds concentrated in the heavier (unextractable) portion of the original oil.
4. This study indicated that care should be exercised when performing material balances on asphaltenes from fractionated oils and that it may be inappropriate to presume that only the pentane-insoluble asphaltene fractions of the original oils are susceptible to precipitate in a given recovery (enhanced oil recovery) or refining process.

Acknowledgements

The financial support of the U.S. Department of Energy through the Laramie Project Office of the Morgantown Energy Technology Center is gratefully acknowledged. The authors wish to thank Professor Alex G. Oblad, Director of the Utah Tar Sand Program for his support and encouragement. The authors would also like to acknowledge support from the mineral leasing funds from the College of Mines and Earth Sciences, University of Utah and the Research Support Committee, University of Utah.

References

1. Speight, J. G., *The Chemistry and Technology of Petroleum*, Second Edition, Marcel Dekker, New York, NY.
2. Mitchell, D. L. and Speight, J.G., Fuel, 1973, **52**, 151.
3. Burke, N. E., Hobbs, R. E. and Kashou, S. F., Journal of Petroleum Technology, 1990, **42**, 1440.
4. Chaback, J. J., Journal of Petroleum Technology, 1991, **43**, 1519.
5. AO STRA, *Syncrude Analytical Methods for Oil Sand and Bitumen Processing*, 1979, Edmonton, Alberta, Canada.
6. Orr, F. M., Jr. and Silva, M. K., SPEJ, 1983, **23**, 272.
7. Orr, F. M., Jr. and Silva, M. K. and Lien, C., SPEJ, 1983, **23**, 281.
8. Peng, D. Y. and Robinson D. B., Ind. Eng. Chem. Fund., **15**, 59, (1976).

Table 1
Selected Properties of the Whiterocks Bitumen

Specific Gravity (288 K)	0.98
Conradson Carbon (wt%)	9.50
Pour Point, K	327
Viscosity (323 K), Pa-s	27
Simulated Distillation	
Volatility, Wt%	32.5
IBP, K	520
IBP-477 K, Wt%	0.0
478-616 K, Wt%	5.6
617-811 K, Wt%	26.9
> 811 K, Wt%	67.5

Table 2
Densities of Propane (g cm^{-3}) at Experimental Conditions
Calculated by the Peng-Robinson Equation of State

Temperature (K)	339	380	422
Pressure			
5.5 MPa	-	0.2585	
10.3 MPa	0.4782	0.3825	0.2672
17.2 MPa	-	0.4416	-

Table 3
Selected Properties of the Residual Oils After
Propane Extractions of Bitumen: Pressure = 10.3 MPa

Extraction	Bitumen		
Temperature (K)	339	380	422
Product Yield(%)			
Extract Phase	40	39	24
Residual Phase	59	58	73
Asphaltene/Maltene			
Asphaltenes, Wt%	12.5	15.0	9.8
Maltenes, Wt%	87.5	85.0	90.2
Asphaltenes Wt% Original Oil	7.4	8.7	7.16
5.9			
Elemental Analysis			
C, Wt%	86.74	86.69	86.66
H, Wt%	10.81	10.80	11.08
N, Wt%	1.95	2.02	1.79
S, Wt%	0.50	0.49	0.47
H/C Atomic Ratio	1.50	1.49	1.53
1.56			

Table 4
Selected Properties of the Residual Oils After
Propane Extractions of Bitumen: Temperature = 380 K

Extraction	Bitumen		
Temperature (K)	339	380	422
Product Yield(%)			
Extract Phase	20	39	48
Residual Phase	79	58	50
Asphaltene/Maltene			
Asphaltenes, Wt%	14.0	15.0	20.2
Maltenes, Wt%	86.0	85.0	79.8
Asphaltenes Wt% Original Oil	11.0	8.7	10.1
5.9			
Elemental Analysis			
C, Wt%	86.78	86.69	86.80
H, Wt%	10.97	10.80	10.58
N, Wt%	1.78	2.02	2.12
S, Wt%	0.47	0.49	0.50
H/C Atomic Ratio	1.52	1.49	1.46
1.56			

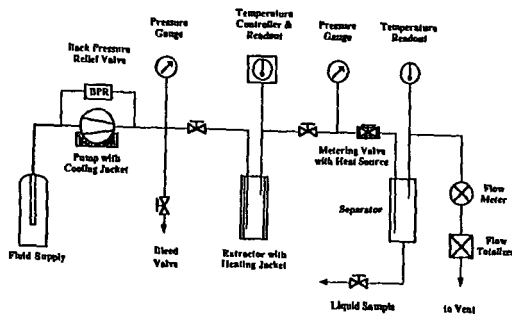


Figure 1: Schematic diagram of the supercritical fluid extraction system

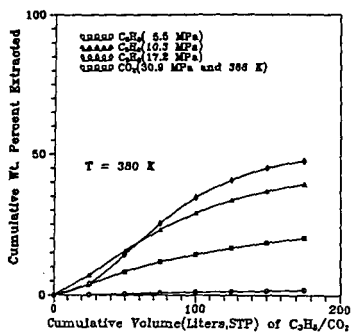


Figure 2: Extraction yields for the native bitumen with propane as function of pressure at 380 K.

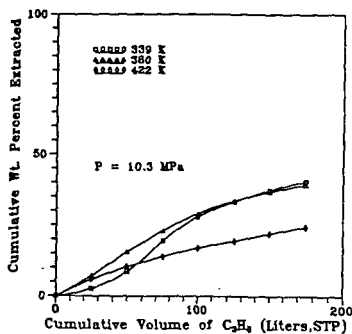


Figure 3: Extraction yields for the native bitumen with propane as function of temperature at 10.3 MPa.

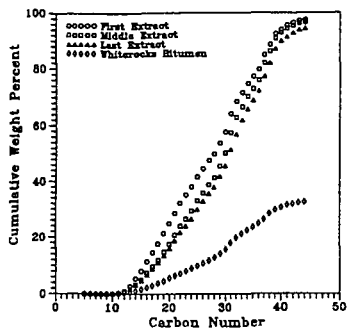


Figure 4: Changing compositions as a function of time for the native bitumen propane extracts at 350 K and 10.3 MPa.

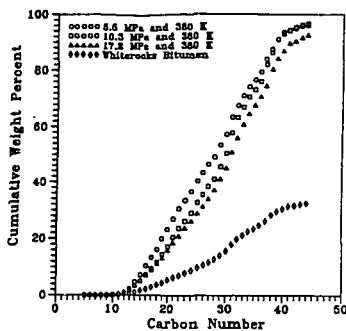


Figure 5: Compositional changes as a function of pressure for the native bitumen propane extractions at 350 K.

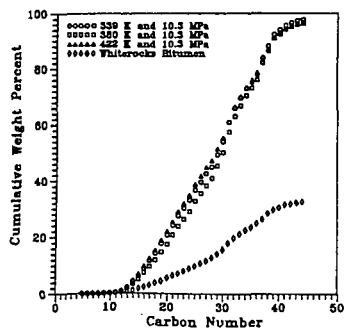


Figure 6: Compositional changes as a function of temperature for the native bitumen - propane extractions at 10.3 MPa.

SMALL ANGLE X-RAY SCATTERING STUDY OF ASPHALTENES

David A. Storm, Eric Y. Sheu and Maureen M. DeTar

Texaco R&D, Beacon, N.Y. 12508

INTRODUCTION

Asphaltenes are molecules that can be precipitated from carbonaceous liquids by certain non-polar solvents¹⁻³. Traditionally they were those molecules in petroleum residuum that were soluble in benzene and insoluble in pentane, but over the years molecules precipitated by other solvents, usually heptane², and molecules precipitated from other materials, such as coal and oil shale liquids have been called asphaltenes³. As such there can be many kinds of asphaltenes, each a mixture of a number of molecules. In this work we have studied the heptane insolubles of vacuum residue from Ratawi crude oil.

Although petroleum asphaltenes have been studied for some time⁴, their physical nature, or macrostructure, in petroleum is poorly understood. Small angle X-ray scattering(SAXS) is a technique that can be used to study asphaltenes in their natural state. Early SAXS experiments confirmed the colloidal nature of crude oil^{5,6}, atmospheric residue⁷, and solid asphaltic materials⁸. Scattering centers were observed with radii of gyration in the range of 30-70 Å, indicating either the presence of macromolecules⁷, or micelle-

like particles.⁸ In more recent studies the authors have tried to obtain more information by fitting the observed scattering intensity with an intensity calculated for model particles.^{9,10} Senglet et al. however noted that polydispersity complicates the analysis.¹⁰ For example the well-known Guinier analysis failed in their study of asphaltenes in toluene, or gas oil.¹⁰ Applying a method suggested by Vonk¹¹, they extracted histograms for the radii of gyration that are quite broad.¹⁰ Recently Sheu¹² suggested some ambiguity can be removed by applying a constraint that follows from the assumption of homogeneous particles. Operationally we have:

$$I(Q) = A \langle F_o^2(Q; \text{shape, size}) \rangle \quad (1)$$

where $I(Q)$ is the measured scattering intensity, and $\langle F_o^2 \rangle$ is the normalized form factor for a particular particle shape and size distribution function. Equation (1) defines A , which also depends on the shape and size parameters used in the fitting. Since the scattering intensity is:

$$I(Q) = N(\Delta\rho)^2 V_p^2 \langle F_o^2 \rangle \quad (2)$$

for identical particles, where N is the number of particles per unit volume, $\Delta\rho$ is the contrast between particles and fluid, V_p is the particle volume and $\langle F_o^2 \rangle$ is the square of the normalized form factor averaged over orientation angles, we would expect for a polydispersed sample that:

$$\alpha - A(shape, size) / (N(size) \langle V^2(shape, size) \rangle \langle F_o^2(shape, size) \rangle) \quad (3)$$

is independent of the shape and size parameters for the right shape and distribution function, since Eq.(3) express the fact that the contrast is constant for homogeneous particles. The constraint is applied by requiring that Eq.(3) remain constant as the concentration is varied; i.e., the parameters of the distribution may change, but the form of the distribution function, and the particle shape can not change. This procedure was used to fit the scattering data obtained with natural and synthetic Ratawi vacuum residue. The asphaltenic particle sizes (radii) are distributed according to a Schultz distribution. The average radius agree well with the radii of gyration reported earlier⁵⁻⁸, and the spherical shape agrees with the recent rheological studies for Ratawi asphaltenes in vacuum residue¹³, and in toluene.¹⁴

EXPERIMENTAL

Ratawi crude oil comes from the Neutral Zone in the Middle East. The vacuum residue was obtained by vacuum distillation; it is the fraction that has an apparent boiling point above 1000 °F. Samples of synthetic vacuum residue were prepared by dispersing appropriate amounts of vacuum residue in the corresponding non-asphaltenic portion. The non-asphaltenic fraction was prepared by first mixing heptane with the vacuum residue in the ratio of 40 parts of heptane for each part of vacuum residue, then stirring overnight at room temperature, and finally removing the asphaltenes by filtration. Heptane was removed from the non-asphaltenic portion by vacuum distillation.

The SAXS measurements were made with the ten meter small angle scattering spectrometer at Oak Ridge National Laboratory. The X-ray generator was a Rigaku-Demki rotating anode with a copper target; the power was 4KW. The K_{α} wavelength of 1.54 Å was selected using a pyrolytic graphite monochromator. The input collimator and a series of pinholes produced a 1 mm² spot at the sample position. The sample to detector distance was 112.6 cm. The detector was a 20 x 20 cm² continuously wired area detector purged by P10 gas. With this configuration the scattering wave vector Q ranged from 0.1 to 0.25 Å⁻¹. The samples were heated to 125 °C and then injected into a Kapton sandwich circular cell with a path length of 1 mm. The temperature was maintained at 93 °C during the experiment. Scattering from empty cells with and without Kapton windows was also measured for subsequent use during data reduction. A

calibrated polyethylene standard of known cross section at the peak position was used to obtain the absolute intensity (differential cross section per unit volume of sample)

RESULTS AND DISCUSSION

As discussed above, the measured scattering intensities were fit according to the procedure suggested by Sheu.¹² The fit obtained for spherical particles with sizes distributed according to the Schultz distribution for the Ratawi vacuum residue is shown in Figure 1. Other particle shapes and distributions were tried, but the alpha values defined in Eq.(3) were not constant. For example, the data for a particular sample could be fit by monodispersed cylinders, but the alpha values were not constant as the concentration was changed.

The Schultz distribution functions is shown in Figure 2. The Schultz distribution is defined as follows:

$$D(R) = [(z+1)/\langle R \rangle]^{z+1} R^z e^{-(z+1)R/\langle R \rangle} / \Gamma(z+1)$$

where $\langle R \rangle$ is the average radius, $\Gamma(z+1)$ is the gamma function, and z is a width parameter related to the polydispersity as

follows:

$$\text{polydispersity} = \sqrt{(\overline{R^2}) - (\overline{R})^2} / (\overline{R}) = 1/\sqrt{z+1}$$

The average radius and the degree of polydispersity is 33.8 Å and 15.4%. There are particles with radii as small as 20 Å and as large as 50 Å in this distribution. The average radius agrees very well with the radii of gyration reported by others for crude oil^{5,6}, atmospheric residue⁷, asphaltic materials⁸, and asphaltenes in solvents.⁵⁻⁸ The distributions are broad, as also found by Senglet et al.¹⁰ using the method due to Vonk.¹¹ The spherical shape for the asphaltenic particles is in agreement with the rheological measurements for these asphaltenes in vacuum residue¹³ and in toluene.¹⁴

ACKNOWLEDGMENT

We thank the Solid State Division of Oak Ridge National Laboratory for granting us beam time, and Dr. J. S. Lin for special assistance during the measurement. The SAXS experiments performed at Oak Ridge National Laboratory are partially supported by the Division of Material Sciences, U. S. Department of Energy under contract number DE-AC05-84OR21400, with Martin Marietta Energy Systems, Incorporated.

REFERENCES

- (1) Long, R. B. 1981. The Concept of Asphaltenes. In: J. W. Bunger and C. Norman (Editors), Chemistry of Asphaltenes. Advances in Chemistry Series 195:17-27
- (2) Speight, J. G. and S. E. Moschopedis, 1981. On The Molecular Nature of Petroleum Asphaltenes. In: J. W. Bunger and Norman C. Li (Editors) Chemistry of Asphaltenes, Advances in Chemistry Series 195:1-15
- (3) Yen, T. F. 1981. Structural Differences Between Asphaltenes Isolated from Petroleum and from Coal Liquid. In: J. W. Bunger and N. C. Li, Chemistry of Asphaltenes, Advances In Chemistry Series 195:39-51
- (4) Speight, J. G. 'The Chemistry and Technology of Petroleum,' Second Edition, Marcel Dekker, Inc., 1991
- (5) Dwiggin, C. W. Jr. *J. Appl. Cryst.* 1978, **11**, 615
- (6) Dwiggin, C. W. Jr. *J. Phys. Chem.* 1965, **69**, 3500
- (7) Klm, Hyo-gun and Long, R. B. *Ind. Eng. Chem. Fundam.* 1977, **18**, 60
- (8) Pollack, S. S. and Yen, T. F. *Anal. Chem.* 1970, **42**, 623
- (9) Herzog, P., Tchoubar, D. and Espinat, D. *Fuel* 1988, **67**, 245
- (10) Senglet, N., Williams, C., Faure, D., Des Courieres, T. and Guilard, R. *Fuel* 1990, **69**, 72
- (11) Vonk, C. G. *J. Appl. Cryst.* 1976, **9**, 433
- (12) E. Y. Sheu, "Polydispersity Analysis of Scattering Data from Self-Assembled Systems", to appear in *Phys. Rev A*
- (13) Storm, D. A., Sheu, E. Y., Barresi, R. J. and DeTar, M. M. International Symposium on the Chemistry of Bitumens, Rome,

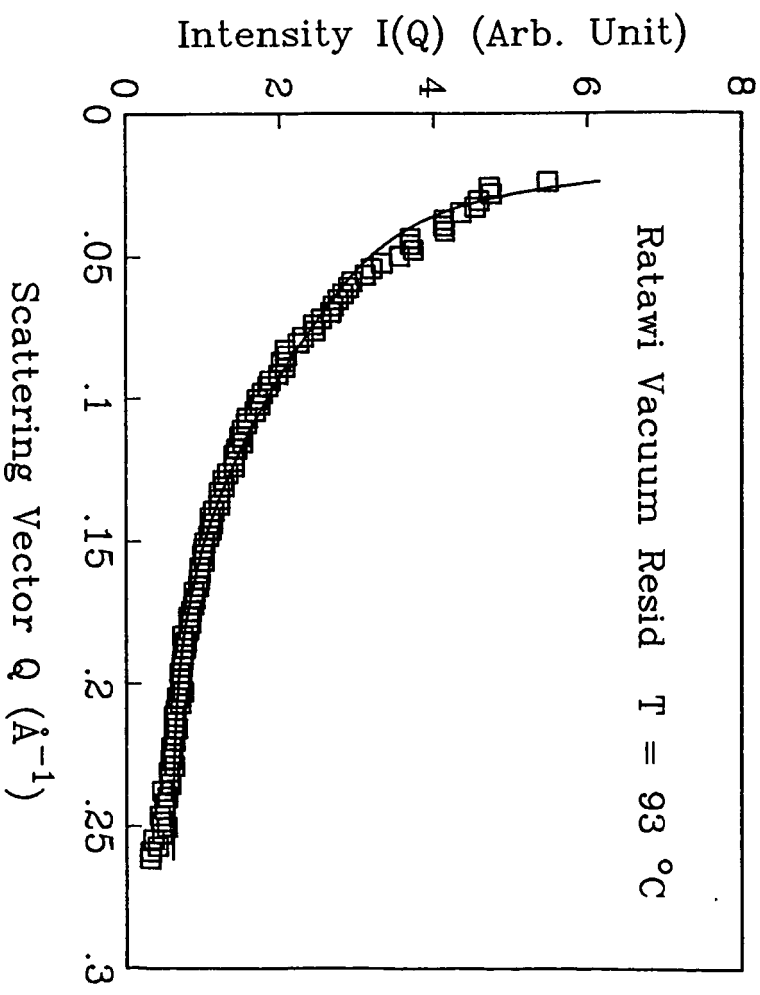
Italy, June 5-8, 1991

(14) Sheu, E. Y., DeTar, M. M. and Storm, D. A. *Fuel* 1991, 70, 1151

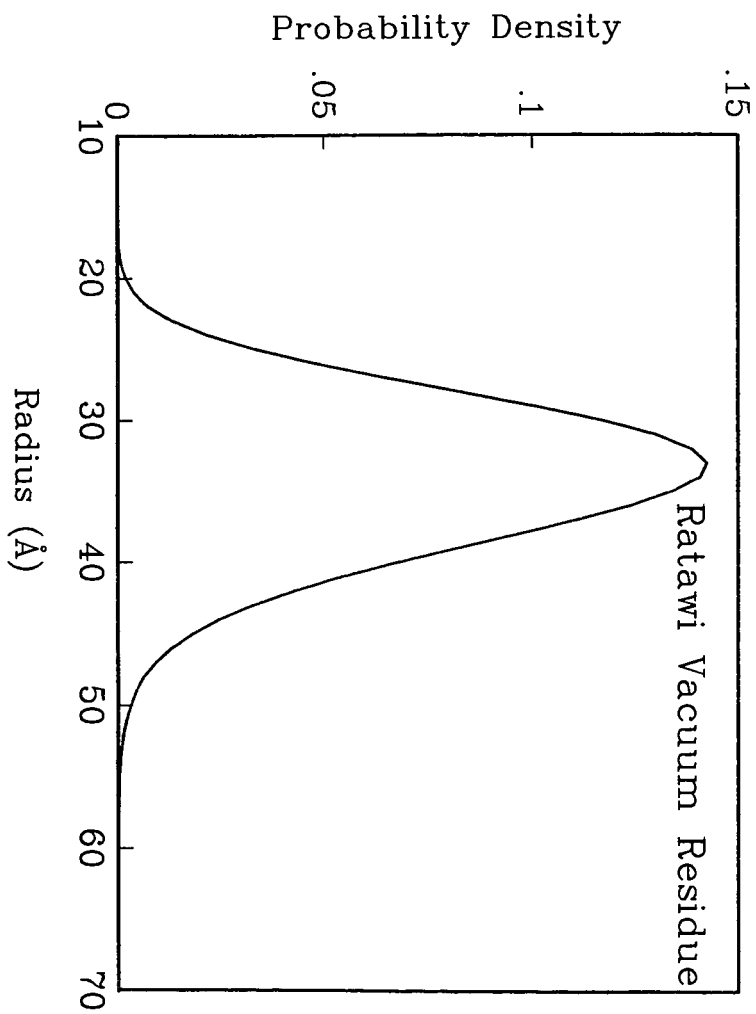
FIGURE CAPTIONS

Figure 1 Scattering intensity for Ratawi vacuum residue at 93° C

Figure 2 Distribution of radii of asphaltenic particles



Particle Size Distribution



COLLOIDAL STRUCTURE OF VACUUM RESIDUE IN SOLVENTS

Eric Y. Sheu, M. M. De Tar, and D. A. Storm
Texaco R & D Dept. P.O. Box 509, Beacon, N. Y. 12508

Key Words: asphaltenes, colloids, small angle neutron scattering (SANS).

I. Introduction

Petroleum asphaltenes form colloidal particles in organic solvents through self-association, when the concentration exceeds a threshold value [1-5]. The self-association process is very similar to the micellization process of surfactant systems [6]. Since the structure, size and the polydispersity of the asphaltene colloids are important parameters for developing technology to upgrade vacuum residue, it is necessary to establish an analytical technique capable of accurately evaluating these parameters. Small angle neutron scattering (SANS) has been successfully applied to the structural characterization of micellar solutions [7]. We employed this technique in this study to investigate asphaltenes. Unfortunately, the polydispersity and the intercolloidal interactions often complicate the data analysis, and lead to ambiguous results, due to local convergence in the data fitting process. Recently, Sheu [8] developed a self-consistent scheme, by which the particle size distribution can be unambiguously determined from a scattering measurement. This technique however, can only be applied for dilute systems, since the intercolloidal interactions were not taken into account.

In this study, we followed up on the polydispersity work of Sheu, with the interparticle interaction taken into account. We also studied the effect of solvent permittivity on particle structure, polydispersity and interparticle interactions.

II. Experimental

A. Sample Preparation

Asphaltene fractions were extracted from Ratawi (Neutral Zone) vacuum residue, by mixing with heptane (1 gram of vacuum residue with 40 cm³ of heptane) at room temperature. After stirring overnight, the solution was filtered with Whatman number 5 filter paper. The insoluble portion was dried under a stream of nitrogen, until constant weight was maintained for a 48 hour period. This insoluble fraction was taken as the asphaltene fraction.

To prepare the samples for the SANS measurement, asphaltenes were dissolved in deuterated toluene/pyridine mixtures of various volume ratios, and aged for several days to ensure thermodynamic equilibrium [9]. Toluene has a permittivity of 2.4, while pyridine is 12, the samples were prepared to exhibit the following permittivities: 2.4, 3.84, 5.28, 6.72, and 9.12.

B. SANS Measurement

The SANS experiment was conducted on the small angle diffractometer (SAD) at Argonne National Laboratory. The neutrons were generated by a neutron generator via Pu-Be reaction. The generated neutron wave lengths were sorted by the time-of-flight method, in order to fully utilize the generated neutrons. The scattering vector Q ($Q = (4\pi/\lambda) \sin \theta$) was computed by built-in software using neutron

energy. Therefore, the sample-to-detector distance was fixed. The temperature was maintained at 22 °C.

III. Scattering Theory

The intensity as a function of the scattering vector, $I(Q)$, represents the differential cross section per unit volume of the sample. $I(Q)$ is a function of concentration, particle-solvent contrast, particle structure, and interparticle interactions [10],

$$I(Q) = C (\Delta\rho)^2 \left[\frac{\langle V_p^2 \rangle}{\langle V_p \rangle} \langle P(Q) \rangle \langle S(Q) \rangle \right] \quad (1)$$

where C is concentration, $\Delta\rho$ is the particle-solvent contrast, $\langle V_p^2 \rangle$ is the second moment of particle volume, and $\langle V_p \rangle$ is the average particle volume. $\langle P(Q) \rangle$ is the average form factor, governed by particle structure, and $\langle S(Q) \rangle$ is the average structure factor, governed by interparticle interactions. The evaluation of $\langle V_p^2 \rangle$, $\Delta\rho$, $\langle V_p \rangle$ and $\langle P(Q) \rangle$ are described in references 1 and 9.

To calculate $\langle S(Q) \rangle$, we approximated $\langle S(Q) \rangle$ by $S(Q)$ (the monodispersed particle structure factor) using $\langle R \rangle$ (the average particle radius) as the particle size. This approximation is generally plausible [10].

We computed $S(Q)$ by solving the Ornstein-Zernike equation using a mean spherical approximation ansatz. A one-tailed Yukawa potential was used as a direct correlation function [10]. A fortran program was developed to compute $S(Q)$, along with $\langle P(Q) \rangle$. This program enabled us to unambiguously determine both particle structure and interparticle interactions.

IV. Results

Fig. 1 displays the scattering intensity $I(Q)$ (open circles) and the fitted curve (solid line). The fitting is reasonable for Q up to $\sim 0.2 \text{ \AA}^{-1}$. Fig. 2 shows the average radius $\langle R \rangle$ and the Yukawa parameter, K , as a function of solvent permittivity. K represents the "diffusiveness" of the Yukawa potential,

$$V(r) = A \cdot \text{Exp}(-Kr)/Kr, \quad r > \langle R \rangle$$

where A is an amplitude factor representing the contact potential at $r = \langle R \rangle$. As one can see from Fig. 2, the average radius does not depend on solvent permittivity, but the diffusiveness of the interparticle interaction increases (K decreases). This indicates that the range of interaction increases. Obviously, this is due to "effective" charges on the asphaltene colloids, which result in long range interactions when solvent permittivity increases. Fig. 3 shows the polydispersity as a function of solvent permittivity. It was found to increase substantially as a function of solvent permittivity. From Gibbs' equilibrium condition this result clearly indicates that for permittivities up to ~ 9.0 , the solvent quality decreases as a function of permittivity [10].

V. Discussion

In aqueous solutions, the K in Yukawa potential is equal to kR , where k is the Debye screening length. In our case, the solvents were oil-like, which may change the meaning of K . Therefore, K can only be visualized as a parameter characterizing the "diffusiveness" of the the potential.

As for the polydispersity, we argue based on the first principle given by Gibbs, about thermal equilibrium. Based on Gibbs' equilibrium condition, the polydispersity should increase when the solvent quality becomes poorer, in order to optimize the free energy through eutropic energy [10.11]. This finding leads us to conclude that the asphaltene colloids behave similarly to surfactant solutions, and by tuning the solvent permittivity, dispersion of asphaltene colloids may be possible. This conclusion may shed light on the upgrading of vacuum residue.

References

- [1] E.Y. Sheu, D.A. Storm and M.M. De Tar, *J. Non-Cryst. Solids*, **131** 341 (1991).
- [2] R.E. Overfield, E.Y. Sheu, S.K. Sinha and K.S. Liang, *Fuel Sci. and Tech. Int'l.*, **1** 611 (1989).
- [3] P.D. Herzog, and D. Espinot, *FUEL*, **67** 245 (1988).
- [4] J. C. Ravey, G. Docouret, and D. Espinot, *FUEL*, **67** 1560 (1988).
- [5] T.F. Yen, *Energy Sources*, **1** 447 (1974).
- [6] E.Y. Sheu, M.M. De Tar, and D.A. Storm, "Aggregation and Kinetics of Asphaltenes in Organic Solvents," to appear in *FUEL*.
- [7] S.H. Chen and E.Y. Sheu, in "Statistical Mechanics and Thermodynamics of Micelle and Microemulsion Systems" ed. by S.H. Chen and P. Rajagopalan, Spring-Verlag (1990).
- [8] E.Y. Sheu, "Particle Size Distribution for a Non-Interacting Dispersed System, Studied by Small Angle Scattering," to appear in *Phys. Rev. A*.
- [9] E.Y. Sheu, K.S. Liang, S.K. Sinha, R.E. Overfield, "Polydispersity Analysis of Asphaltenes in Toluene," submitted to *J. Coll. Int. Sci.*
- [10] E.Y. Sheu and S.H. Chen, "The Hydrophobic Effect, Formation of Micelles and Biological Membranes," *J. Wiley A. Sons, N.Y.* (1980).

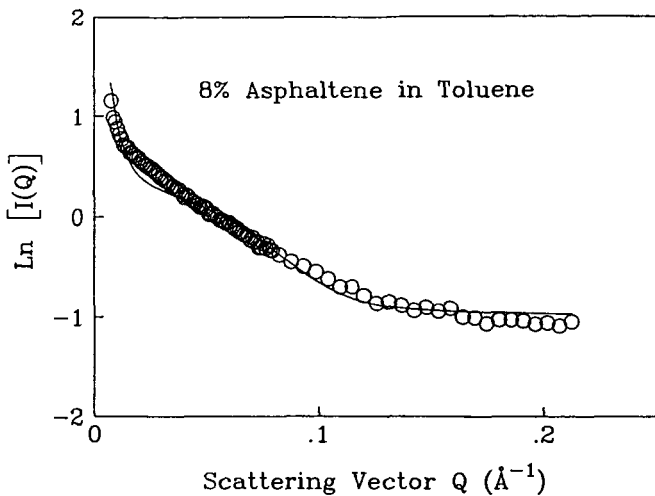


Fig. 1. Fitting of a 8% asphaltene solution. The SANS data (circles), and the theoretical curve (solid line) agree reasonably well, indicating that a one-tailed Yukawa potential is an appropriate representation of the interactions between asphaltene colloids.

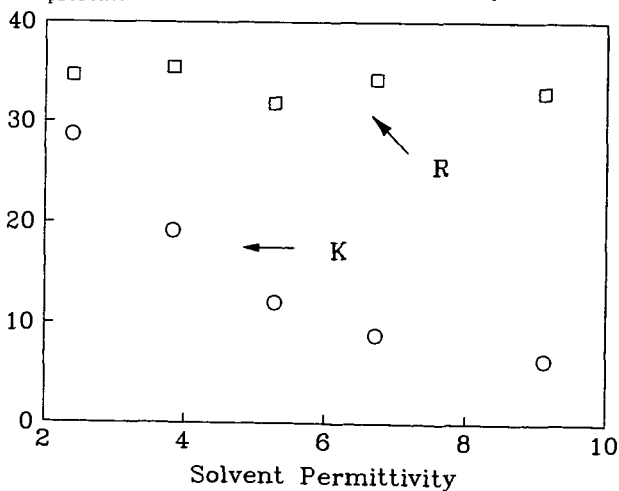


Fig. 2. Average particle radius and potential diffusiveness as a function of the solvent permittivity. The diffusiveness increases (K decreases) as a function of the solvent permittivity, while the average radius remains nearly unchanged.

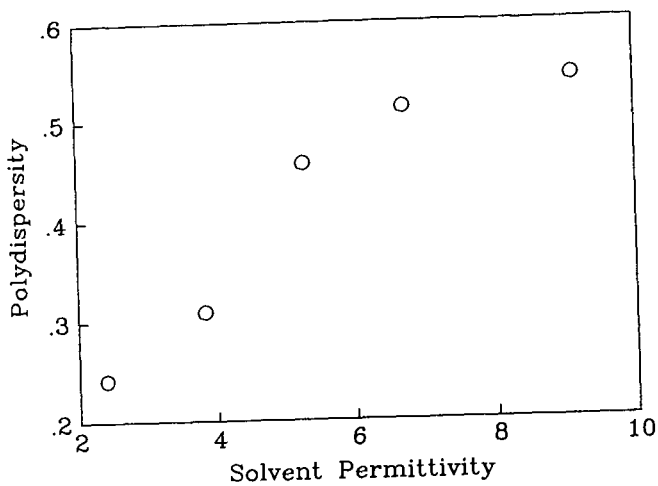


Fig. 3. Polydispersity, as a function of the solvent permittivity, for an 8% asphaltene concentration.

THE ARGONNE COALS DO NOT HAVE AN EXTENDED INTER-CONNECTED PORE NETWORK

John W. Larsen & Patrick C. Wernett
Department of Chemistry
Lehigh University
Bethlehem, Pennsylvania 18015

Keywords: pore structure, gas adsorption, surface area

ABSTRACT

The sorption of N_2 , CO_2 , ethane, cyclopropane, cyclobutane, cyclopentane, and cyclohexane has been studied on all of the Argonne premium coals. For all of the bituminous coals, the CO_2 BET surface areas are as expected and much higher than all of the other molecules studied. Plots of \log (moles adsorbate in monolayer) vs. \log (cross section area of adsorbate) are straight lines whose slopes are very steep (-5.5 to -11.6) and inconsistent with the known fractal dimensionalities of the coal pore surfaces. For Zap lignite, the CO_2 BET surface area is $274m^2/g$, while all of the hydrocarbons give lignite surface areas of $8 \pm 3m^2/g$. These data are inconsistent with adsorption in an inter-connected pore network. For bituminous coals, the dependence of the amount sorbed vs. molecular diameter is similar to the dependence of diffusivities through glassy polymers on molecular diameter. We conclude that the pores in coal are isolated from each other and can only be reached by diffusion through the solid, glassy, macromolecular coal.

INTRODUCTION

It is widely accepted that coals contain an inter-connected network of slit like pores and that the connections between pores are often bottlenecked.¹ This conclusion is based almost entirely on experimental studies of gas adsorption. We have recently completed a study of the adsorption of a series of gases on the Argonne coals and obtained results which are inconsistent with this model. Our data for Illinois #6 coal have already been published and we will here discuss our results for some of the other Argonne coals.²

Small angle X-ray studies have been carried out on all of the Argonne coals and demonstrate that the pore surfaces are well behaved fractals.³ Being surfaces, their fractal dimensionalities are constrained to lie between 2 and 3. Fractal dimensionalities can also be obtained by determining the dependence of measured surface area on the size of the adsorbate molecule.⁴ Fractal dimensionalities obtained in this way should agree with those obtained by other techniques. The basis of the measurement is that small molecules will follow a rough surface more precisely than will larger molecules and thus report a larger surface area. The difference between the surface areas reported by a small and a large molecule will increase with the degree of surface roughness, that is with the fractal dimensionality. The fractal dimensionalities calculated from adsorption measurements carried out using ethane, cyclopropane, cyclobutane, cyclopentane, and cyclohexane

are reported in Table 1. The dimensionalities do not lie between 2 and 3 demonstrating that the process under investigation cannot be a simple equilibrium surface adsorption.

Perhaps the most impressive feature of these data are the great size of the calculated "fractal dimensionalities". They vary from 11 to 23. The amount of gas adsorbed varies with the cross sectional area raised to at least the 5th power. Stated another way, the amount of gas sorbed by these coals exhibits an extraordinarily steep dependence on gas molecular size, that dependence being between the 5th and 12th power of the cross sectional area. Any model for coal structure must rationalize this extraordinary fact.

This enormous sensitivity to molecular size is rare. Diffusivities through glassy polymers are known to have similar and even greater sensitivities to molecular size.⁵ We propose that the process occurring here is not gas adsorption on the surface, but rather diffusion of the gases through a glassy polymer to reach an internal pore surface. We are suggesting that the BET surface areas measured using these gases are not equilibrium values, but are controlled by the rate of diffusion of these gases through the glassy coal. This was confirmed by following the uptake of ethane by Illinois No. 6 coal at 177°K which had not reached equilibrium after 5.5 days.

We look to the surface areas measured using the individual gases for confirmation of the idea that it is diffusion through glassy polymers which is occurring, not diffusion through a more-or-less rigid pore network. We have already pointed out for Illinois No. 6 coal that we were unable to rationalize the reported surface areas based on diffusion through a interconnected network.² Figure 1 contains the data for Bruceton coal and the results are similar. CO₂, which is known to swell coals, has a ready diffusion pathway and reports a high surface area.⁶ Ethane, which differs in size from CO₂ by only 16% and which has a similar cylindrical shape, reports a much lower surface area. It is hard to rationalize this difference if both materials are diffusing through a rigid pore network. Cyclopropane has the same surface area as ethane, but a significantly different shape. It is hard to believe that two materials, one planar and the other cylindrical, would pass equally through a rigid pore system and report the same surface area. Similar results have been obtained for all of the other Argonne bituminous coals. These data support the notion that the coals do not have an interconnected pore network, but rather isolated pores like bubbles in a solid which are reached only by diffusion through the solid coal.

Finally, we consider the surface area measurements for ZAP lignite shown in Figure 2. Hydrocarbon gases should be essentially insoluble in this high oxygen, highly polar low rank coal. If the pore structure is a rigid network, this should have no effect on the surface areas measured. The data are shown in Figure 2 and reveal that within experimental error, all of the hydrocarbon gases report the same surface area, 8 ± 3 m²/g. This is to be contrasted with the CO₂ area which is 274 m²/g. We are unable to rationalize these data using a pore network structure. They are nicely consistent with a pore model which involves

isolated pores which can be reached only by diffusion through the solid.

We conclude that the pore structure of these coals is isolated pores which can be reached by diffusion through the coals and that an interconnected pore network which provides access to a large internal surface by pore diffusion does not exist. This structure model has a number of consequences, a few of which can be elaborated here. The first is that CO₂ surface areas are approximately correct. Because it is somewhat soluble in coals, CO₂ has a rapid diffusion pathway and can quickly reach all of the pore surfaces where it is adsorbed as it would be on any surface. These reported surface areas are undoubtedly somewhat in error because of the amount of CO₂ dissolved in the coal. We believe these errors are small compared to the fundamental uncertainties of the measurement. Likewise, we believe that helium densities give accurate pore volumes. Diffusion rates vary inversely with molecular size and helium is small enough to have reasonably rapid passage through the coal and reasonable equilibrium times. Because coal surface areas depend on the diffusion rate of the molecules used to probe it, measured surface areas will depend on the nature of the molecular probe. This would be true in any case because the surfaces are fractal, but we are concerned with a much greater sensitivity to molecule size and polarity. Molecules which interact with coals (are soluble in them) will have a rapid diffusion pathway and will report much greater surface areas than will non-polar hydrocarbons and other molecules which do not interact specifically.

EXPERIMENTAL

Complete experimental descriptions of all procedures used may be found in the Ph.D. thesis of Patrick Wernett.⁷

ACKNOWLEDGEMENTS

This work was supported by the U. S. Department of Energy Contract #DE-AC22-38PC89757. We gratefully acknowledge this support. Numerous discussions with Dr. Peter Hall played an important role in the development of our ideas and we are grateful to him.

REFERENCES

1. Bond, R. L. Nature **1956**, 104-105. Mahajan, O. P.; Walker, P. L., Jr. Analytical Methods for Coal and Coal Products, **1**, C. Karr Jr., Editor, Academic Press: New York, NY, 1979. Marsh, H. Carbon **1987**, 25, 49-58.
2. Larsen, J. W.; Wernett, P. Energy & Fuels **1988**, 5, 719-720.
3. Hall, P.J.; Wernett, P.C.; Larsen, J.W. unpublished.
4. Farin, D.; Peleg, S.; Yavin, D.; Avnir, D. Langmuir **1985**, 1, 399-407. Farin, D.; Volpert, A.; Avnir, D. J. Am. Chem. Soc. **1985**, 107, 3368-3370. Pfeifer, P.; Avnir, D. J. Chem. Phys. **1983**, 79, 3558-3565.

5. Crank, J.; Park, G. S. Diffusion in Polymers Academic Press: New York, NY, 1968. Van Krevelen, D. W.; Hoftyzer, P.J. Properties of Polymers Elsevier Scientific Publishing Company: New York, NY 1976. Berens, A. R.; Hopfenberg, H. B. J. Membr. Sci **1982**, 10 283-303.
6. Reucroft, P. J.; Patel, H. Fuel, **1986**, 65, 816-820. Walker, P.L., Jr.; Verma, S.K.; Rivera-Utrilla, J.; Khan, M.F. Fuel, **1988**, 67, 719-726.
7. Wernett, P. C. Ph.D. Thesis, Lehigh University, 1991.

Table 1. Fractal Dimensionality of Argonne Coal Surfaces Measured by BET Adsorption of Ethane, Cyclopropane, Cyclobutane, Cyclopentane, and Cyclohexane

Coal	%C dmmf	Dimensionality	Correlation Coefficient
Pocahontas #3	91.8	12	0.998
Upper Freeport	88.1	11	0.995
Lewiston-Stuchton	85.5	15	0.942
Pittsburgh No. 8	85.0	16	0.987
Blind Cargon	81.3	14	0.990
Illinois No. 6	80.7	23	0.999
Wyodak	76.0	11	0.867

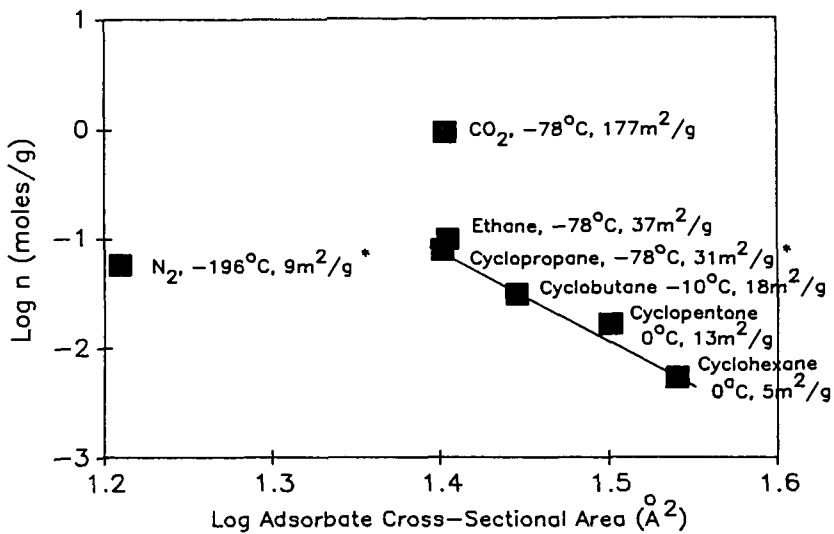


Figure 1. Fractal Analysis of the Cyclic Hydrocarbon Gas Adsorption on Argonne Pittsburgh No. 8 Coal (n is the Number of Moles Required for Monolayer Surface Coverage Obtained from the BET Equation). The Adsorbate Gas is Given Followed by the Adsorption Temperature and the Measured BET Surface Area.

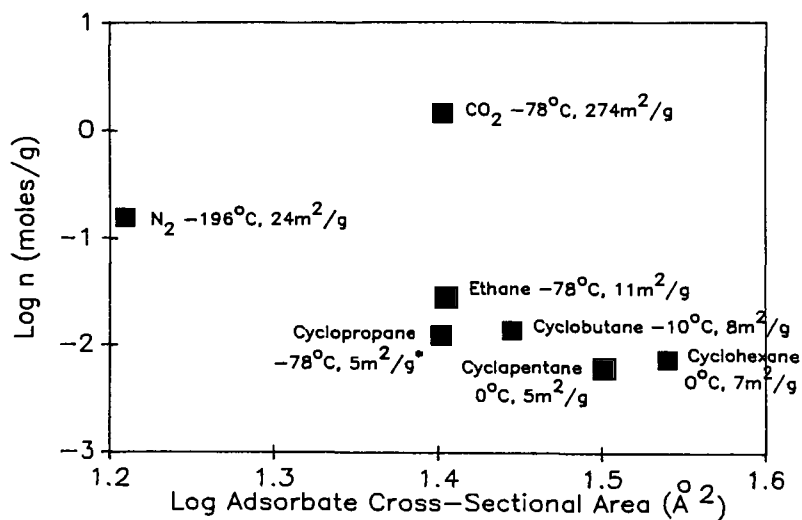


Figure 2. Fractal Analysis of the Cyclic Hydrocarbon Gas Adsorption on Argonne Beulah Zap Lignite (n is the Number of Moles Required for Monolayer Surface Coverage Obtained from the BET Equation). The Adsorbate Gas is Given Followed by the Adsorption Temperature and the Measured BET Surface Area.

Structural Changes in High-rank Bituminous Coals Caused by Solvent Swelling and Heat

Yongseung Yun and Eric M. Suuberg
Division of Engineering, Box D
Brown University, Providence, RI 02912

(Key Words: Bituminous coal structure, Solvent swelling, Differential Scanning Calorimetry)

INTRODUCTION

High-rank coals (>86 %C daf) have been known to exhibit fundamentally different response characteristics to heat and solvent treatments than lower-rank coals (< 86 %C daf). Sakurovs et al.[1] reported that heat is more effective than pyridine for creating mobility in coal structure, for coals of 86-90 %C daf. Also Iino et al.[2] showed that extraction yields using solvent mixtures of CS₂/N-methyl-2-pyrrolidinone(MP) (1:1 v/v) increase with carbon content up to 86 %C daf and then fall rapidly with further increase in carbon content.

High-rank coals do not significantly swell in pyridine, while most lower-rank coals show a substantial amount of swelling in that solvent. However, some combinations of solvents, especially with CS₂, yield for the higher-rank coals similar swelling ratios as can be obtained in lower-rank coals. The work of Iino et al.[2-4] is especially noteworthy, since they first reported the benefit of mixing CS₂ (which is a known good solvent for fats, resins, and rubbers) with several solvents (i.e., pyridine, dimethylsulfoxide, dimethylformamide, dimethylacetamide, MP), in enhancing extraction yield and volumetric swelling of coal, particularly around 86 %C daf.

It has also been demonstrated that the structure of high-rank bituminous coals can be thermally loosened, to yield high volumetric swelling ratios in pyridine (when the coals are heated to above 350°C)[5,6]. These swelling ratios are similar to those which can be obtained at room temperature in mixtures of CS₂/pyridine, CS₂/dimethylsulfoxide, or CS₂/dimethylformamide as will be shown in this paper.

In order to understand the underlying structural changes caused both by mixed solvents and heat, as well as to explore possible effective pre-liquefaction strategies for these high-rank bituminous coals, two coals, viz., Upper Freeport (mvb) and Pocahontas No. 3 (lvb), were studied using differential scanning calorimetry (DSC) and solvent swelling techniques.

EXPERIMENTAL

Aliquots of several coal samples, obtained from the Argonne National Laboratory - Premium Coal Sample Program, were analyzed by DSC and solvent swelling techniques. These samples included Illinois No. 6 (-20 mesh), Blind Canyon (-20 mesh), Upper Freeport (-100 mesh), and Pocahontas No. 3 (-20 mesh) coals. They were used as-received. Detailed petrographic, chemical, and physical analysis data on these coals can be found elsewhere [7].

Differential Scanning Calorimetry A DuPont 2910 DSC system with a liquid nitrogen cooling accessory (LNCA-II) was employed in this study. The sample cell was operated under a nitrogen flow rate of 90 ml/min in order to keep the cell free of oxygen during measurement. Aluminum sample pans were used in an unsealed mode. This was done by just pushing down the

top sample pan cover gently onto the bottom pan containing the coal. Samples were initially isothermal for five minutes and then heated from 30°C at 8 °C/min or 10 °C/min. Typically 6-9 mg of sample was used in an experiment. Cooling of the cell between consecutive heating scans normally involved air convection in the heating assembly, but the sample itself was always kept under nitrogen.

Solvent Swelling Coal samples were placed in constant diameter tubes (3 mm i.d., ca. 5 cm long) and centrifuged at 7500 rpm for 3 min in a roughly 30 cm horizontal rotor (SAVANT HSC-10K high speed centrifuge), after which the initial height of the sample was measured by a caliper. The choice of 7500 rpm was rather arbitrary and selected only to be as high as could be comfortably tolerated by the equipment. Solvent was then added and stirred until a visual check showed the total submergence of coal in solvent. The stirring was repeated frequently (normally 3 times) during the first 30 min following solvent addition. At the desired measurement times, the sample tubes were centrifuged again (7500 rpm for 3 min), the swollen coal height measured, and the solvent replaced with the clean solvent. This assured that the concentration of extractable was not so high as to interfere with the measurement.

Samples (22-28 mg) for solvent swelling were prepared in the DSC at a heating rate of 8 °C/min under a nitrogen flowrate of 90 ml/min. After reaching the desired temperature, each sample was cooled immediately by contacting the bottom of the sample pan with ice or cold water. Swelling solvents employed were all reagent grade and were used without any further purification.

Sample Pretreatment In order to determine the main parameters governing the relaxation of coal structure, several treatments were performed before subjecting the samples to DSC or solvent swelling. These include preswelling by solvent, pyridine Soxhlet extraction, acetylation, and heat treatment. Solvent preswelling was performed in two ways. One method involved swelling coal samples in the constant diameter glass tubes, which were used in the normal swelling experiments described earlier. The swelling was performed in excess solvent at room temperature for about 3-4 days with frequent replacement of extract-laden solvent with fresh solvent. The samples were subsequently dried under vacuum (<30 inHg) at room temperature for about two days. Another approach involved Soxhlet extraction of samples with pyridine for about two days, until the color of pyridine in the extraction tube indicated no further extraction. Then the sample was washed with deionized water, filtered using a water aspirator, and dried under vacuum (<30 inHg) at room temperature for about two days. Thus in the first case the samples were swelled but not exhaustively extracted, whereas in the second case the samples were exhaustively extracted (as well as presumably being fully swelled). Acetylation of hydroxyls was accomplished by mixing coal with excess pyridine and excess acetic anhydride at room temperature for about three days, and then excess acetic anhydride was destroyed by reaction with water while excess pyridine was removed by washing the sample with water. The acetylated sample was subsequently dried under vacuum at room temperature for about two days.

RESULTS AND DISCUSSION

Figure 1 shows difference DSC spectra, solvent swelling ratios in pyridine and tetrahydrofuran (THF), and pyrolytic mass loss for the Upper Freeport and Pocahontas No. 3 coals. The mass loss curves indicate the total loss observed from individual samples heated at 8°C/min and then immediately quench-cooled from the specified temperature by contacting the bottom of the sample pan with ice or cold water. The mass loss around 100°C shows the loss of moisture (around 1% in each sample) and the upturn at around 300°C heralds the onset of pyrolytic weight loss. It is presently unclear at what temperature pyrolysis reactions actually begin in these samples, since the mass loss at near 300°C might include physical evaporation of small molecules, in a manner analogous to the loss of water at 100°C. This point will be further discussed below.

The solvent swellability of the raw Upper Freeport and Pocahontas No. 3 samples is very low, prior to heat treatment (see middle panels of Figure 1). Both exhibit a volumetric swelling ratio of roughly 1.1 in pyridine, prior to heat treatment. As we discussed in our earlier papers [5,6], heat treatment appears to irreversibly "relax" the coal structure somewhat, such that both swellability in pyridine and THF is greatly enhanced, as is also seen in Figure 1. The temperature at which increased swellability is first observed is around 300°C in both the Upper Freeport coal and the Pocahontas No. 3 coal, although it takes considerably higher temperatures to achieve maximum swellability in the latter.

As we earlier noted [5], such irreversible changes in swellability correspond with events observed by DSC (see the top panels of Figure 1). In both coals, the dramatic rise in swellability coincides with a significant endothermic peak in the DSC spectra. The spectra are shown as difference spectra, obtained by scanning through the same temperature range three times with the same sample. The first minus second and first minus third scan spectra show the peaks distinctly, centered at 350°C in the Upper Freeport coal and at around 425°C in the Pocahontas No. 3 coal. The peaks around 100°C involve moisture loss. The second minus third scans show the absence of these peaks, confirming the irreversibility of the processes.

Figure 2 shows the actual raw DSC spectra for the two coals of interest here, compared with two spectra for lower-rank bituminous coals. While somewhat less distinct in feature than the subtracted spectra of Figure 1, the curves in the top panel show the clear endothermic peaks at 350°C and 425°C for the Upper Freeport and Pocahontas No. 3 coals, respectively. Such distinct peaks are not visible in the spectra of the lower rank coals in the lower panel in Figure 2, in which water evaporation process (endothermic) is followed by a more or less straight DSC response curve corresponding to the heat capacity of coal, and then followed by thermal degradation process where a peak occurs in the exothermic direction, in part due to weight loss. What is notable from the top panel is that the endothermic peaks corresponding to the irreversible relaxation of the structures of the higher rank coals are well separated from the main pyrolysis events, seen as major disturbances in the DSC curves. The sharp peak into the exothermic direction in the Upper Freeport coal is mainly caused by the sudden expansion of sample volume, with the development of plasticity.

The above observations do not establish the nature of the events resulting in the endothermic peaks coinciding with the relaxation event in the high-rank coals. They might be reaction endotherms, occurring prior to the main pyrolysis reactions, or they could be physical events of an endothermic nature (such as "melting"). The fact that the events are irreversible does not necessarily rule out an explanation based on physical processes, since the coal obviously does not have to reassume the same physical form upon cooling as it had in the raw state. We believe that the events have a high probability of having physical origin, based upon other observations. First, the endothermic peaks for two high-rank bituminous coals are similar to the "hysteresis" peak normally occurring just after the glass transition temperature in stressed polymers [8]. The hysteresis peak is mainly caused by stress relief of the structure by heat, quite often observed in amorphous polymers, e.g., epoxies, polycarbonate, polystyrene. Second, we believe that the behavior of one of the coals in certain solvents supports the hypothesis of a physical process.

It has been noted [2-4] that higher rank bituminous coals show a remarkably high degree of extractability in mixtures of certain solvents with CS₂. The Upper Freeport coal shows a sharp increase in room temperature swellability in a mixture of pyridine and CS₂, as noted in Figure 3. There is no need to heat treat the coal to achieve significant swellability, which suggests that a physical relaxation of the structure is all that is involved. There is, of course, the possibility that CS₂ undergoes chemical reaction with the coal, cleaving similar numbers of bonds as are cleaved

during heat treatment, but there is no strong reason to believe that this should be so. Moreover, as the data of Figure 3 show, there is a maximum in swelling ratio for the 1:1 by volume mixture of pyridine and CS_2 . It would be difficult to understand why, if CS_2 is a chemically reacting agent, such a stoichiometry would be needed, when solvent is in large excess. We thus are led to the tentative conclusion that the CS_2 /pyridine mixtures are effective mainly because of specific solvent properties.

The fact that the CS_2 /pyridine mixture relaxes the coal structure in a manner similar to heat, is established in Figure 4. Treating the coal with CS_2 alone, pyridine alone, or chloroform/pyridine mixtures leaves intact the DSC peak, corresponding to the relaxation of the structure. The Upper Freeport coal treated in CS_2 /pyridine, however, no longer shows such a relaxation event at 350°C. The CS_2 /pyridine mixture is not nearly as effective a swelling agent for Pocahontas No. 3 coal as for Upper Freeport coal. This, too, is confirmed by the DSC which still records a significant relaxation event for the previously pyridine/ CS_2 treated Pocahontas No. 3 coal (see lower panel of Figure 4). Apparently this specific solvent combination is only effective for a certain range of ranks. This is consistent with the observations of Iino et al.[3].

There is nothing particularly unique about the choice of pyridine in mixture with CS_2 . As Iino et al. earlier showed [2,3], N-methyl-2-pyrrolidinone/ CS_2 mixtures are also effective. We have established, as Iino et al. noted, that CS_2 /dimethylsulfoxide(DMSO) and CS_2 /dimethylformamide are also effective mixtures (see Table 1). Thus the solvent pair need not even include a nitrogen base, since DMSO is not. All the effective solvents in CS_2 mixtures are, however, fairly good electron donors.

Pyridine was tried in admixtures with other solvents of similar solubility parameter to CS_2 , and with other solvents that could serve as effective electron acceptors (see Table 1). None of these other combination rivaled the ability of the CS_2 /pyridine mixture to swell the Upper Freeport coal. Of course, these solvents did not yet include particularly strong electron acceptors (strong acids) and work on this point continues.

Pretreatment of the coal by pyridine extraction has little effect on its subsequent behavior in CS_2 /pyridine (see Table 1). Pretreatment of the coal by acetylation does little to change the behavior of the coal with respect to swelling in CS_2 /pyridine mixtures. This means that the structure is not irreversibly expanded to a significant extent by the acetylation alone. This suggests that it is not, for example, a xanthate formation type of process [9-11] involving CS_2 and the hydroxyl groups in the coal that results in the greater swellability of the coal in CS_2 /pyridine mixtures. The completeness of our acetylation has not yet been established, so its conclusion is still tentative.

Pretreatment of the coal in CS_2 , followed by removal of the CS_2 by evaporation and then subjected to pyridine swelling, showed again the importance of the interaction of pyridine and CS_2 . The sequence resulted in pyridine swelling comparable to that of the raw untreated coal (see Table 2). Reversing the order of sequential exposure was also not effective (again see Table 2).

When the coal was "relaxed" by exposure to CS_2 /pyridine mixtures, it was more swellable than in the raw state, by either of these solvents (see Table 2). The fact that the swellability was not as great as that induced by the thermal treatment to 350°C is also seen in Table 2. This is because

once swollen in pyridine/CS₂ mixture, it is difficult to fully remove all of the pyridine from the coal by vacuum drying. Thus the coal is already in a partially swollen state, due to the irreversibly bound pyridine. Heating a CS₂/pyridine swollen coal to 350°C results in a higher subsequent pyridine swellability (relative to the vacuum dried CS₂/pyridine swelled coal), because the pyridine is fully lost upon heating.

Results of swelling by solvents for low volatile bituminous Pocahontas No. 3 coal (91.1 %C daf) are illustrated in Table 3. As can be expected from DSC responses for CS₂/pyridine-swollen Pocahontas No. 3 coal (see Figure 4), even CS₂/pyridine mixture was not as effective in swelling as for Upper Freeport coal. However, heat treatment up to 450°C can relax the coal structure enough to induce swelling of more than 60% by THF and pyridine. At present, only heat appears to be an effective agent for loosening the structure of low volatile bituminous coal significantly.

CONCLUSIONS

- Two high-rank bituminous (Upper Freeport: mvb, Pocahontas No. 3: lvb) coals exhibit a distinct endothermic DSC peak corresponding to the irreversible relaxation of the structure. The endothermic peaks are well separated from the main pyrolysis events and appear to originate from physical processes rather than from chemical reaction processes.
- Even strong solvents (e.g., pyridine) cannot swell the structure of high-rank coals more than ten percent at low temperatures (<250°C). Heat treatment above 300°C can enhance the swelling of both Upper Freeport and Pocahontas No. 3 coals significantly. Solvent swelling by mixtures of solvents (e.g., with CS₂) is effective in relaxing the structure of medium volatile bituminous Upper Freeport coal, but not for low volatile bituminous Pocahontas No. 3 coal.
- The efficacy of mixed solvents containing CS₂ and certain solvents (e.g., pyridine, dimethylsulfoxide, dimethylformamide) appears to be physical. The work to confirm more conclusively this hypothesis is in progress.

ACKNOWLEDGEMENT The work reported here was financially supported by the Department of Energy Contract No. DE-AC22-91PC91027.

REFERENCES

1. Sakurovs, R.; Lynch, L.J.; Barton, W.A. In *Coal Science II*; Schobert, H.H., Bartle, K.D., Lynch L.J., Ed.; ACS Symposium Series 461; ACS: Washington, DC, 1991; Chapter 9, p 111.
2. Iino, M.; Takanoashi, T.; Ohsuga, H.; Toda, K. *Fuel* **1988**, *67*, 1639.
3. Takanoashi, T.; Iino, M. *Energy Fuels* **1990**, *4*, 452.
4. Iino, M.; Matsuda, M. *Fuel* **1983**, *62*, 744.
5. Yun, Y.; Otake, Y.; Suuberg, E.M. *Prepr. Pap.- Am. Chem. Soc., Div. Fuel Chem.* **1991**, *36(3)*, 1314.
6. Suuberg, E.M.; Otake, Y.; Deevi, S.C. *Prepr. Pap.- Am. Chem. Soc., Div. Fuel Chem.* **1991**, *36(1)*, 258.
7. Vorres, K.S. *User's Handbook for the Argonne Premium Coal Sample Program*; Argonne, Illinois, 1989.
8. Meesiri, W.; Menczel, J.; Gaur, U.; Wunderlich, B. *J. of Polymer Science* **1982**, *20*, 719.
9. Petrucci, R.H. *General Chemistry*; The Macmillan Co.: New York, 1972.
10. Morrison, R.T.; Boyd, R.N. *Organic Chemistry*; Allyn and Bacon, Inc.: Boston, 1983.
11. Roberts, J.D.; Caserio, M.C. *Modern Organic Chemistry*; W.A. Benjamin, Inc.: New York, 1967.

Table 1. Volumetric Swelling Ratio by Mixed Solvents (1:1 v/v) for Upper Freeport Medium Volatile Bituminous Coal

Pretreatment	Solvent mixture (1:1 v/v)	Solvent characteristics			Q**
		Solvent	Acceptor Number	$\delta(H)$ *	
None	CS ₂ /pyridine	pyridine	14.2	10.4	1.95
	CS ₂ /dimethylsulfoxide	dimethylsulfoxide	19.3	12.8	1.75
	CS ₂ /dimethylformamide	dimethylformamide	16.0	11.5	1.92
	CS ₂ /n-butylamine	n-butylamine	-	-	1.21
	pyridine/water	water	-	9.4	1.08
	pyridine/methanol	methanol	41.3	12.9	1.09
	pyridine/chlorobenzene	chlorobenzene	-	9.5	1.12
	pyridine/chloroform	chloroform	-	9.3	1.13
	pyridine/methylene chloride	methylene chloride	-	9.7	1.14
	pyridine/nitroethane	nitroethane	-	11.1	1.09
	Pyridine Soxhlet extracted	CS ₂ /pyridine	CS ₂	-	10.0
Acetylated	CS ₂ /pyridine	CS ₂	-	10.0	1.71

* δ : solubility parameter in Hildebrand which is equivalent to $\text{cal}^{1/2}\text{cm}^{-3/2}$ **Q: volumetric swelling ratio

Table 2. Solvent Swelling Results for Upper Freeport Medium Volatile Bituminous Coal

Pretreatment	Solvent	Solvent Properties				Q*	Swelling number** ($\times 10^3$)
		Donor No.	Acceptor No.	$\delta(H)$ ¹	Molar Vol.(cc/mol)		
None	pyridine	33.1	14.2	10.4	80.9	1.14	1.73
	CS ₂	-	-	10.0	60.3	1.08	1.33
	n-butylamine	-	-	-	99.8	1.12	1.20
	THF	20.0	8.0	9.1	81.1	1.08	0.99
	dimethylsulfoxide	29.8	19.3	12.8	71.0	1.09	1.27
	dimethylformamide	26.6	16.0	11.5	77.4	1.08	1.03
CS ₂ swelled	pyridine	33.1	14.2	10.4	80.9	1.12	1.48
Pyridine Soxhlet extracted	pyridine	33.1	14.2	10.4	80.9	1.19	2.35
	CS ₂	-	-	10.0	60.3	1.07	1.16
CS ₂ /pyridine (1:1 v/v) swelled	pyridine	33.1	14.2	10.4	80.9	1.40	4.94
	CS ₂	-	-	10.0	60.3	1.30	4.97
Heated under N ₂ up to 350°C	THF	20.0	8.0	9.1	81.1	1.82	10.11
	pyridine	33.1	14.2	10.4	80.9	2.17	14.46
	CS ₂	-	-	10.0	60.3	1.50	8.29
	dimethylsulfoxide	29.8	19.3	12.8	71.0	1.49	6.90
	chlorobenzene	-	-	9.5	101.7	1.40	3.93
CS ₂ /pyridine swelled and heated up to 350°C	pyridine	33.1	14.2	10.4	80.9	1.83	10.26
Acetylated	pyridine	33.1	14.2	10.4	80.9	1.10	1.24
	CS ₂	-	-	10.0	60.3	1.06	0.99

¹ δ : solubility parameter in Hildebrand which is equivalent to $\text{cal}^{1/2}\text{cm}^{-3/2}$ *Q: volumetric swelling ratio ** (Q-1)/molar volume

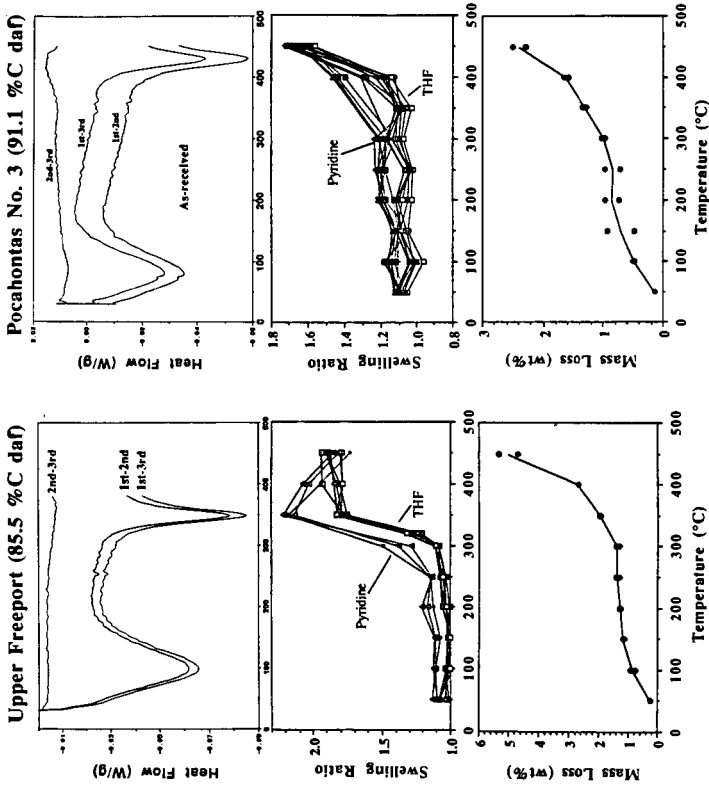


Figure 1. DSC difference thermograms as well as profiles of swelling ratio and weight loss for Upper Freeport (-100 mesh) and Pocahontas No. 3 (-20 mesh) coals. DSC was performed at 8°C/min under N₂ atmosphere.

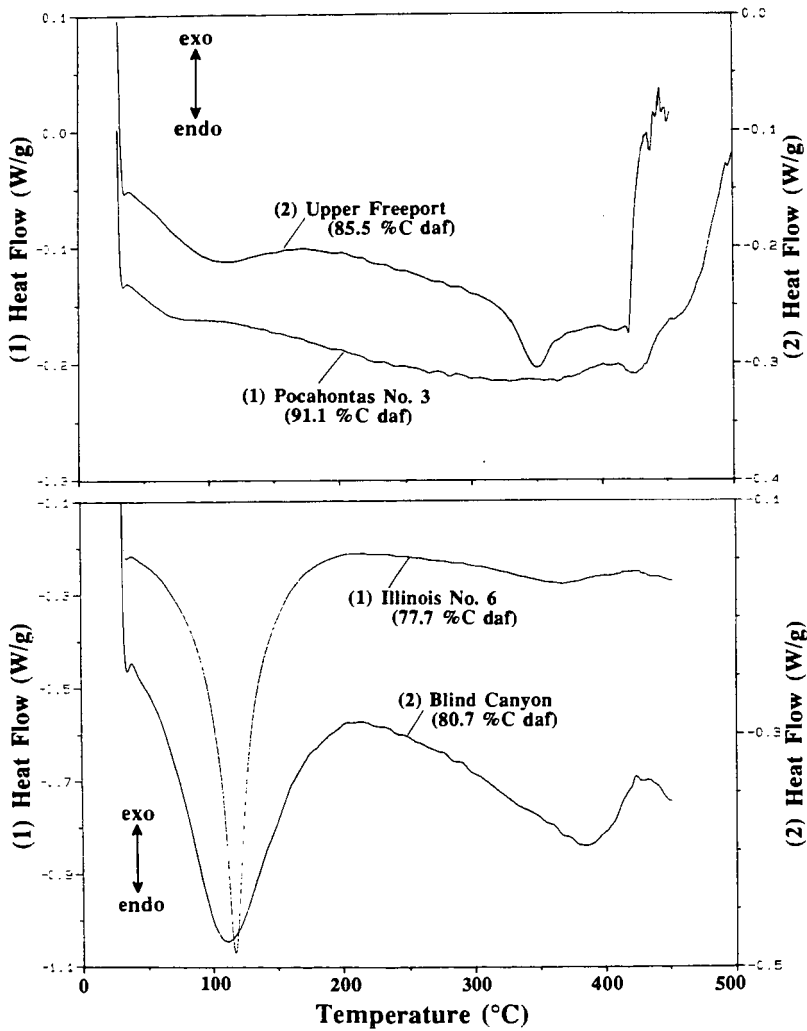


Figure 2. Comparison of DSC thermograms obtained at 8°C/min for different rank bituminous coals.

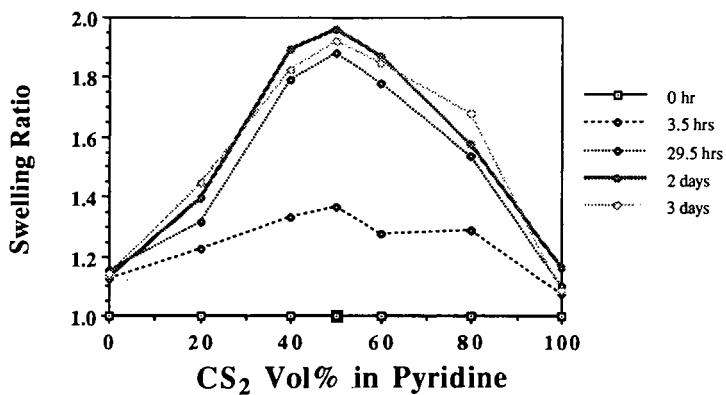


Figure 3. Changes of volumetric swelling ratio by mixed solvents of CS₂ and pyridine for Upper Freeport coal.

Table 3. Solvent Swelling Results for Pocahontas No. 3 Low Volatile Bituminous Coal

<u>Pretreatment</u>	<u>Solvent</u>	<u>Q</u>	<u>Swelling number (x10³)</u>
None	pyridine	1.12	1.48
	CS ₂	1.16	2.65
	THF	1.10	1.23
	CS ₂ /pyridine (1:1 v/v)	1.16	-
CS ₂ swelled	pyridine	1.13	1.61
Heated under N ₂ up to 450°C	THF	1.65	8.01
	pyridine	1.72	8.90

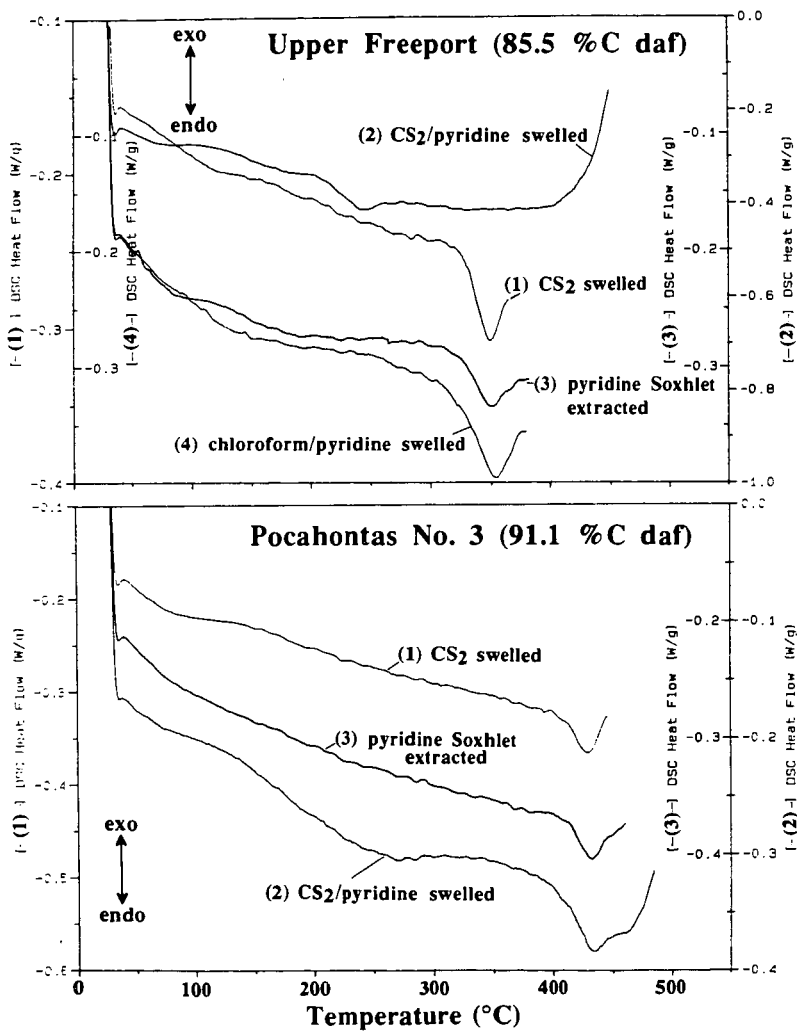


Figure 4. DSC thermograms obtained at 10°C/min for differently pretreated samples, illustrating the relaxed coal structure already at room temperature in CS₂/pyridine (1:1 v/v) swelled Upper Freeport Coal.

THE VISCOELASTIC BEHAVIOR OF SOLVENT-SWOLLEN COAL

George D. Cody, Alan Davis, Semih Eser,
Patrick G. Hatcher, Paul Painter
The Pennsylvania State University
University Park, PA

Keywords: Coal, Macromolecular Structure, Viscoelasticity

Introduction

Under conditions typical of most industrial processes, such as liquefaction, coal is subjected to thermal and pressure-driven stresses. Deformation, diffusion, and chemical reaction all occur simultaneously during liquefaction; in order to optimize process conditions, it is important to understand the nature of such internal processes occurring within coal. Details on the time dependences of such processes could reveal much about the architecture of coal's macromolecular network.

Viscoelasticity is an important time-dependent phenomenon in terms of elucidating aspects of coal's structure. Coal's viscoelastic properties in the glassy state have been measured by numerous researchers¹⁻⁵; under such conditions the measurements only detect deformational mechanisms which are rapid and correlate over a very short contour interval, where the contour describes the spatial arrangement of a macromolecular chain. At higher temperatures ($T > 250^\circ\text{C}$) deformational mechanisms involving larger scale contour relationships become important. It is these larger scale motions which dominate coal's physical response to process conditions. The thermo-mechanical behavior of coals has also been measured; in addition to viscoelastic behavior at elevated temperatures thermal degradation also accompanies the viscoelastic deformation. The presence of such parallel processes greatly hinders interpretation of macromolecular characteristics, i.e. under conditions of thermal degradation the state of the coal's network structure is also time dependent. The optimum experiment would be to characterize coal in a rubbery state at room temperature. Brenner demonstrated that coals immersed in appropriate solvents, such as pyridine, exhibit rubbery characteristics. He subsequently quantified this observation by measuring coal's elastic modulus while in the swollen state⁶; the magnitude of this was shown to lie in the range of stiff rubber. The experiments of Brenner constituted an important step towards characterizing coal's macromolecular structure. This present paper continues the investigation and focuses on a set of simple experiments designed to highlight aspects of the viscoelastic behavior of solvent swollen coals.

Experimental

The experiments described in this presentation involve monitoring creep (i.e. time-dependent strain) under compressive

stress. The two samples used in this study were procured from the Penn State Coal Sample Bank; both coals are high volatile C bituminous in rank from the Illinois No. 6 and the Lower Kittanning seams, respectively. Details on the samples are presented in table 1 under the designation PSOC-1539 and PSOC-1274, samples 1 and 2, respectively. The sample selection and preparation protocol has been described in detail elsewhere⁹. The crucial characteristics of an optimum sample for such studies are 1) that it be homogeneous, i.e. entirely vitrinite, 2) that it be exhaustively extracted in pyridine, and 3) that it be free of cracks. Using the protocol described in reference 9, these ideal characteristics are very closely approached. The instrument employed to measure strain is a microdilatometer also previously described⁹. In brief, vertical displacement of a piston is measured using a linear variable differential transformer (LVDT); the analog signal is sent to a chart recorder so that strain can be continuously monitored. All measurements reported here are made while the sample is immersed in solvent.

Two different experiments were conducted; in the first, a constant compressive stress was applied to the sample, while the resultant strain was measured as a function of time; a standard creep test. In the second, the sample was subjected to a progressively greater stress up to a maximum on the order of 0.6 MPa. Upon reaching the maximum, the stress was progressively reduced. The stress rates in both loading and unloading are on the order of 0.2 MPa/min. To avoid introducing uncertainties in the position of the piston upon complete unloading, it was necessary to unload only to approximately 0.1 MPa before initiating the next stress cycle. The subsequent stress cycle was begun only after the strain recovery rate reached zero.

The precision of the instrument is such that displacements on the order of 0.5 μm are detectable. The compliance of the instrument is very low; at the maximum stress the LVDT recorded a displacement of less than 5 μm , whereas the typical displacement of a swollen coal sample at stress maximum is on the order of 70 μm in the case of the first experiment and on the order of 300 μm in the second.

Results and Discussion

The time dependent compressive strain of solvent-swollen coal while under a constant stress can be separated into three fundamental deformational modes. These have been illustrated schematically in figure 1. The first is an instantaneous (time-independent) element (E_0 in figure 1, which here appears Hookean, but is, in fact, nonlinear, see below). The second mode is a time-dependent, reversible viscoelastic element ($K-V$ in figure 1; signifying that the strain response in this region can be described with a Kelvin-Voigt model). The third mode is a time-dependent, irreversible element (N in figure 1; indicating that strain in this region is largely viscous in nature and thus can be considered as a Newtonian fluid with a coefficient of viscosity, η).

The time-dependent strain behavior of sample 2 is presented in figure 2 (the strain presented in this figure is compressive, strain = $-(\Delta L/L)$). The applied stress is on the order of 0.1 MPa; the instantaneous elastic strain component has been factored out and only the time-dependent deformation is presented. Therefore, the magnitude of the strain is calculated from height of the instantaneously compressed sample. The magnitude of the instantaneous deformation, under a small stress applied in this manner, accounted for approximately 50 percent of the strain. As will be discussed below, however, the instantaneous strain is nonlinear and its contribution to the total strain diminishes with progressively increased stress.

The first part of figure 2 corresponds to viscoelastic deformation which can be described with a generalized Kelvin-Voigt element model (i.e. a model in which elements composed of a Hookean solid spring in parallel with a Newtonian fluid dashpot are arranged in a series). At longer times ($t > 30$ minutes) the deformation is essentially linear and can be modeled using a single Newtonian fluid dashpot. The viscosity of the "fluid" in this case is calculated to be approximately 3×10^8 centipoise.

The behavior of this coal at small strains (figure 2) suggests that linear viscoelastic models could be applied to parameterize sample 2's strain behavior. Investigations at higher stresses, however, indicate that the overall viscoelastic behavior is significantly non-linear. Non-linearity in the instantaneous reversible strain component is demonstrated in figure 3 (sample 1), where the incremental displacement accompanying incremental stress clearly decreases. A noteworthy point is that magnitude of the incremental displacement for a given stress is apparently independent of the other deformational mechanisms.

The viscoelastic behavior of sample 1 with cyclic stress loading is presented in figure 4. In this figure, the strain is presented as the ratio of the height to the original height. Several interesting features are evident. First, there is a progressive shift to greater strains with each subsequent cycle, the result of superposition of viscous irreversible deformation on the reversible viscoelastic deformation. Second, upon compression, the stress-strain slope remains essentially constant, i.e. the time-dependent compliance remains the same for each cycle. Third, the magnitude of energy dissipation evident upon stress reduction is also nearly constant. The implication is that the same retardational strain mechanisms are being utilized upon each cycle. Also, it appears that these modes are independent of the viscous strain superposed on the entire strain process.

Conclusions

Solvent swollen coals, exhibit three apparently independent strain modes. The first is reversible and time-independent; although it exhibits regular reproducible behavior it is nonlinear;

i.e. non-Hookean. The second mode is reversible and time-dependent; it is reproducible, hence predictable. The third strain mode is entirely viscous and appears to be independent of the previous two and is readily treated using a Newtonian fluid model. These results indicate that swollen coal's viscoelastic behavior can be described through a constitutive equation where the individual elements, e.g, Maxwell or Kelvin-Voigt elements, are nonlinear with respect to stress. Coal's viscoelastic behavior, therefore, can be parameterized, e.g. in terms of a retardation spectrum; this has the potential to yield fundamental information on the nature of coal's macromolecular structure.

Acknowledgement

We gratefully acknowledge the financial support of the sponsors of the Penn State Cooperative Program in Coal Research

References

1. Bangham, D. H.; Maggs, F. A. P. *Proceedings of the Conference on Ultra-fine Structure of Coals and Cokes*; British Coal Utilization Research Association: London, 1943.
2. Hiorns, F.J., *Fuel* 1953, 32, 113.
3. Terry, N. B., *Fuel* 1957, 37, 309.
4. van Krevelan, D. W., *Coal*; Elsevier Scientific: New York, 1981.
5. Weller, M.; Wert, C., *J. Appl. Phys.* 1982, 53, 6205.
6. Howell, J. M.; Peppas, N. A., *Fuel* 1987, 66, 810.
7. Brenner, D., *Fuel* 1984, 63, 1324.
8. Brenner, D., *Pre. Pap.-ACS Div. Fuel Chem. Prepr.* 1986, 16.
9. Cody, G. D.; Davis, A.; Esser, S.; Hatcher, P. G., *Pre. Pap.-ACS Div. Fuel Chem. Prepr.* 1991, 1307.

TABLE 1- SAMPLES

<u>SAMPLE</u>	<u>%C*</u>	<u>%H*</u>	<u>%O*</u>	<u>H/C*</u>	<u>O/C*</u>	<u>%R_m**</u>	<u>%Q***</u>
1539 (1)	81.0	5.5	9.4	0.8	0.1	0.58	2.3
1274 (2)	82.1	5.9	8.0	0.9	0.1	0.63	2.1

* DAF basis

** Mean-Max Reflectance in oil

*** Volumetric Swelling Ratio

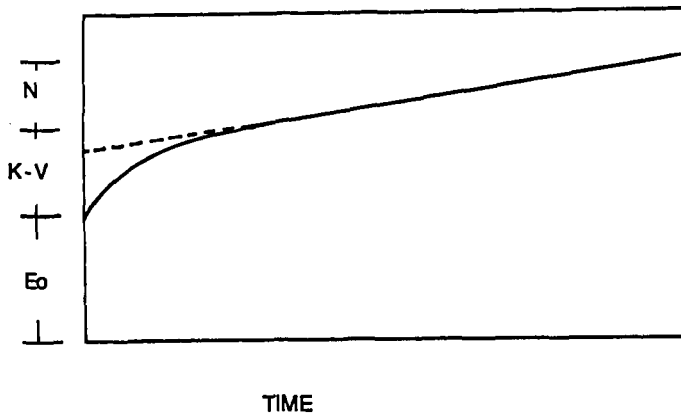


Figure 1: Typical strain vs time curve for a constant applied stress. E_0 = instantaneous elastic strain, K-V = reversible viscoelastic strain, N = irreversible viscous strain.

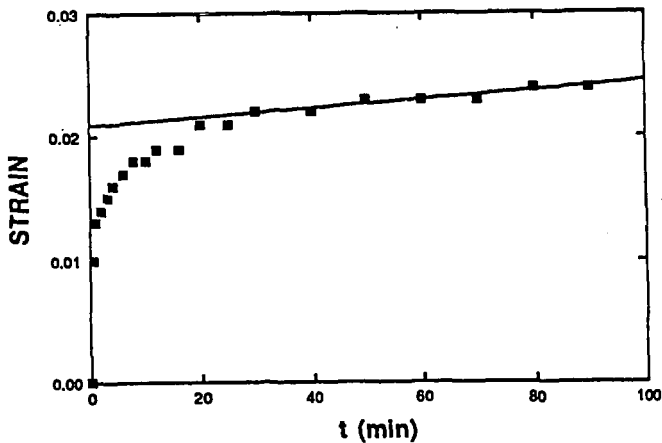


Figure 2: Characteristic Creep curve, sample 2, stress = 0.1 Mpa

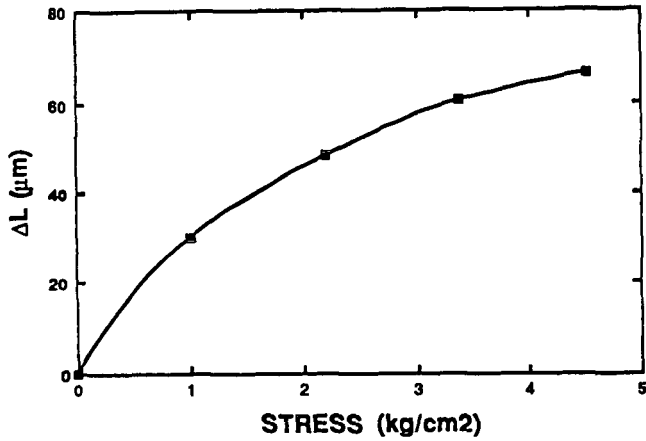


Figure 3: Incremental displacement due to instantaneous strain vs. stress, sample 1.

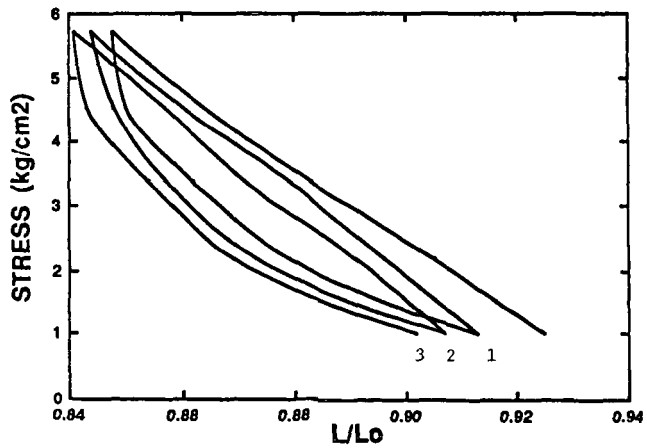


Figure 4: Compressive stress - strain cycles, sample 1. The stress rate is 0.2 Mpa/min

DO GLASS TRANSITIONS REPRESENT GLOBAL CHANGES TO COAL STRUCTURE?

Peter J. Hall and Alexander J. Mackinnon
Department of Pure and Applied Chemistry
University of Strathclyde, Glasgow G1 1XL
SCOTLAND

Key Words: Glass transition, Differential Scanning Calorimetry

Introduction

At room temperature coals are glassy solids. The existence of thermal glass to rubber transitions has been claimed for coals in a number of publications. Typically, coals have glass transition temperature (T_g) in the region of 600K. There is a certain amount of contradictory experimental data published. For example, Green *et al.*¹ have presented data which suggest a second order phase transition at 573K for APCS Illinois #6 which looks like a traditional glass to rubber transition. Conversely, Lucht *et al.*² claim a second order phase transition at 655K for PSOC Illinois #6 in which the specific heat baseline is displaced downwards. It may be claimed that this difference is due to the difference in the origin of the coal but nevertheless, this raises doubts about the reproducibility of these second order phase transitions. The existence of such transitions may be important to coal processing because diffusion rates through rubbery materials are orders of magnitude faster than through the corresponding glass.

The question to be considered here is whether glass transitions represent truly global changes in the viscoelastic properties of coals. In many polymers, which have tend to have much more uniform chemical and physical structures than coal, physical properties such as Young's moduli typically reduce by two orders of magnitude³. Direct measurement of Young's moduli for coals is difficult and unreliable because of the existence of cracks and a well defined bedding plane.

The objective here is to use Differential Scanning Calorimetry (d.s.c.) to investigate thermal and solvent effected glass transitions in coals and, by comparison with another polymer system, determine whether they represent global changes to structure.

The process of quantifying glass transitions will be achieved by interpreting specific

heat (C_p) data in terms of two component Einstein C_p models. It has been shown by Merrick⁴ and Hall and Larsen⁵ that the C_p of coals from ~100K to pyrolysis temperatures can be described by Einstein C_p models that consist of two components. One component comes from easily excited atomic vibrations and has a weighting of 1/3. The second component originates from vibrations that are harder to excite and has a weighting of 2/3. C_p at any temperature, T , is given by:

$$C_p = \left(\frac{R}{a} \right) [1/3 g_1(\Theta_1/T) + 2/3 g_2(\Theta_2/T)] \quad 1$$

where $g(\Theta/T)$ is the Einstein function:

$$g = \frac{\exp(\Theta/T) (\Theta/T)^2}{(\exp(\Theta/T) - 1)^2} \quad 2$$

a is the mean atomic weight and Θ is the Einstein temperature. Equation 1 provides a two component fit to empirical C_p data, Θ_1 and Θ_2 being adjustable parameters. One advantage of Equation 1 is that it explicitly separates the mean atomic weight and the Einstein temperatures Θ . Θ is therefore independent of the chemical structure and provides a basis for comparing chemically different structures.

Hall⁶ has shown that Equation 1 provides a good description for C_p data of a Dioxane Lignin (DL) obtained by Hatakeyama *et al.*⁷. DL is a good model for certain aspects of coal structure because it is a heterogeneous aromatic-based crosslinked polymer. However, it is simpler to understand the structure of DL because there are no analogues to coal macerals, mineral matter contamination or bedding planes. The chemical structure is more uniform than coal. Hall⁶ demonstrated that Θ_2 decreased from 1630K below T_g to 1230K above T_g , a decrease of 400K. This is taken as the bench mark figure for a material that has well-defined glass to rubber transition.

Experimental

A Mettler DSC 30 was used with standard aluminium pans. A detailed experimental procedure has been described previously⁸. The only difference was that C_p errors due to convective heating at low temperatures were minimized by minimizing the volume of the pan and reference chamber using a low temperature lid. Exhaustive calibration meant that temperatures were determined to ± 0.1 K, enthalpies were determined to ± 0.01 J/g. DSC was performed at 10 K/min in a carrier of dry nitrogen.

Coals were obtained from the Argonne Premium Coal Bank. The ultimate analyses from APCS was used for calculating mean atomic weights. The coals were dried in the DSC chamber at 373K until the heat flow indicated that no water remained.

Results and Discussion

A number of coals were tested. Ten separate samples of Illinois #6 were tested. Very slight second order phase transitions were detected in two cases. In three others displacement of the C_p baseline downwards was noted, similar to the observations of Lucht *et al.*² The temperature of these transitions varied between 520K and 630K. In the other experiments there were either no second order phase transitions observed, they were too small or ambiguous. Figure 1 shows a mean of the runs, overall there are no obvious second order phase transitions. The Einstein temperatures for fresh Illinois #6 were calculated to be 380K and 1200K. In the cases where a second order phase transition resembling a glass transition was observed, the reduction in the higher Einstein temperature following a glass transition was 50K. This is much less than the change of 400K calculated for DL⁵. Our conclusions are that if genuine glass to rubber transitions do indeed exist for Illinois #6 then they do not represent global changes to structure. Differences in the behaviour are probably due to sample inhomogeneity.

Pittsburgh #8 presented different problems in the identification of a possible glass to rubber transition. Figure 2 shows a typical d.s.c. result. The dashed lines mark what may be a second order phase transition followed by what may be a slight exotherm. Another interpretation of this is that it may be a first order endotherm caused by some pyrolysis effect. On the basis of the data presented here these possibilities cannot be distinguished. The problem is that the onset of softening in high swelling coals such as Pittsburgh #8 is accompanied by the evolution of tars. This result illustrates the difficulties of using d.s.c. alone to investigate glass transitions.

Two higher rank coals, Upper Freeport and Pocahontas were also investigated. We were not able to find any evidence of glass to rubber transitions for these coals below the onset of pyrolysis.

The only situation in which we were able to produce a significant, reproducible and well defined glass to rubber transition was for Wyodak coal following heat treatment. Figure 3 shows d.s.c. for Wyodak coal dried at 373K. Run 1 is on the dry coal and Run 2 is on the same sample of coal that has been heated to 573K in the d.s.c. and cooled to room temperature. Run 1 shows a well defined endotherm at 478K and a rather broad endotherm at 430K. Run 2 shows a well defined second order phase transition at 380K.

Equation 1 has been used to model the C_p data for Run 2 both below and above the glass transition. There was not enough sample to determine the elemental composition

of the Wyodak following Run 1 and the assumption is made that there is no significant change in the mean atomic weight. This is a reasonable assumption since the weight loss on Run 1 was only 3%. Figure 4 shows that Θ_2 values of 2250K and 1850K give the best fits. In other words, Θ_2 reduces by 400K as a result of the glass transition. This is the same as previously observed for the DL. We therefore conclude that this particular glass transition represents a global change to the Wyodak structure. The reasons for this are a matter for speculation but the following discussion is at least consistent with the experimental results presented here and with what is known about the molecular structure of Wyodak coal. It is known that Wyodak has a large oxygen content and a relatively large concentration of carboxylic acid groups. The first order phase transitions in Run 1 could be caused by the dissociation of these groups. The fact that they are very much reduced in Run 2 suggests some chemical change, rather than a melting phenomenon. In the original coal these acid groups would give rise to hydrogen bonding in the coal macromolecule. When they are removed the coal may become effectively less heavily crosslinked and therefore has a well defined glass to rubber transition.

References

- 1 T.K. Green, T.K.; Pan, W-P; Clark M.A. *ACS Fuel Div Preprints*, **1991** 36(2), 814.
- 2 Lucht, L.M.; Larson, J.M.; Peppas, N.A. *Energy and Fuels*, **1987**, 1, 56.
- 3 Billmeyer, F.W. *Text Book of Polymer Science*, Wiley, New York, 1966.
- 4 Merrick, D *Fuel*, **1983**, 62, 540.
- 5 Hall, P.J.; Larsen, J.W. submitted to *Energy and Fuels*, **1992**.
- 6 Hall, P.J. in press, *Polymer Communications*, **1992**.
- 7 Hatakeyama, H.; Nakamura, K.; Hatakeyama, H, *Polymer*, **1982**, 23, 1801.
- 8 Hall, P.J.; Larsen J.W. *Energy and Fuels*, **1991**, 5, 228.

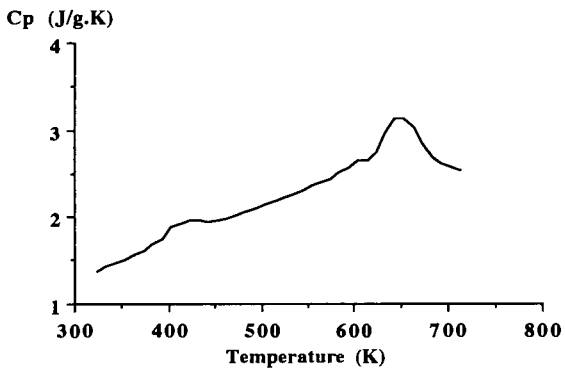


Figure 1: DSC at 10K/min for dry Illinois #6 coal.

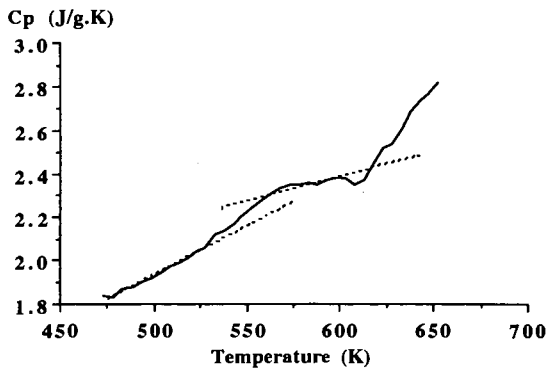


Figure 2: DSC at 10K/min for dry Pittsburgh #8 coal.

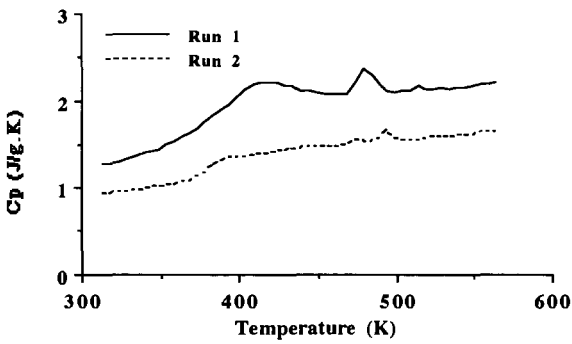


Figure 3: DSC at 10 K/min for dry Wyodak coal and a re-run of the same sample.

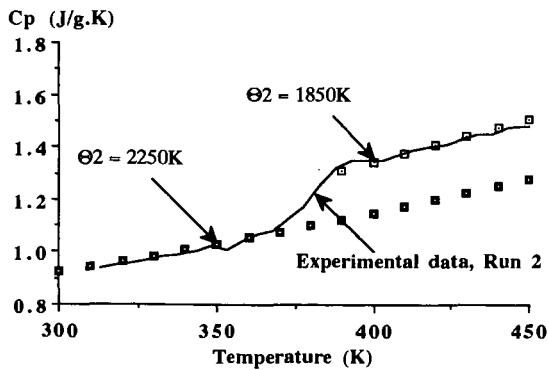


Figure 4: DSC at 10 K/min for Wyodak coal heated to 573K then cooled to room temperature together with two-component Einstein C_p theory fits to the experimental data below and above the glass transition.

THE ASSOCIATED MOLECULAR NATURE OF BITUMINOUS COAL

Masaharu Nishioka

BCR National Laboratory, 500 William Pitt Way, Pittsburgh, PA 15238

Keywords: coal structure, association, intermolecular interactions

INTRODUCTION

Coal is a complex mixture of organic material and inorganic components. Detailed characterization of the organic material is still impossible, even when using today's highly developed sophisticated analytical techniques. This is primarily due to the amorphous nature of high-molecular-mass mixtures. The understanding of the physical structure of these materials is an important step in the study of coal structure. The extent to which coal molecules may be (A) covalently cross-linked and/or (B) physically associated is illustrated in Figure 1.

A cross-linked, three-dimensional macromolecular model (Model A) has been widely accepted as a model of the organic material, with this framework occluding some solvent-extractable components. It is, however, this author's opinion that the evidence is indirect and there is little information to elucidate the real state of the physical structure of coal.

Intra- and intermolecular (secondary) interactions play an important role in Model B, but differentiation between covalent bonds and the strong secondary interactions has not been thoroughly studied. Our recent work (1-6) demonstrated the significance and importance of relatively strong secondary interactions in all ranks of coal. Therefore, the conventional coal structural Model A needs to be reinvestigated.

In this paper, our recent results will be summarized and investigated along with the relating past work. From this analysis, it is reasonable to deduce that significant portions (far more than generally believed) of coal molecules are physically associated.

EXPERIMENTAL

Most of the experimental procedures have been already reported in the previous papers (1-7). The followings are some of these outlines. American Chemical Society reagents and h.p.l.c.-grade solvents were used without purification. Coal samples were obtained from the Premium Sample Program at Argonne National Laboratory (8), the Pennsylvania State University Coal Bank and Exxon Research and Engineering Co.

Approximately 5 g of coal was placed in 100 ml of solvent in a 250 ml flask or a 300 ml autoclave and magnetically stirred under nitrogen. The mixture was either stirred at room temperature, heated, or mildly refluxed in an oil bath or in an autoclave heater. The cooled mixture was dried using a rotary evaporator, mixed with methanol, and filtered, while being rinsed with methanol several times. The coal was dried in a vacuum oven at 95°C overnight.

The experimental procedure of coal swelling is based on the earlier reported method (9,10). The measurements were performed in the disposable Wintrobe Tubes (Fisher Scientific) of 3 mm inner diameter and 115 mm in length with graduations in 1 mm divisions. After placing three weighed coal samples into the tubes, these tubes were centrifuged for 5 min (at 3600 rpm in a 30 cm diameter horizontal rotor). Bulk density of each coal under the condition was determined by the average height centrifuged. Each initial height before solvent swelling was calculated from weight of samples by using the bulk density. This is tedious compared to the conventional procedure but essential

to obtain reproducible results particularly at low coal concentration. Solvent was added to each weighed sample after measuring its volume, and the content was vigorously stirred with a thin rod. The tubes were centrifuged for 5 min at 3600 rpm. The volumetric swelling ratio (Q) was calculated by the difference between these heights of samples (9,10). Separate samples were employed for determining the extents of swelling as a function of time and coal concentration.

RESULTS AND DISCUSSION

Solvent extractability

There is a long history, over a century, of coal-solvent extraction. Only a small fraction of most coals is extractable in organic solvents. This amount may reach 20-30 wt%, and it has been thought that this limited solubility or extractability is consistent with Model A. Hydrogen bonds have been primarily considered in addition to relatively weak van der Waals' forces and they are assumed to be broken with one of the best solvents, pyridine (11,12). Caution, however, is advised against the limited extractability of coal, because it seems that the limited extractability originates from the disregard of various relatively strong secondary interactions caused by polyfunctional groups in coal.

The variety of relatively strong secondary interactions are present and their abundances are highly rank-dependent because of the dependence of the abundance of diverse functional groups on coal rank (1,4,6). It was estimated (1,4,6) that the Coulombic force is predominant in lower-rank coal due to ionized groups, that charge-transfer complexes involving non-ionizable but transferable electrons are important in medium-rank coal, and that dispersion forces involving polarizable π -electrons in polycyclic aromatics (π - π interactions) are major contributors in higher-rank coal.

Any single solvent does not appear to be able to disrupt all of these relatively strong secondary interactions and allow an efficient single step extraction. Macromolecules with relatively strong secondary interactions co-operatively interact (13). The co-operativity may make solubilization of coal more difficult. Therefore, another extraction procedure appropriate for coal needs to be explored.

A multistep sequence was proposed with the aim of minimizing various interactions step by step in the recent papers (6). Each step was selected to minimize the possibility of cleaving covalent bonds. Detailed mass balances and additional experiments to investigate the breaking of different secondary interactions were shown in the paper (6).

Each step to break or solvate relative strong secondary interactions has to be selected according to ranks of coals because of the rank dependence of the abundance of these interactions. The concept of this rank dependence may be represented as shown in Figure 2. For subbituminous coal, ionic forces and then charge-transfer interactions should be solvated step by step in addition to hydrogen bonds. For high-volatile bituminous coal, the solvation of π - π interactions would be important after breaking charge-transfer interactions.

The pyridine extraction yields for Argonne Premium coal samples by single step and multistep procedures were compared (6). Total extraction yields of 38-73 wt% (daf) were obtained by using multistep extractions except for low-volatile bituminous coal. These procedures are tedious but straightforward, and the extractabilities are much larger than those obtained by using the conventional extraction. Other results of high extractability using different methods has been available for selected ranks of coal (14-17).

Above results indicate that coal is extractable to a large extent if

various relatively strong secondary interactions are properly weakened. Therefore, limited extractability using a single step with an individual solvent may give a misleading information about coal structure. It is not logical to deduce any concept from the values.

Associative equilibria

If the relatively strong secondary interactions or physical associations are significant in coal, associative equilibria of coal should be observed in solvents. The associative equilibria, however, have not been fully appreciated for the system of coal and solvent regardless of such numerous observations for polymer solutions.

The solvent-induced association has been observed and interpreted as associative equilibria (1,2). Self-associations of high-volatile bituminous coal and its pyridine extract is induced by the solvent soaking. Heating or immersing these materials in poor solvents or in good solvents, followed by the removal of good solvents (the solvent treatment), caused decreases in their pyridine extractability. Any significant chemical reaction during the solvent treatment was experimentally ruled out.

Other associative equilibria were seen as changes in precipitation of extract solutions and molecular weight at different temperatures (3). It was observed that such associative equilibria are highly rank-dependent. This resulted in remarkable differences in extraction rate, effect of preheating on extraction and effect of solvent-soaking on extraction for A region (< ca. 87 % C), B region (ca. 87 to 90 % C) and C region (> ca. 90 % C) coals (3). This coincides with the significant rank dependence of types and abundances of relatively strong secondary interactions in coal considered for multistep extractions in the previous section.

From the above discussion, relatively strong secondary interactions exist in coal, and coal components (or molecules) equilibrate between association and dissociation due to these interactions even in good solvents such as pyridine. So, differentiation between chemical bonds and strong secondary interactions should be considered, although the quantitative assessment of their abundances is very difficult. Because of the presence of relatively strong secondary interactions, it is suggested that apparent networks experimentally observed, which have been often regarded as representing Model A, are much deviated from the phantom (real) networks, if any.

Solvent swelling

The behaviour of solvent(-induced) swelling without complete dissolution in any organic solvent has been often referred to the evidence for Model A. Sanada and Honda (18) applied the statistical theory of rubber elasticity to coal in order to estimate the average molecular weight between cross-links. Since then, solvent swelling has been used to characterize the macromolecular nature of coal by many workers (19,20). The author critiques this line of evidence for Model A on the grounds that coal swelling is not reversible and highly dependent upon coal concentration. Although a series of full papers will be reported elsewhere (21), some of recent results on these issues are shown.

1 Irreversibility of solvent swelling. Distinctively different physical phenomena have been observed in a solvent between the A and B region coals (3). Accordingly, pyridine swellings of Illinois no. 6 (IL: the A region) and Upper Freeport (UF: the B region coal) were compared. The swelling ratio Q at room temperature is very small as seen by UF-1 in Table 1, whereas the Q value at 70°C is larger and increased with time (UF-2). If the pyridine swelling is

mainly due to cross-linked covalent bonds in the coal, the significantly different Q between the two temperatures cannot be explained by elastic swelling. The result can be rationalized due to more disruption of secondary interactions at high temperature (70°C) (3).

The UF coal once swollen in pyridine, followed by the removal of pyridine, gave nearly the same Q value (UF-3) and pyridine extractability (3) as the raw coal. However, decreases in the Q value (IL-1 and 2 in Table 1) and extractability (3) were observed for the IL coal by the swelling/deswelling procedure.

Thermally induced dissociation which is significant for the B region coal was observed for UF-2 as shown above. However, if pyridine is removed from the B region coal after thermally induced dissociation by refluxing in pyridine, relatively strong association may occur as seen for the A region coal (3). The UF coal was refluxed in pyridine for 3 days, followed by the removal of pyridine, and then the swelling ratio Q of this sample was measured at room temperature (UF-4) and 70°C (UF-5). Both Q values at room temperature and 70°C of the sample were nearly equal to that of the raw coal. It is noted that an increase in the Q value was not observed at 70°C .

If pyridine solubles is removed from the coal after thermally induced dissociation, the coal may increase solvent swelling even when the coal was dried, because the solubles do not associate back with the residue. In fact, the swelling ratio Q of the pyridine extracted UF coal (PI) (UF-6) was larger than that of the raw coal. This is also notable, because PI of the IL coal (IL-3) showed the smaller Q value than the raw coal.

Therefore, solvent swelling is irreversible for the IL and the UF coals. The irreversibility is quite different between the IL and the UF coals. These distinctive differences are consistent with different physical phenomena between these ranks of coals discussed above.

2 Dependence of coal concentration on solvent swelling. The change in associative equilibria for residue may be detected by the dependence of coal concentration on solvent swelling. Therefore, swelling ratios of various coals and their PI were measured at various coal to solvent weight ratios (C/S) in room temperature pyridine.

The results for PSOC-1491 coal (high-volatile C bituminous coal) are summarized in this section. Swelling ratios of the raw coal and its PI versus C/S values are shown in Figure 3. In both cases, swelling ratios are highly dependent on coal concentration.

Most of Q by the volumetric method have been obtained at the large C/S value, and these Q can be regarded as the saturated value (Q_{∞}) (9,10). A gravimetric (18) and a piston type (22) of measurements are under the condition of the quite large C/S value without agitation. Therefore, these methods must also give the saturated swelling ratios. Because of the small dependence of concentration on solvent swelling at the larger C/S value, the conventionally obtained Q should be approximately reproducible regardless of C/S. However, caution should be exercised when coal structure is investigated by using these Q_{∞} , because the Q_{∞} are apparent values.

If soluble material during coal swelling significantly affect solvent activity and change solvent swelling, swelling of coal and residue must be significantly different against the C/S value. However, the results (Figure 3) show the approximately same dependence on sample concentration. The effect of solubles on solvent swelling was further examined. The PI from the PSOC-1491 coal was mixed with its PS, and their pyridine swelling ratios were measured at various mixing ratios at the C/S value of 0.2.

It was found that the swelling ratio Q of the mixture containing solubles

is simply determined by the additive of swelling of each fraction. As PS cannot completely dissolve in room temperature pyridine at the C/S value of 0.2, the undissolved PS behaves like residue and is swollen with pyridine. No significant effect of solubles in the solvent on the solvent activity was observed.

From these results, the dependence of coal concentration on solvent swelling indicates that secondary interactions are solvated more at lower concentration, associated coal dissociates more, and coal is swollen more.

A mono- or two-phase model?

It has been proposed that coal is composed of a macromolecular network (immobile phase) with relatively small molecules (mobile phase) occluded in the macromolecular network. This idea was recently described as the so-called two-phase model (23,24). The essence of this model states that only some portions (ca. 10-20%) of the mobile phase can be extracted using the regular extraction procedures because of restricted orifice sizes of the immobile phase. The two-phase model is readily compatible with Model A. However, there is no direct evidence to prove the two-phase model as reviewed in a recent paper (7). The problem is that no work has differentiated (a) between the extent of covalent bonds and physical associations, and (b) between the disruption of covalent bonds and physical dissociations.

The proposed two-phase model has been studied by two different approaches (7,25). Since major portions (70-90%) of high-volatile bituminous coal can be extracted with THF after heating (350°C) in *n*-butylamine (26), the physically trapped mobile phase should be released in the extract. The Illinois no. 6 coal extract from this treatment was further pyrolyzed, and typical mobile phase compounds were semi-quantitated in these samples (7). Although the detailed solvation mechanism in *n*-butylamine is not clear, the differences in amounts of such compounds between the original extract and further pyrolyzed samples are unequivocally due to degradation of chemical bonds. As the results showed, typical mobile phase molecules such as *n*-alkanes and polycyclic aromatic hydrocarbons were not released during the *n*-butylamine treatment, but were released by the thermal degradation of coal macromolecules. From this result, it was concluded that the two-phase model is not applicable for high-volatile Illinois bituminous coal. This work and another work (25) showed that *n*-alkanes, alkylbenzenes, alkyl-naphthalenes, phenanthrene, and alkyl hydroaromatic pentacyclic triterpanes, which were regarded as the mobile phase, are important partial constituents of coal molecules regardless of molecular mass.

Consequently, coal can be regarded as a monophase rather than the two-phase model. The monophase model is more consistent with Model B rather than Model A.

CONCLUSION

On the basis of the preceding discussion, it can be suggested that the three major indications of Model A: (a) limited solvent extractability, (b) reversible solvent swelling and (c) the present concept of the two-phase model, are not entirely persuasive. It is reasonable to deduce from various results shown above that significant portions (far more than generally believed) of coal molecules are physically associated.

REFERENCES

- 1 Nishioka, M. and Larsen, J. W. Energy & Fuels 1990, 4, 100
- 2 Nishioka, M. and Larsen, J. W. Prepr. Am. Chem. Soc. Div. Fuel Chem. 1990, 35(2), 319
- 3 Nishioka, M. Energy & Fuels 1991, 5, 487
- 4 Nishioka, M., Gebhard, L. A. and Silbernagel, B. G. Fuel 1991, 70, 341
- 5 Nishioka, M. Energy & Fuels 1991, 5, 523
- 6 Nishioka, M. Fuel 1991, 70, 1413
- 7 Nishioka, M. and Gorbaty, M. L. Energy & Fuels 1990, 4, 70
- 8 Vorres, K. S. Energy & Fuels 1990, 4, 420
- 9 Green, T. K., Kovac, J. and Larsen J. W. Fuel 1984, 63, 935
- 10 Otake, Y. and Suuberg, E. M. Fuel 1989, 68, 1609
- 11 Larsen, J. W. and Baskar A. J. Energy & Fuels 1987, 1, 230
- 12 Painter, P. C., Sobkowiak, M. and Youtcheff, H. Fuel 1987, 66, 973
- 13 Tsuchida, E. and Abe, K. Adv. Polym. Sci. 1982, 45, 77
- 14 Iino, M., Takanohashi, T., Ohsuga, H. et al. Fuel 1988, 67, 1639
- 15 Mallya, N. and Stock, L. M. Fuel 1986, 65, 736
- 16 Miyake, M. and Stock, L. M. Energy & Fuels 1988, 2, 815
- 17 Chatterjee, L., Miyake, M. and Stock, L. M. Energy & Fuels 1990, 4, 242
- 18 Sanada, Y. and Honda, H. Fuel 1966, 45, 295
- 19 Larsen, J. W. and Kovac, J. in 'Organic Chemistry of Coal' (Ed. J. W. Larsen), American Chemical Society, Washington, DC, 1978, Ch. 2
- 20 Lucht, L. M. and Peppas, N. A. in 'New Approaches in Coal Chemistry' (Eds. B. D. Blaustein, B. C. Bochrath and F. Friedman), American Chemical Society, Washington, DC, 1981, Ch. 3
- 21 Nishioka, M. to be published
- 22 Aida, T and Squires, T. G. Am. Chem. Soc. Div. Fuel Chem. Prepr. 1985, 30(1), 95
- 23 Given, P. H. in 'Coal Science Vol. 3' (Eds. M. L. Gorbaty, J. W. Larsen and I. Wender), Academic Press, New York, 1984, pp. 63-252
- 24 Given, P. H., Marzec, A., Barton, W. A. et al. Fuel 1986, 65, 155
- 25 Nishioka, M. and Larsen, J. W. Energy & Fuels 1988, 2, 351
- 26 Tagaya, H., Sugai, J., Onuki, M. et al. Energy & Fuels 1987, 1, 397

Table 1 Swelling ratio (Q) in pyridine of UF and IL coals at room temperature (r.t.) and 70°C (21) (coal/solvent wt ratio: 0.20-0.25)

Code	Sample	0	2h	4h	8h	16h	24h	48h	72h
UF-1	Raw coal (r.t.)	1.2	1.1	1.1			1.2	1.1	1.1
UF-2	Raw coal (70°C)	1.2	1.2	1.4	1.7	1.8	2.2		
UF-3	Coal swollen in pyridine followed by drying (r.t.)	1.0					1.0	1.1	1.1
IL-1	Raw coal (r.t.)	2.3	2.1	2.2	2.1	2.3	2.2	2.3	2.2
IL-2	Coal swollen in pyridine followed by drying (r.t.)	2.0	2.0	2.0	2.0		2.0	2.0	
UF-4	Coal refluxed in pyridine followed by drying (r.t.)	1.0					1.1	1.0	
UF-5	Coal refluxed in pyridine followed by drying (70°C)		1.0	1.1	1.0	1.1	1.1	1.1	
UF-6	Pyridine extracted coal (r.t.)	1.4					1.4	1.3	
IL-3	Pyridine extracted coal (r.t.)	2.0	2.0				2.1	2.0	

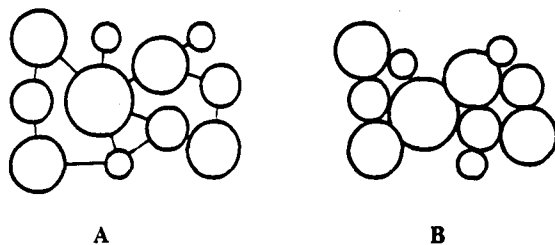


Figure 1 (A) Covalently cross-linked and (B) physically associated models of coal structure

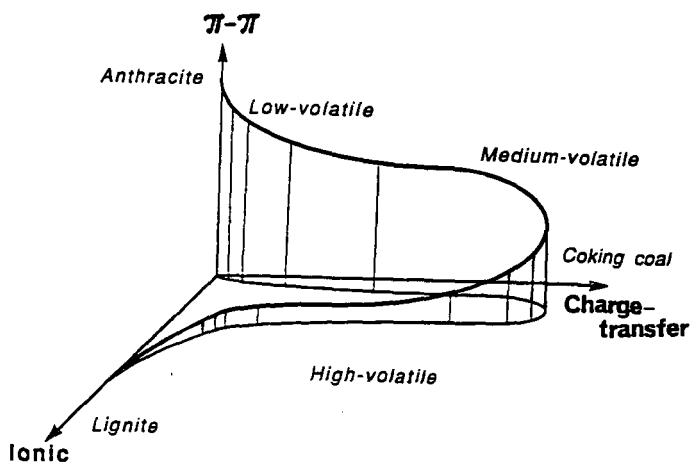


Figure 2 Proposed dependence of relatively strong intra- and intermolecular interactions on coal rank

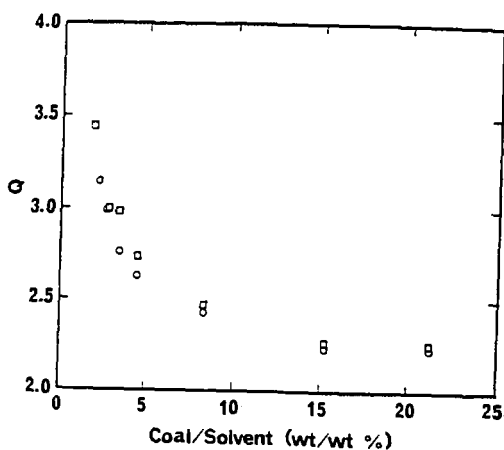


Figure 3 Swelling ratios (Q) in pyridine of PSOC-1491 native (\square) and its pyridine extracted (\circ) coals as a function of coal/solvent wt% (21)

A THREE DIMENSIONAL STRUCTURAL MODEL FOR VITRINITE FROM HIGH VOLATILE BITUMINOUS COAL

Patrick G. Hatcher, Jean-Loup Faulon, Kurt A. Wenzel
and
George D. Cody

Fuel Science Program
The Pennsylvania State University
University Park, PA 16802

Keywords: vitrinite, coal structure, molecular modeling

Introduction

In recent years, several models have been proposed for the chemical structure of coal (1-4). Some of these models have been visualized in three dimensions by use of computer graphics (5). The models have been constructed by considering elemental, spectroscopic, and pyrolysis/gas chromatography/mass spectrometry data. While the models have provided a visual framework for evaluating the kinds of structural elements that are contained in coal macromolecules, they fail to depict the chemical heterogeneity that exists in coal due to the many varied macerals. Developing structural models for individual macerals such as vitrinite would limit some of the heterogeneity, but vitrinite, a petrographically defined component, can also have a heterogeneous composition. There are numerous petrographic forms of vitrinite.

The approach towards defining a more homogeneous maceral component of coal used in our laboratory is one which has focused on coalified wood as a representative for vitrinite derived from xylem in ancient trees (6-9). Structural models were developed from a lignin template, because lignin has been determined to be the major source of chemical structures in coalified wood. By examining the chemistry of series of woods from peat to coalified woods from ancient rocks and seams, we have been able to discern changes in the lignin framework induced by coalification to the rank of subbituminous coal. The models were then developed by applying the observed changes to the lignin template. The model for lignin was that proposed by Adler (10).

Detailed examination of coalified wood samples of higher rank, high-volatile bituminous coal, have allowed us to extend the model to this rank range. This paper presents the data and the model for vitrinite from coalified wood of high volatile C bituminous coal rank. The model is constructed from elemental, solid-state ^{13}C NMR, and flash pyrolysis/gas chromatography/mass spectrometric data.

Methodology

The sample is a fossil stem which was recovered from a lacustrine shale from the Midland Formation (Triassic) near Culpeper, Virginia. Elemental and ^{13}C NMR data for this sample have been previously published, but are here reevaluated for purposes of developing a structural model. Flash pyrolysis/gas chromatography/mass spectrometry was employed in a manner analogous to that described previously (6). Pyrolysis products were quantified by integrating the total ion chromatogram (TIC), assuming equivalent response factors for individual components, and normalizing the concentrations to the total peak area for all peaks in the pyrogram.

The solid-state ^{13}C NMR data were obtained by both the method of cross polarization with magic angle spinning (CPMAS) and by a Bloch decay. The CPMAS conditions were similar to those described previously (7). The cycle time for the Bloch decay was 45 sec. Both NMR data

sets were transferred to a PC computer format and the peaks were deconvoluted by Lab Calc software available from Galactica Industries, Inc.

Results

The elemental and NMR data for the coalified wood sample are shown in Table 1. The carbon content of 85.5% and a vitrinite reflectance value of 0.6 (N. Bostick, personal communication) indicate that the rank of this sample is equivalent to high volatile C bituminous coal. The oxygen content of 5.9%, measured by direct analysis (7), is significantly lower than oxygen contents (13.9%) of coalified logs of subbituminous rank (7). A significant amount of nitrogen, 2.2%, is also observed.

Comparison of the NMR data obtained by CPMAS and by Bloch decay indicates that the two methods yield virtually identical spectra (Figure 1). The Bloch decay does show greater aromaticity and possibly a higher yield of phenolic carbon (Table 1). In both spectra the broad peaks for aromatic (100 - 160 ppm) and aliphatic (0-60 ppm) carbons dominate. Discernible shoulders at 140 and 153 ppm are observed in the aromatic carbon region, and these can be assigned to aromatic bridgehead or nonprotonated aromatic carbons and phenolic carbons, respectively. With a ratio of aryl-O to total aromatic carbon of about 0.12, it appears that nearly all aromatic rings have at least one phenolic OH or aryl ether carbon. The aliphatic carbon region also exhibits fine structure with a distinct peak at 17 ppm which can be assigned to methyl carbons. Dipolar dephasing studies confirm that this peak is that of methyl carbons (7). Deconvolution of the aliphatic region shows that approximately one third of the aliphatic carbons are methyl carbons. Due to insufficient spinning speeds of the sample rotor, spinning sidebands are observed at 260 and 0 ppm.

Flash pyrolysis data for the coalified wood sample are shown in Figure 2 and the peaks are identified and quantified in Table 2. Phenol and alkylphenols are the most readily visible pyrolysis products. Of these, the three cresol isomers, 4-ethylphenol, and 2,4 dimethylphenol predominate. Other isomers of C₂-phenols are apparently minor or trace components. Only 4 isomers of C₃-phenols predominate, trimethyl phenol, 2 isomers of ethyl, methyl phenols, and propylphenol. The specific substitution sites have yet to be discerned. As a whole, the phenols account for approximately 60% of the aromatic pyrolysis products and 40% of the total pyrolyzates. Benzene and alkylbenzenes are the second most prominent components, accounting for about 11% of the pyrolyzates. C₁, C₂, and C₃ benzenes with undetermined substitution patterns comprise the prominent components eluting in the 0-10 min retention time window.

Other pyrolysis products which account for numerous other peaks in the pyrogram are naphthalenes, alkylidibenzofurans, and n-alkane/n-alkene pairs. C₁, C₂, and C₃ alkyl naphthalenes are present as various, as yet undetermined isomers. The n-alkane/n-alkene pairs show a range of carbon numbers ranging from C₆ to C₂₂. The lower molecular weight homologs predominate and the distribution tapers off with increasing carbon number. Quantitatively, the n-alkanes/n-alkenes contribute to 33% of the pyrolyzate, a rather large percentage as a whole. At higher retention times in the pyrogram, peaks for alkylidibenzofurans are found. These contribute to only 3.5% of the pyrolyzate and 5.2% of the aromatic products.

Discussion

The quantitative information on carbon types afforded by the NMR data and the molecular-level information supplied by the flash pyrolysis data provide sufficient detail to allow construction of a molecular model from a lignin template. It is clear that the original lignin structures have been modified by coalification because the coalified wood does not show any characteristics of the lignin-derived methoxy phenol structures. Previous studies (8,9) have suggested that lignin undergoes a series of coalification reactions that include 1) B-O-4 aryl-ether cleavage, 2) demethylation to form catechol-like structures, 3) dehydroxylation of the 3-carbon side chain, and 4) dehydroxylation of catechols to form phenols. In this previous study, a structural model was developed for ranks of brown coal, lignite, and subbituminous coal, using the lignin template published by Adler (10), and modifying the aromatic structures according to the coalification reactions observed for each rank level.

It is a logical progression to take the model developed in this prior study for subbituminous coal and to alter it in a way which would reflect the changes in chemistry observed between the high volatile C coal in the present study and the subbituminous coal in the previous study whose elemental and NMR data are shown in Table 1. The major changes between the two coalified woods in going towards higher rank include 1) a decrease in oxygen content from 13.9% to 5.9% with a corresponding increase in carbon content and 2) a significant increase in benzene and alkylbenzenes in pyrolyzates. Interestingly, the carbon aromaticity does not change greatly, but the fraction of aryl-O carbon to total aromatic carbon decreases by about half. This and the significant loss of oxygen from the elemental data would imply that the primary transformation of the catechol and alkylphenolic structures in subbituminous coal is a loss of aryl-O -containing structures and a condensation of the phenols to diaryl ethers.

While tracing a template through coalification is certainly a valid approach, we have begun to investigate other approaches to molecular modeling, using primarily computer methods that have recently been described (11, 12). Using a molecular modeling software similar to the one developed by Faulon et al. (12), we have generated two models, one which will be described in this paper and the other to be described by Faulon et al. (13). The model generated here provides a three dimensional graphical display of a structure constructed from a lignin framework. Briefly, the input to the model is the quantitative NMR information and the elemental data. The pyrolysis data is not used in a quantitative sense but rather a qualitative sense to input structures found that relate to lignin structural units. The lignin skeletons and inferred bonding sites are deduced from the pyrolysis data and from the previous studies on the coalification of wood showing the reactions of the various functional groups associated with lignin. For example, it is clear that the presence of 2,4 dimethylphenol in pyrolyzates indicates a lignin-derived phenol where the attachments to other structural entities are at the 2 and 4 positions. Indeed, the three-carbon side chain of lignin is in the C-4 position and a significant number of lignin units are also linked at C-2. From previous studies of coalified woods of low rank, we have deduced that the methoxy group is lost and that the three-carbon side chain is reduced to a propenyl group.

From a practical point of view, to verify the correlation between the lignin and our structure, three molecular fragments were introduced in the computerized model: propylbenzene, 4-propylphenol, and dipropylphenol. These fragments were built and stored in a library using the molecular modeling software PCMODEL (Serena software). Then, our program was asked to generate a structure containing these fragments by taking account of all analytical data. This operation was realized in two steps. First, the program computed the correct amount of fragments and connections between fragments to obtain a structure consistent with ^{13}C NMR and elemental analysis. The model of lignin used as template in our previous publication (9) contains 115 carbon atoms, therefore we asked the program to find all the solutions between 95 and 135 carbon atoms. The best solution found is $\text{C}_{113}\text{H}_{105}\text{O}_5$ and is composed of 3 propylbenzenes, 2 propylphenols, and 2 dipropylphenols. The connections between these fragments are the following: 4 biphenyl bonds, 5 benzylphenyl ether bonds, 8 bibenzyl bonds, 3 biphenylpropane bonds, and one biphenylethane bond. In a second step, from the previous list of fragments and bonds, the program was run to generate automatically a 3D structure. The program estimated first the number of structures which can be generated. The number found was too big to build all of them, therefore one structure was chosen randomly and constructed in 3D space.

Figure 3 shows a two-dimensional projection of the 3D model built by the program. There are some important features of this model that need explanation. It is important to highlight the fact that this displayed model is only one of numerous possible models that the program has calculated, and as such should be viewed as only an example whose chemistry is consistent with the chemical information provided to the program. Note that all aryl-O carbons are phenolic ethers and that the structure is composed of principally one- and two-ring aromatic systems. Also, the presence of dibenzofurans is a characteristic feature that is consistent with the pyrolysis data. In fact, the entire structure can be visualized as providing pyrolysis fragments which match rather well with the distribution of aromatic pyrolysis products. What is conspicuously absent is the presence of long-chain aliphatic structures which could give rise to the n-alkane/n-alkene pairs observed in

pyrolysis. We feel that these components are minor components of the coalified wood and are not derived from lignin structural units. It is likely that they were incorporated into the coal from either external materials migrating into the sample or from microbial remains present within the wood as it decomposed and was later coalified. It is also likely that the flash pyrolysis accentuates these substances because they are more readily pyrolysed in comparison with the lignin-derived materials. Also absent are the nitrogen-containing structures. Elemental data for this sample shows about 2% nitrogen (8). We do not have any data concerning the types of nitrogen-containing structures that might be present in this sample. Thus, we choose to omit these structures until which time we might have enough information to include them.

The three dimensional display is not readily visualized in two dimensions, but examination of the structure in Figure 3 shows the connecting points which imply that the structure is three-dimensional. The visualization of the structure in three dimensions is important from the standpoint that we must visualize coal reactivity as a three dimensional phenomenon. The ability to utilize sophisticated computer graphics displays adds to our ability to eventually utilize such structures for the prediction of coal reactivity.

Literature Cited

1. Given, P. H., *Fuel*, **39**, 147, 1960.
2. Wisner, W. H., *Proc. of the Electric Power Research Institute Conf. on Coal Catalysis*, 1973.
3. Solomon, P.R., in *New Approaches in Coal Chemistry*, Am. Chem. Soc. Symp. Series No. **169**, 61, 1981.
4. Shinn, J. H., *Fuel*, **63**, 1187, 1981.
5. Carlson, G. A., and Granoff, B., in *Coal Science II*, Advances in Coal Sciences series **461**, 159, 1990.
6. Hatcher, P.G., Lerch, H.E., III, Kotra, R.K., and Verheyen, T.V., *Fuel*, **67**, 1069, 1988.
7. Hatcher, P.G., *Energy and Fuels*, **2**, 48, 1988.
8. Hatcher, P.G., Lerch, H.E., III, and Verheyen, T.V., *Int. J. Coal Geol.*, **13**, 65, 1989.
9. Hatcher, P. G., *Organic Geochemistry*, **16**, 959, 1990.
10. Adler, E., *Wood Sci. Technol.* **11**, 69, 1977.
11. Faulon, J. L., *Prediction Elucidation and molecular modeling : Algorithm and Application in Organic Geochemistry*, PhD Thesis, Ecole des Mines, Paris, 1991.
12. Faulon, J. L., Vandenbroucke, M., Drappier, J. M., Behar, F., and Romero, M., *Advances in Org. Geochem.*, **16**, 981, 1990.
13. Faulon, J. L., Hatcher, P. G., and Wenzel, K. A., *Fuel Div. ACS, Preprints*, this volume, 1992.

Acknowledgments

Financial support for this study was provided by the U. S. Department of Energy, Sandia National Laboratories under contracts DE-AC04-76DP00789 and 12-5543. We also acknowledge financial support from DOE contract DE-AC22-91PC91042 from the Pittsburgh Energy Technology Center. We thank Jackie M. Bortiatynski for assistance in assembling the data and manuscript.

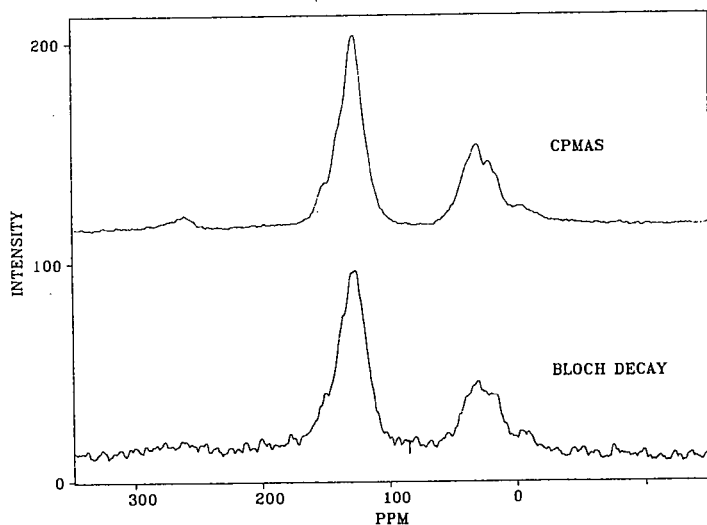


Figure 1. Solid state C NMR data for the high volatile C bituminous coalified wood obtained by the CPMAS and Bloch decay methods.

Table I. Solid-state ^{13}C NMR data for coalified wood samples.

Parameter	Hv Bituminous coal	Subbituminous coal
% carbon*	85.8	77.5
% hydrogen*	6.5	5.28
% oxygen*	5.9	13.9
% nitrogen	2.2	1.0
carbon aromaticity	0.64 (0.61)	0.59
aryl-O/aryl	0.11 (0.13)	0.22
methyl/total aliphatic	0.33 (0.28)	
aryl-H/aryl	0.44	0.40

*- moisture and ash-free values in () are for Bloch decay data

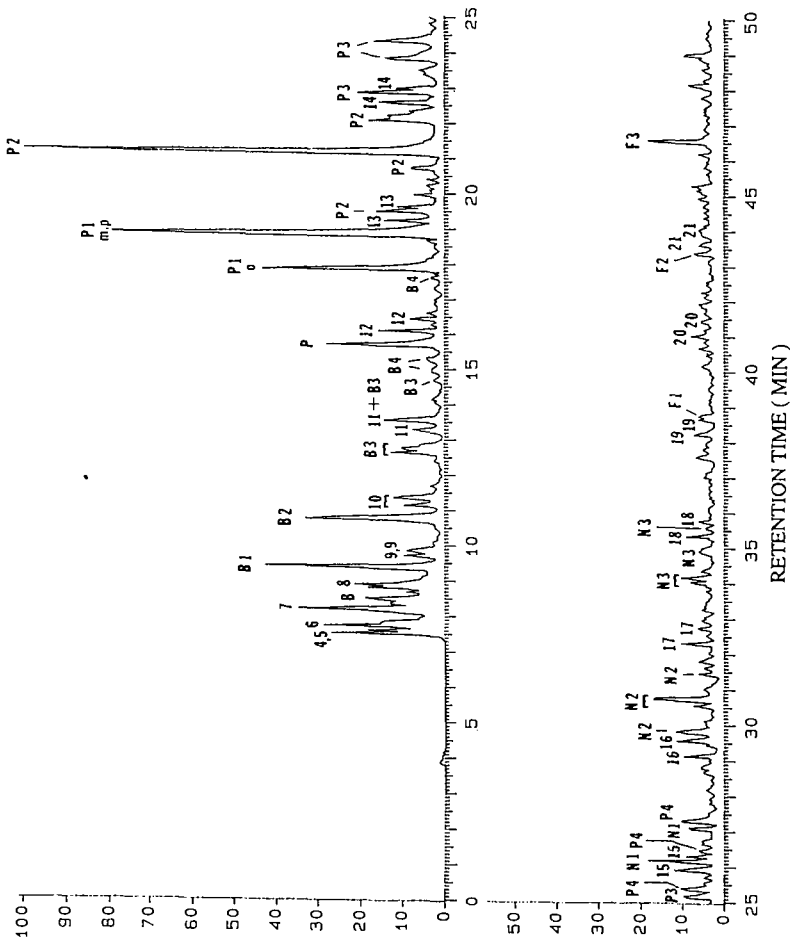


Figure 2. The pyrolysis/gc/ms trace of total ion current for the sample of Hv Bituminous coalified wood. Peak identifications are given in Table 2.

Table 2. Flash pyrolysis data for Hv C bituminous coalified wood

compound	peak designation in Figure 2	weight %	weight % normalized to aromatics
benzene	B	2.2	3.3
toluene	B1	3.2	4.8
C-2 benzenes	B2	3.4	5.2
C-3 benzenes	B3	2.6	3.9
Total benzenes		11	17
phenol	P	2.3	3.6
<i>o</i> -cresol	P1	3.7	5.7
<i>m</i> + <i>p</i> -cresol	P1	8.9	13
2,4 dimethylphenol	P2	8.2	12
other C-2 phenols	P2	6.8	11
C-3 phenols	P3	7.2	11
C-4 phenols	P4	3.2	4.8
Total phenols		40	61
alkylnaphthalenes	N1, N2, N3	11	17
alkyldibenzofurans	F1, F2, F3	3.4	5.2
C ₄ - C ₂₂			
n-alkane/alkenes	4- 22	33	

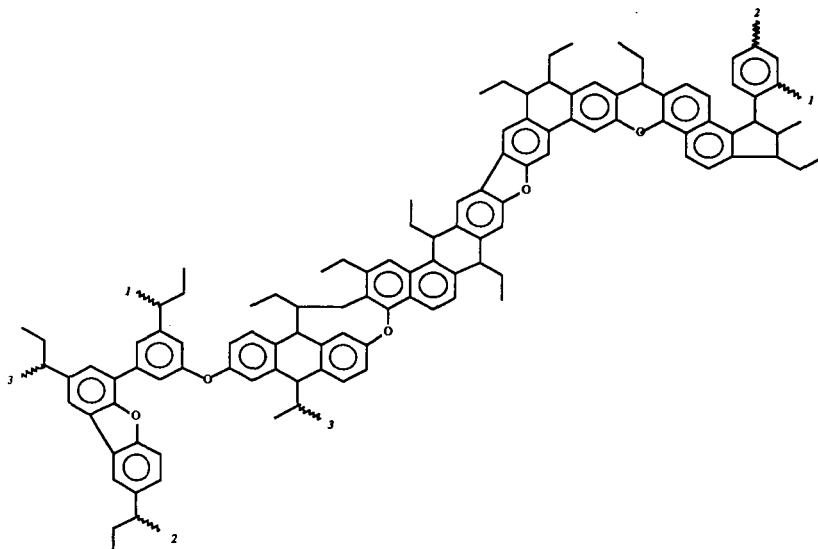


Figure 3. The two-dimensional display of the three-dimensional structural model for high volatile bituminous coalified wood.

POSITRON ANNIHILATION IN ARGONNE ILLINOIS #6 COAL

Peter J. Hall *, Alexander J. Mackinnon and Richard A. Pethrick

Department of Pure and Applied Chemistry

University of Strathclyde,

295 Cathedral Street Glasgow G1 1XL

SCOTLAND

Key Words: Electronic structure, positron annihilation.

* - To whom communications should be addressed.

Introduction

The electronic structure of coals has received little attention but has been the subject of a recent investigation by Larsen *et al.*¹ At a molecular level, the coal becomes increasingly more unsaturated with increasing rank, consistent with generation of a pseudo graphitic structure. Electronically the maturing of coal may be visualized as a transformation from an insulator to a semi conductor. Studies of coal have indicated that a decrease in resistance occurs with increasing temperature consistent with coal being classed as a semi conductor.² Recently there has been considerable interest in the electrical properties of conducting polymers generated by doping conjugated macromolecules³⁻⁵. The conductivity of these materials is influenced by the efficiency of electron diffusion within the conjugated chain structure and hopping between chains which usually involves donor-acceptor sites. Conjugated polymers are very poor semi conductors and it is only when they are doped either by the addition of strong Lewis acids or bases or alternatively the incorporation of heteroatoms into the conjugated structure that semi conductor or metallic behaviour is observed. It is reasonable to assume that similar criteria will be operative for coal, the detailed processes being a function of the rank and chemical composition of the coal. If conductivity were to be measured on a block, there would be complications from any cracks present, together with complications from the bedding plane and the local maceral structure. Direct measurement of the conductivity of powders is difficult in itself.

Positron annihilation has been used for a number of years in the investigation of the effects of radiation damage on metals and ceramic and recently in the study of free

volume in polymers and glasses. The generation or occurrence of defects on an atomic scale allows trapping of positrons as positronium. The typical positron annihilation experiment involves firstly the generation of a positron with an energy of approximately 1.28 MeV; and it is this which when it passes through an organic media will induce radiation damage, combining with a free electron and forming positronium [Ps]. In polystyrene, the diffuse Ps becomes thermally equilibrated and trapped in a molecular size void associated with free volume. Positronium can exist in two spin states; ortho [o-] and para [p-] Ps. The pPs state undergoes annihilation via an allowed transition and has a lifetime of 0.125ns, whereas the oPs state which undergoes annihilation via a forbidden transition which has been predicted by Dirac to have a lifetime of 140ns. In a molecular insulator, spin exchange processes shorten the lifetime and a proportionality with the size of the void has been established. The intensity of the oPs component is a function of the ionization potential of the molecular structure and hence reflects the ability of the thermalizing positron to induce radiation damage. In amorphous polymeric materials, the annihilation spectra are usually composed of three components. The two shortest lifetime components correspond respectively to the self annihilation of p-Ps and free positrons with lifetimes of 0.125ns and 0.4ns. In general, neither of these annihilations will have any significant interaction with media and are independent of its physical and chemical properties. The intensity of the p-Ps will be influenced by the trapping thermalization probability of the positronium which is intimately connected with the occurrence of voids. In the case of a conductor, the positron can interact with the intrinsic delocalized free electron density and trapping will only occur if the radiation spur is larger than the domain structure of the material. Studies of doped polypyrrole has shown that in contrast with the usual situation in most amorphous polymer insulators, annihilation gives rise to a two component spectrum which contrasts strongly with that of the typical amorphous polymer. In this case the positron is assumed to combine with the delocalized electronic structure of the extended conjugated backbone of polypyrrole and its annihilation is a probe of the spin states of this structure. This paper reports the first positron annihilation studies of coal and attempts to compare these observations with the results of related studies on other amorphous materials.

Results and Discussion

Materials

Illinois #6 was selected from the Argonne premium Coal bank for this study. The coal was used as supplied and was subjected to exhaustive extraction using pyridine. The pyridine was completely removed by rotary evaporation prior to use.

Positron Annihilation Spectroscopy

Figure 1 shows a schematic diagram of the apparatus used. A sealed ^{22}Na source was used to generate 1.28 MeV positrons and an accompanying gamma ray. The source was constructed by the evaporation of a concentrated solution of $^{22}\text{NaCl}$ onto a polyamide [Kapton] film. The source was then covered with a second layer of film and the sandwich sealed using a room temperature curing epoxy resin [Araldite]. The positron lifetime was determined from the time delay between the observation of the initial 1.28 MeV gamma ray and the detection of two 0.511 MeV gamma rays which mark the annihilation process. The spectrometer used in this study was a fast-slow coincidence system which incorporates a time-to-pulse height conversion unit and the data is collected using a multichannel analyser, Figure 1. The gamma rays are detected using two fast plastic scintillators coupled to fast photomultiplier tubes [PMT]. The processes are characterized by the emissions at 1.28 and 0.511 MeV which are energy selected and provide the start and stop signals respectively. Discrimination between the start and stop pulses is achieved in the slow circuit and removes any ambiguity of the nature of the pulse arriving at the photomultiplier tubes. The positron annihilation spectra used in this study were obtained from an accumulation of 10^5 counts. The spectrum obtained was analysed using the computer programme POSITRONFIT⁶. The timing resolution of the system had previously been determined using the full width at half peak maximum obtained from a ^{60}Co source. The instrumental resolution function was determined by analysing the lifetime spectrum for annihilation in benzophenone which has a single lifetime of 0.33ns. POSITRONFIT EXTENDED uses the results from the calibration experiments and fits the deconvoluted curve to a sum of exponentials:

$$f(t) = \sum_i A_i \exp(-t/\tau_i) \quad 1$$

where i represents the the number of components present. The relative intensity of

each component is calculated from the area under the corresponding lifetime curve. The adjustable variable in the computer fitting of the data can be altered allowing the selection of the number of components and whether or not each is to be fixed or allowed to be freely adjustable. The quality of the data fit is obtained from the value of σ . For these experiments the powdered coal sample as was loaded into a 5ml vial (diameter 10m) and the ^{22}Na source with its plane perpendicular to the axis of the PMT's. The glass vial was placed coaxially in a second larger vial which was itself inserted between the PMT's⁷. All measurements were carried out at room temperature.

Results and Discussion

Two samples of powdered coal were examined in this initial investigation; a sample of Illinois #6 and a sample of the same coal which has been extracted with pyridine. This extraction removes low molecular mass fractions and may be expected to increase the *free volume* in the material. Ps annihilation spectra for the two samples were obtained and fitted using two component lifetimes. Attempts to fit the data using the traditional three component fits fails, there being no appreciable long lifetime component. The lifetimes and the fits are presented in Table 1. A typical spectrum for the fresh Illinois #6 is shown in Figure 2.

The process of extraction appears to have the effect of increasing the lifetime. Increases in the lifetime of oPs in polymers such as polystyrene can be interpreted in terms of an increase in the lifetime associated with the generation of *free volume* in the matrix. However, in the case of coal the observed spectra resembles more closely that observed in doped polypropylene than that obtained for polystyrene, as shown in Table 2.

Spectra obtained from coal can therefore be seen to resemble those of the semi conducting polymer polypyrrole rather than the insulator polystyrene. The shorter lifetime τ_1 can be associated with free positron annihilation and would not be expected to be significantly influenced by the nature of the matrix. The values of 0.34 and 0.32 ns for the coal and polypyrrole can be assumed to be the same within experimental error. The second component, τ_2 is however clearly a more sensitive probe of the matrix and has a longer time in the coal than in the conducting polymer. The electron mobility may be expected to be greater in the case of the p-toluenesulphonic acid doped polypyrrole than that of the coal. However, these data would suggest that at a microscopic level these values are comparable. Extraction of the low molecular weight fraction appears to

increase slightly the lifetime and this would be consistent with a reduction in the electron mobility. It is probable that the extractable material will not only fill voids in the coal but can also aid electron mobility. Removal of this fraction may generate voids into which the positronium might be trapped and will reduce electron mobility which will further increase the lifetime. It is not possible from these preliminary observations to deduce which of these effects will dominate, however, this data does indicate that positron annihilation may be useful in obtaining information about the nature of the micro-structure of coal.

References

- 1 J.W. Larsen, R.A. Flowers, P.J. Hall, B.G Silbernagel & L.A. Gebhard 1991 **Int. Coal Conf.**, Butterworth-Heinemann, (1991).
- 2 M.G.B. Mahoubin Jones & R.A. Pethrick, **Polymer Yearbook** (Ed R.A. Pethrick) Harwood, New York (1985).
- 3 J.R. Steven & A.J. Mao, **Appl. Phys.**, 41, 4273, (1970).
- 4 R.N. West, **Positron studies of Condensed Matter**, Taylor & Francis, London (1974).
- 5 S.E. Doyle, M.G.B. Mahoubin Jones & R.A. Pethrick, **Polymer Communications**, 26, 262-264, (1985).
- 6 P. Kikegaard & M. Eldrup, **Comput. Phys. Comm.**, 3.204 (1972), 7.40 (1974).
- 7 B.D. Malhotra & R.A. Pethrick, **Macromolecules**, 16, 1175-1179, (1983).

Table 1 Positron Annihilation Study of Illinois #6 Coal

	τ_1 (ns)	σ_1 (ns)	τ_2 (ns)	σ_2 (ns)	I ₁ (%)	σ_1 (%)	I ₂ (%)	σ_2 (%)
Illinois #6	0.746	0.092	0.345	0.007	10.411	3.273	89.589	3.27
Pyridine Ext. Illinois	0.843	0.101	0.345	0.005	7.987	1.785	92.013	1.78

Table 2 Lifetimes and Intensities for Related Polymer Systems

	τ_1 (ns)	τ_2 (ns)	τ_3 (ns)	I_1 (%)	I_2 (%)	I_3 (%)
Polystyrene (room temperature)	0.125	0.450	1.20	-	-	-
Doped Polypyrrole (room temperature)	0.32	0.68	-	18.0	78.0	-

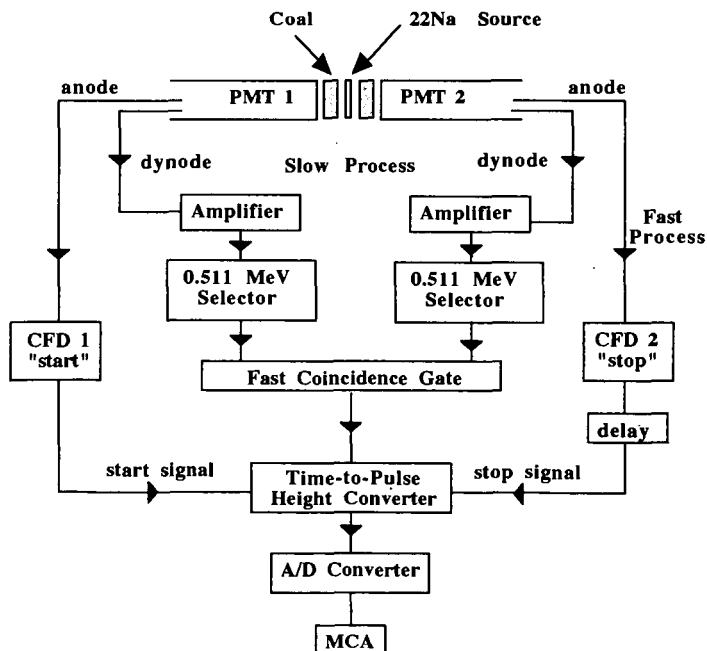
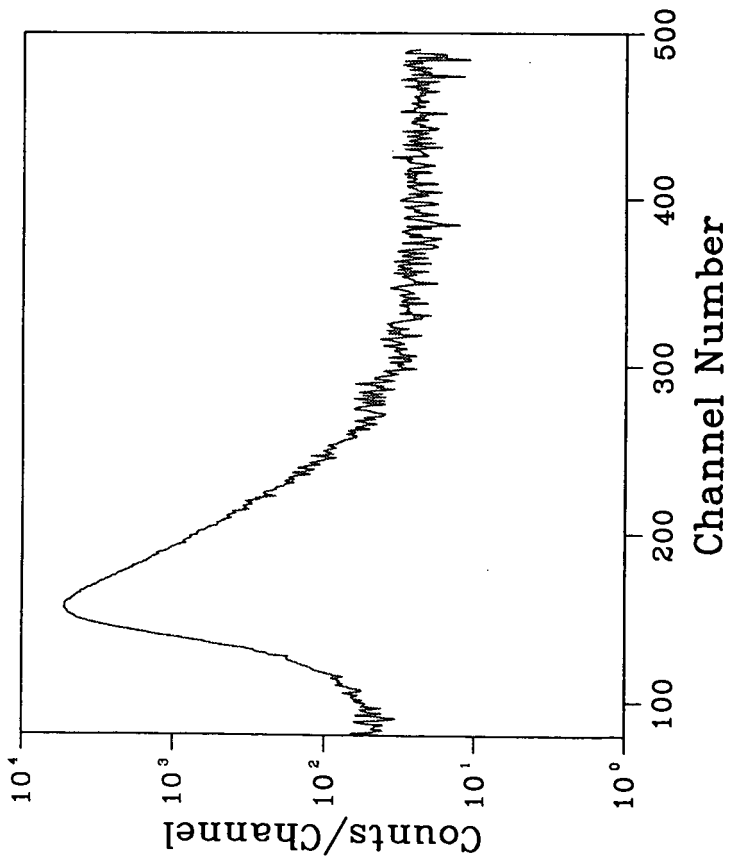


Figure 1 Schematic diagram showing the fast-slow coincidence system



A COMPUTER ASSISTED STRUCTURAL ELUCIDATION FOR COAL MACROMOLECULES.

Jean-Loup Faulon, Patrick G. Hatcher,
and Kurt A. Wenzel.

Fuel Science Program,
The Pennsylvania State University,
University Park, PA 16802.

Keywords : coal structure, molecular modeling, computer aided structure elucidation.

INTRODUCTION

Study of the chemical structure of coal has been the subject of fundamental research for decades and we are now beginning to better understand this structure. It is well recognized that coal is chemically and physically a highly heterogeneous material mainly consisting of organic matter (macerals) and some inorganic materials (minerals). Organic matter which is the object of our interest is composed of carbon, hydrogen and oxygen with lesser amounts of sulfur and nitrogen. The amount, the distribution, and the chemical structure of various macerals in coals depend on the chemical nature of the original coal forming material and the conditions of coalification. Individual macerals may themselves be heterogeneous assemblages of sub-macerals with different chemical structural compositions. The nature of each phase progressively changes during coalification (with rank). For example it is well known that the carbon content of coal increases with its degree of maturation (1). In short, coals are very diverse, and even within any given coal type there is considerable heterogeneity.

Nonetheless, because of the strong link between structure and reactivity, there have been many attempts to model the molecular structure of various coals. For example, chemical structural models have been developed for vitrinite, a major component of coal, ranging in rank from lignite to subbituminous coal (2). For bituminous coals, the most widely accepted molecular models developed during the past 30 years have been the aromatic/hydroaromatic structures. These models are formed by fragments containing about three linked aromatic and/or hydroaromatic rings including appropriate numbers and types of heteroatoms. The fragments are interconnected by hydroaromatic, etheric or aliphatic linkages (3-6). These models have been built using available chemical and structural data on coal, without the aid of computers. They are certainly not unique and the same analytical data can produce similar but different models. Because of the highly heterogeneous character of coal these models are only intended to be representative structures, or average structures. The main limitation of these molecular structures are their two dimensional nature which necessarily ignores most of the interfragment interactions and three dimensional properties such as density and porosity.

Recently Spiro (7) and Carlson (8) have constructed 3D models of several of these structures. Using a space-filling model, Spiro identified several steric difficulties in the original structures and proposed some modifications. To determine the optimal structural conformations of the previous models (3-6), Carlson has used molecular mechanic and dynamic programs. Once minimized, some characteristics such as energy, density porosity can be systematically evaluated

for each model (8). An important result is that for all the models no porosity volumes were found since bituminous coals do clearly show substantial porosity.

The result of these studies have led us to reconsider the modelization of coal. Considering the complexity and the heterogeneity of this material, our intention is not to define another new general model but more specifically to establish a set of average 3D structures which can be correlated to different macerals at different rank levels. In this paper we have chosen to modelize only one maceral of high volatile bituminous coal : the vitrinite. The sample is specifically a coalified wood sample described by Hatcher et al. (9). Our method will involve use of chemistry and a computer. By chemistry we mean we will consider all the chemical analytical results already employed in the previous models but also new techniques which were not used in the past. By computer, we will see that it is possible to generate automatically 3D models from the analytical results and characterize these models in terms of statistics.

METHOD

From a chemical point of view, the task of determining the molecular structure is becoming simpler with the advent of many spectroscopic methods such as NMR, FTIR and flash pyrolysis/gas chromatography/mass spectrometry (py/gc/ms). ^{13}C NMR with cross polarization-magic angle spinning and dipolar dephasing can be used to analyze the overall distribution of various types of carbon structures present in coal such as aliphatic, oxygen-containing, aromatic and hydroaromatic structures (2). By using dipolar dephasing techniques, we can also identify protonated and non-protonated carbons (Table I). Information on the nature of pyrolysis products produced upon heating a coal particle can be obtained using py/gc/ms (2). Results of elemental analysis, and NMR are directly conducted on the coal macromolecule (9) and we can then define what we call a signature for this macromolecule. The signature is simply a series of numbers which count different types of atoms in a specific environment (Table II). The information obtained by py/gc/ms does not describe directly the macromolecule but degradation products or fragments of this macromolecule (Fig. 1). The information given by py/gc/ms is qualitative and defines the fragments which once connected together, in an appropriate amount, constitute the macromolecule. The problem is therefore to find the correct quantity of each fragment and each connection between fragments (interfragment bonds) to form a macromolecule which is consistent with all the structural information. Retrieval of molecular structure from a set of analytical results can be accomplished by an empirical method which consists of a repetitive trial-and-error process to find the correct structure. This method was probably used by the previous authors (3-6), but it is not an entirely satisfactory technique for at least two reasons :

- 1- The process to build a structure is empirical, is accomplished through manual fitting, and can be time consuming for large molecules.
- 2- Generally, many structures can be built from the same analytical data, the reason one structure is chosen instead of an other cannot be clearly defined. This is probably one of the reasons why the coal models cited previously are so different.

Many studies have been conducted in the 30 past years to resolve by computer the general problem of retrieving a structure from analytical data. The generic name for these studies is *computer-aided structure elucidation* (10). Unfortunately the techniques used in these studies are useful only for small molecules and, therefore, cannot be helpful for coal. Recently Faulon et al. (11) have developed a technique which is efficient for macromolecules such as coal. More precisely the data used by this technique are the quantitative chemical information regarding the macromolecule (a signature) and qualitative information concerning a set of fragments. The authors have shown that it is possible from a set of chemical data to compute the amount of fragments and the connections between fragments (interfragment bond) by resolving a linear equation (signature equation). Briefly, the quantitative data given by elemental analysis and NMR defines the signature of the macromolecule, the qualitative information defined by py/gc/ms identifies the molecular

fragments. The structure of each fragment is known from mass spectrometry, therefore it is possible to calculate a signature for each of them. It is also possible to determine a signature for each possible interfragment bond. The amount of fragment and interfragment bonds is obtained by solving the signature equation :

$$\text{signature of fragments} + \text{signature of interfragment bonds} = \text{macromolecular signature}$$

This equation is defined in a discrete space and can admit several solutions. Once resolved, the equation defines the pieces (fragment) and the relations between the pieces (interfragment bonds) of the unknown model which is at that point still an unresolved "puzzle". To "reconstruct the puzzle", a combinatorial program has been developed (12). The program computes first an estimation of the number of solutions : how many models can be built considering a set of pieces and the relation between pieces. When this number is reasonable, the program calculates automatically all the models which correspond to the analytical results. Otherwise the program builds randomly one or a fixed quantity of different models. In all cases the solutions are 3D structures coherent from a chemical point of view : the bonds lengths and the angles between bonds are consistent with the values defined in the literature. These structures can be read and displayed by molecular modeling softwares such as PCMODEL (Serena software), DISCOVER (Biosym) and can be submitted to energy minimization using programs of molecular mechanics like for example MMX (13). Once minimized, physical properties, such as energy, density, porosity can be evaluated.

RESULTS

The analytical results introduced in the program are described in the paper presented by Hatcher et al.(9). From a practical point of view the atomic information (elemental analysis and NMR data listed in Tables I and II) was stored in a file. The molecular fragments (Fig. 1) and the interfragments bonds (Fig. 2) were built using the molecular modeling software PCMODEL (Serena Software) and stored in a library.

The signature equation (11) has been applied for the previous information and all the molecular structures containing a number of carbon atoms between 140 and 180 has been searched. The signature equation found 7 solutions listed in Table III. The best structure with the least error is structure number 6 (molecular formula $C_{178}H_{164}O_8$). This structure is composed of the following fragments: 2 toluenes, 3 C2 benzenes, 1 C3 benzene, 1 o-cresol, 3 m- and p-cresols, 3 C2 phenols, 1 C4 phenol, 3 alkylnaphthalenes, 3 propyls, 9 ethyls, and 7 methyls. The interfragment bonds are 6 benzene-benzenes, 8 benzene-phenols, 10 benzene-toluenes, 5 toluene-toluenes, 7 ethylbenzene-ethylbenzenes, 3 propyl-benzenes, 9 ethyl-toluenes, and 7 methyl-ethylbenzenes. The fragments and inter-fragments bonds are the structures listed in Fig. 1 and 2. Benzene and phenol which appear in the py/gc/ms results are not present in the solution but they can be obtained by pyrolysis from any alkyl benzene or alkyl phenol. C3 phenol is also not present in the solutions. This compound is formed by connecting cresol to ethyl or ethylphenol to methyl. In the same way, alkyldibenzofuran is formed by bonding alkyl benzene and alkyl phenol with a benzene-phenol bond and a benzene-benzene bond.

The combinatorial program presented in (12) has been applied to determine how many models can be built for the structure number 6. This structure is composed of 36 fragments. Considering the structure of the fragments and the global percentage of hydrogen, each fragment must be attached to the rest of the molecule by an average of 3.05 bonds. The total number of bonding sites is therefore $36 \times 3.05 = 110$; this number is also equal to the number of interfragment bonds (55) multiplied by 2. The first bonding site cannot be connected to itself, and there is $110 - 1$ or 109 possible connections. After this operation, $110 - 2$ or 108 bonding sites remain. For the same reason, there is $108 - 1$ or 107 possibilities to connect the second bonding site, 105 for the third, 103 for the fourth, and so on. Consequently the maximum number of structures that can be built is $109 \times 107 \times 105 \times 103 \dots \times 1$: this number is greater than 10^{86} ! However most of the

structures are identical and most of them do not respect the classical chemical constraints and the quantity of interfragment bonds calculated by the signature equation. By avoiding the redundancies and respecting all the analytical constraints, the program found around 1,000,000 possible structures. All these structures are composed of the same fragments and inter-fragments bonds but are different. Fig. 3 shows one of these structures randomly generated by the program. This structure has been subjected to an energy minimization to find a conformationally correct form (MMX program 13). Fig. 4 is the 3D representation of the structure after minimization. All the fragments analyzed by py/gc/ms can be retrieved in this solution, especially C3 benzene and alkyldibenzofuran which were not present in the initial data but obtained by combination of other fragments.

CONCLUSION

The conclusion which can be made from the above results is that for coal the number of models is too large to build all of them. Therefore, in such cases the following question has to be considered : *how many and which structures must be selected and built ?*

The theory of sampling assumes that when the size of a finite population is known, it is possible to extract a subset (a sample) of this population which, in terms of probability, is a good representation. Many techniques of sample design are possible : random sampling, stratified sampling, and sampling with unequal probability of selection (14). The most simple technique which can be applied as a first approximation for our problem is the simple random sampling without replacement (SRSWOR). With this technique it is possible to define an optimal size for a sample (Mean Square Error Method : 15) and extrapolate the mean sample value of a certain characteristic to the whole population. Clearly, according to the theory of sampling, it will be possible to define a sample of average structures which represents the studied coal. It will be also possible to evaluate on this sample certain characteristic such as the energy, the density, the porosity, and to extrapolate these characteristics to the whole population of coal models.

The computer program developed for this study is built in such a way that any new experimental result can be introduced, at any time, without modification of the program. The same program will be useful in the future, when from new experimental data, new models will be needed. Furthermore, we can point out that the program can be applied for any other bituminous coal maceral and any other molecule studied in coal science such as lignite, subbituminous coal, or anthracite. Because different ranks of coal can be modeled, the program can be helpful in understanding the process of coalification. In fact the method is based on an original study made for the kerogen macromolecule (11), and is a general system of structure elucidation efficient for any unknown molecular structure. Therefore, it is realistic to consider applications in organic geochemistry, fuel science and petroleum science such as modelization of humic acids, peat, asphaltenes, crude oil, jet fuel, etc.

REFERENCES

1. Van Krevelen, D. W., *Coal*, Elsevier, Amsterdam, 1961.
2. Hatcher, P. G., *Advances in Org. Geochem.*, **16**, 959, 1990.
3. Given, P. H., *Fuel*, **39**, 147, 1960.
4. Wiser, W. H., *Proc. of the Electric Power Research Institute Conf. on Coal Catalysis*, 1973.
5. Solomon, P.R., in *New Approaches in Coal Chemistry*, Am. Chem. Soc. Symp. Series No. **169**, 61, 1981.
6. Shinn, J. H., *Fuel*, **63**, 1187, 1981.
7. Spiro, C. L. *Fuel*, **60**, 1121, 1981.
8. Carlson, G. A., Granoff B., in *Coal Science II*, Advances in Coal Sciences series, 159 1990.
9. Hatcher, P. G., Faulon, J. L., Wenzel, K. A., Cody, G. D., *this volume*, 1992.

10. Smith, D. H., *Computer-Assisted Structure Elucidation*, Am. Chem. Soc. Symp. Series No. 54, 1977.
11. Faulon, J. L., Vandenbroucke, M., Drappier, J. M., Behar, F., and Romero, M., *Advances in Org. Geochem.*, **16**, 4-6, 1990.
12. Faulon, J. L., *Prediction Elucidation and molecular modeling : Algorithm and Application in Organic Geochemistry*, PhD Thesis, Ecole des Mines, Paris, 1991.
13. Alinger, N. L., *J. Am. Chem. Soc.*, **99**, 8127, 1977.
14. Dalenius, T., in *handbook of statistic 6 - Sampling*, Elsevier, Amsterdam, 1988.
15. Rao, J. N. K., in *handbook of statistic 6 - Sampling*, Elsevier, Amsterdam, 1988.

ACKNOWLEDGMENTS

Financial support for this study was provided by the U. S. Department of Energy, Sandia National Laboratories under contracts DE-AC04-76DP00789 and 12-5543. We also acknowledge financial support from DOE contract DE-AC22-91PC91042 from the Pittsburgh Energy Technology Center. We thank Jackie M. Bortiatynski for assistance in assembling the data and manuscript.

Table I. The atomic information. These values are taken from Hatcher et al.(9).

ELEMENTAL ANALYSIS			¹³ C NMR			
	WEIGHT %	for 100 C		Value 1	Value 2	AVERAGE
C	85.8	100	fa	0.64	0.61	0.63
H	6.5	91.2 ± 1	Aro-O / Aro	0.11	0.13	0.12
O	5.9	5.2 ± 1	Aro-H / Aro	0.44		0.44
			CH ₃ / Ali	0.33	0.28	0.30

Table II. The macromolecular signature. The notations used by the signature are the potential types defines in Biosym softwares : h_ represents an hydrogen atom, c_ an aliphatic carbon, cp an aromatic carbon, and o_ an oxygen atom. The values are given for 100 carbon atoms, h_ = 91.2 means that the ratio H/C is equal to 0.912, c_(c_h_h_h_) = 9.2 means that there is 9.2% of carbon which is aliphatic, linked to one other aliphatic carbon and three hydrogen atoms.

SIGNATURE

	MIN	MAX	AVERAGE
h_	90.2	92.2	91.2
o_	4.2	6.2	5.2
c_	34.2	39.8	37.0
cp	60.2	67.8	64.0
c_(c_h_h_h_)	11.1	13.3	12.2
cp(cp cp h_)	25.3	29.9	27.6
cp(cp cp o_)	6.6	8.9	7.7

Table III. The solutions of the signature equation. The error listed is the difference between the model and the analytical results

solution number	molecular formula	error for 100 C
1	C ₁₅₂ H ₁₄₀ O ₇	0.92
2	C ₁₆₁ H ₁₄₈ O ₈	0.91
3	C ₁₆₂ H ₁₄₈ O ₈	0.83
4	C ₁₇₀ H ₁₅₆ O ₉	0.94
5	C ₁₇₁ H ₁₅₆ O ₉	0.86
6	C ₁₇₈ H ₁₆₄ O ₈	0.82 (-)
7	C ₁₈₀ H ₁₆₄ O ₁₀	0.97

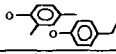
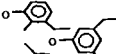
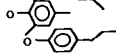
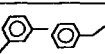
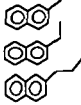
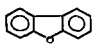
NAME	WEIGHT %	CHOSEN STRUCTURE	NAME	WEIGHT %	CHOSEN STRUCTURE
methyl ethyl propyl			C2 phenol	23.0	
benzene	3.3		C3 phenol	11.0	
toluene	4.8		C4 phenol	4.8	
C2 benzene	5.2		alkyl naphthalene	17.0	
C3 benzene	3.9				
phenol	3.6				
o cresol	5.7				
m and p cresol	13.0		alkyl dibenzo furans	5.2	

Fig. 1. The molecular information. These fragments are results of flash pyrolysis/gas chromatography/mass spectrometry. The weight percentages and the different isomers for the chosen structures are discussed in Haicher et al.(9). The fragments are considered by the program only as qualitative information. Once connected together in an appropriate amount these fragments form the unknown macromolecule.

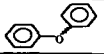
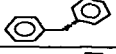
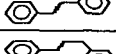
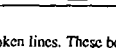
BOND	STRUCTURE
benzene-benzene	
benzene-phenol	
benzene-toluene	
toluene-toluene	
ethylbenzene-ethylbenzene	
propyl-benzene	
ethyl-toluene	
methyl-ethylbenzene	

Fig. 2. The inter-fragment bonds are shown as broken lines. These bonds represent the different ways to connect the fragments listed in Fig. 2.

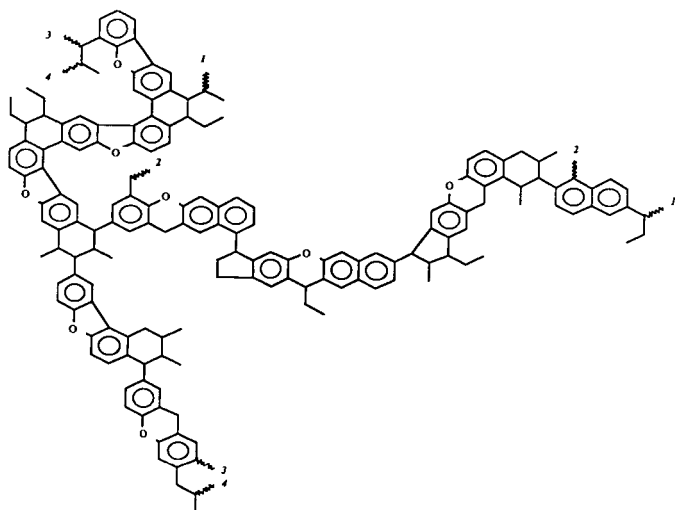


Fig. 3. One possible 2D representation for vitrinite from high volatile bituminous coal. Some other models are possible. An other possibility is given in Hatcher et al. (9). The number indicates the bonding sites (e.g. 1 -> 1).

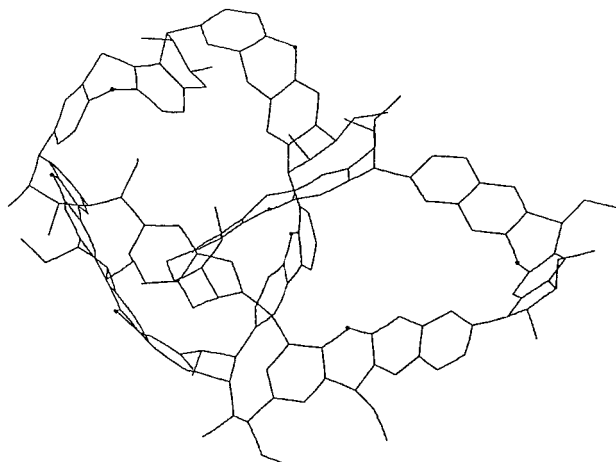


Fig. 4. One possible 3D structure for vitrinite from high volatile bituminous coal. This structure is the 3D representation of Fig. 3.